

# Investigation into the effect of the Thermal Management system of a Diesel engine on the rate of heat transfer through the combustion chamber

Lewis, Andrew

*Award date:*
2014

*Awarding institution:*
University of Bath

# Investigation into the effect of the Thermal Management system of a Diesel engine on the rate of heat transfer through the combustion chamber

**Andrew Graham John Lewis**

**A thesis submitted for the degree of Doctor of Philosophy**

**University of Bath**

**Department of Mechanical Engineering**

**October 2014**

# Abstract

Modern diesel engines are being continuously developed in order to improve their specific output thus reducing the fuel consumption. This is in response to both increasingly stringent regulations and to the demands of the customer evolving. With this in mind a more detailed understanding of some of the fundamental processes within the engine are required. A prime example of one of these processes is heat transfer. In the region of 17-35% of fuel energy will pass to the coolant, therefore the rate of heat transfer has a considerable effect on the design and function of the engine. This thesis describes a method to calculate heat transfer through a combustion chamber wall of a modern production engine and uses the data to improve the understanding of the impact of active thermal management systems on the rate of heat transfer and how this can be incorporated into empirical modelling, also improving fundamental understanding and evaluating established correlations focusing on the warm-up period.

Development of prototype engines over extended test schedules can prove expensive, therefore in order to reduce the necessary test and development period of a new engine it is useful to be able to predict the heat transfer within the combustion chamber using modelling data. A large number of correlations have been developed over the years, however with the rate of development of the diesel engine; some of these correlations have been left behind.

A number of steady state operating conditions were employed to approximate the New European Drive Cycle. By approximating the drive cycle performance it was possible to further the understanding of the effect of changing the engine operating conditions on the temperature distribution in key areas of the engine, including the crankshaft bearings, camshaft bearings and combustion chamber walls. The main focus of this thesis is the cylinder wall temperatures and the rate of heat transfer through the cylinder wall from the combustion gases. It was found that there was a temperature rise of 7°C between the oil in the main oil gallery and that used to lubricate the journal bearings; however the oil in the camshaft bearings was found to decrease in temperature along the inlet camshaft but increase along the exhaust camshaft. In addition the temperature and heat transfer profiles were significantly different between the inlet and exhaust sides of the engine. Existing correlations

were found to in general over-predict the gas side convective heat transfer coefficients at high power conditions. The accuracy of these correlations could be improved by 77.6% by modifying the correlation coefficients; however the introduction of a cylinder wall temperature component, in addition to modifying the correlation coefficients, led to an improvement in the correlation by a further 17.4%.

Prototype hardware and a Design of Experiments (DoE) based test programme were used to investigate the impact of actively changing the external oil and coolant circuits during a New European Drive Cycle on the engine warm-up. It was found that the driving force for improved warm-up when throttling the engine coolant flow was the increase in the gas side wall temperature, and the reduction in the local coolant temperature. The coolant local to the combustion chamber wall was cooler as it remained isolated from the majority of the external cooling system. In addition, the low engine coolant flow retained the heat energy which had been transferred through the cylinder wall, within the engine structure. This unique approach of combining cylinder wall temperature measurements and active thermal management systems allowed for the fundamental heat transfer paths to be explained.

The insight obtained during the steady state experiments and the transient tests was then used to evaluate the potential to calculate the convective heat transfer during different stages of the engine warm-up. A strong correlation, a R-squared of between 0.77 and 0.83, was found between the rate of energy transfer to coolant across the engine and the gas side convective heat transfer coefficient during early stages of the drive cycle, however this decayed as the engine warmed up. A correlation was also found between the convective heat transfer coefficient and the temperature used by the ECU for engine control, in this case measured in the cylinder head. The modified convective heat transfer correlation developed in this thesis allows for the gas side convective heat transfer coefficient to be estimated at different stages of the engine warm-up based on the average cylinder wall temperature. This was not possible with existing correlations and could significantly improve thermal modelling during engine warm-up.

The findings of this thesis are relevant to engine designers, combustion simulation engineers and thermal management teams as 1-D modelling will continue to play a significant role in the development process of internal combustion engines for the foreseeable future. This is

primarily due to the cost implications of high performance computers for 3-D modelling; therefore the development of these models remains vital.

# Acknowledgements

I would like to express my thanks and appreciation to Prof Chris Brace and Dr Sam Akehurst for the guidance, supervision, support and open door policy throughout this work. The occasional feedback and continued encouragement has helped me to persevere.

I would also like to thank Dr Richard Burke, Allan Cox and Sam Hurley for all their efforts in installing, operating and maintaining the test facility during this time.

I must also thank the Ian Pegg and Roland Stark at the Ford Motor Company for their support during the experimental phase of this work, which was conducted with the financial support of the Technology Strategy Board, Ford Motor Company, BP and Mahle Powertrain and their funding is acknowledged.

I would also like to thank all my other colleagues at the PVRC and the wider automotive community for their support, whether they are aware of it or not, it is their continued questioning "How is the PhD coming along?" which has kept me going. Particular mention must be made to Dr. Rishin Patel, Dr. Jamie Turner, Dr. Simon Pickering, Ed, Karl, Huayin, Qingning, Deepak, Bob and Jim.

Finally I would like to thank my good friends and family for their support, especially my mum who read this thesis from cover to cover during her holiday. Without these people standing by me and forcing me to carry on I am certain I would have given up and walked away long ago.

# Table of Contents

# Notation

| | |
|---|---|
| a, b, c, C, m, n | experimental coefficients, constants, parameters and exponents |
| A | instantaneous surface area exposed to heat transfer ($m^2$) |
| B | Cylinder bore or diameter (m) |
| BMEP | brake mean effective pressure (bar) |
| $C_d$ | valve discharge coefficient |
| CDF | valve discharge coefficient (forward flow) |
| CDR | valve discharge coefficient (reverse flow) |
| CHTC | convective heat transfer coefficient ($W/m^2K$) |
| $C_p$ | constant-pressure specific heat (J/kgK) |
| $C_u$ | peripheral gas velocity (m/s) |
| $D_h$ | Hydraulic duct diameter (m) |
| DI | Direct injection |
| ECU | engine control unit |
| $g_0$ | force-mass-acceleration constant ($m/s^2$) |
| h | heat transfer coefficient ($W/m^2K$) |
| $h_c$ | convective heat transfer coefficient ($W/m^2K$) |
| H | enthalpy (J/kg) |
| IDI | indirect injection |
| k | thermal conductivity (W/mK) |
| $\dot{m}$ | mass flow rate (kg/s) |
| $\dot{m}_f$ | fuel mass flow rate (kg/s) |
| $n_c$ | number of revolutions per cycle |
| n | engine rotational speed (rev/min) |
| Nu | Nusselt number |
| P | power (W) |
| p | instantaneous cylinder gas pressure (bar) |
| Pr | Prandtl number |
| q | heat flux rate (heat transfer per unit area per unit time) ($W/m^2$) |
| Q | heat transfer rate (heat transfer per unit time) (W) |
| r | radial distance from cylinder axis (m) |

| | |
|---|---|
| R | gas constant of air (287 J/kgK) |
| Re | Reynolds number |
| t | time (s) |
| T | temperature (K) |
| T | Torque (Nm) |
| TMS | Thermal management system |
| $c_m$ | mean piston speed (m/s) |
| V | instantaneous cylinder volume ($m^3$) |
| $V_d$ | displacement volume ($m^3$) |
| $V_s$ | swept volume ($m^3$) |
| $w_c$ | ratio of carbon content in the fuel by mass |
| x | distance measured along one particular coordinate (m) |
| $\Delta x$ | difference in distance (m) |
| $\Delta T$ | difference in temperature (K) |
| $\alpha_s$ | scaling factor |
| $\varepsilon$ | surface roughness parameter |
| $\gamma$ | ratio of constant-pressure to constant-volume specific heats |
| $\mu$ | dynamic viscosity (kg/ms) |
| $\nu$ | kinematic viscosity ($m^2/s$) |
| $\theta$ | crank angle (degrees) |
| $\varrho$ | density ($kg/m^3$) |
| $\sigma$ | Stefan-Boltzmann constant ($5.67x10^{-8}$ $W/m^2K^4$) |
| $\omega$ | angular rotational speed of crankshaft (rad/s) |

**Subscripts**

| | |
|---|---|
| a | indicates ambient conditions |
| bb | denotes blowby |
| c | denotes coolant |
| cyl | denotes cylinder |
| g | denotes gas |
| tf | total friction |
| w | denotes wall |
| x | denotes reference to one particular coordinate |
| 0 | refers to stagnation conditions |

| | |
|---|---|
| 1, 2 | denotes reference to coordinate values or crank angle steps |
| Tot | denotes total or overall value |

# List of Figures

# List of Tables

# Further Publications

The work that will be presented has led to a number of publications at internationally recognised conferences. A list of these publications is provided below and references to these will be provided as necessary within the chapters of the thesis.

## *Refereed conference articles*

**The effect of forced cool down on cold start test repeatability**

A. Lewis, CJ. Brace and A. Cox., presented at SAE 2009 International Powertrains, Fuels and Lubricants Meeting (June 17th 2009) Paper No. 2009-01-1976

**Dynamic measurement of heat flux through the cylinder wall of a modern HSDI engine a New European Drive Cycle**

A. Lewis, CJ. Brace, K. Robinson and CA. Finol., presented at SAE 2010 World Congress (Detroit, Michigan – June 12th 2010) Paper No. 2010-01-0322

**Spatially resolved heat flux measurements from a HSDI engine over NEDC**

A. Lewis, CJ. Brace, S. Akehurst, K. Robinson and I. Pegg., presented at Vehicle Thermal Management Systems (VTMS) 2011 (Heritage Centre, Gaydon – May 16th – 19th 2011)

**Estimated total energy transfer over an NEDC through steady state performance evaluation**

A. Lewis, CJ. Brace, S. Akehurst, K. Robinson and I. Pegg, presented at ASME 2012 Internal Combustion Engine Division Spring Technical Conference (Torino, Italy – May 6th – 9th 2012) Paper No. ICES2012-81192

# Chapter 1. Introduction

## *1.1 Key motivations*

Modern diesel engines are required to meet increasingly stringent regulations with regard to emissions and performance criteria. This drive is mainly due to the increasing concerns of the impact that vehicles have on the environment such as Global Warming. When petrol or diesel is burnt in an internal combustion engine the main by-products are water and Carbon Dioxide. Carbon Dioxide has been found to be contributing significantly to Global Warming. To reduce the impact of vehicle emissions on the environment, targets have been enforced amongst vehicle manufacturers since 1997 to drastically reduce the emissions from any new passenger vehicle. In recent years the advances in engine technology have brought about vast improvements in the emissions control and power output of the internal combustion engine. Such advancements in diesel engine technology include the high pressure common rail and variable fuel injection strategies, the introduction of exhaust gas recirculation, high levels of intake boost pressure provided by a single or double stage turbocharger and inter-cooling. Even with these large steps forward in technology it is important to continue investigation into all aspects of the internal combustion engine development process, from concept to manufacture.

Current market trends show that the consumer expects high performance whilst maintaining the lowest possible fuel consumption. To achieve this, the specific power of an engine must be increased, however this means running at higher operating temperatures and pressures which will consequently lead to greater thermal loads on a large number of components within the engine. A better understanding of the heat transfer paths through the engine and between different components will be significantly beneficial in developing new engines to meet the new regulations and guidelines. There are several fundamental components, such as cylinder bores, exhaust valves, valve bridges, valve seats and piston crowns that directly affect the output possibility of an engine due to durability constraints. The constraints are due to the component material and its performance under higher temperatures. To guarantee a long and reliable life of an engine it is important that there is adequate lubrication throughout and all components temperatures are kept within their operating range.

Lubrication not only affects the mechanical life of the engine but it is also affects the day-to-day running of the engine from a consumer's point-of-view as it is known that a considerable amount of fuel is used to overcome friction between internal components. The level of friction is known to be dependent on various temperatures inside the engine as the lubricant has an ideal operating window, this implies that a greater knowledge of the temperature distribution of components would aid in the improvement of fuel economy. One solution to reducing the level of friction is to reduce the time taken to achieve the working temperature of the lubricating fluid; another solution is to reduce the size of the engine whilst maintaining the same level of performance, which is known as 'down-sizing'.

As with all aspects of engine calibration there is a trade-off when implementing changes to improve an engine's thermal efficiency. Increasing the thermal efficiency of an engine will help to reduce the emissions of $CO_2$ but will often cause an increase in NOx; therefore with an increased understanding of the heat transfer through the combustion chamber walls an optimum point can be achieved. For example, local hot points around the combustion chamber will increase the NOx production. The combustion processes taking place inside the cylinder make the heat transfer extremely complicated as it is a function of both the instantaneous in-cylinder temperature and pressure. The heat transfer from the gases to the cylinder walls and subsequently to the coolant and the oil also occurs by the three different modes of heat transfer. Current methods for predicting the heat transfer from the combustion chamber walls is based on extremely outdated engine technology, with some empirical correlations dating back to 1939 with limited development taking place more recently. Investigations of this type have an inherently high cost and thermal management systems are sized for the worst case scenario therefore little focus has been placed on work of this type. Therefore the implementation of established correlations may be producing results which are vastly different from actual conditions.

## *1.2 Aims and Objectives*

The primary aim of this thesis is to improve the understanding of heat transfer in modern production diesel engines through the measurement of combustion chamber wall heat transfer under both steady state and transient operation. A significant proportion of the work was the design and evaluation of an appropriate technique for the measurement of the cylinder wall temperature. As well as this an evaluation of established convective heat transfer models and the proposal of an improvement to these models was made, alongside an

investigation of the fundamental heat transfer effects of different active thermal management systems over a series of transient drive cycles.

In order to achieve the overall project aim a series of more specific objectives had to be completed, these are as follows:

1. Review literature relating to engine performance technologies, current trends in thermal management systems and their subsequent impact on the heat transfer in modern diesel engines.

2. Review combustion chamber wall measurement techniques and the empirical convective heat transfer correlations which have been established.

3. Apply this knowledge in the design of a temperature sensor to be installed in the combustion chamber wall of a production engine at a number of different locations.

4. Develop and implement an experimental programme to evaluate the rate of heat transfer through the combustion chamber wall across a targeted operating envelope. Analyse the resulting data and use to evaluate established convective heat transfer models used in 1-D engine simulations.

5. Improve the accuracy and/or highlight fundamental deficiencies in the application of empirical convective heat transfer correlations in their current forms in 1-D simulation codes due to the inclusion of modern technologies in engine systems.

6. Design and manufacture a number of mechanical components to allow for a series of thermal management system build changes to be performed.

7. Develop an understanding of how different active thermal management systems impact the rate of heat transfer from the combustion chamber through the cylinder wall.

8. Combine findings from both the steady state experiments and the transient experiments to improve the understanding of heat transfer within a modern diesel engine.

## 1.3 Summary of chapters

This thesis contains the following chapters:

- Chapter 1 contains an introduction, the principle aim of the thesis, the targets to achieve this objective and a summary of the chapter contents.

- Chapter 2 introduces a number of fundamental engine technologies which have been implemented to improve fuel consumption and the recovery of waste heat. A brief overview of the current market trends in thermal management systems is given to give context to the changes which will be applied in this study.

- Chapter 3 contains an overview of the development of convective heat transfer correlations including the experimental methods. Additionally the use of in-cylinder pressure measurement has been explained and how this is closely connected to the understanding of in-cylinder heat transfer.

- Chapter 4 describes the experimental facilities and engine hardware used for this investigation; this includes the data acquisition equipment that was used to control the engine test facility. The coolant system and additional active thermal management system components have also been outlined and the methods used to integrate them into the production system are discussed. A brief overview of the experimental programme is also given. Finally the calculation and data processing methodologies are described.

- Chapter 5 details the design and development of a temperature sensor used to measure the combustion chamber wall temperature and subsequently calculate the rate of heat transfer from the combustion gases to the engine coolant through the cylinder liner. The development of this temperature sensor also involved establishing

a calibration and installation process which would improve the accuracy of the sensor and its reliability respectively.

- Chapter 6 analyses the results obtained from the different experimental procedures undertaken. The first results were obtained from a series of motored tests to identify the level of friction within the engine. Steady state tests were subsequently used to evaluate the measured rates of heat transfer through the cylinder walls and how changes in the engine operating condition affected the heat transfer. In addition in-cylinder pressure data was used to evaluate established convective heat transfer correlations and how they compared to time-averaged measured data. Finally transient tests were used to assess whether changes to the external oil and coolant circuits had significant impact on the rates of heat transfer through the cylinder walls.

# Chapter 2. Review of engine technologies and thermal management trends

This chapter aims to review recent engine technologies which have increased the overall performance and heat generation from modern diesel engines, as well as detail the fundamental components which are included in a production engine cooling circuit.

Also included in this chapter is an overview of the energy balance which is present in the engine during operation, this details the methodology for calculating each proportion of the equation as well as some key findings.

In addition an explanation of the basic modes of heat transfer which take place within the engine is given and how these are effected by the coolant composition and boiling regime.

It is known that heat is a fundamental energy loss within internal combustion engines which has been a focus of an increasingly large number of investigations with the aim to improve fuel consumption by using this heat in a productive manner. Projects, such as this one, aim to understand the heat generation and utilise additional components or fundamental changes in thermal management strategies to convert this energy loss back into useful work. A number of these studies and technologies have been detailed here.

## *2.1 General I.C. engine technologies affecting performance and heat generation*

Internal combustion engines used in on-road applications typically adhere to a four-stroke mechanical cycle whether it is a spark-ignition or compression ignition engine. To understand the thermodynamic processes taking place in the complex cycle it is common to analyse the mechanical cycle using an air standard cycle. In air standard cycles a certain mass

of air operates in a complete thermodynamic cycle where the heat is added and rejected using external sources and the processes are reversible. There are a number of air standard cycles but high-speed compression ignition engines can be compared to the Diesel Cycle, shown in Figure 2.1 and is made up of the following four processes:

- Isentropic compression
- Addition of heat at constant pressure
- Isentropic expansion
- Rejection of heat at constant volume

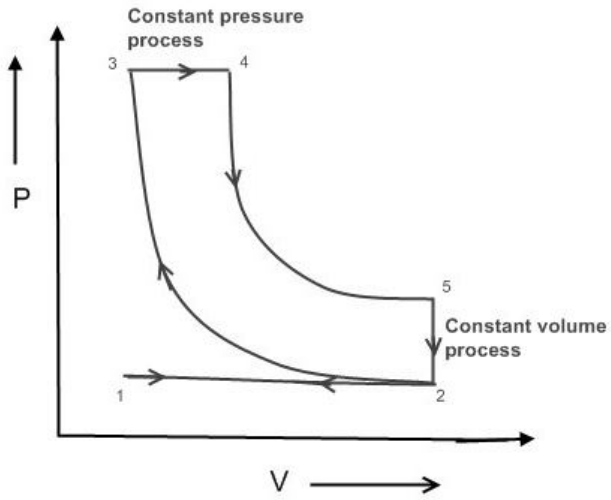


**Figure 2.1 – Diesel thermodynamic cycle (p-V diagram) [1]**

In this cycle the combustion event can be considered as a process of heat addition at constant pressure due to the fuel being injected as the piston is moving down, therefore evaporating and filling the increasing volume, thus keeping the pressure inside roughly the same. The Otto cycle which is used for spark-ignition engines considers the combustion event as a heat addition at constant volume. Combustion does not occur at either constant pressure or volume but is initiated at a point dependent on injection timing or spark timing and continues over a period during the compression stroke. This is one of the reasons for the thermodynamic cycle being an approximation to the true events.

For combustion to occur both air and fuel are required in the combustion chamber. For improved peak power and to ensure sufficient air flow, modern engines have four valves per cylinder, allowing the fuel injector, in direct injection engines, to be positioned centrally and vertically above the piston to improve mixture preparation [2]. There are two main types of

fuel injection in compression ignition engines; direct injection (DI) into the main chamber, or indirect injection (IDI) into a separate chamber. In a DI engine the fuel injection pressures must be greater than an IDI, typically in the region of 1500 bar, and utilise multiple-hole nozzles due to reduced air movement. Fuel can be delivered to the injectors via either a common-rail fuel injection system or an injection pump system. A common-rail system is preferential as it allows the system pressure to be controlled. The injection timing is controlled by the Engine Control Unit (ECU) and can consist of a pilot and main injection depending on the operating condition. The pilot injection is designed to reduce the occurrence of diesel knock, which is caused by a pressure rise in the cylinder which is faster than that occurring due to the ignition delay; the main injection event produces the engine power. The combustion process in a compression ignition engine is much slower than in a spark ignition engine and as a result the maximum obtainable engine speed is also lower. There are four distinct stages to the combustion process:

- Ignition delay, the period after injection before combustion occurs, during which the fuel is breaking up into droplets, being vaporized and mixing with air.
- Rapid combustion, a very rapid rise in pressure due to the ignition of the prepared mixture.
- Controlled combustion, combustion occurs at a rate determined by the preparation of the air/fuel mixture.
- Final combustion, rate of combustion is determined by diffusion until all fuel and air is used.

The process of combustion is the main source of heat within the engine, with improving technologies resulting in higher cylinder pressures and temperatures the amount of heat generated is only increasing. Torque is produced from the force of the combustion gases on the piston and can be measured at the crankshaft using a torque transducer coupled to the engine dynamometer. Using Equation (1) the brake power output of the engine and the brake mean effective pressure can be calculated. Brake mean effective pressure (BMEP) is the work output of an engine as measured by the dynamometer and is independent of engine size so is a useful metric when comparing engines of different displacements or when operating conditions are across a range of speeds and loads.

$$P = \frac{2\pi n}{60} T \qquad BMEP = \frac{T n_c}{V_d} 2\pi \qquad (1)$$

All modern diesel engines are now turbocharged to increase peak power and efficiency. Traditionally this would be with a fixed geometry turbocharger (FGT) but it is becoming increasingly more common to utilise a variable geometry turbocharger (VGT) as the technology becomes more refined and the systems to control the mechanism become cheaper. A FGT converts the exhaust gas energy into useful work via a turbine and compressor assembly, this increases the inlet charge air to a pressure of 1 bar gauge, and about 150°C. The high pressure gas is then cooled by an intercooler, reducing the temperature back down to about 50°C. This process increases the inlet air density (21% oxygen) allowing more fuel to be injected producing more power and achieving an improved volumetric efficiency. The increase in peak in-cylinder pressures and temperatures results in much higher rates of heat transfer to the coolant system through the combustion chamber walls.

Another technology now common place in modern I.C engines is Exhaust Gas Recirculation (EGR) of which there are two types, internal and external. Internal recirculation is achieved by late exhaust valve closing, therefore increasing the valve overlap period, whereas external recirculation requires a gas feedback loop. In an external EGR circuit the exhaust gas flows from the exhaust manifold (upstream of the turbocharger) through a gas-to-liquid heat exchanger in the main engine coolant circuit. The aim of this heat exchanger is to bring the exhaust gas temperature down from about 500°C to 150°C. It is important that the exhaust gas is sufficiently cooled otherwise the resultant NOx emissions would increase and the volumetric efficiency would be severely reduced. The amount of gas which flows through this heat exchanger is controlled by a motor driven valve on the outlet. The EGR gas consists of in the region of 16% oxygen and is combined with the compressed air from the compressor prior to the inlet manifold. This mix has significant impact on the exhaust emissions, e.g. NOx emissions are reduced with increased EGR rates but induce a penalty of an increase in THC emissions, resulting in a trade-off. EGR gases have the following three effects on combustion:

- Dilution effect: The lack of oxygen in the cylinder reduces the formation of NOx but at the same time inhibits PM oxidation. Studies have shown that this is the principle effect of EGR.
- Thermal effect: The EGR gases increase the specific heat capacity of the cylinder charge acting as a heat sink, reducing the overall peak temperatures. It was also found that the use of EGR causes an increase in ignition delay and a shift in the location of the start of combustion.
- Chemical effect: Increased concentrations of $H_2O$ and $CO_2$ produce more endothermic dissociation reactions, absorbing heat energy and reducing peak temperatures within the cylinder. A dissociation reaction is a chemical reaction where a compound breaks apart into two or more parts.

The mix of EGR gas and fresh inlet gas is dependent on the pressure in the exhaust manifold and the extent the EGR valve is open, which is controlled by the engine management system.

All engine designers' aim for high volumetric efficiency as the engine output is directly dependent on it. An essential part of achieving high volumetric efficiency is the engine cooling system. The cooling system is also important in ensuring proper combustion and reliable mechanical operation of the engine. A simple expression was produced in 1957 by Alcock which stated that the total heat loss from an engine could be based purely on the fuel flow rate, regardless of the engine speed, air-fuel ratio, throttling or charging system. Equation (2) was found based on two high-speed, four stroke engines (one petrol and one diesel) and states that the total heat flow is proportional to the gross fuel consumption [3]. By using fuel flow rate the effect of engine load is taken into account but some differences due to changes in air charge temperature and pressure, and engine speed were found but considered to be second-order effects. It must be noted that the tested engines utilised simple intake air system charging systems and had very narrow operating conditions compared to modern engines.

$$Q_{Tot} \propto \left(\dot{m}_f\right)^{0.64} \tag{2}$$

The advances in engine charging and other technologies, as well as increased engine speed ranges have led to a number of inaccuracies in this equation. Findings made by Taylor et.al found that the coefficient should be increased to 0.75 for the local heat transfer rate [4].

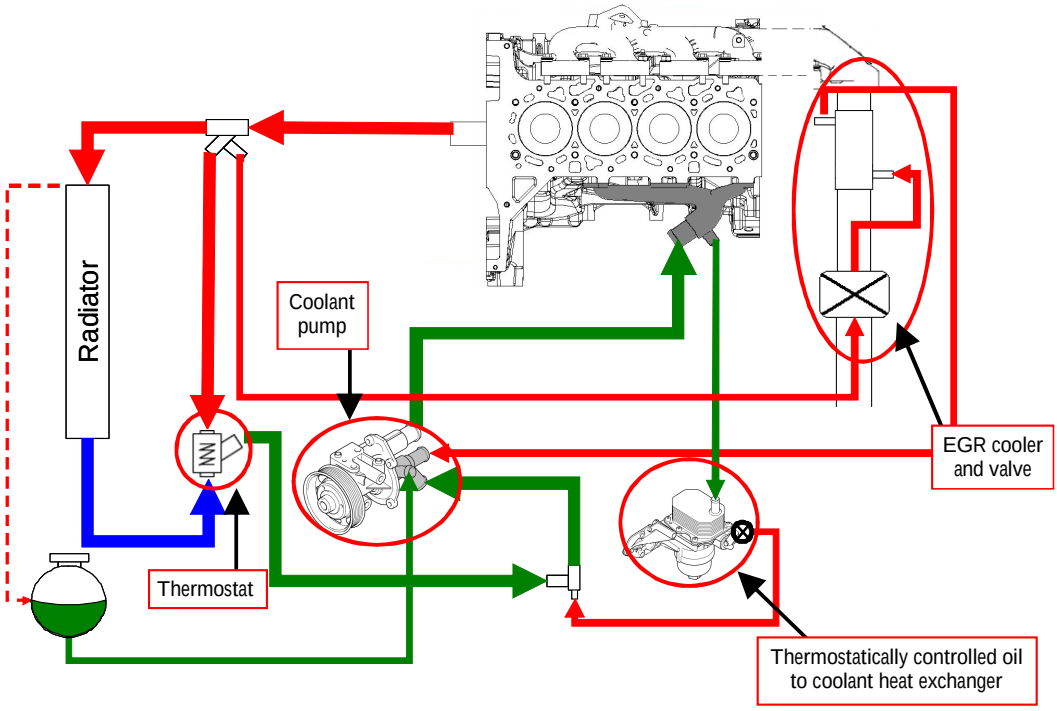


**Figure 2.2 – Production engine coolant circuit**

Figure 2.2 shows a basic cooling system consisting of an EGR cooler and valve assembly, a mechanical coolant pump and a thermostatically controlled oil-to-coolant heat exchanger. A basic understanding of the energy flows within the system can be obtained by applying the first law steady flow energy conservation equation to a control volume surrounding the engine.

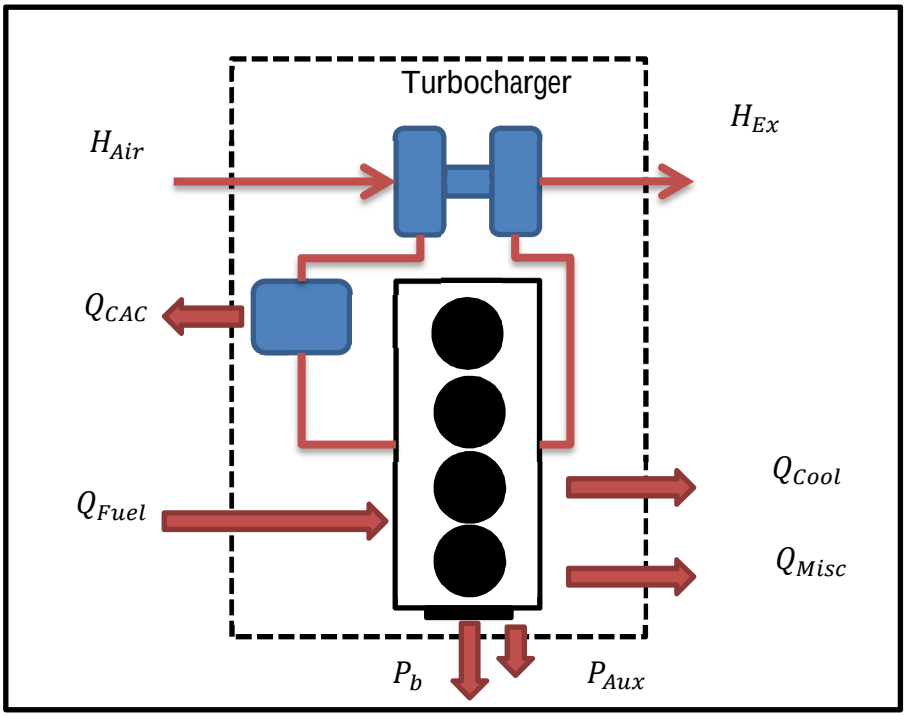


**Figure 2.3 – System control boundary for heat balance application**

Equation (3) shows this applied to the control volume shown in Figure 2.3. There are eight components to the energy balance, the two inputs to the system are the injected fuel and consumed air, and the outputs are the useful work or brake energy, the auxiliary power, the heat lost to coolant and exhaust, and external heat rejection of the engine, such as that to overcome friction and lost to radiation from the structure.

$$Q_{Fuel} + H_{Air} = P_b + P_{Aux} + Q_{Cool} + Q_{Misc} + Q_{CAC} + H_{Ex} \quad (3)$$

It is difficult to measure the external heat rejection of the engine, therefore it is often assumed to be the remainder left over from the energy balance. However this will hide any inaccuracies or errors in the measurement procedure. A possible method to measure the heat rejection is to construct a box surrounding the engine and measure the air flow through it and subsequent temperature difference, this is known as a climatic chamber engine test bench [5, 6]. This kind of setup is not always appropriate or possible due to the extensive set up required. The brake power can be calculated directly from the measured dynamometer torque and speed as given in Equation (1). The auxiliary power consists of electrical power the alternator delivers to external devices, hydraulic power the steering pump delivers to the steering system and cooling power the air conditioning compressor delivers to the cabin. These outputs would be calculated from the measured voltage and current for the alternator, and for the pumps, the appropriate temperatures, pressures and flow meters would be

required. There was no external power output of the auxiliaries during the measurements taken in this thesis so no effective auxiliary power had to be taken into account.

To calculate the fuel energy accurately the fuel composition would need to be known so that the enthalpies of formation of the reactant species could be determined. However as the exact composition is not known, the lower heating value can be used. This is measured in a calorimeter and represents the heat of reaction per unit mass at a standard temperature of 25°C for complete combustion of the fuel. Also required is the fuel flow rate. There are three methods of estimating the fuel flow rate; these are the gravimetric method, the carbon balance and the ECU fuel demand. The gravimetric consumption is simply the change in the mass of fuel in a beaker over a specific time interval such as a drive cycle. The ECU fuel demand is calculated from the control strategy volumetric demand based on engine air flow and torque demand. Burke et al. found large discrepancies between these fuel measurement methods which can be reduced if certain corrections are employed [7]. It was found that the most accurate method for calculating the fuel energy is by using the fuel flow rate estimated by a corrected British Standard carbon balance method applied to the emissions data collected using a Horiba MEXA 7000 series gas analyser [8].

$$FC_{CB} = \frac{1}{w_c}\left(w_c \times m_{THC} + 0.428 \times m_{CO} + 0.273 \times m_{CO_2}\right) \quad (4)$$

The overall fuel consumption is obtained using Equation (4), where $w_c$ is the ratio of carbon content in the fuel by mass, and 0.428 and 0.273 represent the ratio of the atomic weight of carbon to the molecular weight of carbon monoxide and carbon dioxide respectively. Further details of the estimation method are given in work by Burke, where the difference between this method and the gravimetric method were found to be less than 10g (1%) over a New European Drive Cycle. When calculating NEDC fuel consumption the emissions data must be synchronised so that the emission measurement corresponds to the correct 'slug' of exhaust gas. The total delay is due to the analyser response, sample line transport time and the exhaust transport [9]. The fuel energy is subsequently given by:

$$Q_{Fuel} = \dot{m}_{Fuel} \times Q_{LHV} \quad (5)$$

Gas enthalpy fluxes have to be calculated for fresh air and exhaust gas as well as for the air before and after the charge air cooler to draw the energy balance. The gas enthalpy can be taken from standard tables at the same reference temperature to that used for the determination of the fuel heating value, i.e. 25°C. Therefore the enthalpy flux can be given as a function of temperature by:

$$H(T) = \dot{m} \times h(T) \tag{6}$$

Or in the case of the exhaust enthalpy where it consists of a number of components, the overall enthalpy flux consists of the sum of all individual components:

$$H(T) = \sum_{i=1}^{n} \dot{m}_i \times h_i(T) \tag{7}$$

The specific heat capacity of the coolant is also a function of temperature. The specific capacity has a non-linear characteristic therefore it is necessary to calculate the enthalpy change across the heat exchanger given by:

$$Q_{Cool} = \dot{m}_{Cool} \times \int_{T_{upstream}}^{T_{downstream}} C_P(T) \times (dT) \tag{8}$$

In this work the coolant flows were measured using non-intrusive electromagnetic mass flow meters and the temperatures were measured using k-type thermocouples located in the hoses both upstream and downstream of the heat exchangers. There are additional energy exchanges such as that across the oil heat exchanger, the EGR cooler and dissipated by the radiator, in this case the radiator is outside the control volume however the other energy exchanges are within the boundary. The energy transfer to the coolant across the engine is made up of a number of components, which include the heat from combustion and friction from the pistons and valve train. The energy distribution for an engine as an isolated system is shown in Figure 2.4 [2]. The heat losses have been put into the context of total vehicle losses for a NEDC in Figure 2.5 for a 3.6 litre V6 SIDI gasoline engine.

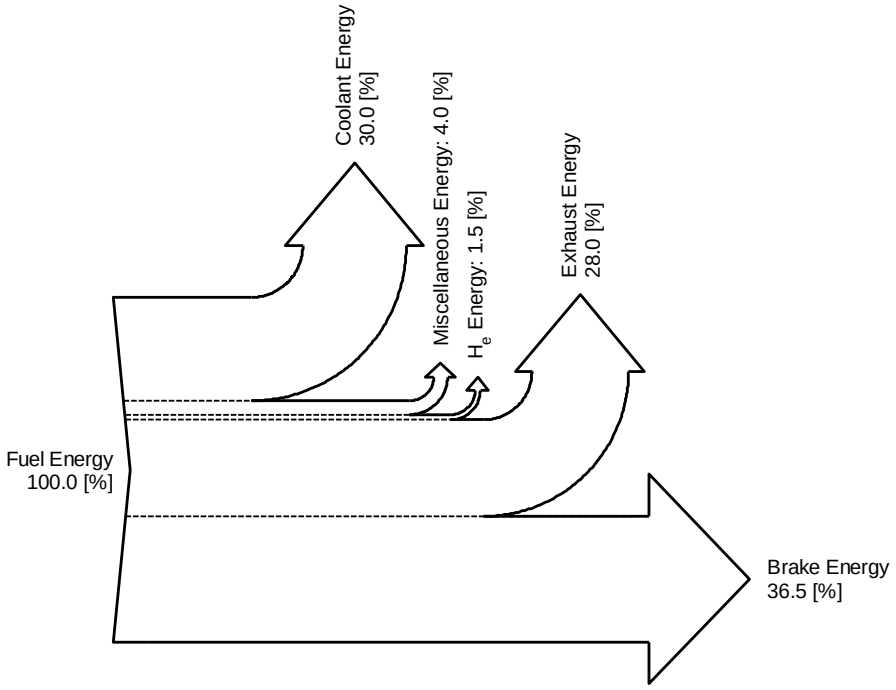


**Figure 2.4 – Sankey diagram of fuel energy usage**

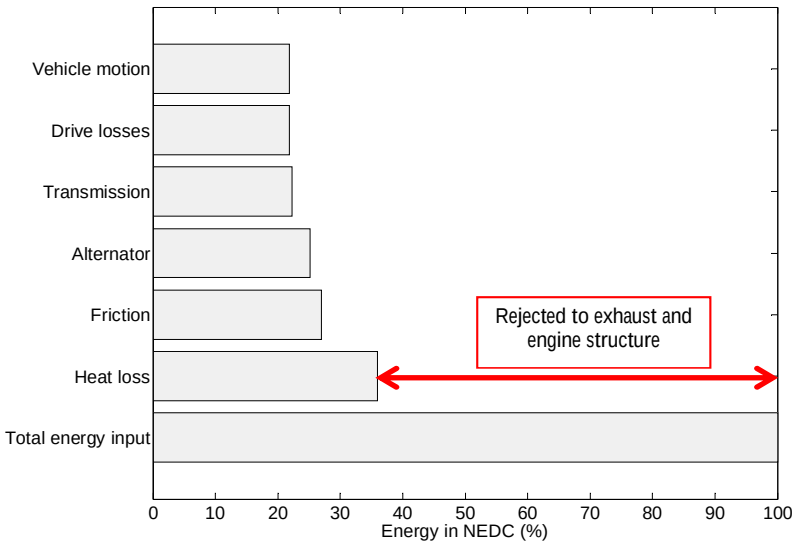


**Figure 2.5 – Energy dissipation for a vehicle over a NEDC [10]**

Figure 2.5 highlights that 64% of the total energy input is lost to the exhaust or engine structure, in comparison to the 2.9% lost in the transmission or 9% used to overcome engine

friction[1]. Table 1 gives typical values for the components of Equation (3) at maximum power for both a spark ignition engine and a diesel engine.

**Table 1 – Typical energy balance percentage ranges at maximum power output for both spark ignition and compression ignition engines**

| | $P_b$ | $Q_{cool}$ | $Q_{misc}$ | $H_e$ | $Q_{exh}$ |
|---|---|---|---|---|---|
| | (Percentage of fuel heating value) | | | | |
| SI engine | 25 - 28 | 17 – 26 | 3 - 10 | 2 - 5 | 34 - 45 |
| Diesel | 34 - 38 | 16 – 35 | 2 - 6 | 1 - 2 | 22 - 35 |

The energy balance will give a rough guide to the required engine cooling however insufficient cooling can lead to engine failure, possibly caused by thermal loading [11]. Similar work was performed by Lakshminarayanan, in which an energy balance to the oil was investigated [12]. Thermal strain is directly proportional to the temperature gradient through a component, a single occurrence of a high temperature gradient will typically not cause an issue, however if this condition is repeated thermal fatigue will occur. Areas most likely to suffer from this surround the combustion chamber where high temperatures and high temperature gradients are experienced, such locations include the valve bodies; therefore these areas require significant focus when designing a coolant system [13].

Engine thermal management systems (TMSs) offer a reasonably large potential for innovation with most systems having used very similar components over the past 20 years. In addition to maintaining the thermal integrity of the engine structure the engine TMS performs a number of other tasks around the vehicle. These include a significant influence on the oil temperature, the EGR gas temperature and features for passenger comfort and safety, mainly the demist capability and interior thermal comfort. A cooling system does however come with some disadvantages, such as the volume of coolant requires heating to an optimum temperature, in the same way the engine does, which leads to a slow engine warm-up, and therefore an increased short journey fuel consumption. Slow engine warm-up also affects the life of components within the engine as the oil will remain outside its working temperature for longer.

[1] Bars indicate the energy remaining once the quantity for each variable shown has been removed from the total energy input.

The heat transfer within an internal combustion engine occurs both directly from the working fluid as well as from friction, the study of these heat interactions is very important for a number of reasons, such as to improve the engine efficiency, the design of the cooling system, and possibly the most important of all for the understanding of the operating temperatures of different regions of the engine. The process of heat transfer from the combustion gas to the metal of the internal combustion engine is a highly complex one. There are three modes of heat transfer, radiation, conduction and convection.

- The smallest contribution is made by radiation, which is defined as the heat transfer through space and it is known to be more significant in compression ignition engines than spark ignition engines. In compression ignition engines the gas radiation was found to be negligible compared with soot radiation which can account for more than one-fifth of the in-cylinder heat transfer owing to the formation of highly radiative soot particles during combustion. The magnitude of the radiative heat flux to the cylinder head was found to vary significantly from the cylinder axis to the bore edge due to the greater exposure to the burned zone [14].

- The second method is conduction, which is defined as the process of heat transfer by molecular motion through solids and fluids at rest, such as from the piston rings to the cylinder wall. Through the cylinder wall the heat transfer is entirely by conduction [2].

- Finally convection, which is the heat transfer through fluids in motion and between a fluid and a solid surface in relative motion. There are two forms of convection, natural and forced. Natural convection is when the fluid motion is caused by differences in the density whereas forced convection is when the fluid motion is caused by an external force other than gravity. Heat from the combustion gases is transferred to the metallic components mainly by forced convection; this is necessitated by the piston motion as well as the combustion itself [15]. Combustion gases also transfer heat to the oil layer inside the surface of the cylinder liner, either directly or via the piston rings [12]. Free convection is insignificant in the internal combustion engine. Some of the heat absorbed by the piston is transferred to the combustion chamber wall by conduction via the piston rings and skirts. Forced

convection is also responsible for the transfer of heat from the metal surface to the coolant [2].

Heat transfer from the combustion chamber is very important as it affects the engine performance, the engine size and the required cooling capacity. The rate of heat transfer will have a large effect on the conditions within the cylinder pre and post a combustion event and therefore is of critical importance to the combustion chemistry and as the in-cylinder temperature and pressure is vital in controlling emission formation, there is a knock on effect. An exact value of fuel energy passing to the engine coolant cannot be given, however a range of 17-35% has been proposed, as shown in Figure 2.4 meaning that a sufficient cooling system is essential [4]. The range given here is very wide due to a large number of factors which affect the amount of heat transferred to the coolant such as the engine configuration, material and operating condition.

As previously mentioned the removal of heat into a liquid coolant can be by forced convection, additionally nucleate sub-cooled boiling (where the bubbles detach when small and collapse into the bulk fluid that is below its saturation temperature) and saturated boiling (where large bubbles form and no condensation in the bulk fluid) also occur. Nucleate sub-cooled boiling is the process of bubbles forming in micro cavities adjacent to the wall and occurs when the boundary layer of the coolant side of the combustion chamber wall is allowed to operate at its boiling temperature, therefore small bubbles of vapour form at the convective surface of the fluid and subsequently detach into the bulk fluid. If the bulk fluid is below its saturation temperature the vapour bubbles quickly condense back into the fluid. This process makes the removal of heat from the surface more efficient and therefore the pumping work can be reduced as the overall flow requirement is lower. However it is important that the vapour condenses back into the bulk fluid and saturated boiling does not occur as this will lead to high coolant system pressures.

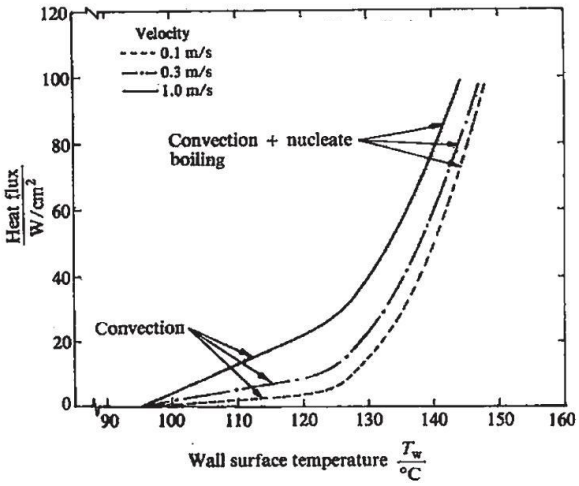


**Figure 2.6 – The effect of engine coolant velocity on heat flux due to nucleate boiling [16, 17]**

Figure 2.6 shows the heat flux as a function of the wall surface temperature, the change in gradient indicates the transition point from forced convection to nucleate boiling. The fluid velocity has a small effect on the surface temperature at which this transition occurs; for a 50-50 mix of glycol and water this transition temperature can be given to be 128°C as this is the stated boiling temperature for this particular fluid. Saturated boiling is when the bulk fluid temperature is equal to its saturation temperature and large pockets of vapour form on the wall surface. Some then detach from the surface and do not condense back into the bulk fluid, rising to a free surface, if available, and escape from the liquid. This results in a departure from nucleate boiling and if the heat flux was to increase further bubbles would form more readily and rapidly, making it difficult for the liquid to rewet the surface forming a vapour blanket on the surface and dramatically reducing the rate of heat transfer. This is known as film boiling and once it has occurred it is extremely difficult for liquid coolant to penetrate the vapour layer and cool the surface back down. A jet of coolant directly impinging on the wall will prevent film boiling from occurring and will greatly improve the rate of heat transfer. Film boiling conditions would lead to very high component and surface temperatures, although the temperature distribution may be improved and the associated thermal stresses reduced [18-20]. This indicates that nucleate boiling and saturated boiling can provide some heat transfer benefits, with comparable levels to purely convective mechanisms at much lower flow rates. However prolonged high temperatures from saturated boiling could result in catastrophic failure, it is due to this that the majority of engines are designed for forced convection cooling with nucleate boiling acting as a safety margin.

A large amount of experimental work has been performed in this area, with investigations having been conducted into the effect of coolant velocity, wall surface temperature and pressure on the rate of heat transfer and the possible reductions in fuel consumption which can be obtained due to faster warm-up and reduced parasitic pumping losses. An example of this experimental work developed an extended convective heat transfer model correlation for predicting flow boiling heat transfer which took into account the difference between Chen [21] and Dittus-Boelter. The Dittus-Boelter equation for fully developed turbulent flow (i.e. a Reynolds number greater than 2100) is:

$$Nu = 0.023 Re^{0.8} Pr^{0.4} \frac{k}{D} \quad (9)$$

The exponent of the Prandtl number, 0.4, is used where the fluid cools the wall; this would be different if the wall was cooling the fluid. The new model takes into account undeveloped flow, surface roughness and temperature sensitivity and is given in Equation (10) [22-24].

Nusselt Number = (Dittus-Boelter Correlation) x (entrance factor) x (unheated starting length factor) x (roughness factor) x (viscosity loading factor)

$$Nu = 0.023 Re^{0.8} Pr^{0.4} \frac{\left[1 + 23.99 Re^{-0.23} \left(\frac{x}{D_h}\right)^{n}\right]}{\left[1 - \left(\frac{x_0}{x}\right)^{9/10}\right]^{1/9}} \left[0.091 \left(\frac{\varepsilon}{D_h}\right)^{-0.125} Re^{0.363\left(\frac{\varepsilon}{D_h}\right)^{0.1}}\right] \left(\frac{\mu_{bulk}}{\mu_{wall}}\right)^{0.14} \quad (10)$$

n - 2.08 x $10^{-6}$

Re – 0.815

x – Distance downstream from duct entrance

$x_0$ – Distance downstream from the duct entrance to the start of the heated surface

All properties are evaluated at the liquid film temperature except for $\mu_{bulk}$ and $\mu_{wall}$ which are evaluated at the bulk and wall temperatures respectively.

$$T_{film} = \left(\frac{T_{bulk} + T_{wall}}{2}\right) \quad (11)$$

The modified model was found to give a good representation of the experimental data for different values of fluid velocity, inlet temperature, pressure and surface roughness. The experimental engine block to be used in this study is sand cast from iron therefore the metal-to-coolant interface is a rough surface which would aid heat transfer as there is an increased surface area. A review of established empirical correlations for the estimation of heat transfer in engine cooling systems has shown that the majority do not account for the physical mechanisms involved in the heat transfer process and are based on curve fitting to experimental datasets. This is suitable for internal combustion engines where the overall heat transfer rate is sufficient but would not provide enough information for systems where the transition from liquid to vapour phases can have further implications [25].

It is important to consider that engine coolant is typically a 50/50 mixture of a form of glycol and water, as pure water contributes to corrosion in the radiator, engine and the vehicle's heater. Investigations into the use of entirely non-aqueous fluids have been performed where they were found to have significantly lower heat transfer coefficients due to the lower thermal conductivity, higher viscosity and higher boiling points [26]. The glycol provides the antifreeze element to the mixture and increases the boiling temperature of the fluid as well as aiding in the prevention of corrosion. The most common form of glycol in antifreeze is ethylene glycol; however other forms, such as propylene glycol, are being increasingly used as they have been found to be less toxic. Interestingly, pure water actually transfers heat better than a chemical coolant therefore by increasing the glycol content the heat transfer effectiveness of the fluid will be reduced, causing an increase in the metal temperature. It has been found that propylene and ethylene glycol based coolants are comparable for typical driving conditions but propylene glycol solutions show improved performance in nucleate boiling heat transfer [27]. A study looking at a copper, aluminium and cast iron section found that the onset of nucleate boiling flow became unsteady in all three sections; however it was much more violent in the copper section. In addition saturated boiling occurred earlier in the copper section at low fluid velocity and there was evidence that it would occur at lower rates of heat flux at higher fluid velocities than with the other wall materials [28]. Studies of this type will influence the design of coolant systems and the materials used to construct engine components.

## 2.2 Current trends in thermal management systems

Increases in engine performance has put increased demands on the engine cooling system; over a twenty year period the overall rate of heat transfer in internal combustion engines has increased by 50-100% [29, 30]. On-going research in the area of TMSs often attempts to isolate singular components and focus improvements in efficiency on them alone rather than looking at the global system. Some previous studies have investigated the effects of heating parts of the powertrain or decoupling the coolant flow rate from the engine speed to improve the system efficiency [31]. Decoupling the coolant flow rate is usually achieved by replacing the mechanically driven pump and thermostat with an electric pump and control valve. The reason behind this is due to a conventional engine cooling system being designed to manage the engine's temperature at extreme conditions (inclined, high load), and therefore operates excessively during most driving conditions. For example, under motorway driving conditions this results in excessive pumping work and overcooling of the engine. Electric pump systems allow independent control over the coolant flow around the engine and aim to reduce fuel consumption due to reducing the pumping work when high flow is not necessary [32]. These systems work by controlling to an important metal temperature rather than controlling to the top-hose temperature as with a traditional thermostat. By controlling to a metal temperature the engine cooling can be allowed to run hotter during low load conditions when it is preferable to have higher coolant temperatures, hence higher oil temperatures and reduced frictional losses. However it is still important to monitor the coolant temperature to prevent boiling and catastrophic failure. This approach has however been found to incur a high cost penalty due to the increased complexity of the pump and the additional control system for the flow valve [33-35]. The inherent cost of these systems will reduce as they become more widespread, especially when the electric pump technology will serve more than just the engine thermal management, such as in electric vehicles (EVs) and hybrid electric vehicles (HEVs) where mechanical drive will not be available [36]. Brace et al. found by throttling the main coolant flows during a cold start that the fully warmed up engine temperatures could be effected, however this showed no improvement to the rate of engine warm-up [37]. Whereas by stopping coolant flow completely a faster warm-up could be achieved [38]. A pressure regulated thermostat could be used to replace the standard thermostat, this is still based on the wax element, however it senses both the top hose and

bottom hose temperatures, therefore if there is a large cooling potential available from the radiator but a relatively small amount of heat being produced by the engine, such as driving down a gradient, the system will not experience overcooling as the thermostat will tend to remain closed [37].

Exhaust heat recovery is another method which has been explored for improving engine warm-up; one example utilized a coolant-to-exhaust gas heat exchanger prior to the oil-to-coolant heat exchanger. This system yielded a 8-10% fuel consumption benefit when comparing cold-start tests with a hot start test with an impact on specific fuel consumption of 14% during the first 6 minutes from a cold start [39]. However systems which are implemented using waste heat from the exhaust flow are likely to have significant effects on the after-treatment devices. In general the most beneficial methods for improving fuel consumption using the engine TMS have been to heat the oil up more rapidly to reduce frictional losses.

The system shown in Figure 2.2 (Page 32) is the production coolant circuit for the engine used in this study. It consists of a coolant pump, mechanically driven from the engine crankshaft via the ancillary belt on the front of the engine, a thermostat which reacts to the top-hose temperature preventing the flow of coolant through the radiator until a set coolant temperature is achieved, typically 85°C. This is a simple method to reduce the engine warm-up time. Once the thermostat is fully open the coolant flow to different regions of the engine is controlled by the diameter of the coolant passages. Oil is mainly used for lubrication; however it is also used to cool a number of components within the engine, such as the underside of the piston. The flow to the underside of each piston is controlled by a piston cooling jet. An internal gallery within the piston directs oil around the circumference which results in the centre of the piston maintaining a higher temperature than the perimeter. Numerical models have been developed to predict the heat transfer through the piston to the oil. The rate of heat transfer was found to be a function of the oil type, jet diameter and the jet velocity [40]. To cope with the additional heat transferred to the oil, direct injection engines typically have an oil-to-coolant heat exchanger, shown in Figure 2.2, therefore heat flow to coolant usually includes the heat removed from components by the oil. The coolant flow through the oil-to-coolant heat exchanger is controlled by a thermostat on the coolant outlet. During engine warm-up the thermostat prevents flow of coolant through the heat exchanger as it would be detrimental to the oil warm-up and take heat from the oil to the

coolant, thus increasing the oil warm-up time and losses to friction. However it is required to cool the oil during hot running conditions. Developments within the function of TMSs concentrate on engine warm-up as this is where the largest benefits to fuel consumption can be obtained.

The internal structure of an engine block consists of a complex series of passageways for both coolant and oil. The coolant jacket surrounds each of the combustion chambers and channels coolant up into the cylinder head. The coolant jacket is shaped to promote cooling in certain areas and the condition of the metal/coolant interface can have a significant effect on the heat transfer coefficient. However the cooling system can inadvertently overcool some areas of the engine but the following advanced methods have been proposed to overcome this problem and others:

- Precision cooling
- Dual circuit cooling
- Controlled component temperature cooling
- Evaporative cooling

All these methods aim for a more uniform engine temperature, with less sensitivity to the engines operating point, some of which will be discussed later. Precision cooling is implemented primarily for prevention of component failure and is a technique which focuses cooling inside the block and cylinder head more intensively on critical areas by adjusting piping and introducing jets into the flow [41, 42]. It involves adjusting the coolant velocities within the coolant jacket to match the local heat fluxes to avoid excessive or insufficient cooling. By increasing the coolant velocity through modifications to the passageways the convective heat transfer improves, therefore more heat is extracted, but without increasing the overall coolant flow rate requirements and in some cases allowing the pump work to be reduced. It was found that this technique resulted in a coolant flow reduction of 65% but an increase in the pressure drop across the engine of 30%, which produced a 54% reduction in the pump power consumption [43]. The nature of precision cooling means that the coolant volume is reduced which aids the rate of warm-up. Some early work was conducted using one-dimensional analysis and pipe network theory; this has now been incorporated into computational fluid dynamics models to optimize coolant jackets but these are still approximations.

Dual circuit cooling or split cooling concepts are also designed to reduce the coolant pump power consumption by distributing the coolant more effectively to the cylinder head and cylinder block. Another advantage to this system is that the cylinder head can be run cooler than the cylinder block without an additional thermostat or coolant pump through control of coolant flow rates [44]. This is an interesting concept when it is considered that Donn et.al found that the ratio of coolant heat input between the cylinder head and the engine block was nearly constant at 2:1 for the complete operating map of a state-of-the-art automotive diesel engine [6]. This investigation was performed in a climatic chamber where the energy balance at steady state operation could be analysed and the impact of operating parameters such as EGR rate and injection strategy quantified.

As previously mentioned, one of the aims of improving the engine cooling system is to improve the vehicles cold start fuel economy; this can be by improving the engine efficiency. Methods achieve this include reducing parasitic loads on the engine, such as the electric coolant pump over a mechanical pump or another option is a variable flow oil pump. Currently the majority of production engines utilise a fixed displacement oil pump mechanically driven from the crankshaft, therefore the higher the engine speed the higher the oil pressure within the engine. This component will be specified to maintain above satisfactory oil pressure in all running conditions, however for the most part this exceeds the engine's requirements. A variable flow oil pump is still driven mechanically but the pump displacement can be varied. Over a cold drive cycle a reduction in fuel consumption of 3.4% and 2.6% was found, for an internal rotor design or a vane type design respectively. As expected the largest reduction in fuel consumption was during the early stages of the drive cycle when the oil was coldest and most viscous [45].

Significant fuel consumption savings can be achieved with greater knowledge of the heat flow through an engine as further optimisation of ancillary devices could be made. Therefore the heat flow would be better managed and directed to regions where the greatest benefits could be extracted. The main source of heat in an engine is combustion and further investigation into the measurement and prediction of its distribution as it is dissipated from the combustion chamber would aid this development process.

## 2.3 Chapter summary and conclusions

A review of current engine technologies, trends in thermal management strategies and an explanation of fundamental modes of heat transfer and how they are affected by some key aspects of engine coolant system design has been outlined in this chapter. A number of key technologies, such as turbochargers, have enabled a step increase in engine peak performance, which leads to higher in-cylinder temperatures. It is this increase in heat generation which has pushed the development of more complex thermal management systems. The key outcomes from this chapter have been highlighted below:

- A simple heat balance can be performed on an engine by applying the first law steady heat flow energy conservation equation. It has been shown that 16 – 35% of fuel energy is transferred to the coolant, whilst 22 – 35% is transferred to the exhaust gas.

- There are three fundamental modes of heat transfer, conduction, radiation and convection. Within a diesel engine combustion chamber soot radiation was found to contribute to more than one fifth of in-cylinder heat transfer.

- The rate of heat transfer from the combustion chamber is very important as it affects the overall engine performance as well as the requirements of the engine cooling system, in order to maintain optimal operating temperatures of key components.

- Current trends in thermal management systems are tending towards more complex strategies which involve decoupling the engine coolant flow rate from the engine operating condition, with the use of an electric coolant pump for example. Other technologies include a pressure regulated thermostat and variable flow oil pump.

- The majority of work has been performed with the aim to improve fuel consumption by reducing the engine warm-up time and by utilising waste heat in a productive way, such as with a coolant-to-exhaust gas heat exchanger.

- The addition of these and other engine technologies has led to established methods for estimating heat transfer rates to become outdated.

# Chapter 3. Combustion chamber temperature measurement and heat transfer correlations

This chapter aims to review the techniques and methodologies that have been employed to measure the operating temperatures of a combustion chamber cylinder wall. Detail is given of the different approaches to calculating the rate of heat transfer through the combustion chamber wall and how the measurement type can affect the accuracy of results.

Also discussed in this chapter are the factors which affect the rate of heat transfer through the cylinder wall and how their influence can affect the complexity of prediction techniques. This leads on to details of the empirical convective heat transfer correlations which have been developed from numerous experimental investigations.

Finally in this chapter the measurement of fast in-cylinder pressure data is discussed and how it is used in the engine development process.

## *3.1 Fundamentals of temperature measurement with the focus of combustion chamber walls*

It has been recognised that the heat transfer through the combustion chamber walls of an internal combustion engine is an extremely important factor to consider when designing an engine and the operation of ancillaries. Research in this field looks at all routes of heat transfer from both an experimental and modelling point-of-view. Heat from the combustion chamber is lost in all directions and through a variety of paths, such as via the piston rings to the combustion chamber walls, directly to or via the main gasket to the cylinder head and to the oil. However there have been significant findings which suggest that the majority of heat

is transferred radially through the cylinder wall, with only a relatively small amount transferred in the axial direction [46]. Heat transfer from the combustion chamber is a highly complex process and has been shown to vary periodically with the thermodynamic cycle and in different regions of the cylinder. Suzuki et.al found that there was significant variation radially from the cylinder axis; points located radially inwards were influenced more by the combustion flame as it was presumed this occupied the region around the central piston axis [47]. These findings supported that of Yoshida et.al, who found the variations to be dependent on the gas temperature, the wall surface temperature and the gas flow, with measurements indicating that the heat loss from the piston crown was 7% and 5% from the exhaust port at full load [48]. Other factors to affect the heat flux from the combustion gases include compression ratio, injection timing, injection demand, engine speed and in-cylinder temperature and pressure [49].

Fundamentally all thermocouple measurement techniques are based on the Seebeck effect. In 1821, Thomas J. Seebeck discovered that it was possible to create an electrical voltage by soldering two different metals together, this creation of a voltage is known as the Seebeck effect [50, 51]. The dissimilar metals create an electro-motive force (EMF) which can be detected at the other end of the metals by a voltmeter and was found to be proportional to the thermal gradient between the hot and cold junctions. The simplest form of temperature measurement is a pair wire thermocouple. The primary consideration when selecting or designing instrumentation to measure temperature is the accuracy at measuring the 'true' temperature, the 'true' temperature being that which would exist if the thermocouple was not installed. In order to achieve measurements of the highest accuracy a large number of I.C. engine thermal studies have utilised custom manufactured instrumentation to suit their particular purpose. This ranges from the simple pair wire thermocouples to the more complicated fast response thermocouples and thermopiles. Fast response thermocouples are based on the Seebeck effect but can employ it by different means, commonly described as coaxial and thin-film. The coaxial type is more typically used for measurement on metal surfaces, whilst the thin-film type has been developed specifically with the intention to minimise the disturbance to the measurement field.

The first recorded attempt to use a pair wire thermocouple to measure instantaneous surface temperature in a combustion chamber was in 1939 by Eichelberg [52-56]. Eichelberg employed two 0.3mm diameter wires of copper and Constantan or nickel and chrome,

depending on the expected metal temperature to be measured. These wires were electrically insulated using a ceramic insulation with high dielectric strength from the outer wall using quartz tubes and contacted the wall at a depth of exactly 0.25mm from the inner surface of a combustion chamber. The contact was direct to the cylinder wall or via a conical pin (made of the cylinder wall material). This measurement method allowed for accurate position referencing and fast response time, however the thin wires were very fragile, suiting the large two-stroke engines rotating at target speeds up to 300rpm which Eichelberg used for the published research. The coaxial probe was found to illustrate good dynamic response within a firing engine, however in order to achieve the fast response times required when investigating the temperature variations across a single combustion event, i.e. 5-$10\mu s$, it was required that the sensor was mounted flush with the combustion chamber surface [57-60].

Thin-film thermocouples (TFTs), also known as eroding thermocouples employ the coaxial or pair wire principle but utilise a conductive film on the measurement surface to provide an electrical connection between an insulated fine wire penetrating the core of a second wire [48, 61]. The two wires are typically insulated from each other using an oxide layer or glass wool. The thermocouple junction on the surface can be formed by gently sanding the end surface or by applying a material layer on the surface, therefore the TC junction can be in the region of 1-$2\mu m \text{ in thickness}$ [62-64]. The earliest work found which employed this technique was that of Bendersky [65]. An example of a TFT is shown in Figure 3.1. This thermocouple was used to characterise the thermal sensitivity of the wall surface temperature of the piston and cylinder head of a gasoline HCCI engine to changes in the coolant temperature [57]. It was found that the coolant flow direction within the head caused a temperature difference and the local surface temperatures decreased linearly with decreasing coolant temperature, but the spatial difference between measurement locations was consistent. These findings implied that if the engine warm-up time was reduced that engine components would reflect the increase in temperature. It was also found that by reducing the local coolant temperature the rate of heat transfer also reduced, now this might sound counterintuitive; however it was concluded that this was due to the effect on combustion phasing. The lower coolant temperatures caused a slower burn rate and reduced combustion efficiency, in the author's opinion this highlighted that combustion was the main driver of the heat transfer process rather than the coolant side temperature. This phenomenon may only be true in a HCCI engine where the start of combustion is directly dependant on the spontaneous combustion of the homogenous charge, which would be impacted by the

combustion chamber temperature, whereas in a normal CI or SI engine the start of combustion is a result of the fuel injection or spark timing respectively.

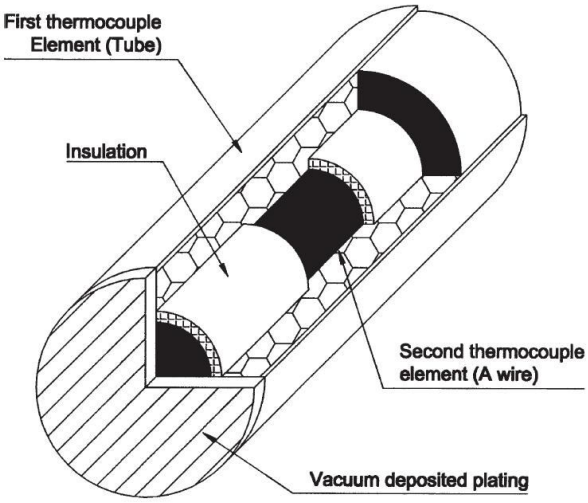


**Figure 3.1 – Internal construction of a coaxial thermocouple [58, 60]**

Measurement techniques of this type have been found, under certain conditions outside of engine research, to detect a temperature rise of 200°C in less than 10ns when a laser pulse was focused on the junction due to the thin nature of the measuring junction [66, 67]. However this type of sensor has also shown to produce measurement errors due to the dynamic behaviour within the probe itself, i.e. the heat sink surrounding the centre wire is unable to cool it fast enough to control the transient response. This error can be minimised by constructing the sensor of a material with accurately known thermal properties as well as a good thermal insulating layer, such as an oxide layer. It was found that an air gap surrounding this outer metal would help provide a one-dimensional heat conduction condition [68]. Marr et al. showed that a copper layer applied to the surface increased the ability for the heat to be conducted from the constantan wire to the aluminium substrate, equalising the temperature and improving the accuracy of the 'true' temperature measurement [69]. The installation is shown in Figure 3.2.

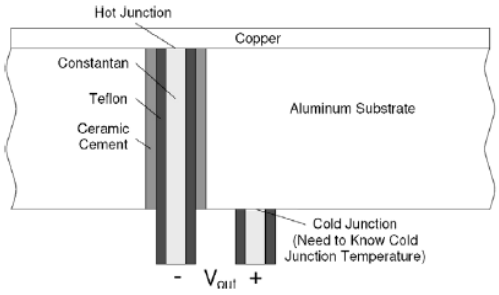


**Figure 3.2 – Thermocouple schematic used by Marr et.al to measure surface temperatures in a single cylinder engine [69]**

Another source of error for sensors which penetrate the combustion chamber wall is that they have a tendency to over predict the peak heat flux due to the potential presence of combustion deposits on the surface of the probe [70]. Investigations were performed by Yamada et.al to quantify these effects by artificial depositing soot on a TFT sensor located in the piston crown. They found that the presence of deposits reduced the amplitude of the measured heat flux and the phase of the maximum value was delayed [71]. Sensors of this type have been installed in a variety of locations around single cylinder engines, such as the piston crown surface, cylinder head surface, pre-combustion chamber surface and exhaust port surface to measure the variation in heat flux [48].

These installations provide a fast response single point surface temperature measurement, and are typically coupled with an additional single point thermocouple positioned a set distance back from the measurement surface in order to estimate the heat flux through the area of material. Heat flux is defined as the energy transit due to a temperature difference per unit cross-sectional area normal to the direction of the flux. There is no device that can directly measure this flow of energy therefore it must be monitored and inferred [72]. There are multiple measurement techniques for determining heat flux; they can be separated into the following groups:

- Differential temperature
- Calorimetric method
- Energy supply or removal
- Mass transfer analogy

To measure heat flux by the differential temperature method a minimum of two temperature measurements are required along the same plane. The separation between the measuring points must be known to calculate a thermal gradient between the points. If additional measurement points are available along the plane a more accurate thermal gradient can be calculated. The heat flux is the thermal gradient multiplied by the thermal conductivity of the material and is a measure of the flow of energy per unit of area per unit of time. This measurement technique is based on Fourier's one dimensional law of conduction given in Equation (12).

$$q = -k\frac{\delta T}{\delta x} = -k\frac{(T_1 - T_2)}{(x_1 - x_2)} \tag{12}$$

This calculation is based on the assumption that the heat transfer is one dimensional between the measurement points with two and three dimensional effects reducing the accuracy of the measurement [73]. As with all measurement techniques, the aim is to obtain the required data whilst minimising the disruption to the measured material. Matching the sensor material to the surface material can reduce the thermal disruption, however if this is not possible it could be compensated for through a calibration process.

One method of obtaining differential temperatures is a traversing thermocouple employed by Alcock et al. [3] to measure the heat flow through the cylinder liner of three different engines. This system allowed for a series of measurements to be obtained at set distances from the combustion chamber surface so a temperature gradient could be determined. The thermocouple consisted of a hypodermic tube containing manganin-constantan coupled wires which were clamped to a simple micrometer at the outer end allowing for 1mm movement of the measurement point for a single rotation of the wheel. The installation shown in Figure 3.3 was designed for use in single cylinder engines and would not lend itself well to a multi-cylinder engine due to inner surface washers and seals.

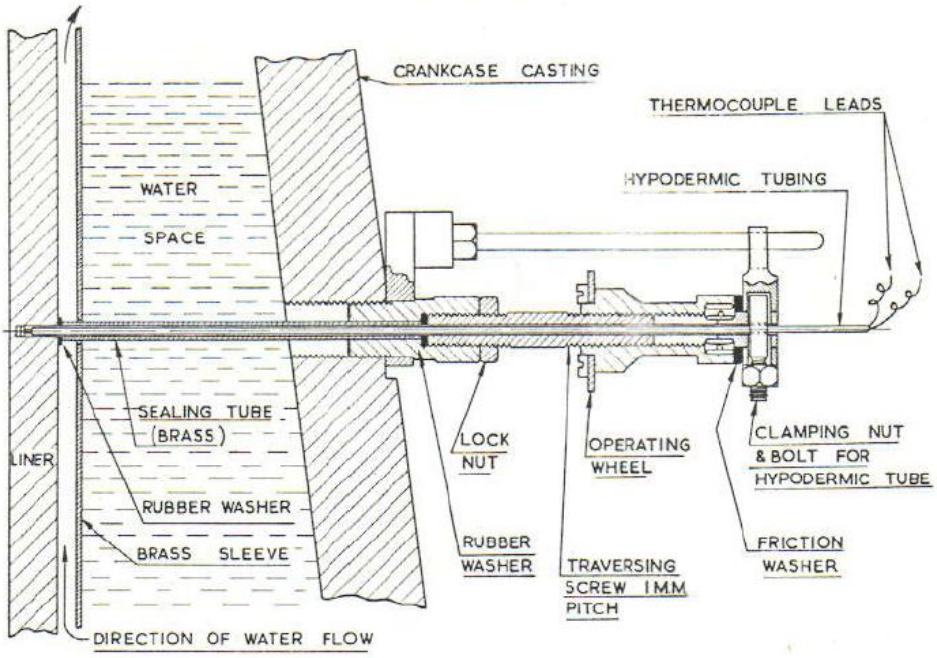


**Figure 3.3 – Traversing thermocouple in position, used by Alcock et al. [3]**

Another method to obtain steady state heat flux measurements is a second thermocouple positioned a set distance below the surface [74-77]. This method employs a fast response thin-film thermocouple developed to measure the surface temperature and a surface temperature set back from the combustion chamber. An example designed to measure the impact of changes to different engine parameters on the local instantaneous heat flux is shown in Figure 3.4. It was constructed using Constantan and Mica as the insulation material, and was installed in the cylinder head of a single cylinder engine. This setup produced very good results and showed that the local heat flux and in-cylinder pressure were highly sensitive to combustion variations, brought about by altering the intake air temperature, the injection pressure and the EGR rate for controlling the oxygen concentration at the intake [78]. It is interesting to note that the combustion chamber of this single cylinder engine is located in a separate section above the piston and is not exposed to the piston motion. Therefore the results obtained from this investigation may differ from a traditional combustion chamber as the gas motion and subsequently the temperature distribution will be considerably different.

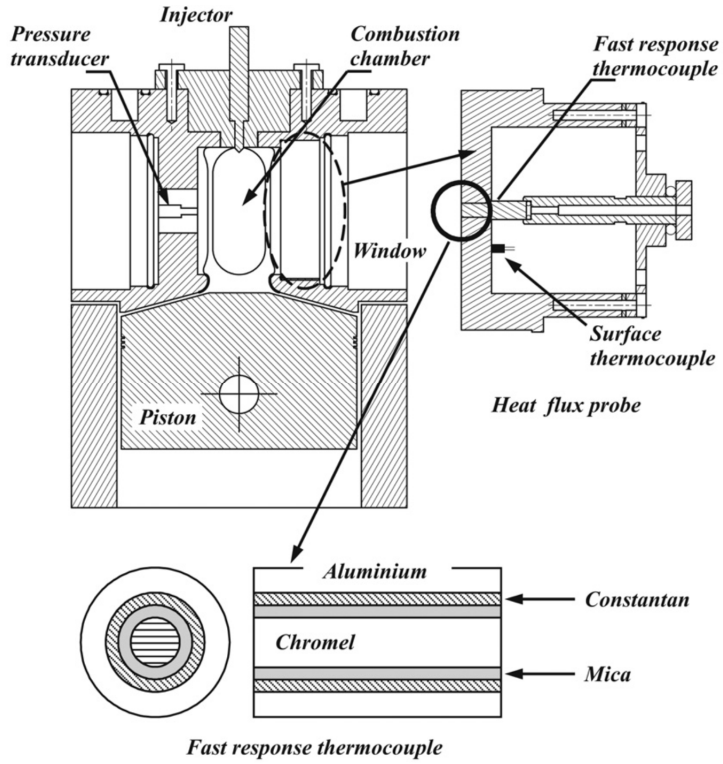


**Figure 3.4 – Cross-sectional view of an instrumented cylinder head and fast response thermocouple**

A large amount of previous work since 1953 has prioritised focus on the heat transfer through the combustion chamber walls of single cylinder experimental rigs over very short periods of time, i.e. a single combustion event [58, 73, 79, 80]. To this end, the majority of the needle type sensors, i.e. a sensor of tubular construction which penetrates from the outside into the required structure, were found to require a depth over that available in the production combustion chamber wall or had a very large outer diameter of 8.74mm [81]. As shown in Figure 3.4 these sensors are suitable for research engines where space can be made available for mounting, however the installation area on a production engine is much more restricted due to ancillary devices and additional cylinders.

The technique for this study would be required to monitor the heat transfer through the cylinder wall of a production engine over much longer periods, to establish time-averaged heat transfer rates rather than instantaneous or crank angle based values. A further option which has been developed for measuring heat fluxes and surface temperatures are multipoint temperature probes [82]. An example sensor utilises several thermocouples which are held in contact with the measured surface using conductive split rings. This sensor has a very complex internal structure and requires a large sealing surface. A simplified version of this probe would be a multipoint thermocouple sensor. This would be a single outer sheath

containing a number of single point thermocouples at different depths, it would not utilise the split ring design and therefore would rely on good thermal contact with the outer sheath and good conducting material surrounding the thermocouple junctions. A sensor of this type would simplify the instrumentation of the engine over separate single point thermocouples and would also allow the sensors to be tested before installation [83]. There was some uncertainty over whether a multipoint thermocouple without the conductive split ring design or exposed thermocouple junctions would be able to respond to small changes in temperature accurately, it was therefore important that a range of different multipoint sensor designs be evaluated for both steady state performance and dynamic response. The materials with which the multipoint sensor body would be constructed had to be considered as this had been found to produce a measurement error in other studies [84].

## *3.2 The challenges of combustion chamber heat transfer prediction*

The overall energy balance was previously discussed and an equation for the engine as a control volume given. In this section the established convective heat transfer correlations will be discussed. In order to understand how these correlations were formulated an understanding of the factors which affect the heat dissipation through the engine is required. These factors can be expressed simply as:

$$Q_{Fuel} = Q_{Gas} + Q_{Coolant} + Q_{Oil} + Q_{Rad} + P \quad (13)$$

$Q_{Coolant}$ – Energy to the coolant radiator

$Q_{Oil}$ – Energy to the oil radiator

$Q_{Rad}$ – Energy escaping directly from the engine (can be called radiation)

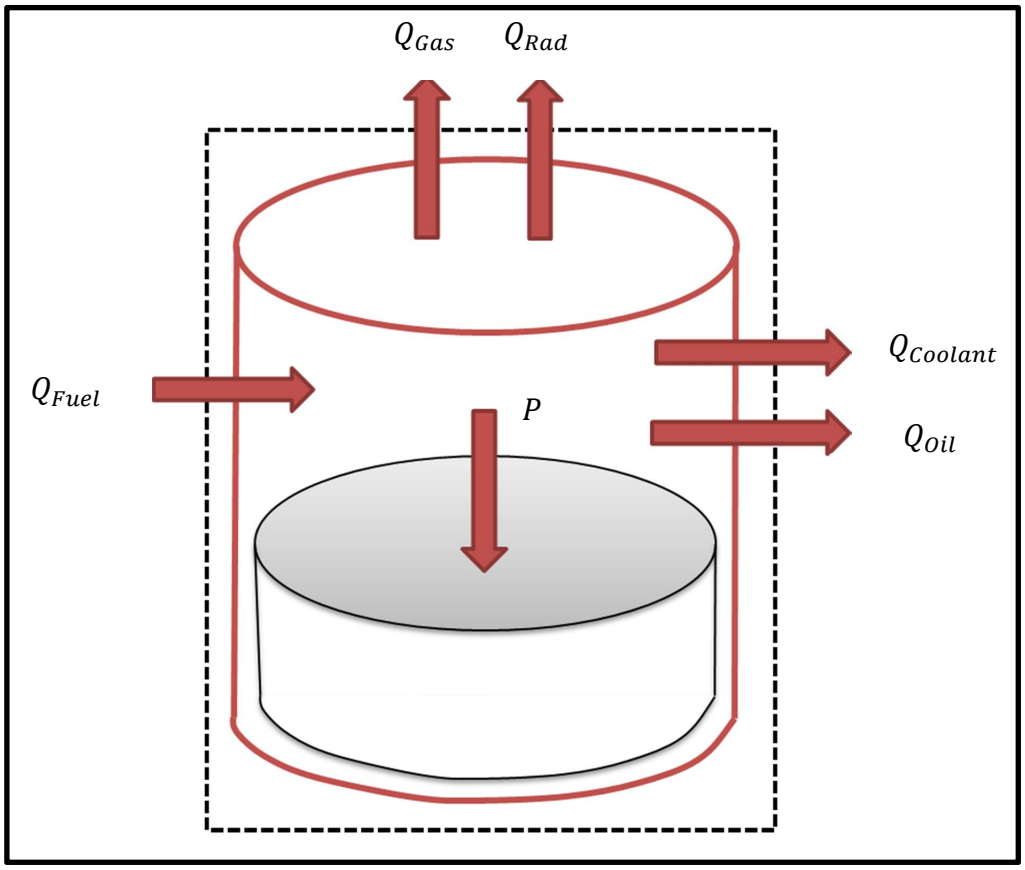


**Figure 3.5 – Control volume for cylinder energy balance**

Each of these components can be easily affected by a large numbers of engine operating parameters, such as:

- Piston speed
- Inlet temperature and pressure
- Coolant temperature
- Coolant composition
- Engine deposits

Investigations into the thermal conditions in an engine are designed to improve the methods for accurately predicting them on subsequent innovative technologies. The potential benefits from better predictive capabilities include: enhanced cooling systems, reduced thermal loading and fatigue, and advances in engine modelling and simulation. Models are based on the fundamental heat transfer in basic systems with certain assumptions having been made. Therefore if an engine design is based on these mathematical models the design will only be as good as the assumptions made in the model. Figure 3.6 shows the input factors used in the convective heat transfer correlations to be discussed as well as additional variables used

to either calculate the heat transfer through the cylinder wall or which impact the heat transfer rate.

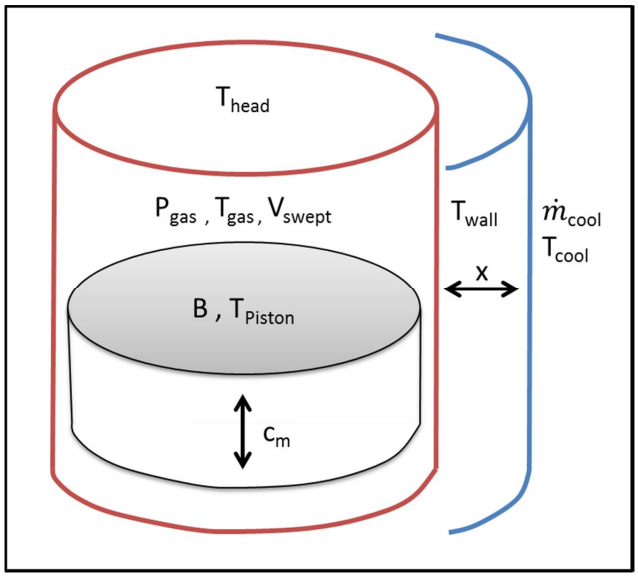


**Figure 3.6 – Factors affecting the rate of heat transfer from combustion gas to surrounding environment**

The combustion chamber can be described as three distinct surfaces, the cylinder liner, the piston crown and the cylinder head [85]. The heat from the combustion gases can be transferred to any of these surfaces and the distribution to each is dependent on a large number of variables. Established empirical correlations currently concentrate on the prediction of the heat transfer from the combustion gases to the cylinder liner, with some additional work having been performed to investigate the heat flow to the cylinder head and piston crown. The complexity of the heat flow within an engine combustion chamber can be attributed to the following reasons:

- The gas flow rate and motion within the cylinder is very unsteady
- The geometry of the flow system is not uniform and it changes periodically as the crankshaft rotates and the combustion chamber volume changes
- The gas temperature varies significantly with position in the system
- The conductivity through the walls varies with location and is affected by wall thickness and any deposits on the surface
- The surface temperatures are not uniform
- There is the additional heat transfer due to friction and heat flow along the length of the cylinder wall [86].

These considerations cause heat transfer models to be of varying complexity and subsequently varying accuracy. Models which have been established using differing assumptions can be grouped depending on the type of heat transfer they predict, there are correlations to predict:

- time-averaged heat flux (used for estimating the total heat given up by the gases for energy balance calculations, typically based on a pair of temperatures measured at a distance sufficiently far from the combustion gases that the values are considered as steady).
- the instantaneous spatially-averaged heat flux (used for predicting power output and efficiency).
- the instantaneous local heat fluxes (used for thermal analysis of engine components as well as engine modelling).

The latter two types are much more difficult to calculate both experimentally and analytically as they require a surface mounted fast-response thermocouple and a second temperature measurement far enough from the surface measurement to be regarded as steady. A large number of heat transfer correlations are based on Equation (14), which is a general expression to allow experimental data to be correlated to three dimensionless groups rather than seven variables. The dimensionless groups are the Nusselt, Reynolds and Prandtl numbers.

$$Nu = aRe^{m}Pr^{n} \tag{14}$$

The Dittus-Boelter equation (Equation (9)) discussed earlier is a particular derivative of Equation (14) used to describe turbulent flow in circular tubes. Significant developments have been made to the different heat transfer correlations since the understanding of the thermal properties within an engine have improved. During this time there have also been leaps forward in the technology used in an internal combustion engine so it is important that the predictive methods are able to develop at a similar rate. Each of the types of correlations will be explored and reviewed in the following sections. All the methods to be discussed assume that the conduction from the cylinder only occurs radially outwards from the central axis of the cylinder bore.

## Correlations for the time-averaged heat flux

Time-averaged correlations require the simplest form of instrumentation and therefore typically lead on to the most basic of correlations. Correlations of this type are used to estimate the overall heat transfer from the combustion chamber in order to size the cooling requirement for the engine. For this type of correlation the complexities in combustion chamber heat transfer can be reduced by employing the following assumptions:

- The heat transfer due to radiation is included in the convection process. By combining these terms, Taylor et.al found that there was not significant error introduced in the estimated total heat transferred to the coolant [4].
- The shape and variations in the gas and coolant flow systems are taken into account by using the correct mean values.
- The variation in temperature is overcome by utilising a steady uniform temperature which would result in the observed heat flow.

To establish an overall heat transfer coefficient for the transfer of heat from the combustion gases to the cylinder liner and subsequently to the cooling medium, an understanding of the correlation between the engine operating condition and temperatures within the engine is essential. In order for this to be applied to future engine designs, data must be obtained from a range of engines of different types and displacements to validate the model [87]. It is commonly regarded that the heat flow between the working fluid and the cooling medium in an engine can be approximated by employing the assumption that the heat flow process is similar to that in a heat-exchanger. When using this method it is assumed that the Prandtl number, *Pr*, varies little in gases and any variations can be accounted for in the coefficient, *a*. Therefore Equation (14) can be reduced to Equation (15) and this leads to Equation (16) by substituting in the Nusselt and Reynolds numbers definitions.

$$Nu = aRe^{m} \tag{15}$$

$$\frac{hL}{k} = a\left(\frac{GL}{\mu g_0}\right)^{m} \tag{16}$$

G - mass flow of gas per unit time divided by the cross-sectional area of the test passage

$g_0$ - the force-mass-acceleration constant

Based on Newton's law of cooling an overall engine heat transfer coefficient is shown in Equation (17).

$$h_{Tot} = \frac{\dot{Q}}{A_s(T_g - T_c)} \tag{17}$$

By assuming that Equation (17) can be expressed in the same form as Equation (16) and the characteristic length is the cylinder bore, *B*, then:

$$\frac{h_{Tot}B}{k_g} = a\left(\frac{GB}{\mu g_0}\right)_g^m = aRe_g^m \tag{18}$$

By using data gathered from 19 commercially available engines of different sizes and configurations, over a wide range of piston speeds, fuel-air ratios and inlet air densities, the coefficients, *a* and *m*, were given as 10.4 and 0.75 respectively, and were found by Taylor to represent the average overall heat transfer to the coolant quite well [88]. The data used for the heat loss from the combustion gases was obtained from measurements of heat to coolant, plus heat to oil, minus heat to friction where available. However not all data was available for all engines, subsequently if only the heat to coolant was given; it was assumed that the heat to oil was equal to the heat of friction. Therefore it must be highlighted that the energy balance used in some instances was incomplete, this would inherently lead to some inaccuracy in the derived coefficients given for this correlation.

$$\frac{h_{Tot}B}{k_g} = 10.4\left(\frac{GB}{\mu g_0}\right)_g^{0.75} \tag{19}$$

Equation (17) combined with Equation (19) gives a correlation for a time-averaged overall heat transfer rate and can be used to predict the convective gas-side heat transfer coefficient providing the fuel-air ratio and the mass flow are known or can be estimated.

$$h_{Tot} = 10.4\frac{k_g}{B}Re_g^{0.75} \tag{20}$$

$$\frac{\dot{Q}}{A_s} = 10.4\frac{k_g}{B}\left(T_g - T_w\right)Re_g^{0.75} \quad (21)$$

The accuracy of this correlation is based entirely on the critical parameters chosen, which are piston speed, the characteristic length and the thermodynamic properties. Utilising a single correlation to estimate the overall heat transfer for a wide range of engine types will compromise the individual accuracy for each engine type. Therefore this method can be used to give an overview of the thermal load predictions which can then be used to influence the overall design of coolant systems but further improvements to the method would be required to highlight small improvements where possible. However this method could be developed to accurately predict the heat transfer for a particular engine if a detailed experimental study was first performed. With the data and knowledge obtained from an experimental study of this nature, future iterations within that particular engine family would substantially benefit.

## Correlations for instantaneous spatially averaged heat flux

A correlation for instantaneous spatially averaged heat flux is important for predicting the engine power and efficiency and is more widely used in engine simulation and modelling. The convective heat transfer coefficient from the gas to the cylinder wall is known to vary with position and time, therefore knowledge of these variations is required to be able to predict the thermal stresses within the engine. When considering engine performance through modelling, emissions are of less concern which leads to the requirement for a spatially averaged heat transfer correlation rather than a time averaged. If considering emissions then accurate local surface temperature measurements would be very important as they have a strong effect on emissions, especially NOx formation. The first known instantaneous spatially averaged correlation produced from recorded engine data was developed by Eichelberg in 1939. The Eichelberg correlation was a development of the work completed by Nusselt in 1923 on a spherical bomb, in which Nusselt introduced a factor ($1+1.24c_m$) to allow for the influence of the piston motion in the engine.

$$h_g = \alpha_s(1 + 1.24c_m)\left(\sqrt[3]{p^2T_g}\right) \quad (22)$$

$$c_m = \frac{2Ln}{60} \quad (23)$$

Eichelberg's method of measuring the temperature within the combustion chamber wall has been discussed in Chapter 3 Section 2.1, and it was used to determine the temperature fluctuation at or near the combustion chamber wall inner surface in order to calculate the temperature of the working gas. The rate of heat transfer curve could be deduced from the measured temperature fluctuations in the wall. The relationship of which can be inferred from the unsteady heat flow equation.

$$\frac{\delta T}{\delta t} = \alpha \frac{\delta^2 T}{\delta x^2} \tag{24}$$

$$\alpha = \frac{k}{\rho C_P} \tag{25}$$

Eichelberg developed his expression, Equation (26) utilising the square root of the absolute value of the temperature and the square root of pressure (rather than the cubed root of temperature and pressure to the power of 2/3 as suggested by Nusselt) based on experimental results. The exponents were modified to account for radiation and convection in a combined term.

$$\frac{Q_s}{A_s} = \alpha_s\left(\sqrt[3]{c_m}\right)\left(\sqrt{pT_g}\right)\left(T_g - T_w\right) \tag{26}$$

Therefore the convective heat transfer coefficient can be given by:

$$h_g = \alpha_s\left(\sqrt[3]{c_m}\right)\left(\sqrt{pT_g}\right) \tag{27}$$

The Eichelberg correlation is relatively similar to that proposed by Nusselt, with the most notable difference being the coefficients of the piston motion term, used to account for the motion of the in-cylinder gas. Recent developments and experimental evaluations of Eichelberg's equation have generally found inaccuracies which have been attributed to there being no separate radiation term. It was also found in 1951, that the time-averaged heat transfer rates calculated using this correlation diverged from experimental results obtained from a large supercharged diesel engine. The introduction of a supercharger would result in elevated temperature and pressures within the cylinder invalidating the correlation. This illustrates that the correlations quickly become outdated and need to be developed alongside the technological developments made in order to keep the predictions accurate.

The next attempt to produce a correlation able to predict an instantaneous heat transfer coefficient was made by Annand in 1963 [89]. From early examination of the problem, it was decided that the Reynolds Number was the main parameter affecting convection and that the power law would better describe the relationship, see Equation (14), rather than the unsteady heat transfer equation. As previously noted, the Eichelberg correlation lumped the radiation term with the convection term, Annand highlighted the inaccuracies this would cause so proposed a radiant heat transfer term shown in Equation (28); where 'c' is the constant for radiant heat transfer, equal to 0 for the compression stage and constant for combustion and expansion stages but different values for different surfaces and engine types.

$$q_{rad} = A_s c\left(T_g^4 - T_w^4\right) \tag{28}$$

This leads to the total rate of heat transfer to be given by:

$$\frac{Q}{A_s} = a\frac{k_g}{B}(Re)^{0.7}\left(T_g - T_w\right) + c\left(T_g^4 - T_w^4\right) \tag{29}$$

a - 0.35 – 0.8, depending on the intensity of charge motion (adjusted to suit flow characteristic of engine)

b - 0.7

c - 0, during intake, compression and exhaust when radiation is negligible

c - $1.6 \times 10^{-12}$, during combustion and expansion for diesel engines

Nearly ten years later, in 1972, Sitkei and Ramanaiah further highlighted in experimental work that there was a significant effect of radiant heat transfer on the overall rate of heat transfer in an internal combustion engine. Extensive testing was performed on a single-cylinder engine designed to allow radiation measurements to be taken using a Foster photoelectric pyrometer. It was found that radiation due to carbon particles in combustion gases can account for 20-30% of the total heat transfer at full load [90]. Therefore Annand was correct not to ignore it, and to include a separate radiation term rather than including it within the convective term. Annand continued his work on his correlation (Equation (29)) in conjunction with Ma [91]. A naturally-aspirated, air-cooled, single-cylinder, four stroke engine was instrumented with surface thermocouples in the cylinder head to investigate

variations across the bore. The variation in measured surface temperature was found to be considerable from sensor to sensor and there was not a simple relationship to engine speed and fuel-air ratio. Analysis of the data obtained from this engine led to the introduction of a term that represented the rate of change in temperature in order to compensate for the non-steady nature of the temperature within the cylinder. It was concluded that some improvement was achieved with the introduction of this term however further experimental investigation was required to establish whether the added complexity was necessary. Including this additional term the overall rate of heat transfer can be given as:

$$\dot{q} = \frac{Q}{A_s} = \frac{k}{B}(Re)^{0.7}\left[a\left(T_g - T_w\right) - \frac{b}{\omega}\frac{\delta T_g}{\delta t}\right] + c\sigma\left(T_g^4 - T_w^4\right) \tag{30}$$

$\omega$ - angular rotation rate of the crankshaft (rad/s)
a - 0.12,
b - 0.20,
c - 1.50, set to zero up until ignition

Reducing the equation of the additional temperature derivative leads to a simpler gas side convective heat transfer coefficient.

$$h_g = a\frac{k}{B}(Re)^{0.7} + c\sigma\frac{\left(T_g^4 - T_w^4\right)}{\left(T_g - T_w\right)} \tag{31}$$

Another highly established correlation is that of Woschni [15]. Woschni replicated experiments performed by Nusselt utilising a spherical bomb and then employed two different methods to determine the heat transfer coefficient. The first investigating the internal energy of the gas (as performed by Nusselt) and the second involving the time curve of the wall surface temperature as a boundary condition for solving a Fourier differential equation. It was found that the outcome of these two methods differed considerably, and it was deduced by Woschni that the evaluation of the internal energy provided a mean heat transfer coefficient in terms of location within the spherical bomb, whereas the evaluation of the surface temperature provided a local heat transfer coefficient value at the point where the surface thermocouple was positioned. By comparison to work performed by Schmidt it was concluded that the evaluation of the internal energy yielded results closer to the heat transfer

caused by free convection rather than forced convection [92]. Therefore Woschni regarded the work completed by Nusselt and Eichelberg as inaccurate for the association with the internal combustion engine, where the majority of heat transfer is controlled by forced convection, caused by either the piston movement or by combustion itself. The wall surface thermocouple method will, however, provide localised values and will vary quite significantly from cycle to cycle due to incidental irregularities such as local disturbances, and position and timing of fuel sprays. Cycle-to-cycle variability has been shown to significantly affect the measured surface heat flux in both magnitude and phasing in a spark-ignition engine. Stone et.al found that in spark-ignition engines the differences in measured surface heat flux was due to the variations in flame propagation through the combustion chamber [93]. Therefore for improved accuracy in the estimate of a heat transfer coefficient it is important to utilise mean values over a large number of consecutive cycles to exclude the cyclic variability especially in spark-ignition engines [94]. The Woschni correlation is based on the power-law for steady state forced convection heat transfer in turbulent flow. Equation (32) follows if density, viscosity and conductivity of the gas are expressed as functions of pressure and temperature, $\alpha_s$ is a scaling factor used for tuning of the coefficient to match a specific engine geometry.

$$h = \alpha_s B^{m-1} p^m w^m T^{0.75-1.62m} \tag{32}$$

By first considering only the unfired engine the local average gas velocity in the cylinder can be assumed to be the same as the mean piston speed. The combustion process was then broken down into its different phases, by first considering the scavenging period and utilising a test engine with a special double-symmetrical camshaft the coefficients of Equation (32) were found to be as follows:

$$h = \alpha_s (B^{-0.2} p^{0.8} (C_1 c_m)^{0.8} T^{-0.53}) \tag{33}$$

Equation (33) estimates the convective heat transfer coefficient from the combustion gases to the cylinder wall during the scavenging period, whereas the total heat transferred to the cylinder walls during this period can subsequently be found when Equation (33) is combined with Equation (34) (an integral of the difference in the mean gas temperature and the mean wall surface temperature, and the total surface area integrated over the crank angle for a complete cycle).

$$Q_w = \int_{cycle} hA_s(T - T_s)\,\delta\emptyset \tag{34}$$

Calculated values from Equation (34) were then compared with measured data during the scavenging phase and a strong correlation was found, when the constant $C_1$ was set to 6.18. By similar methods it was found that during the compression and expansion phase in an unfired engine $C_1$ was 2.28. Fundamentally this correlation has very limited applications until it can estimate the rate of heat transfer for a firing engine. As such, an additional component for the gas velocity due to combustion must be incorporated. The heat transfer coefficient decreases rapidly once combustion is complete so it is logical to apply the change in pressure as the measure of the change in the internal energy of the working gas.

$$w_c = C_2 \frac{V_s T_1}{p_1 V_1}(p - p_0) \tag{35}$$

Equation (35) attempts to represent the gas velocity due to combustion and is in addition to the velocity caused by the piston motion. This is taken into account by utilising the difference in pressure between the motoring and fired conditions. It can then be incorporated into Equation (33); therefore the convective heat transfer coefficient during scavenging, combustion and expansion can be estimated. The resulting expression is given in Equation (36). There is not an explicit radiation term given in this correlation, but it was assumed that the radiation term was included in the additional combustion term, as this is the time which the contribution by radiation would be significant. Comparing measured data from several test conditions the constants for each phase could be deduced to give a good correlation, $C_2$ was found to be $3.24 \times 10^{-3}$ for combustion and expansion of direct-injection engines (otherwise set to zero for compression and scavenging phases). By employing different coefficients based on the period during the cycle, like the Annand correlation, it is proposed that better matching will be achieved throughout the cycle. Lawton found that during the compression the heat transfer coefficient to the liner was much larger than during the expansion, even noting heat flow from the surface to the gas during this period [95].

$$h = \alpha_s B^{-0.2} p^{0.8} T^{-0.53} \left( C_1 c_m + C_2 \frac{V_s T_1}{p_1 V_1}(p - p_0) \right)^{0.8} \tag{36}$$

In Equation (36), $p$ and $T$ correspond to the instantaneous in-cylinder conditions, whereas $T_1$ and $p_1$ are conditions at a known working value which correspond to a volume of $V_1$ of a reference state, such as the inlet valve closure or beginning of combustion. This formula agrees with the laws of similarity of convective heat transfer and was found by Woschni to correlate well with measured data from engines of different displacements. Further developments were made to the constants used in this equation according to Watson to take account of changes in swirl, which will affect the gas velocities within the combustion chamber [96].

$C_1 = 6.18 + 0.417\frac{C_u}{V_P}$ is valid for scavenging periods, and $C_1 = 2.28 + 0.308\frac{C_u}{V_P}$ is valid for the compression and expansion phases i.e. when the valves are closed, with $C_u = \pi B N_D$, the circumferential gas velocity, calculated using an anemometer 0.7B below the cylinder head, measured on steady state tests.

The Woschni correlation was further developed by Wang et.al to use the instantaneous chamber height rather than the cylinder bore [97], additionally Chang et.al increased the temperature exponent to 0.73 and reduced $C_2$ by 1/6 of its original value [58]. By using the instantaneous chamber height as the characteristic length, better matching in the expansion stroke was found compared to the cylinder bore [97]. The modifications by Chang et.al were made to better approximate the gas velocities to those found in an HCCI engine. The original Woschni correlation was found to result in much higher velocities than in an HCCI due to the gas velocity not being impacted by the advancing flame front as in HSDI. Heinle et.al made additions to the Woschni correlation to take into account the variations in combustion-generated convection allowing a single correlation to be applied to all common combustion principles. This was achieved by introducing a term which determines the differential speed between the expansion velocity of the burned gas and the penetration velocity of the unburned cylinder mass into the flames. Additionally a further term was introduced to determine the heat loss in the piston top land area [98]. The Woschni correlation and its derivatives are very complex as they utilise different coefficients during different portions of the cycle and an additional component for the in-cylinder gas velocity. Hohenberg found that this led Woschni's correlation to over-estimate the convective heat

transfer coefficient during combustion and under-estimate during the motored conditions [99]. Hohenberg therefore proposed a simplified form of this correlation with the aim of reducing the inaccuracies.

$$h = C_1 V_S^{-0.06} p^{0.8} T^{-0.4} (c_m + C_2)^{0.8} \quad (37)$$

$C_1$ = 130
$C_2$ = 1.4

The Woschni correlation (Equation (36)) utilises the cylinder bore as the characteristic length, however Hohenberg considered that the use of the cylinder bore as the characteristic length would adversely affect the accuracy of the correlation due to it limiting the effect of the mass air flow. Subsequently he decided to use the instantaneous cylinder volume as the characteristic length, which is crank angle dependent.

Figure 3.7 shows a comparison between the most commonly used instantaneous heat transfer correlations discussed in this review. It shows that there are significant variations between them; the main reason for these differences can be attributed to the selection of different significant parameters, most notably the flow velocity and the characteristic length. The Woschni correlation illustrates a significantly different response to the other correlations due to the step changes in the coefficients employed in the calculation of the heat transfer coefficient. These are at the inlet valve closing (crank angle 253°), exhaust valve opening (crank angle 491°) and most notably the increase due to the fuel injection. The fuel injection process results in an additional term used to describe the increase in the working gas velocity due to combustion. The other correlations do not incorporate a change due to the fuel injection but only respond to changes in cylinder pressure. Prior to the fuel injection the Woschni prediction follows the same magnitude as the Eichelberg correlation due to its root similarity (The step changes in convective heat transfer coefficient would not be the true response in cylinder but are used to represent the effect of the events.). The convective heat transfer coefficient average for the cycle was found to be comparable for each correlation. Attempted developments and refinements on these correlations are continuously taking place. For example, Woschni has since modified his equation after continued experimental investigations during low load and motored conditions. This development was due to the discovery of the influence of soot deposits on the heat losses through the chamber walls. It

was found that the soot layer thickness increased with increasing load and that Woschni's original equation gave a value for the heat transfer coefficient of less than half the true value due to it including the thermal conductivity of the soot layer; this development has not been included in the Woschni correlation evaluated here [100]. Other studies have been performed which evaluate the correlations for different engine applications, Soyhan et.al concluded that the Hohenberg correlation was better suited to HCCI engines as there was no explicit combustion compression velocity term [101].

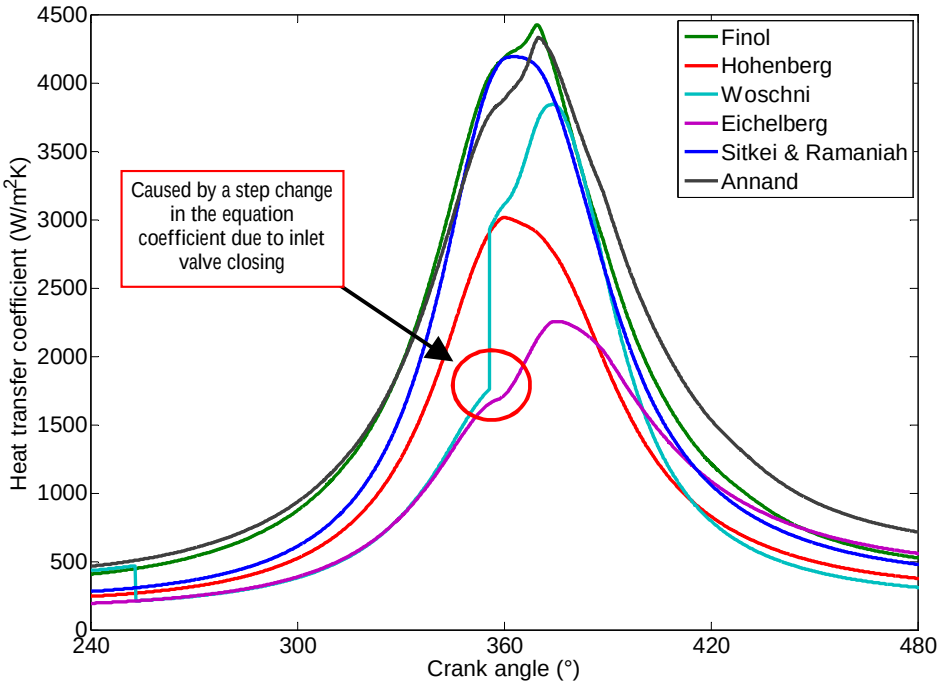


**Figure 3.7 – Predicted heat transfer coefficient comparison using measured data from this study**

A more recent correlation for calculating the convective heat transfer coefficient on a crank angle base was developed on a modern 2.0 litre diesel engine [102]. The experimental work was performed across the engine's full speed and load range, utilising a three thermocouple installation to measure the temperature gradient through the combustion chamber wall. The thermocouples did not penetrate the combustion chamber surface with the innermost thermocouple positioned 2mm from the gas-metal interface, therefore the response time would be less than usually required to develop a correlation of this type and would also mean that the surface temperature would be extrapolated from the calculated gradient. The correlation was developed by investigating the results from the established correlations and how they correlated with measured data. The correlation is based on the fundamental forced convection relationship where the mean piston speed is used as the characteristic velocity to

represent the gas velocity in the cylinder. The coefficient $C_1$ was obtained from experimental data at the maximum power condition as uncertainties were found at part load conditions. The relationship for calculating the gas side convective heat transfer coefficient is shown in Equation (38) [102-104].

$$h = C_1 B^{(C_2-1)} k \left( C_3 \frac{\rho c_m}{\mu} \right)^{C_2} \quad (38)$$

A value of 0.0947 for $C_1$ was found to match the cycle-averaged data from experimentation and the coefficient $C_2$ was taken from work by Woschni and Hohenberg to be 0.8. This was found to be sufficiently large to take into account the effects of radiation from soot particles. $C_3$ was found to equal 1.5 in order to adequately estimate the cycle-averaged convective heat transfer coefficient at the maximum power condition.

The only method to determine which of these correlations is correct is to install a measurement method which accurately measures the relevant temperatures and allows for the convective heat transfer coefficients to be calculated. This is currently not possible therefore there is no definitive correct correlation and an improvement to the accuracy is essential.

## Correlations for instantaneous local heat flux

LeFeuvre highlighted that the majority of the previously discussed correlations, such as Nusselt, Eichelberg, Annand and Woschni, utilise instantaneous wall temperature data at a particular location or temperature data averaged across an area of the cylinder wall, combined with an average in-cylinder gas temperature, i.e. mean gas properties for all calculations, to estimate the total heat transfer from the combustion gases to the cylinder wall [15, 52, 91, 105]. An equation for predicting instantaneous wall heat flux on the cylinder head and piston at different radial distances from the bore axis was subsequently proposed, this was to use instantaneous local wall temperatures in addition to instantaneous gas temperatures.

$$q = a \frac{k}{r} Re^{0.8} Pr^{0.33} \left( T_g - T_w \right) \quad (39)$$

Equation (39) is based on a Reynolds number used in the correlation of friction factors and heat transfer coefficients in rotating flow systems. This correlation was developed based on motored tests of a direct-injection, super-charged single cylinder engine and was intended to predict the convective heat transfer taking into account forced convection by the piston motion only, so was not expected to perform well under firing conditions when there is the combustion component added to the piston motion for forced convection. This was found to be the case at one of the two locations monitored in the test engine at 2000 rev/min and an injection timing of 20° BTDC, where the heat transfer was largely over-predicted for the majority of the cycle. The over prediction can be attributed to the inputs used in the correlation, such as $T_g$, the mass-averaged gas temperature, which highlights that the assumption of a uniform gas temperature may be incorrect during combustion when spatial variations may be extremely high especially during early stages of flame growth. Therefore a correlation to predict local instantaneous heat flux will require significant instrumentation, measuring a large number of locations within the combustion chamber wall and cylinder head to establish the localised mass-averaged gas temperature and the wall surface temperature. Another method proposed to calculate local instantaneous heat flux is to solve a one-dimensional transient energy equation using a Fast Fourier Transform [78]. To employ this method the following assumptions are made:

- The wall is a semi-infinite solid
- Heat transfer is one-dimensional and perpendicular to the wall
- Initially the system is of uniform temperature
- The measured temperature of the internal wall changes periodically and can be expressed as a Fourier series

Using the one-dimensional heat conduction equations and the assumptions above, the following boundary conditions can be deduced:

$$T(L,t) = T_0$$

$$T(x,0) = T_0$$

$$T(0,t) = T_m + \sum_{n=1}^{N} A_n \cos(n\omega t) + B_n \sin(n\omega t)$$

These can then be applied to the one-dimensional unsteady heat conduction equation and according to the Fourier law the heat flux through the probe would be:

$$\dot{q} = k\frac{T_m - T_0}{L} + k\sum_{n=1}^{N}\sqrt{\frac{n\omega}{2\alpha}}[(A_n + B_n)\cos(n\omega t) + (B_n - A_n)\sin(n\omega t)] \quad (40)$$

Therefore the heat flux through the chamber can be estimated from instantaneous gas side and back side temperatures. The coefficients can be selected by Fourier analysis of the instantaneous gas side wall temperatures also. This method was used by Oude Nijeweme et.al to investigate the unsteady in-cylinder heat transfer in a spark ignition engine. By installing twelve fast response thermocouples and measuring an adjacent steady reference temperature in a single-cylinder engine it was found that during the expansion stroke, heat is transferred from the wall to the cylinder gases, even though the bulk gas temperature was higher than that of the wall. It was determined that this was a result of areas of the combustion gas local to the wall having a temperature below that of the wall, i.e. unsteady flows in the gas side thermal boundary layer. These findings would impact the phasing of all correlations based on the general equation given in Equation (14) [106]. Outlined here is a different method of calculating the heat transfer through the cylinder liner, which utilises the same invasive experimental methodology as the other established correlations. From this equation the gas-side convective heat transfer coefficient could be calculated by applying Equation (17).

## *3.3 The uses of in-cylinder pressure measurement*

The aim of this section is to explain why in-cylinder pressure measurement is important in engine development and how the different factors, including in-cylinder heat transfer prediction affect the accuracy of the calculated parameters. In-cylinder pressure measurement is integral to the combustion chamber development process and therefore requires the highest possible accuracy; however there are a large number of factors which affect the accuracy of the recorded data.

In-cylinder pressure data allows for detailed monitoring of conditions within the combustion chamber, which leads to a more complete understanding of the combustion process. For accurate analysis there are three main areas of pressure measurement which must be considered. They are the association of the pressure data to the crankshaft position, the pressure referencing, or pegging, and the pressure sensor accuracy [107]. From this data a large number of parameters can be calculated, such as the rate of heat release, start of combustion, burn rates, peak temperatures and the mode of combustion. These parameters can uncover important information for a wide variety of applications, such as engine output, operating condition and emissions analysis.

## The effect of convective heat transfer on heat release analysis

The methods of analysis of cylinder pressure data originate from the first law of thermodynamics for an open quasi static system, i.e. the system can be considered to have transfer across its boundaries and uniform in both temperature and pressure. An adaptation of this law is given in Equation (41) for a single zone model shown in Figure 3.8. This means that the trapped volume inside the cylinder is treated as homogeneous. A number of more complex methods have been proposed where the cylinder is split into multiple zones to allow for local conditions to be predicted. These methods allow for more detailed analysis of emissions formation; however there has been limited validation with experimental data and are much more complex to apply.

$$dU = dQ_c - dQ_w - pdV + \sum_i \dot{m}_i h_i \tag{41}$$

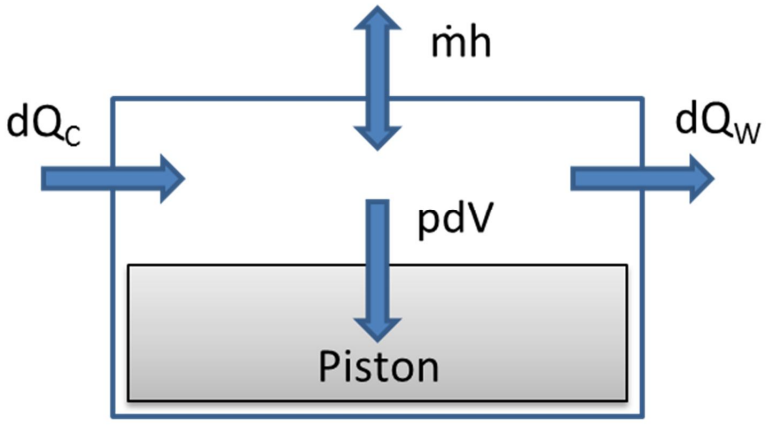


**Figure 3.8 – Heat release single zone system diagram**

The first term, U is the energy of the material contained inside the system boundary, the second is the heat transfer rate from combustion, the third is the heat transfer rate across the system boundary into the system, the fourth is the rate of work transfer by the system due to the system boundary motion, $m_i$ is the mass flow rate into the system at any location, $i$, and $h_i$ is the enthalpy of flux entering or leaving the system. Mass flow rate to and from the system occurs through the valves, as blow-by and as injected fuel.

The concept of heat release rate is very important when understanding the combustion process. It is defined as the rate at which the chemical energy of the fuel is released by the combustion process to produce the observed pressure rise. In order to calculate heat release a number of assumptions are required. A common assumption is to assume the same single zone model as above and that the working gas within the system is perfect. The calculation is solved numerically in the crank angle domain and to simplify the calculation it is common to only consider the period between the inlet valve closing and exhaust valve opening, therefore the mass flow through the valves can be neglected. To further simplify the calculation the heat transfer from the combustion gases to the cylinder wall can be ignored; this is known as the net heat release, whereas with the inclusion of heat transfer it is called the gross heat release. The gross heat release can be solved by applying Equation (42).

$$dQ_c = m_{cyl}c_v\frac{dT_{cyl}}{d\theta} + P_{cyl}\frac{dV_{cyl}}{d\theta} + \frac{dQ_{ht}}{d\theta} + \frac{dm_{bb}}{d\theta}h_{cyl} \tag{42}$$

The process of diesel combustion does not lend itself well to the application of the first law of thermodynamics in this way due to a number of reasons. The injection of fuel into the cylinder which mixes with the air does not result in a uniform distribution and it also varies with time, therefore it is not quasi static. The resulting gas from combustion is also not uniform due to the chemical processes taking place. Therefore all methods for calculating heat release etc. are seen as approximations rather than true values. Other factors which affect the accuracy of calculated heat release to different degrees are listed below:

- Pressure phasing
- Pressure referencing
- Transducer calibration
- Trapped mass

- Heat transfer
- Blow-by mass
- Gas properties
- Compression ratio

There does not seem to be an agreement on which factor affects the accuracy the most as they all contribute an error to some degree, however it has been claimed that the greatest uncertainty is caused by assuming the wrong rate of heat transfer between cylinder charge and the combustion chamber walls [108]. A number of the factors named above can be mitigated by implementing a number of procedures.

- Pressure phasing, otherwise known as TDC determination ensures that the pressure trace is aligned correctly with the cylinder volume, i.e. the signal obtained from the crankshaft encoder. A 1° error in the recorded TDC position to the actual can result in a 10% error in the calculated IMEP. The pressure phasing can be determined by motoring the engine at a range of speeds at elevated boost conditions or by using a TDC detector.

- Pressure referencing or pegging is a method to reduce the effect of the sensor drift by correcting the measured data to a known reference value at a specific point in each cycle. Typically the inlet manifold pressure prior to compression, i.e. when the inlet valve is still open, is used. The pressure transducers are subject to a calibration procedure by the manufacturer to a reference condition as part of their manufacturing process; these factors are then input into the data acquisition equipment.

- Sensors are also prone to electrical noise and can be affected by the combustion process itself, such as the oscillation caused by the injection pressure. As the heat release calculations are based on differential pressure, it is important to filter the pressure signal to reduce the noise caused by small oscillations of the pressure sensor diaphragm due to the pressure ripples within the combustion chamber.

- Finally, the gas properties in a simple heat release model, including the ratio of specific heats of the combustion gases can be assumed to be a fixed value, however it has been found that this distorts the calculated heat release at low speed and load conditions. Therefore it is more accurate to implement a temperature based model to predict gamma [109, 110].

In order to estimate the heat transfer from the working fluid to the chamber walls for the estimation of gross heat release, an empirical heat transfer correlation must be used when measured data is not available. Any of the previously discussed correlations could be implemented, such as Woschni, Hohenberg or Annand, in which the mean combustion gas or charge temperature is obtained from the measured cylinder pressure data by assuming a charge temperature at a specified location and applying the perfect gas law, assuming that the in-cylinder mass is constant. The use of convective heat transfer correlations to predict the energy transfer from the cylinder is not entirely accurate and is highly dependent on the correlation which is employed. This is due to the different methods used to establish each correlation, resulting in different instantaneous convective heat transfer coefficient and therefore, leading to a variation in the calculated rate of heat transfer through the cylinder wall; this in turn could introduce a sizeable error. In addition there are small regions within the combustion volume, such as between the piston, rings and cylinder wall, where the gas is considerably cooler than the majority and therefore exhibiting different properties. The difference in properties could significantly increase the rate of heat transfer. The differing heat transfer rates will result in different gross heat release rates. This further highlights the importance of accurate estimation of the convective heat transfer coefficient from the working fluid to the combustion chamber wall.

## The calculation of indicated power

Cylinder pressure data can be used to calculate the indicated engine power. The area enclosed on a p-V trace or indicator diagram is the indicated work of an engine and is calculated using Equation (43). In a four-stroke cycle the net indicated work is made up of two parts, the combustion loop and the pumping loop. The pumping loop is the negative work completed during both the induction and exhaust strokes of the cycle when fresh air is drawn into the engine and the burned gas is expelled from the cylinder. This can be subtracted from net indicated work to give the gross indicated power of the engine.

$$P_{ind} = \sum_{All\_Cyls} \sum_{0}^{720} p \frac{dV}{dt} \quad (43)$$

As with BMEP the indicated power can be discussed in terms of mean effective pressure. The net indicated mean effective pressure ($IMEP_n$) is therefore a measure of the indicated work output per unit swept volume of an engine; independent of engine speed and number of cylinders for the entire four strokes of the cycle. The gross indicated mean effective pressure ($IMEP_g$) is the work delivered to the piston over the compression and expansion strokes of the cycle and the difference can be described as the pumping mean effective pressure (PMEP).

$$IMEP_g = IMEP_n + PMEP \quad (44)$$

## Engine friction measurement

The indicated work from the gases contained inside the cylinder is not all transferred to the drive shaft as useful work. The engine brake power is always less than the indicated power with the difference dissipated in a variety of ways within the engine and to auxiliary components. This is known as friction work. Engine friction occurs in a number of areas including piston rings and skirt, con rod bearings, crankshaft bearings, valve train elements and belt and chain drives. Engine friction has been found to generally follow a power law dependent on the bulk oil viscosity except during the early seconds of engine operation. The relationship is shown in Figure 3.9.

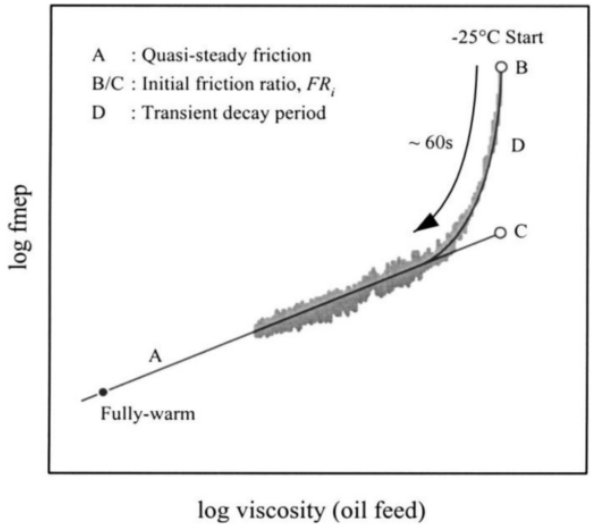


**Figure 3.9 – Friction response to changing oil viscosity during warm-up [111, 112]**

The frictional losses can be a significant proportion of the indicated work and affect the maximum brake torque and the minimum brake fuel consumption directly. The majority of friction losses appear as heat in the coolant and oil and therefore have a knock-on effect on the sizing of the radiator and oil-cooling system, subsequently knowledge of the friction power is vital. Friction work is defined as the difference between the work delivered to the piston by the working fluid whilst it is within the cylinder (i.e. during the compression and expansion) and the usable work transferred to the driveshaft. The losses consist of three areas:

- Pumping work (the work to draw the fresh air through the intake system and into the cylinder, in addition to the work to expel the burned gases from the cylinder and through the exhaust system)
- Mechanical (the work to overcome resistance of the motion of all the moving parts within the engine)
- Auxiliaries (the work to drive the engine auxiliary components, including the fan, water pump, oil pump, fuel pump, alternator, power steering pump and cabin heater)

Friction in the piston elements can be described by a number of lubrication regimes, the piston skirt is generally accepted to operate in the hydrodynamic regime throughout the cycle, whereas the piston ring varies [113-116]. The variation in the piston ring lubrication regime is due to the change in in-cylinder pressure and piston velocity during a cycle. The

rings are pushed against the liner as a result of their static tension and the in-cylinder pressure building up behind the ring in the groove. When the piston velocity is highest, i.e. mid stroke, the oil film is sufficient for hydrodynamic lubrication, however towards TDC or BDC where the velocity is reduced, the film breaks down into mixed or boundary lubrication [117]. The total friction work is the sum of these three areas and is given by Equation (45). Pumping work can also be known as the turbulent friction and is proportional to the fluid velocity; in this case this is engine speed. Mechanical losses are a result of two surfaces moving relative to each other with a lubricant in between. This lubricated friction is dependent on the relative velocity of the two surfaces. There are a number of techniques developed to measure friction in an engine; these can be split into two categories: bench test, where a small part of the engine is replicated in a controlled and isolated environment and those conducted on engine. The most common method of measuring the total friction work is in a hot motoring test, in which the engine is motored with coolant and oil temperatures held at firing engine levels. A test of this type measures the sum of pumping, piston-crank and auxiliary losses. As a result the gross indicated power can be calculated as the sum of the brake power and friction power. However if cylinder pressure data is available the pumping power can be determined directly.

$$W_{tf} = W_P + W_{mf} + W_a \tag{45}$$

A method for measuring friction in a firing engine is to use the indicated method, which finds the total frictional mean effective pressure ($FMEP_{tf}$) as the difference between the gross indicated mean effective pressure ($IMEP_g$) and the brake mean effective pressure (BMEP), given in Equation (46). A number of inaccuracies can be introduced when employing this method, such as when calculating the BMEP and IMEP from motored tests it is crucial that the coolant and oil temperatures are stable as FMEP is very sensitive to small changes in oil temperature as this affects the oil viscosity. When calculating the FMEP from fired tests the measure is ill-conditioned as it is the small difference between two large measurements, in addition to the TDC alignment of the in-cylinder pressure measurement having a significant effect on the IMEP calculation.

$$FMEP_{tf} = IMEP_g - BMEP \tag{46}$$

A number of correlations have been established to predict the frictional losses of an engine on a cycle-averaged basis. These correlations give a good indication of the overall frictional losses; however it has been found that friction does vary significantly over the 720° crank angle. Cycle-averaged correlations are based primarily on a fixed term, to cover the auxiliary losses, and a speed element such as engine speed or mean piston speed, to estimate the mechanical friction losses. Chen-Flynn and Winterbone included an additional term to account for the effect of pressure loading on the piston with a maximum cylinder pressure term. Other established correlations from Barnes-Moss, Millington and Hartles (Equation (47)), and Heywood include a velocity squared term to estimate the pumping losses. Equation (47) utilises a term based on the engine compression ratio to predict a constant friction term.

$$FMEP = \frac{(r_v - 4)}{14.5} + 0.475\left(\frac{n}{1000}\right) + 3.95 \times 10^{-3} c_m^2 \quad (47)$$

Each correlation was derived from different data and for different purposes, for example the Barnes-Moss correlation was derived for spark ignition engines, whereas the Millington and Hartles was derived for diesel engines. These further differ from the Chen-Flynn and Winterbone correlations as they were developed under motoring conditions rather than fired. Heywood suggested a simple quadratic empirical model for $FMEP_{tf}$ in diesel engines given in Equation (48).

$$FMEP = C_1 + \left(\frac{48n}{1000}\right) + 0.4c_m^2 \quad (48)$$

n – Engine speed (rev/min)

$c_m$ – Mean piston speed (m/s)

The most complex model currently used is a modified Chen-Flynn correlation used in simulation packages, given in Equation (49). This incorporates elements from the other correlations discussed, including a constant accessory term, a peak cylinder pressure term, a mechanical friction term and a pumping losses term.

$$FMEP_{tf} = C_1 + C_2(P_{MAX}) + C_3(S_{FACT}) + C_4(S_{FACT})^2 \quad (49)$$

$S_{FACT}$ = Engine Speed X (Stroke/2)

Each of the correlations has been evaluated against motored friction data from the experimental engine in Chapter 6.

## 3.4 Chapter summary and conclusions

The combustion chamber wall measurement techniques, the factors which affect the prediction of the rate of heat transfer, the established empirical correlations for predicting convective heat transfer and how these impact the calculation of parameters using in-cylinder pressure measurement have been discussed in this chapter. There were a number of key outcomes from this chapter which have been listed below:

- The primary consideration when selecting instrumentation to measure temperature is the accuracy of the technique to measuring the 'true' temperature. There are a number of methods to improve this accuracy, including using like materials to the measurement material and using a good insulating layer between the sensor materials and the outer surface, such as an oxide layer.

- The most common method for calculating heat flux is the differential temperature method which uses a series of measurement points to allow for a temperature gradient to be calculated. Using Fourier's one dimensional law of conduction the rate of heat transfer can be calculated.

- The rate of heat transfer from the working fluid in the cylinder to the cylinder walls is influenced by a large number of factors, which results in the prediction methods varying greatly in their complexity and accuracy.

- Experimental investigation has been undertaken since 1939 to establish methods to predict the rate of heat transfer from the combustion process to varying degrees. During this time the correlations have evolved and been developed as new measurement techniques and technologies have been introduced. However no single empirical correlation has been found to accurately predict the convective heat transfer coefficient across different engine sizes and operating conditions.

- There are some key factors which affect the accuracy of parameters calculated from measured in-cylinder pressure data. One of these factors is the rate of heat transfer from the combustion gases, as this affects the calculation of gross heat release. Therefore an improvement in the calculation of heat transfer will improve the thermal modelling of engines in the development process.

# Chapter 4. Experimental facilities, hardware and testing procedure

This chapter describes the internal combustion engine which was modified and extensively instrumented for this study and the facility in which the experimental programme was completed. The facility description includes details of the data acquisition equipment and the standard instrumentation installed for normal experimental programmes. Details of the additional prototype thermal management hardware are discussed and a brief introduction to the experimental programme and the rationale behind it is also given.

A detailed investigation into a forced cool down procedure which could be implemented in the test facility to improve productivity was also completed and the findings have been detailed in this chapter.

## *4.1 Test Facilities and standard equipment*

All experiments were performed in an engine test cell located in the Powertrain and Vehicle Research Centre at the University of Bath. The test bed equipment consisted of an A.C. dynamometer, a gravimetric fuel flow measuring unit, a main control system, combustion analysis equipment, exhaust emissions analysis equipment and an additional computer monitoring all ECU parameters [118]. The computer systems are located in a control room adjacent to the test cell to allow safe operation of the engine by an engineer. The emissions analysers are also located in a dedicated room; therefore the samples are transported via a heated line to prevent the gas from condensing in the line. This means that there is a sample delivery time requiring that the emissions data is time adjusted to match the engine conditions. The sample delivery time would not be an issue during steady state testing but would need consideration during any transient experimental work.

The control system used in the test cell is called Cadet, and is a product of Sierra CP Engineering Systems. It is designed to control and monitor the engine performance in real time, to control the test cell ambient conditions and to record all test variables, including the

emissions data. The system is capable of continuously logging the data at the acquisition control frequency, at a defined time interval or averaged over a time period. The ECU is controlled via a separate computer and interface called ATI Vision; however a link via an ASAP3 protocol allows selected variables to be recorded by the host system. Important parameters such as injection timing, injector flow rate and air mass flow rate were recorded for the completed experimental programme. The test cell was recently upgraded and the ventilation system was capable of controlling the ambient temperature to ±1°C. The test cell ventilation system is discussed in Section 4.6.

## 4.2 Data acquisition system

Data for the experimental programme was recorded on two different systems, primarily the test cell host system, but the steady state in-cylinder pressure data was recorded on a D2T Osiris combustion analysis system. The host system continuously records all variables including engine parameters, room conditions and temperatures. The additional temperature measurement requirements of this programme required extra thermocouple logging channels due to the large number of measurement locations on the engine. The original system had the capability of recording 32 thermocouple channels, however the completed experimental thermal survey required in the region of 120 channels. The additional thermocouple loggers were positioned inside the test cell local to the engine to minimise possible errors. The host system recorded all the temperature data at 2Hz and to three decimal places. In order to achieve repeatable thermal equilibrium in different areas of the engine, i.e. engine structure, oil and coolant, a parameter settling algorithm was available. This allowed for a threshold to be set for a number of temperature channels. As thermal equilibrium was crucial for accurate results the threshold would be set particularly low. Therefore a change in temperature of less than 0.1°C in 5 seconds had to be satisfied for that temperature to be regarded as stable; all monitored temperatures had to be stable before logging could begin. A minimum wait time of 120 seconds was also implemented to ensure a change in operating condition had impacted the monitored temperatures.

## 4.3 Engine coolant system hardware

The test engine for this study was a production 2.4 litre four-cylinder, common rail, direct-injection, fixed geometry turbocharged diesel engine. Details of the engine geometry are given in Table 1. The engine was installed in the transient test facility described above with

the gearbox being replaced by a single shaft. The typical application for this engine is a light-commercial goods vehicle and the simulated load was provided by the dynamometer for the dynamic testing. The test engine cooling circuit was designed to best replicate the vehicle installation, utilising a production radiator and road speed fan. The cabin heater portion of the cooling circuit was removed from the test cell installation, as was the alternator. All other ancillary devices, such as the water pump, oil pump, fuel pump and radiator were incorporated to best replicate the vehicle installation. The coolant circuit had a number of minor differences to that of the production circuit with the addition of five ultrasonic flow meters, flow control valves and a non-production pressure regulated thermostat (PRT). The additional measurement components were located such that minimal disruption to the production circuit was made in order to best replicate the vehicle installation. The coolant circuit diagram is shown in Figure 4.1, highlighted in the diagram are the positions of the flow meters and hose thermocouples. It is important to note that the coolant inlet manifold is located on the air inlet side of the engine. The location of the inlet manifold will affect the coolant temperature distribution and subsequently the convective heat transfer coefficient and rate of heat transfer through the cylinder wall. The branch manifold feeds coolant directly alongside all four cylinders at four discreet locations at the top of the cylinder block as shown in the coolant schematic.

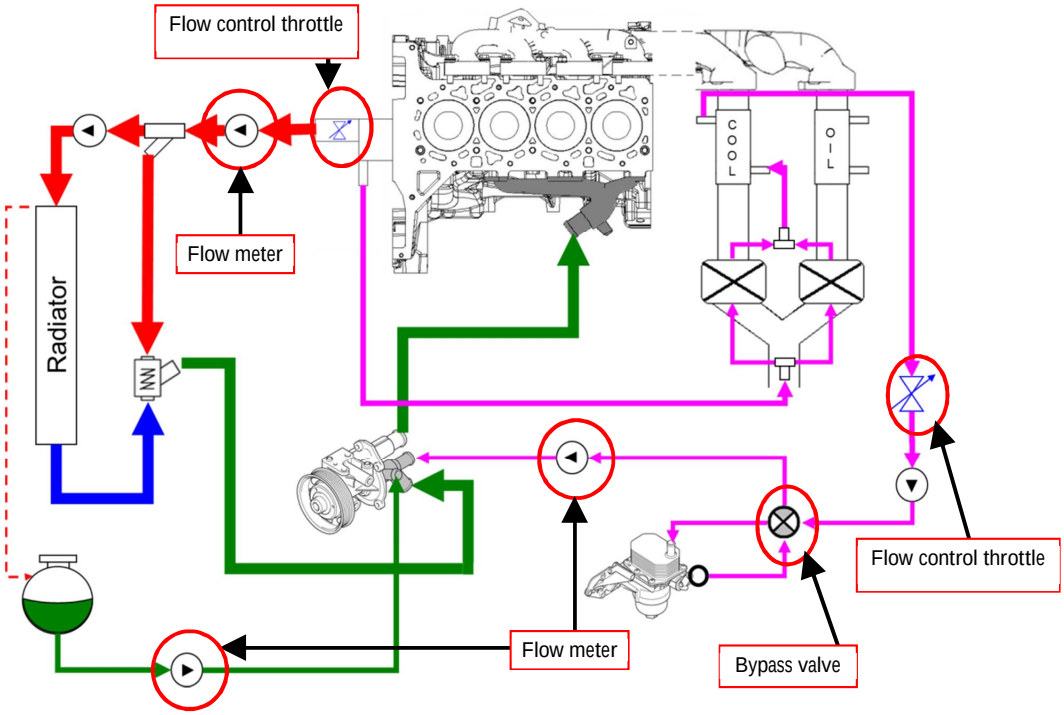


**Figure 4.1 – Experimental engine coolant circuit with additional hardware**

**Table 1 – Experimental engine specifications**

| | |
|---|---|
| Engine Type | Diesel |
| No. of Cylinders | 4 |
| No. of Valves | 16 |
| Block | Cast Iron |
| Head | Aluminium |
| Horsepower | 103 kW (140PS) at 3500 rpm |
| Torque | 375 Nm at 2000-2250 rpm |
| Displacement | 2402 cc |
| Bore | 89.9 mm |
| Stroke | 94.6 mm |
| Connecting Rod Length | 149.8 mm |
| Compression Ratio | 17.5 : 1 |
| Fuel System | Common Rail<br>Electronic Throttle |

The engine was fully dismantled to allow the installation of the sensors in both the engine block and cylinder head. The method used to install the multipoint sensors and their positions within the engine are detailed in Chapter 5. During the engine rebuild the standard glow plugs in each of the four cylinders were replaced with high temperature fast-acting pressure sensors. The data from these was recorded using a high frequency acquisition system and was aligned with the crank angle position using a shaft encoder. The D2T combustion analysis system is a standalone system which was triggered once the engine had reached a stable condition at each operating point. The recording duration was limited due to it utilising the base computer storage, however it was capable of recording up to 500 engine cycles, which is sufficient for statistical analysis.

## *4.4 Additional prototype thermal management system hardware*

A number of additional items were incorporated into the production cooling and oil circuits. This included flow control valves, direction control valves, a dual EGR cooler arrangement and a variable flow oil pump. The flow control valves were simple butterfly valves which

were operated by rotary electric actuators (REA). The REA is typically used for actuation of the vanes of a VGT, therefore it can be incorporated into the ECU control strategy. During engine running it was possible to effect the position of each of the flow control valves based on any variable monitored by the ECU. It was decided that the cylinder head metal temperature was a crucial temperature in determining the thermal state of the engine, therefore the valves were mapped based on engine speed, fuelling quantity and cylinder head temperature. The directional control valves worked in a similar manner and allowed for the additional components to be included or bypassed from the system via the ECU control strategy.

The aim of the dual EGR cooler was to allow the EGR gas to be cooled by either coolant, as in the standard system, or by oil. By cooling the EGR gas with oil it was hoped to reduce the oil warm-up time by introducing additional heat into the system during cold start conditions. The second cooler was located parallel to the first, with a simple extension being fabricated to the exhaust manifold. The gas flow through the second cooler was controlled in an identical manner to the original cooler utilising a second coolant cooled EGR valve. The flow of cooling medium through its respective cooler was continuous as the ability for diverting the flow was not incorporated in the system. The system was designed so that the coolers were located in parallel on the engine so as to provide similar gas paths for each. However the coolers were not designed to be used simultaneously but with the EGR gas flow to be directed through one cooler or the other.

The variable flow oil pump was incorporated in the engine build to directly replace the fixed displacement pump normally fitted to the production engine. The variable flow oil pump controlled the main oil gallery pressure by adjusting the amount of flow through the pump. This was achieved by an electro-hydraulic system controlled by the ECU. The target oil pressure was determined from a series of maps within the ECU strategy and could be a function of engine speed and fuelling quantity (i.e. engine load) or simply a flat-mapped value and the closed loop feedback was from the post filter main oil gallery.

## *4.5 Experimental programme*

The project was divided into three phases of experimentation. Each phase was designed to have a distinct outcome with the aim to link the findings from each phase together. The three phases were motored tests, steady state tests and dynamic NEDC tests.

## Motored tests

The motored tests involved running the engine at a series of speed set points in order to achieve thermal equilibrium through the engine. The fuel was subsequently cut via the ECU controller and the engine was motored by the dynamometer. The aim of these tests was to understand the background friction levels of the engine at different speeds. In addition, the motored pressure traces would be used in the evaluation of the empirical heat transfer coefficient correlations previously discussed. The motored test points were at 500rpm intervals across the complete engine speed range, from 1000rpm to 4000rpm.

## Steady state tests

The steady state test points were performed to understand the effect of different speed and load conditions on the heat flow through the engine, without the influence from the additional thermal management devices. The steady state operating conditions were designed so that a comparison to the transient NEDC behaviour could be made. By performing the investigations under steady state conditions the complex interactions during the transient cycles would be reduced and a stable heat flow path would be established. The test programme consisted of 26 operating conditions representing the engine operating conditions from idle to the 120km/h cruise of the EUDC.

## Drive cycle tests

A series of cold and hot start NEDC tests were finally performed to investigate the transient thermal behaviour through the cylinder walls of the engine. The NEDC simulates a 20 min drive with a 14 min urban and a 6 min extra-urban part, for a cold start the vehicle temperature should be completely uniform and in a range between 20°C and 30°C. These tests would also allow for comparison with the steady state test results. The main aim of this series of tests was to investigate the effect of the additional hardware previously discussed on the rate of heat transfer through the cylinder wall and whether changes to the coolant and oil circuits was significant to the cylinder wall temperatures and how the different builds affected the heat flow through the engine. The cold start tests were performed at an ambient temperature of 25°C as specified in the legislation. The engine was soaked at this temperature overnight.

# *4.6 The effect of a forced cool down procedure on test-to-test repeatability*

The requirement for reduced fuel consumption and improved emissions is creating a demand for test procedures which allow for an increased productivity of a test facility whilst maintaining high standards of reliability and repeatability [119]. Currently, before a cold test cycle is performed an engine is often left overnight to achieve stable temperatures throughout; this means that only one cold test can be carried out each working day. The engine can be cooled rapidly to allow more tests to be performed each day; however there is an inherent risk of a loss in test-to-test repeatability. A small change in experimental conditions can have a dramatic effect on the outcome for each test; evidence shows that there can be up to a 10% saving in fuel consumption over a NEDC when completed with a higher engine temperature [120].

Forced cooling involves forcing air and/or operating fluids around the engine to remove heat at a much faster rate than achieved by natural means. In some instances the engine fluids can be pumped into an external heat exchanger to aid the cooling of the engine bulk material, however this is not always suitable as it alters the coolant and oil circuits. The aim of this work was to assess the impact of a forced air cooling procedure on the drive cycle fuel consumption when using the basic test cell ventilation system and some additional dedicated fans. The temperature distribution through the engine is also important, areas must not be overcooled past their ambient conditions; this is known as cold spotting, which can lead to inaccurate results. The mechanism for the erroneous result may be due to a change in the heat physical environment (combustion, heat transfer, viscosity etc.) or a change in the controller behaviour due to the measurement system sensing an unrepresentative temperature. Often a combination of both will be apparent.

## Experimental set-up and approach

The test engine was as described above with a modified cooling circuit, incorporating a PRT and a variable flow oil pump (fixed to allow full flow). The coolant circuit utilised a radiator and road speed fan positioned to the front of the engine rather than a heat exchanger; this was to best replicate road conditions. The test ventilation was very basic as shown in Figure 4.2. In this system the ventilation fan and road speed fan could be either automatically or

manually controlled between 0 and 100%, whereas the recirculation flaps worked on a closed loop control system based on the cell ambient temperature. To aid with the forced cooling process, the option of a free standing fan to provide spot cooling was included. This fan would be positioned on the gearbox side of the engine directed towards the cylinder head and block; due to there being no air incident on this area from the road speed fan or ventilation system.

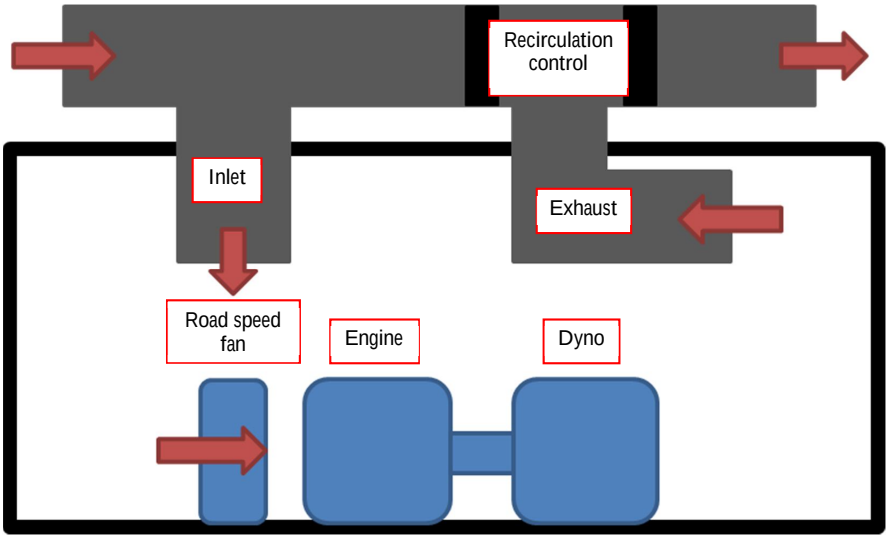


**Figure 4.2 – Cell ventilation schematic used in the forced cool down investigation**

**Table 2 – Overnight soak temperature distribution**

| Location | Average starting temperature (°C) |
|---|---|
| Oil – Sump | 21.7 |
| Coolant – Engine in | 23.6 |
| Coolant – Engine out | 22.8 |
| Fuel – High pressure pump in | 22.4 |
| Engine temperature | 24.5 |

The cell ambient demand temperature was set at 23°C with the average temperature distribution through the engine after an overnight soak from 8 cold start NEDC tests shown in Table 2. A structured experimental approach to the testing was required as very small effects on fuel consumption had to be measured. The three variables considered are shown in Table 3. The percentage indicates 0-100% of their available output.

**Table 3 – Overnight soak test variables**

| Variable | Range |
|---|---|
| Ventilation Fan | 0 – 100% |
| Road Speed Fan | 0 – 100% |
| Spot Cooling Fan | On/Off |

The total fuel consumption over the drive cycle would be compared between the tests performed after an overnight soak to those performed after a forced cool down. The baseline was regarded as the test performed after the overnight soak or natural cool down. An additional baseline test was performed prior to the three repeats of the process shown in Figure 4.3. The forced cool down process took in the region of 11000 seconds (3 hours), after which the second test was carried out. The key target temperature for the forced cool down was an ECU engine temperature of 24°C; however the temperature distribution shown in Table 2 was also targeted.

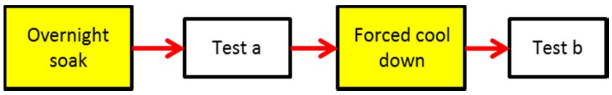


**Figure 4.3 – Forced cool down investigation experimental flow diagram**

## The effect on drive cycle fuel consumption

Figure 4.4 shows the cumulative fuel consumption by three different fuel measurement methods for a single repeat of the drive cycle. Ideally these three methods would show the same fuel consumption, however due to inaccuracies in the calculations there is some variation [121]. The values of fuel consumption at the end of each drive cycle (i.e. 1180 seconds), pre and post forced cool down, for each fuel measurement method is shown in Table 4.

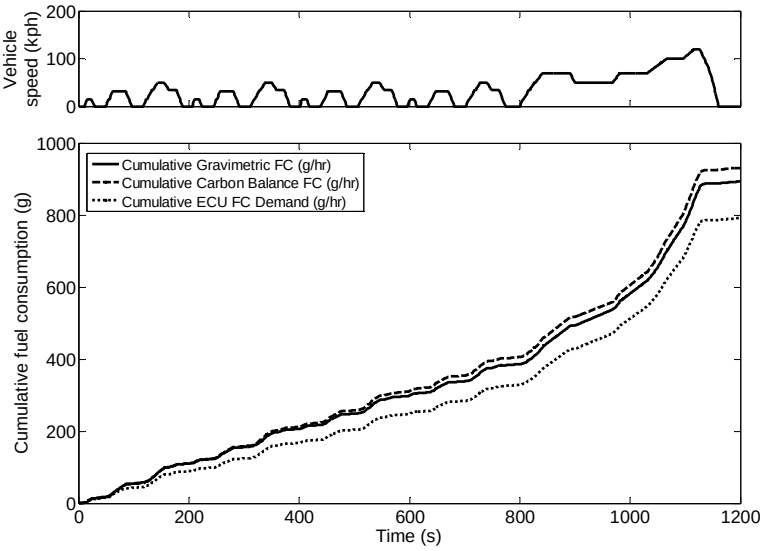


**Figure 4.4 – Cumulative fuel consumption for a New European Drive Cycle as measured by the three available methods**

**Table 4 – Fuel consumption results for all experimental repeats**

| Experiment number | Fuel measurement method | Test a (g) | Test b (g) | Difference (%) |
|---|---|---|---|---|
| 1 | Gravimetric | 837.2 | 829.9 | -0.9 |
| | ECE | 920.1 | 914.6 | -0.6 |
| | ECU | 724.0 | 715.1 | -1.2 |
| 2 | Gravimetric | 834.5 | 830.0 | -0.5 |
| | ECE | - | - | - |
| | ECU | 718.3 | 712.6 | -0.8 |
| 3 | Gravimetric | 834.9 | 830.5 | -0.5 |
| | ECE | 892.9 | 925.9 | 3.7 |
| | ECU | 710.3 | 713.9 | 0.5 |

**Table 5 – Difference in gravimetric fuel consumption between test a repeats**

| Experiment number | Gravimetric fuel consumption (g) | Difference (%) |
|---|---|---|
| 1 | 837.2 | |
| 2 | 834.5 | 0.32 |
| 3 | 834.9 | 0.05 |

The normal overnight variability in the gravimetric fuel consumption measurement for test '*a*' is shown in Table 5. This highlights that there is variation from test-to-test ranging between 0.05 – 0.32% for similar conditions when considering only the gravimetric fuel

consumption measurement method. This must be considered when comparing the '*pre*' and '*post*' forced cool down fuel consumption results. In experiment 2 an error in the ECE fuel measurement method occurred resulting in the missing data set. In addition the 3.7% error in the ECE calculated fuel consumption in experiment 3 is far outside the acceptable range of error (±0.5% would be considered to be representative of standard experimental error) in fuel consumption; however the increase was not conveyed in either of the other measurement methods. Also it would be expected that the fuel consumption would be reduced in the second test, due to residual heat rather than increased. Through further investigation into this anomalous result it was found that there was a fault in the values recorded by the MEXA analyser in the first 11 seconds of the test, resulting in an over prediction of the constituents of the exhaust gas. Therefore the ECE data for this test should be discounted. The ECU method was included for completeness but shows a significant under prediction in fuel consumption compared to the other methods due to the calculation method employed to achieve the fuel consumption figure. The offset between the ECE and gravimetric measurements is less but still notable.

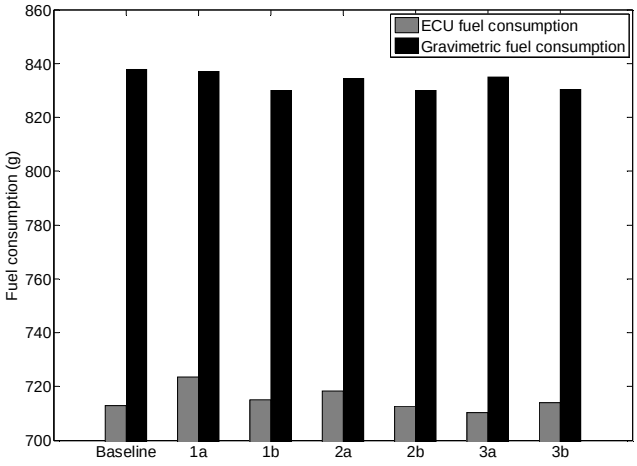


**Figure 4.5 – Comparison of fuel consumption measurement methods across all tests**

Figure 4.5 shows the fuel consumption data for the 6 tests performed compared with the result from the baseline test. The forced cool down process resulted in a reduction in the fuel consumed by an average of 0.63% or 5.4 grams over the NEDC based on the gravimetric method. A repeatability error of this magnitude would not be regarded as acceptable for statistical analysis; therefore further iterations of this method would be required before the method could be implemented. It is commonly considered that the introduction of a new technology, which results in an improvement of 0.5% fuel consumption over a drive cycle, would be regarded as a successful improvement to the

engine performance and this would be masked by this variation in measured fuel consumption. The reduction in fuel consumption after a forced cool down may have been caused by residual heat remaining in the engine structure and fluids; therefore an investigation into the temperature distribution in the engine was performed. The ECU fuel demand was found to be very sensitive to the measured fuel temperature as this is used to calculate the fuel density and therefore the calculated value of injected fuel. The reduction in measured fuel consumption post forced cool down is clearly visible for both the gravimetric and ECU fuel demand.

## The impact of spot cooling on the temperature distribution and forced cool down time

A spot cooling fan was included in the forced cool down procedure, with a separate investigation performed to understand its impact on five key temperatures around the engine. Figure 4.6 shows the effect of the fan on the oil sump temperature with respect to time. The fan was found to increase the cooling by 2°C even though the bulk flow was directed towards the cylinder head and block, reaching the target temperature in 72% of the time without the fan. This is due to the fan promoting heat transfer to this region.

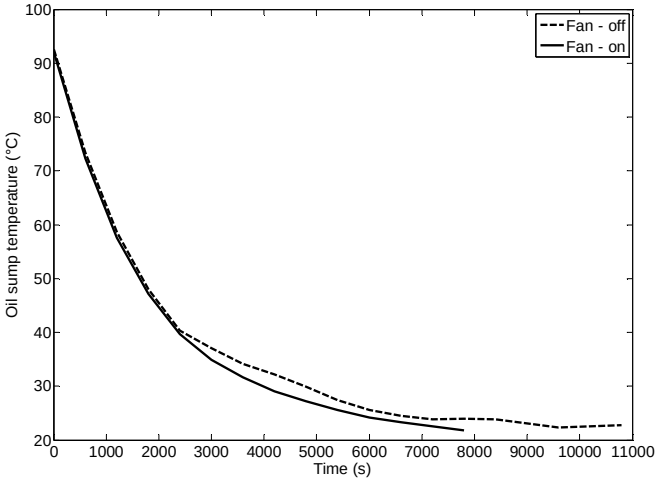


**Figure 4.6 – The effect of spot cooling on oil sump temperature**

The spot cooling fan was found to have a much larger impact on the ECU engine temperature, shown in Figure 4.7. The engine temperature reached 24°C in less than 50% of the time taken without the spot cooling, demonstrating a dramatic reduction in cooling time. The other temperatures investigated were the engine coolant in and out of the engine, and the fuel temperature, all of which showed an increased rate of cooling when the fan was

included in the cool down process. This led to the target temperature of 24°C being achieved in 60% of the time taken without forced cooling.

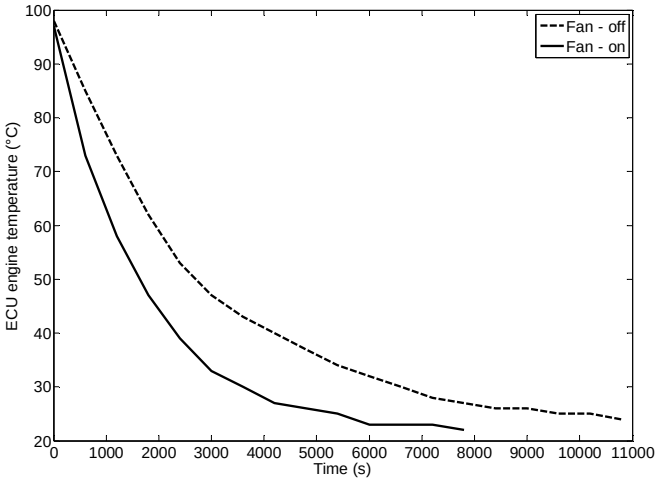


**Figure 4.7 – The effect of spot cooling on ECU temperature**

In summary, the spot cooling fan on the reverse side of the engine reduced the forced cooling time by over 25%; this may be improved further by better control of the forced air path around the engine. A possible method for further reduction of the cooling time is to motor the engine with the dynamometer, which would move the fluids around their respective systems. However further investigation would be required as the impact of heat generated due to friction would have an adverse effect on the cool down.

## Temperature distribution after forced cool down

The temperature distribution through the engine was evaluated to ensure certain areas were not achieving their target temperature faster than others, resulting in an abnormal temperature distribution that would affect the fuel consumption figures. The same key temperatures were used as in the spot cooling investigation.

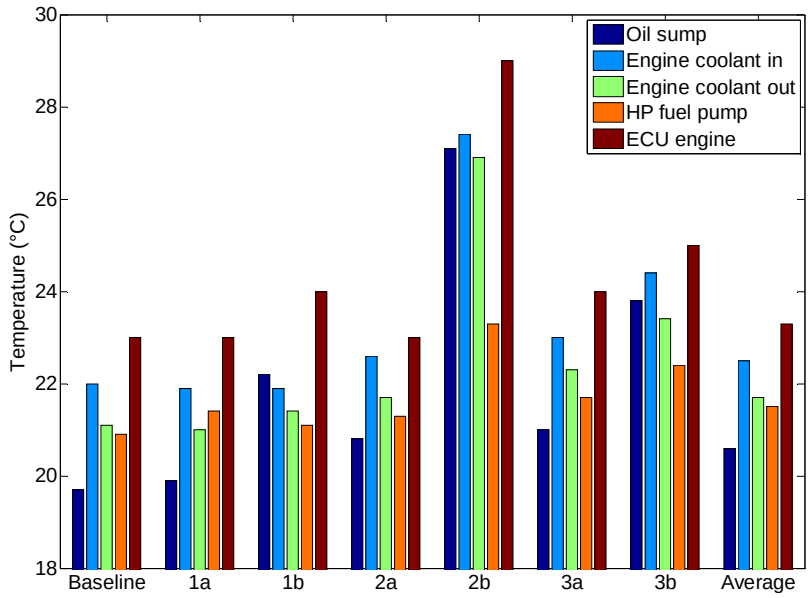


**Figure 4.8 – Temperature distribution in fluids around the engine and the cylinder head ( a – overnight soak, b – forced cool down)**

Figure 4.8 shows the temperatures at the start of each test for both an overnight soak and a forced cool down. The average temperatures after an overnight soak are also included for comparison. The forced cool down used in experiment 2 was insufficient as the starting temperatures for each of the fluids were 5°C higher than after an overnight cool down. This occurred because the forced cool down procedure was stopped at an ECU engine temperature of 28°C, which is hotter than the demanded temperature, due to the fuel temperature coming to within 1°C of its target. The same procedure was performed in experiment 3 where the effect of the forced cool down on the fuel temperature was closely monitored and the ECU engine temperature was forced down to 24°C with no adverse effects on the fuel temperature. The baseline test achieved the lowest temperatures for all the monitored temperatures; in the region of 1°C less than the average. The oil sump temperature was found to be 1°C lower than the other fluid temperatures except for experiment 1b, where the oil temperature was greater than the coolant and fuel temperatures. This is undesirable as it will have an effect on the oil viscosity and other properties [122]. Future implementation of the forced cool down process should be controlled in order to bring the fluid temperatures to within 1°C of their original values. Experiment 3 would have achieved the desired temperature distribution if its method of cooling had been maintained for a longer period of time.

It is interesting to note that using both ventilation and road speed fans at 100%, and the inclusion of the spot cooling fan, did not lead to an uneven temperature distribution in the fluids in the engine. Therefore further investigation utilising different fan speeds was not necessary. A key outcome to the forced cool down procedure was that once the cooling process had been stopped there was residual heat which caused the fluid and metal temperatures to rise slightly, in the region of 0.5°C, therefore the engine should be over-cooled to account for this reheating.

The use of a forced cooling process was found to not adversely affect the temperature distribution through the engine directly but it was shown that a 2°C increase in fluid temperatures would result in a reduction in fuel consumption of 0.63%, proving that the start temperatures for all tests must be within 0.5°C to ensure repeatability.

## Key findings from the forced cool down investigation

The work was specifically undertaken to quantify the impact that the implementation of a forced cool down procedure would have on the fuel consumption of the next test repeat. The following conclusions can be made:

- The implementation of a forced cool down procedure had an effect on the fuel consumption, reducing the gravimetric fuel measurement by an average of 0.63% over 3 test repeats.
- The inclusion of a spot cooling fan reduces the required cooling time by over 25% and improves the temperature distribution through the engine by supplying cooling effects to the reverse side.
- Motoring the engine during the cool down process and maintaining a constant air inlet temperature could potentially improve the cool down time.

The air in the intake duct of the ventilation system ranged between 11°C and 23°C depending on the amount of air being re-circulated. However the cell ventilation system shown in Figure 4.2 was subsequently upgraded prior to this thermal management experimental programme to include an additional fan on the intake section of the system plus a cooling coil, utilising a 6°C refrigerant loop, and a heating element. The new ventilation system allowed the intake air to be conditioned rather than being affected by the outside

ambient temperature. This allowed for accurate control of the inlet air temperature and hence the ambient temperature of the cell.

## 4.7 Chapter summary and conclusions

The experimental facilities, engine hardware and basic testing procedures have been outlined in this chapter. The engine coolant circuit and additional hardware used have also been described. The results of a detailed investigation aimed to understand the impact of a forced cool down procedure on the repeatability of measured fuel consumption from test-to-test have been given. There were a number of key outcomes from this chapter which have been listed below:

- All experimental work was undertaken in a temperature controlled environment which allowed for the ambient temperature to be maintained at 24°C (±1°C) throughout the experimental programme. However the intake air temperature was found to vary significantly due to the volume of recirculated air required to maintain a stable ambient temperature.

- The engine coolant circuit was constructed to best replicate the in-vehicle system, utilising a radiator and road speed fan. However some modifications were required to incorporate flow meters, control valves, a dual EGR system and a variable flow oil pump. The addition of these devices allowed for the evaluation of an active thermal management system on the rate of heat transfer through the combustion chamber wall.

- To improve experimental facility productivity a forced cool procedure was investigated on the experimental engine prior to the test program. It was found to reduce the measured gravimetric fuel consumption over a New European Drive Cycle by an average of 0.63% across 3 experiments. This is a relatively small effect, however in terms of NEDC fuel consumption measurement accuracy this is regarded as unacceptable, therefore natural cool down and force cool down experiments could not be compared with this level of discrepancy.

- The temperature distribution through the engine structure and fluids was found to be acceptable when the following points were adhered to:

    1) Spot cooling fan to the rear of the engine
    2) Forced cooling was maintained until key temperatures were within 1°C of their target value.
    3) The engine should be overcooled by 0.5°C as residual heat resulted in an increase in temperature when the forced cooling process was stopped.

- A forced cooling procedure would increase the productivity of a test facility however further iterations in the procedure must be made before it can be implemented due to the impact on the drive cycle fuel consumption.
- Further iteration of the cooling procedure, which is not reported here, was undertaken prior to the experimental program detailed in this thesis and was implemented to allow two cold start tests to be performed each day.

# Chapter 5. Heat Transfer measurement method

This chapter details the processes undertaken to determine the appropriate measurement technique to be used for the experimental study reported in this thesis. The heat flux measurement through the cylinder wall of an I.C. engine was a significant part of a larger Technology Strategy Board funded project to investigate a number of active thermal management systems on the warm-up and subsequent fuel consumption of a production diesel engine. To support the understanding and conclusions obtained from the wider system evaluation it was decided that the thermal activity inside the engine should also be measured. In order to calculate the heat transfer rate or heat flux through an IC engine, multiple temperature sensors on a single axis of penetration into a medium were required. During the early stages of this project an investigation into the numerous methods for measuring heat flux led to the multipoint temperature sensor method, however as commercially available sensors were not suitable for this application due to size constraints, it was required that a new sensor be designed and developed. The basic design specification for the sensor was that it should:

- Comprise of three measurement points over a distance of 4mm
- Withstand temperatures in excess of 200°C
- Have a maximum outer diameter in the region of 3mm

Four proposed designs were developed and manufactured, each of which required evaluation. Details of the evaluation experiments, the calibration process, installation method and positioning of the sensors are given in this chapter.

It was also important to understand the uncertainties associated with the measurement method used. Therefore the uncertainty analysis performed is also outlined in this chapter.

## 5.1 Sensor evaluation procedure

The suitability of each of the sensors had to be evaluated and compared not only to each other but to a reference measurement, for both the temperature measurement itself and the corresponding heat flux through the sensor. A test rig was designed to hold the four sample sensors plus two single point thermocouples as reference measurements.

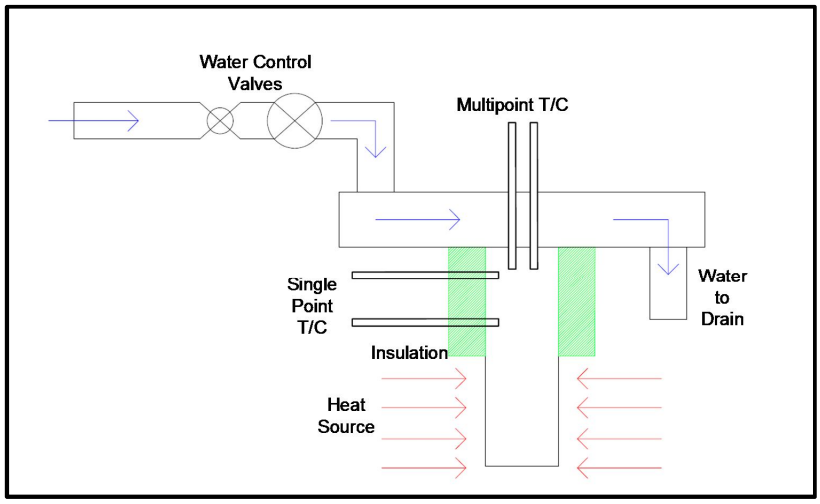


**Figure 5.1 – Multipoint evaluation experimental apparatus schematic**

The experimental setup used is shown in Figure 5.1. The test section was made from mild steel and was lagged with a glass fibre insulating material to promote one dimensional heat flow vertically through the section. Above the insulated section there was a water channel which was included in the apparatus to imitate the coolant jacket present in an engine and promote one directional heat flow to produce heat flux values which reflected values observed in previous engine studies, between 10 $kW/m^2$ and 70 $kW/m^2$ [123]. The water supply was adjusted using a gate valve, behind which was a ball valve so that the water supply could be switched off without adjusting the gate valve between tests. The multipoint sensors were sealed into the section to prevent coolant from passing down between the drilling and the sensor itself, affecting the recorded temperatures. This was also a concern for when the sensors were installed into the test engine. An adhesive sealant capable of withstanding high temperatures, which does not affect the temperature measurement, was therefore required (see Chapter 5 Section 5.4). The single point thermocouples were taken using 1.5mm k-type thermocouples installed in 1.55mm diameter flat bottom drillings employing the same adhesive method as that planned for the multipoint sensors, in order to ensure the most direct comparison. They were positioned with 20mm of separation to enable the reference

heat flux to be calculated over a larger distance than the multipoint sensors in order to help reduce the error by using a representative average heat flux. The calculated temperature gradient was used as a reference for the multipoint sensors to be compared against. The temperature readings were recorded using the test cell host system, where all the temperature channels had been recently calibrated. The heat source was capable of producing a maximum steady state temperature of 600°C with an error of 0.03°C as measured internally at the heater unit. It was not expected that the test section would reach this temperature due to losses through the insulation. The maximum expected cylinder wall temperature in the engine seen on previous instrumented engine blocks was in the region of 125°C. Therefore this would be acceptable for this evaluation experiment. Step changes of 50°C, 200°C, 400°C and 600°C were used as the temperature set points through the test and were reached by the heat source during the warm-up, shown in Figure 5.2. The figure is representative of the input temperatures rather than the measured temperature profile. At each of these temperatures the system was allowed to reach equilibrium.

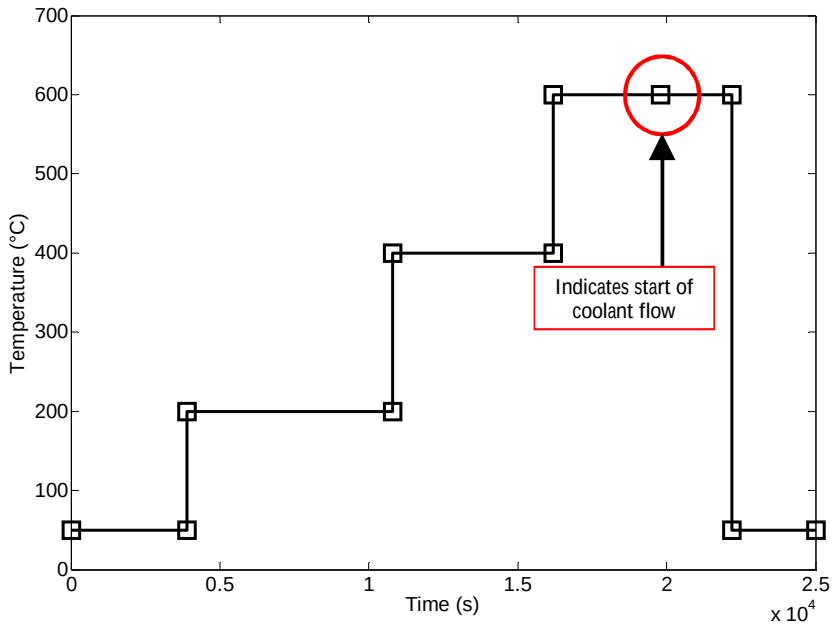


**Figure 5.2 – Input temperature set point profile for multipoint evaluation experiments**

The warm-up period of the test was performed with no flow through the coolant channel. At each of these set points the heater unit achieved the demanded temperature but the recorded temperatures in the test section were significantly lower. When the system had reached equilibrium the coolant was switched on. The temperatures were then allowed to settle before the calibrator temperature was reduced to 50°C to begin the cool down.

# Multipoint designs and experimental instrumentation

The general specification of the multipoint sensors was an outer sheath containing three single point 1mm diameter K-type thermocouples positioned at fixed depths [80]. It has been shown that accurate results with a separation of 6mm between the measuring points of a heat flux sensor can be achieved. However the cylinder wall thickness for the proposed production diesel engine was found to be less than 6mm at certain points. It was decided that the thermocouple junction depths would be 0mm (X), 2mm (Y) and 4mm (Z) from the tip of the sensor. Three thermocouples would be incorporated into each multipoint sensor to improve the accuracy of the calculated thermal gradient; in addition to providing a backup if one thermocouple was to fail. The overall diameter was to be in the region of 3mm and the sensor had to be capable of withstanding temperatures of up to 200°C.

## Multipoint sensor 1

Sensor 1 was produced to the above general specification, the design is shown in Figure 5.3. It consisted of three 1mm thermocouples positioned with the junctions at the appropriate separation, around which the sheath was backfilled with magnesium oxide [124]. The outer sheath was made from stainless steel and had a wall thickness of 0.5mm. The thin wall of the sheath will benefit the transient response of the sensor during testing. The incorporation of a single large pot seal will increase the strength of the sensor and make it much more robust. However the increased diameter and stiffness of having a single pot seal would have to be taken into account for the installation into the engine block as it would have to avoid the engine ancillaries.

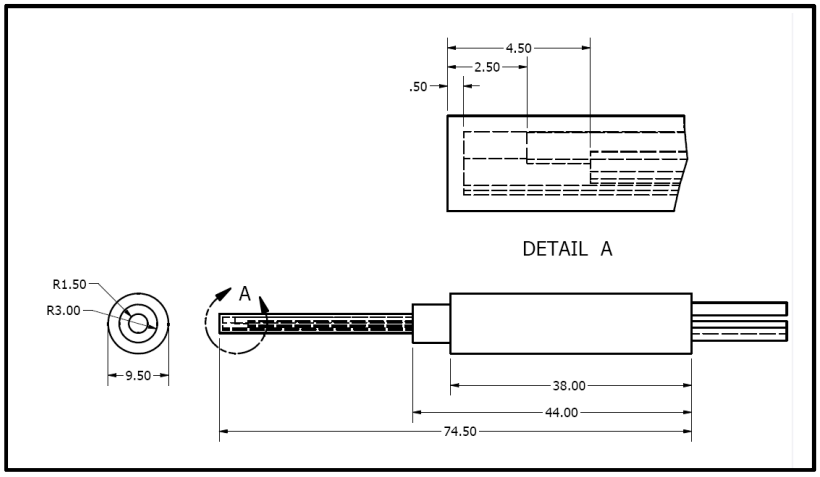


**Figure 5.3 – Multipoint sensor 1 design**

## Multipoint sensor 2

The design of sensor 2 shown in Figure 5.4 has an increased diameter of 4.76mm; this was recommended due to the vibration of the engine when running. It can be seen that the three thermocouple junctions are protruding from the tip of the sheath; this provided a guarantee that the thermocouple junctions were set at the correct separation. It would also allow good thermal contact with the measured surface if a conductive liquid metal sealant was used when installing the sensors rather than conduction required through the sensor outer body. However the increased diameter of Sensor 2 would prove difficult to install in the specified points in the engine block due to the space constraints externally with ancillary devices. The larger diameter may also impact the combustion chamber wall integrity.

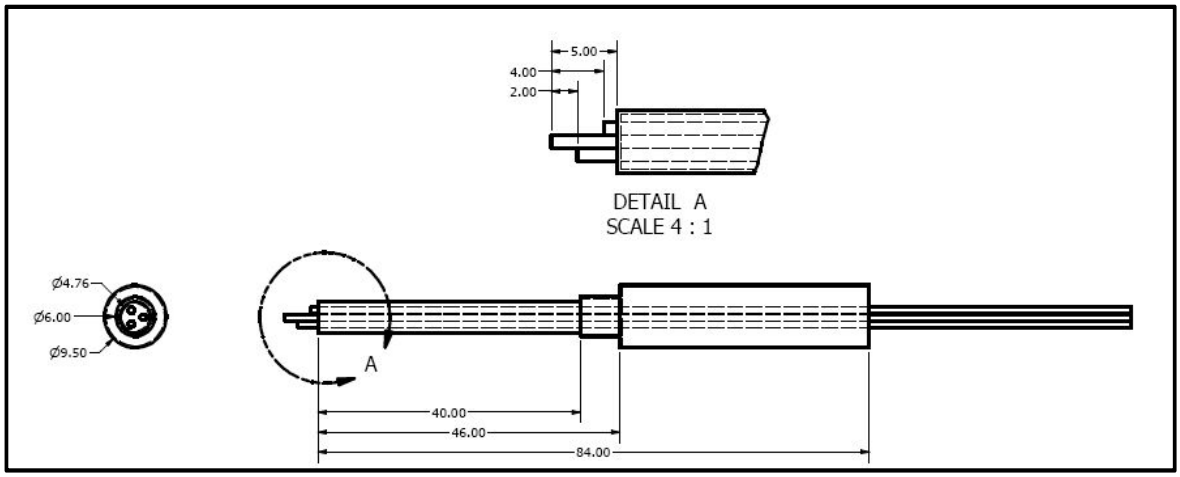


**Figure 5.4 – Multipoint sensor 2 design**

## Multipoint sensor 3

Sensor 3 was designed and manufactured to an American standard; therefore the outer sheath diameter was 0.125" (3.17mm). The sensor was backfilled with magnesium oxide to aid the thermal conductivity. The sensor had a rounded tip with a thickness of 1.5mm shown in Figure 5.5 which was not ideal for insertion into the cylinder wall, as depth was a vital criterion.

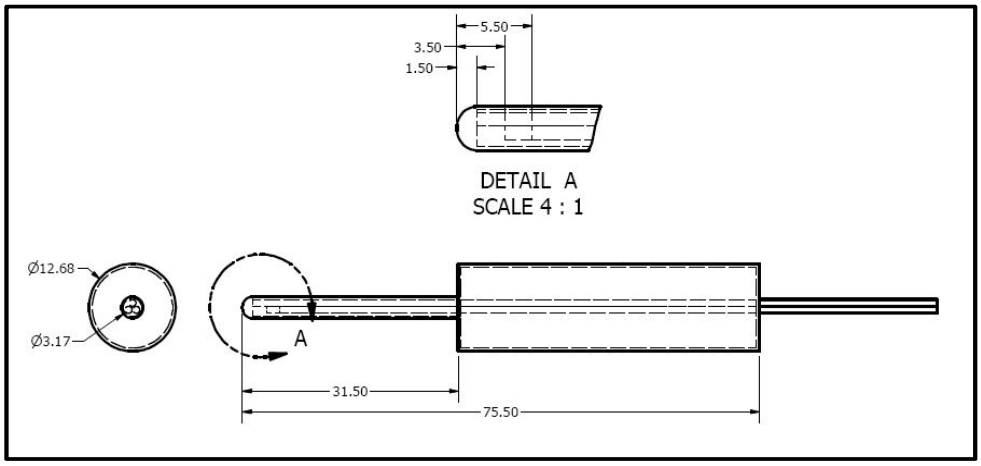


**Figure 5.5 – Multipoint sensor 3 design**

## Multipoint sensor 4

Sensor 4 illustrated a different approach to the general specification set out above. Instead of the large single pot seal utilised by the other three sensors with three extruding PTFE cables, the design consisted of a stainless steel sheath out of which each of the 1mm thermocouples separated to individual pot seals. Initially this design seemed much neater and compact, as there would be no large pot seal sat outside the engine, however due to the small diameter thermocouples protruding from the sheath it was much less robust and therefore there was an increased chance of failure through the period of testing. In addition the area surrounding the thermocouple junctions within the sheath was not backfilled with material which could have an effect on the results obtained.

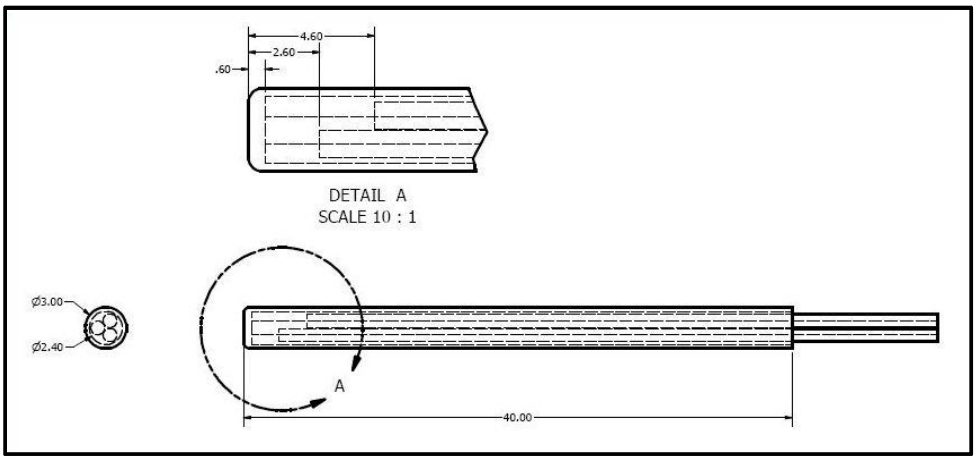


**Figure 5.6 – Multipoint sensor 4 design**

## Calculation methodology

The CP host system, which records all engine parameters and temperature data during experimental work, was also used for the sensor evaluation experiments. The system produces two file types, a trace file and a log file. The trace file contains all data from the initialisation of the test to its close, whereas the log file contains the specific log data which can be averaged over a time period. An importer and analyser were developed in Matlab to access the data files and calculate all necessary parameters.

The differential temperature method was employed to calculate the rate of heat transfer. Therefore the data was used to first calculate a thermal gradient through the metal. The heat flux was calculated using Fourier's one-dimensional law of conduction as the material thermal properties were known. This is therefore assuming one-dimensional heat transfer through the cylinder wall. In its simplest form a temperature gradient can be calculated from two temperature values $T_1$ and $T_2$, measured by thermocouples a certain distance apart, $\Delta x$, by using Equation (50).

$$\frac{\Delta T}{\Delta x} = \frac{T_1 - T_2}{x_1 - x_2} \tag{50}$$

The output from each multipoint sensor was made up of three separate temperature signals recorded at 1Hz to one decimal place. Some fluctuations were expected in the recorded temperatures due to the reduced accuracy and therefore the temperature signals were filtered using a simple zero-phase digital filtering process in both the forward and reverse directions. By filtering in both directions the filtered result shows no phase distortion. Due to having an array of three temperatures within the multipoint sensors a least squares regression line method was applied to the recorded temperatures. The heat flux could then be calculated using the gradient and the thermal conductivity of cast iron (45 W/mK) with Fourier's law of conduction shown in Equation (51). For the engine application the local coolant temperatures and the temperature gradient calculated through the cylinder wall can be used to calculate the convective heat transfer coefficients where appropriate using Equation (52). A similar method was employed to calculate the rate of heat transfer for the single point thermocouples; in this case the simple temperature gradient calculation shown in Equation (50) was used.

$$\dot{Q} = -kA\frac{T_1 - T_2}{x_1 - x_2} = -kA\frac{\Delta T}{\Delta x} \tag{51}$$

$$h_c = \frac{\dot{Q}}{A(T_{wc} - T_c)} \tag{52}$$

## Discussion of experimental findings and sensor evaluation

Figure 5.7 shows the temperature trace for Sensor 1, the step change in the calibrator demand temperature is clearly reflected in the measured temperatures. A maximum temperature in the region of 200°C was reached by the sensor during the testing process; the sharp drop in temperature is due to the cooling water being switched on. The flat region, once the coolant was switched on, was due to the calibrator temperature being decreased to 50°C. A clear temperature gradient is evident in the measured temperatures, as the distance from the sensor tip increases, the measured temperature reduces. The gradient was also found to increase as the calibrator temperature demand was increased, implying a steeper temperature gradient through the measurement section. As the separation between the thermocouple junctions is equal it would be expected that the temperature difference between each thermocouple would also be equal as the heat should be conducted at a constant rate. Figure 5.7 shows that this is not the case and this is further illustrated in Figure 5.8 where the cumulative difference, as well as the instantaneous difference between the recorded thermocouple temperatures is shown for Sensor 1.

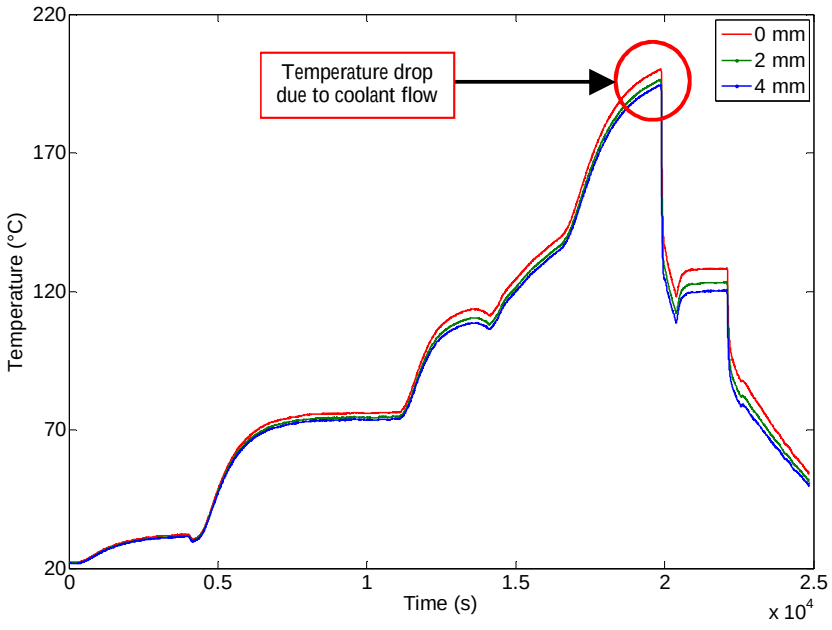


**Figure 5.7 – Temperature response of thermocouples within multipoint sensor 1**

The differences in the thermocouple readings were found to increase as the heat source temperature was increased, the temperature gradient through the sensor should be uniform between each pairing of measurement if the positioning and thermal conductivity were uniform. The difference found within this sensor was likely due to the reduced thermal conductivity of the magnesium oxide filling of the sensor in comparison to the mild steel test rig, which resulted in the tip thermocouple reading a higher temperature than would be predicted by extrapolation of the temperature gradient observed between the second two thermocouples. This is indeed what was observed in practice. The average temperature difference between the sensor at the tip, 'X' and the sensor 2mm from the tip, 'Y' was in the region of 2.5°C, whereas the difference between 'Y' and 'Z' (4mm from the tip) was in the region of 1.4°C. Additionally, positional inaccuracies in the placing of the three thermocouples within the probe would cause a small variation in temperature due to the rates of heat transfer through the sensor and therefore the distance from the heat source. If the separation of 'X' and 'Y' was greater than that between the 'Y' and 'Z' the error pattern would be as observed. Further investigation into this effect with the remaining sensors showed that it was the case for Sensor 2, where the difference between 'X' and 'Y' was greater than that between 'Y' and 'Z'. However the opposite was the case for both Sensor 3 and 4. The separation of the thermocouples in Sensor 2 can be measured as the thermocouples protrude from the sensor body. This implies that the difference measured in Sensor 2 was due to the reduced thermal conductivity of the liquid metal sealant.

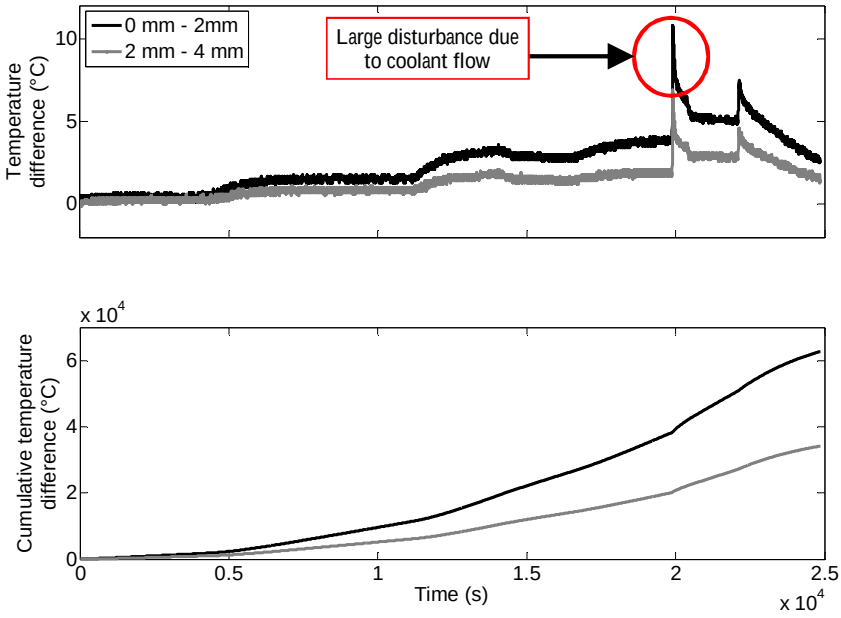


**Figure 5.8 – Cumulative temperature difference between the thermocouples within multipoint sensor 1**

Using Equation (51) the heat flux for each of the sensors was calculated and shown in Figure 5.9. The heat flux calculated from the single point thermocouples is also shown in Figure 5.9. It can be seen that all the sensors follow a similar trend throughout the test process. The traces shown in Figure 5.9 for the four sensors are much noisier than that produced from the single point thermocouples; this is due to the reduced distance over which the calculations were performed and the recorded data having been rounded to one decimal place in the data acquisition equipment. The effect of this quantization error[2] is increased when the temperature gradient is calculated using the difference between the two readings, in subsequent testing the capture accuracy was increased. The heat flux calculated from Sensor 2 was noticeably higher than that from the other sensors; indicating that the temperature difference across the measured section was greater than in the other sensors. This can be attributed to the liquid metal sealant used to install the sensor having a lower thermal conductivity, therefore reducing the rate of heat transfer through the area surrounding the protruding thermocouple junctions.

[2] The difference between the actual analog value and quantized digital value is called the quantization error. This error is due either to rounding or truncation.

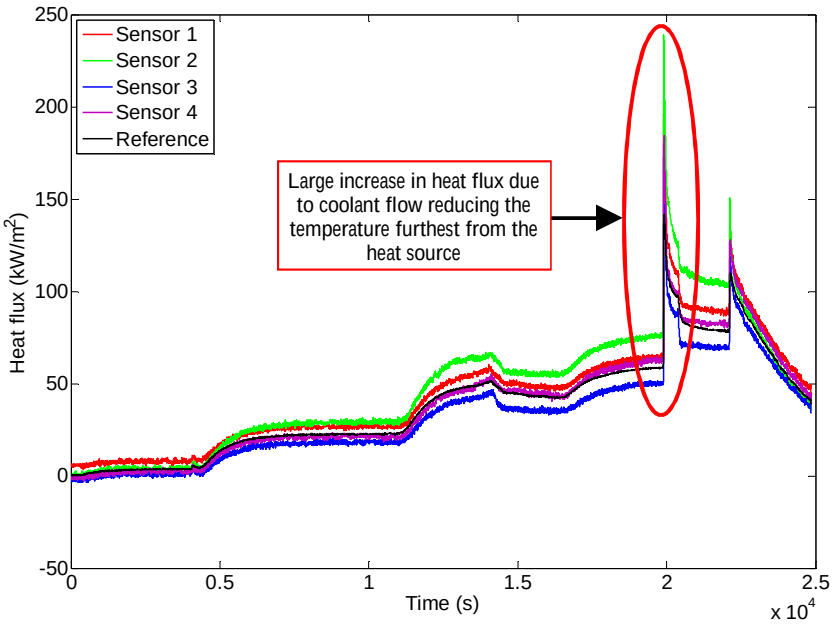


**Figure 5.9 – Calculated heat flux for all evaluated sensors**

In addition to the accuracy of the temperature measurement capabilities of each sensor, it was important to evaluate the mechanical characteristics of each of the designs. The sensors were to be permanently installed in an engine block in a manner which would lead to no leakage or oil and coolant contamination, whilst not affecting the measurement of a 'true' temperature. Each sensor therefore had to be robust enough to withstand a large amount of vibration, as it would have been extremely difficult to replace a failed sensor. Of the two types of construction seen in the four sensors, Sensor 4 was found to be the least robust with no support given to the protruding 1mm thermocouples from the 3mm sheath. Figure 5.10 shows the three temperature signals obtained for Sensor 4, it can be seen towards the end of the test that there was a large oscillation in the recorded temperatures for the middle thermocouple. For this period there was a loss in signal from the thermocouple, therefore these temperatures were not taken into account when calculating the heat flux.

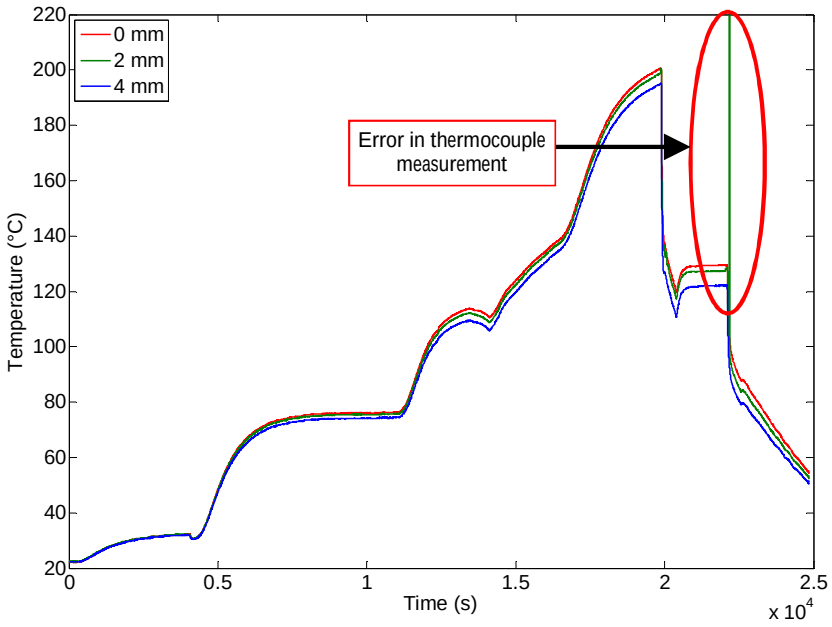


**Figure 5.10 – Temperature response of multipoint sensor 4**

The transient performance of each of the multipoint sensors was also an important factor as they were to be used over a transient drive cycle; therefore the dynamic response had to be fast and accurate. During the test procedure the coolant water remained off until the maximum temperature was achieved. When the coolant was switched on there was a significant increase in the heat flux through the test section due to the drop in temperature in the coolant channel. Figure 5.11 shows a closer view of the performance of each sensor when the coolant water was switched on. The offset between the sensors can be mainly attributed to the design of the sensors and the error in the internal construction, which have not been accounted for in this experiment. For each of the sensors a 10% of the peak point is shown in Figure 5.11. The reference response can be seen to be the slowest in reacting to the increase in heat flux; this will be due to the larger separation between the measurement points. Of the four sensors, Sensor 4 was the slowest to react, taking over 3 seconds longer than Sensor 1, this was attributed to the area surrounding the thermocouple junctions within the sheath being air filled rather than magnesium oxide as in the other sensors. Air is known to be an extremely good insulator causing the delayed response time. Sensor 3 illustrates the fastest transient response with a 10% rise in heat flux after 21 seconds compared with the reference heat flux of 32 seconds.

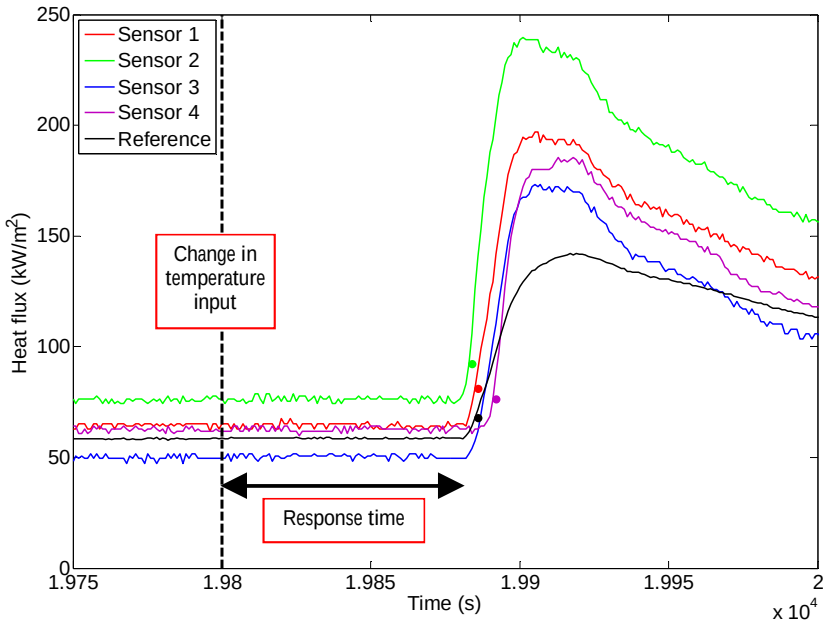


**Figure 5.11 – Transient response of all sensors to a step increase in source temperature**

Due to practical constraints on the sensor dimensions, and taking into account the measurement performances, the four proposed sensors were reduced to two. Sensor 2 had been designed with a larger diameter in order for it to withstand the vibration of the engine; however this meant that the wall integrity may be compromised when installed to within 2mm. Also with the thermocouples protruding from the tip of the sheath it would be more crucial to fill the void with a material with similar thermal properties to that of the engine block with no air pockets and this could not be guaranteed. Sensor 3 accurately followed the heat flux trend of the other sensors; however it consistently produced a much lower value of heat flux. On further investigation it was found that the change in temperature through the sensor was in the region of 30% less than that through the other sensors. This led to a heat flux that was on average 8.0kW/m$^2$ less than that calculated using the single point sensors.

The heat flux calculated from Sensors 1 and 4 as well as the reference heat flux are shown in Figure 5.12. In Figure 5.12 it can be seen that Sensor 4 overlaps the reference heat flux during the lower temperature areas of the test, however some drift is seen further into the test. Sensor 1 seems to have a consistent offset in the region of 4.5kW/m$^2$ from the reference heat flux.

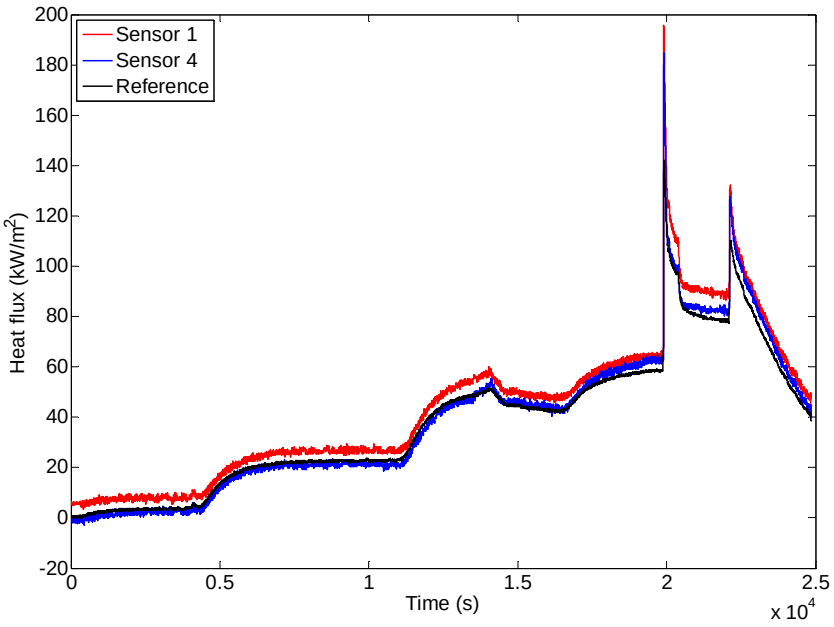


**Figure 5.12 – Comparison of sensor 1 and sensor 4 to the calculated heat flux from the reference single point thermocouples**

Figure 5.13 shows the heat flux data from Sensor 1 with an offset of 4.5kW/m$^2$ applied. The resulting heat flux trace follows the reference data closer than Sensor 4 and provides the most accurate measuring method. A summary of the attributes of the different multipoint sensors is presented in Table 6.

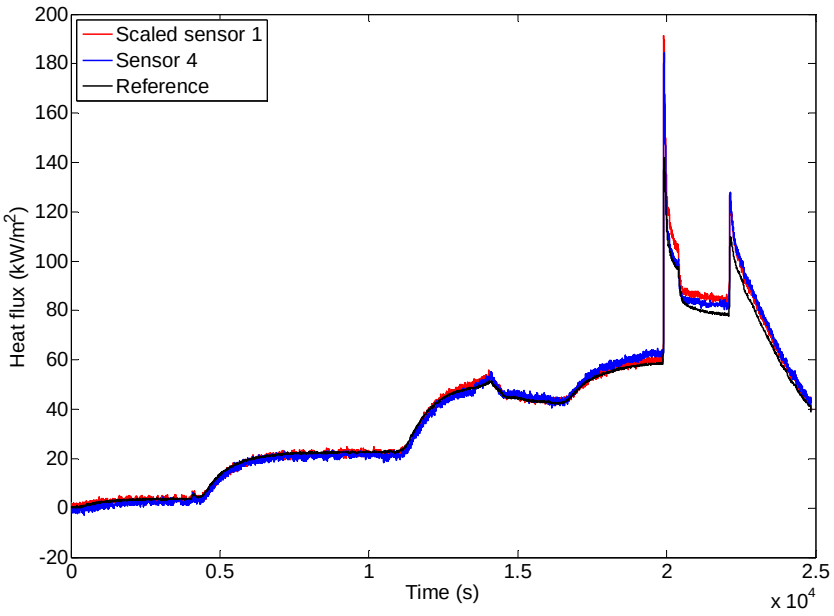


**Figure 5.13 – Comparison of scaled sensor 1 and sensor 4 to the calculated heat flux from the reference single point thermocouples**

**Table 6 – Multipoint sensor evaluation summary**

| Sensor number | Sheath diameter (mm) | Wall thickness (mm) | Positional inaccuracy (mm) | Backfill material | Transient response (s) |
|---|---|---|---|---|---|
| 1 | 3.0 | 0.5 | ±0.5 | Magnesium Oxide | 28 |
| 2 | 4.76 | 0 | N/A[3] | N/A[4] | 27 |
| 3 | 3.17 | 0.5 (1.5 from tip) | ±0.5 | Magnesium Oxide | 21 |
| 4 | 3 | 0.6 | ±0.5 | No material | 30 |

# Conclusion

All the multipoint sensors tested produced a good measurement of the heat flux through the test rig in comparison to the single point sensors. The quality of the heat flux estimates derived from the raw data was encouraging given the very small separation between the measuring points. It was found that the material surrounding the thermocouple junctions

[3] 0.5mm k-type thermocouples protrude from sheath.

[4] Thermocouples protrude form sheath. 0.5mm thermocouples will be backfilled with magnesium oxide as standard.

affected the response time of the sensor with an air filling resulting in a time lag in the region of 3 seconds, with the favoured medium being magnesium oxide. It was found that the difference between the thermocouple at the tip of the sensor and the second thermocouple was not necessarily equal to that between the second and third thermocouples. Two of the four sensors tested were found to have a greater temperature difference between the first and second thermocouples than the second and third, whereas the other two sensors were found to have the opposite. This uncertainty is a result of both the accuracy of the separation of the thermocouple junctions within the outer sheath and the effect of the reduced thermal conductivity of the filling medium. It was concluded that this characteristic was not ideal but could be reduced with calibration of each probe prior to installation in the engine. The evaluation procedure would be valid for a test rig made from another material such as aluminium or mild steel, however the calibration procedure requires a test piece made from a similar material to the experimental installation.

Taking into account the dimension constraints of the sensor and requirement that the sensor had to withstand engine vibration during future experimentation, as well as the results of the evaluation tests explained above, it was decided that Sensor 1 was the most suitable.

## *5.2 Multipoint sensor calibration procedure*

This section describes the calibration process implemented for each of the multipoint sensors prior to their installation into the engine. The multipoint design process highlighted the need for each of the sensors to be calibrated against a range of known heat flux and temperature conditions due to uncertainty in the position of the individual temperature sensors within the heat flux sensor. The calibration process was to ensure that the sensors could be accurately compared to each other, in addition to proving their functionality before being secured in the engine. This section details the experimental process undertaken and the data analysis technique developed.

### Experimental approach

The final design of the multipoint sensor is shown in Figure 5.14. It was designed to fit into a 3mm diameter drilling within the engine structure and to measure the radial heat flux in a 6mm thick section of a cast iron cylinder liner. Each sensor comprised of an array of three k-type thermocouples arranged on a common axis and separated axially by 2mm from each

other, around which the sheath was backfilled with magnesium oxide, the sensor was to be positioned 2mm from the combustion surface. Thermocouples occupy the majority of the space within the probe; with the packing material ensuring thermal contact and to support the outer structure. The outer sheath was made from stainless steel and had a wall thickness of 0.5mm. The thin wall of the sheath will benefit the transient response of the sensor during testing. A single large pot seal was incorporated to increase the strength of the sensor and make it more robust. The length of the probe from the pot seal was to be specified prior to manufacture and customized for each sensor to help avoid engine ancillary components.

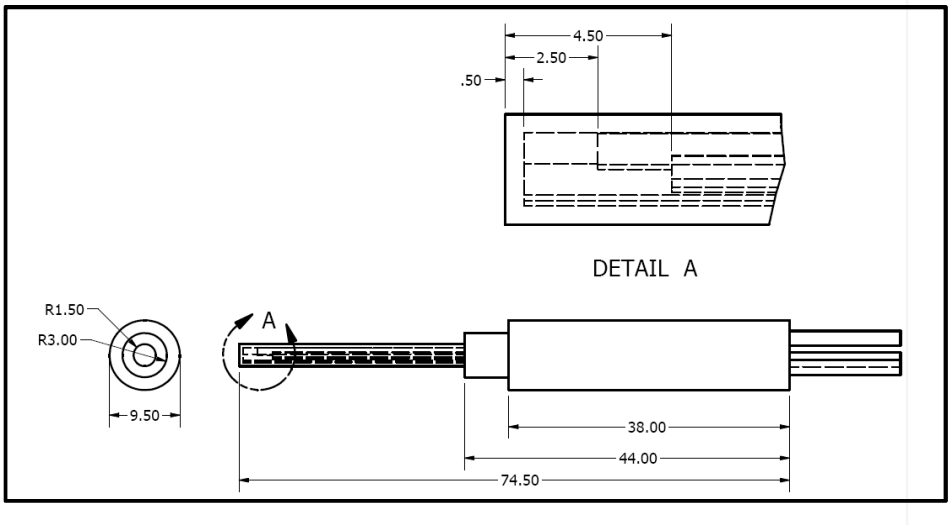


**Figure 5.14 – Selected multipoint sensor design**

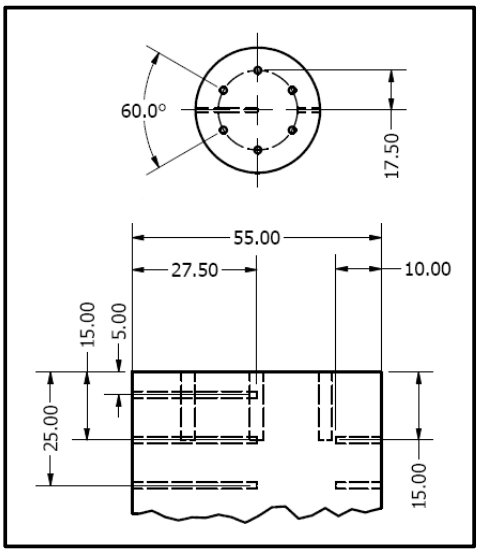


**Figure 5.15 – Detail of the multipoint calibration insert**

A calibration insert was designed to fit into the test rig used in the multipoint selection experimentation outlined above. The calibration insert was manufactured from cast iron to best replicate the material of the cylinder block, therefore the calibration results can only be applied in this application. The positional error within the outer sheath will be accounted for irrespective of the insert material, however the heat transfer through the sensor body will not. Best practice would imply that the calibration procedure must be repeated. Figure 5.15 shows the detail of the test insert, which consists of three K-type thermocouples embedded from the side of the apparatus to the centre of the insert with 10mm separation between each. In addition there are two further K-type thermocouples positioned at the same radial distance as the multipoint sensors. These two thermocouples were positioned to quantify any radial heat flow through the test section. The multipoint sensors were tested in two batches of six as twelve were required for the engine installation. Each group of six multipoint sensors were installed in the apparatus using a small amount of silicon sealant around the multipoint and coolant interface to prevent water from interfering with the temperature measurement. Each test was repeated to allow an average of the calibration factors to be calculated. The multipoint was inserted so that the thermocouple located at the tip of the multipoint was at the same depth as two of the single point thermocouples to allow for direct comparison of the recorded temperatures.

To allow the apparatus to reach a stable start condition the heat source was maintained overnight at 30°C. The water was switched on and allowed to flow prior to the start of the test. Once the apparatus had thermally stabilized the heat source demand temperature was increased to 600°C. Figure 5.16 shows the temperature response of a single point thermocouple within the test piece for the calibration test. The heat source remained constant throughout the test and the apparatus was allowed to reach near equilibrium over a period of 5 hours; there are small fluctuations in the temperature due to outside influences on the process water flow. Over this time a steady one-dimensional heat flow was formed through the apparatus. To ensure that one dimensional heat flow had been achieved a comparison was made between the single point thermocouples positioned at the centre of the insert and the thermocouples positioned at the same radial distance as the multipoint sensors. Figure 5.16 also shows that the temperature difference between the two thermocouples is minimal with the greatest difference observed as the insert was reaching a stable condition, where the central thermocouple was 1.2°C hotter. The difference gradually reduced to the region of 0.9°C.

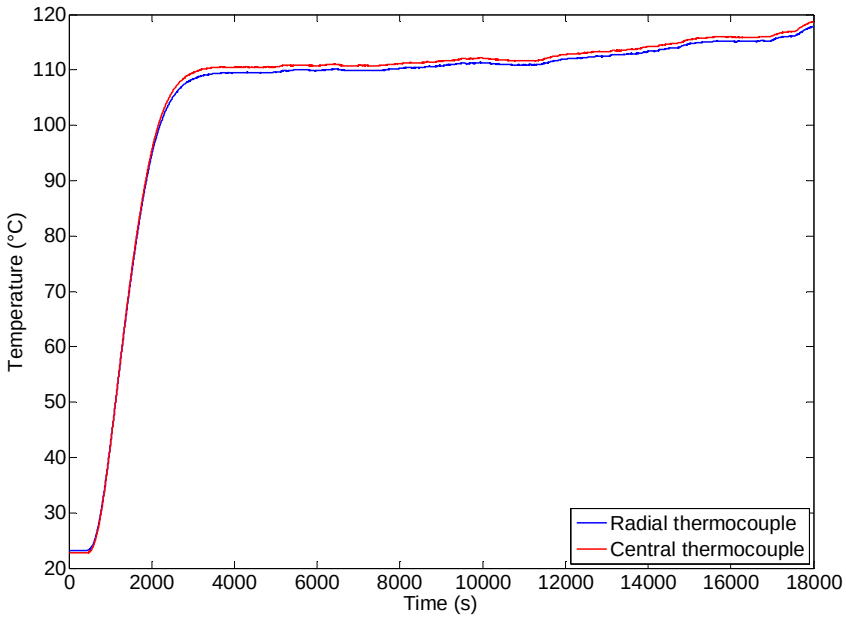


**Figure 5.16 – Calibration experiment temperature profile and comparison of radial temperature measurement to centrally located thermocouple**

The temperature gradient between the single point thermocouples was calculated using Equation (53), which was then used to calculate a predicted temperature for each of the thermocouples within the multipoint sensors using Equation (54).

$$m_S = \frac{S_A - S_B}{x_4} \tag{53}$$

$$m_{SX} = \frac{S_A - X}{x_1} \rightarrow X = S_A - (m_S x_1)$$

$$m_{SY} = \frac{S_A - Y}{x_2} \rightarrow Y = S_A - (m_S x_2) \tag{54}$$

$$m_{SZ} = \frac{S_A - Z}{x_3} \rightarrow Z = S_A - (m_S x_3)$$

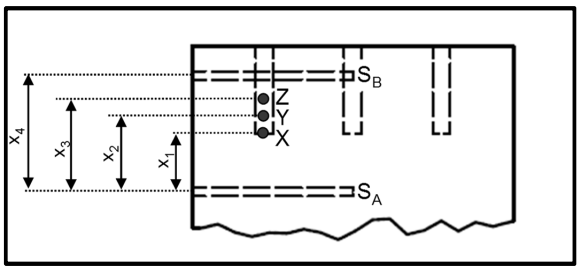


**Figure 5.17 – Multipoint calibration calculation diagram**

To obtain a gain and offset for each of the thermocouples within a sensor the predicted temperatures were compared to the actual recorded temperatures. This calibration procedure attempted to take into account the positional uncertainty of the thermocouples within the multipoint sensor and reduce the effect of the outer sheath of the sensor on the measurements.

# Results and discussion

Figure 5.18 shows an example of the predicted temperature data for thermocouple X within a single sensor compared with the recorded temperature for a calibration test. The figure is made up of a large number of 1Hz data points collected over 18000s. There is a very strong correlation between the predicted temperatures and the recorded. A sufficient temperature was achieved which reflects what was to be expected within the production engine. During the higher temperature region of this test some oscillation occurred in the recorded temperature due to a slight increase in the coolant flow, this explains the variation in the trend. An XY line is shown in Figure 5.18 which highlights that there is a linear correlation; however the predicted temperature is a maximum of 8°C greater than the recorded temperature through the temperature range tested.

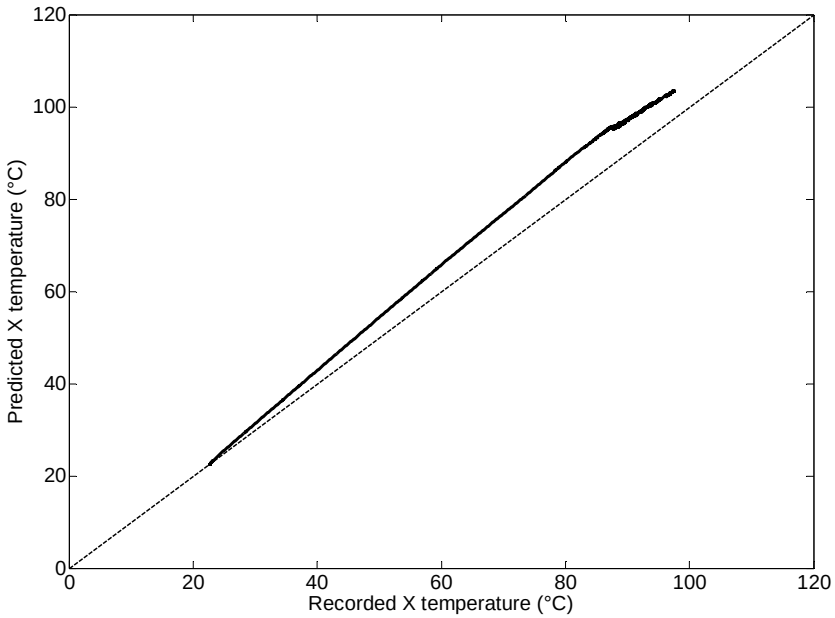


**Figure 5.18 – Example of data used to calibrate multipoint sensor – 18000 data points at 1Hz**

Figure 5.19 shows an example of the effect of applying the calibration gain and offset to each of the thermocouples within the multipoint sensor. The thermocouple temperature error has been included in the raw and single point thermocouple measurements. A temperature increase of 8°C from the raw data is clear for each thermocouple. A least squares linear regression has been applied to the raw temperature, thermocouple Y shows a significant offset from the calculated linear gradient, indicating a possible positional error of that thermocouple within the multipoint sensor. This error has been taken into account in the calibration and the three temperatures illustrate an improved linear relationship. The 8°C offset of the multipoint data to that of the single point thermocouples can be attributed to the sheath material insulating the thermocouples from the measurement material, as this value was consistent for all the multipoint sensors tested. The calibration process was designed to reduce the systematic error from the multipoint sensors and allowed them to be directly compared to each other. By comparing to a much larger temperature gradient the 'true' temperature measurement will also be improved. Further uncertainty analysis has been performed.

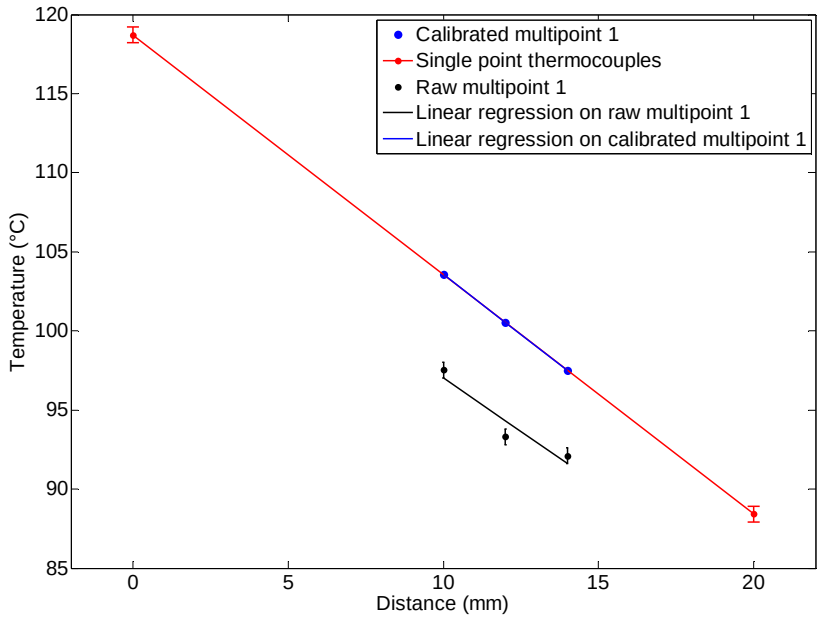


**Figure 5.19 – Impact of calibration on thermocouple measurements at 1200s of the calibration test**

## Conclusion

A calibration procedure for the multipoint sensors was required prior to their installation in the engine due to the positional inaccuracies within the sensor and the impact of the sheath material on the measured temperature within the multipoint sensor. A calibration procedure was developed using a rig designed to best replicate the conditions expected within the combustion chamber wall. The procedure resulted in a calibration factor for each thermocouple within the multipoint sensor to be applied in a post processing routine. The calibration factor drastically reduces the systematic error of the multipoint sensor by accounting for errors in the manufacturing process with respect to the measurement junction location within the sensor.

# *5.3 Measurement errors and uncertainty*

The calibration process aimed to reduce the systematic error introduced from the manufacture of the multipoint sensors as it is important to monitor and evaluate the possibility of error in any measurement process. This section outlines the different types of error, how they can be reduced and the process to calculate the propagation of error through a system.

Systematic error (i.e. from incorrect instrument calibration or the instrument accuracy, its ability to indicate the true value) is one of two different sources of error in any system; the second is random errors (i.e. mistakes or recording errors). Measurement error is defined in Equation (55) as the difference between the true value and the measured or observed value.

$$e \equiv x - x_{true} \tag{55}$$

Ideally a large number of results would be taken around a fixed value for an extended period of time in order to evaluate the accuracy of the measured value. These results could be presented in a plot of the frequency distribution around the mean value. This type of plot can be referred to as a probability density function and the area under the curve represents the probability that a particular value will occur. A typical frequency distribution of data from a measurement application can be represented as a normal distribution with the probability of values falling above or below the mean being equal. When this is the case the standard deviation can be used to determine the probability of obtaining a particular result [125]. However in engineering systems a large number of repeated results can prove to be a costly and time-consuming process. Therefore typically in engineering the "single-sample" approach is undertaken which does not allow for uncertainty to be calculated from multiple readings but means it must be estimated. In this situation the uncertainty relies on the judgement of the experimenter and previous knowledge, in addition to implementing best practice to minimise the introduction of errors. The uncertainty is based on the theory of multiple samples and can be expressed in a similar manner.

In this application the result, the temperature gradient, is derived from a combination of values determined from a number of individual measurements, each thermocouple within the sensor plus its location. Therefore there is propagation of uncertainty from the individual variables to the result. Methods have been proposed for determining the errors in a derived result from single-sample experiments by Kline and McClintock [126]. It was suggested that if a desired result was derived from *n* independent variables or simultaneous measurements [e.g. $R=R(X_1,X_2,\ldots,X_n)$ ] and $\omega_1, \omega_2,\ldots,\omega_n$ are the uncertainties of the independent variables, an expression for the uncertainty of the result can be given by Equation (56).

$$\omega_R = \pm\left[\left(\frac{\partial R}{\partial X_1}\omega_1\right)^2 + \left(\frac{\partial R}{\partial X_2}\omega_2\right)^2 + \cdots + \left(\frac{\partial R}{\partial X_n}\omega_n\right)^2\right]^{1/2} \quad (56)$$

In this experiment the thermal gradient through the combustion chamber wall is based on the temperature rise across the multipoint sensor ($\angle T$) and the change in distance from the combustion gases ($\angle x$). The calibration process previously outlined aimed to reduce the impact of the systematic error by comparing the output from the multipoint sensor to another measurement method, regarded as more accurate, uncertainty analysis of both will be performed here. The calibration process has not directly impacted the ability of the sensor to measure the 'true' temperature but it has improved the accuracy of comparing the measurements from one sensor to another.

The error associated with a k-type thermocouple was given as ±0.5°C and the positional error of the thermocouple within the sensor was given to be ±0.5mm (±0.0005m) [127]. Therefore the uncertainty values for the multipoint sensor are:

$\omega_{\angle T}$ = ±0.5°C
$\omega_{\angle x}$ = ±0.0005m

$$\omega_R = \pm\left[\left(\frac{\omega\Delta T}{\Delta T}\right)^2 + \left(\frac{\omega\Delta x}{\Delta x}\right)^2\right]^{1/2} \quad (57)$$

Substituting an average temperature variation, e.g. $\Delta T \approx 7°C$ and using the known thermocouple separation of $\Delta x \approx 0.004$m, then

$$\frac{\omega_g}{g} = \pm\left[\left(\frac{0.5}{7}\right)^2 + \left(\frac{0.0005}{0.004}\right)^2\right]^{1/2} = \pm 0.14 \quad (58)$$

Thus, the relative uncertainty in the temperature gradient is ±0.14 or ±14%. At high engine powers, where the temperature variation across the sensor is largest the uncertainty is reduced, e.g. $\Delta T \approx 22.2°C$, $\omega_g/g$ = ±0.13 or ±13%. This analysis has highlighted that as the engine power increases the thermocouple error has a reduced impact on the temperature gradient calculation uncertainty. This is a result of the measurement distance not changing

whereas the temperature range increases. These are both systematic errors and cannot be improved without altering the measurement method and implementing a more complex manufacturing procedure. The relationship of the uncertainty error to the temperature variation across the sensor is shown in Figure 5.20. The measurement uncertainty was also calculated for the single point thermocouples used in the calibration process and the thermal gradient error was found to be ±3%, further highlighting the impact of the measurement span. However this does help to support the positive impact of the calibration procedure on the accuracy of the multipoint temperature measurements. Assanis et al. found that coaxial thermocouples capable of measuring transient temperatures within accuracy of 98% would still lead to up to 25% errors in the measurement of peak surface heat flux [128]. These errors were found to be caused by the reaction time of the thermocouple in this application however the magnitude of error was similar. Uncertainty analysis can also be applied to the temperature sensors longitudinally down the cylinder. For an average temperature difference across the sensors and employing an appropriate positional uncertainty, the relative uncertainty of the temperature gradient was found to be ±0.09 or ±9%.

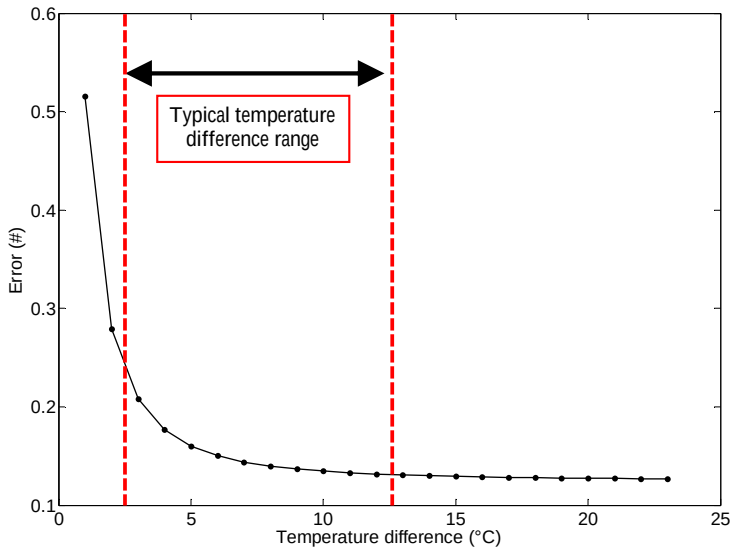


**Figure 5.20 – Heat flux measurement uncertainty for the range of temperature differences across the multipoint sensor**

The occurrence of random errors was mitigated by undertaking a small number of repeats of each of the experimental programmes and some basic statistical analysis of the raw data being completed; this has been detailed in Chapter 6.

An example of the impact of this uncertainty at low engine power conditions, i.e. when the temperature difference across the sensor is small, is the calculation of a negative temperature gradient where one is not present. The propagation of the uncertainty in the thermocouple temperature measurement is shown in Figure 5.21. Example measured data was used to show the possible location of the measured temperature signal within the possible uncertainty limits, illustrated by the dashed box. The red line shows the smallest gradient and the blue line shows the highest. The uncertainty in location for the inner thermocouple is only in one direction due to the thermocouple being located at the tip of the sensor body. An uncertainty of this level could lead to negative gradients being calculated at low engine power conditions when one is not present. Figure 5.22 illustrates graphically what would be required to produce a true negative temperature gradient through the cylinder wall. A bulk coolant or outer temperature far greater than the temperatures measured within the wall would be required due to the boundary layer adjacent to it.

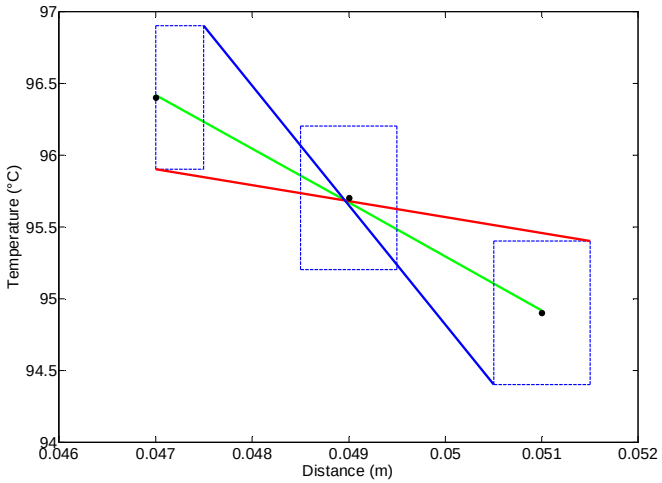


**Figure 5.21 – Temperature gradient uncertainty analysis**

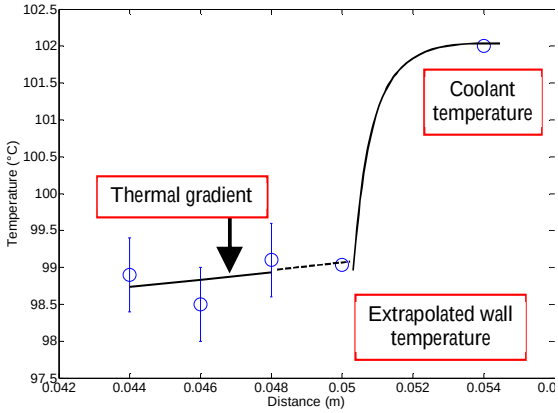


**Figure 5.22 – Visual representation of required temperature measurements to achieve a negative temperature gradient**

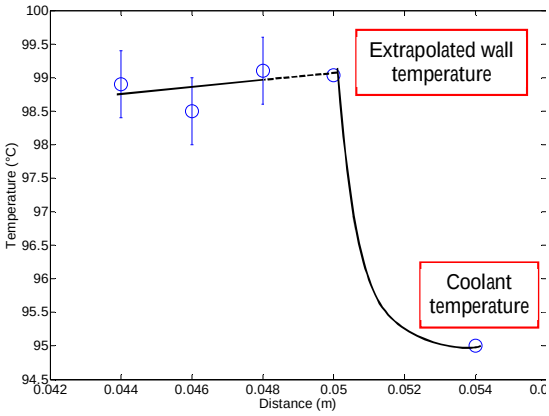


**Figure 5.23 – Uncertainty causing a negative temperature gradient to be calculated**

Figure 5.23 shows a negative gradient which in turn would produce a negative heat flux, however if the inaccuracy of thermocouples is taken into account (±0.5°C) then the gradient of this line could be altered to produce a positive gradient, changing the extrapolated wall temperature also. This would illustrate a ±100% error in the calculated temperature gradient and is shown in Figure 5.20 to require a temperature difference of less than 0.5°C. Errors of this type are more likely to occur at low heat flux conditions as discussed earlier. A number of processes were employed to the experimental program data in order to minimise this error, these included the calibration process and an inspection of the raw temperature data.

## *5.4 Multipoint Installation adhesive*

An investigation into a fixing method for the sensors was performed as the sensors were required to withstand an extensive testing program and a number of engine configuration changes. There were a variety of fixing methods available for the sensors. A large number of temperature sensors utilise mechanical fittings such as BSPT fittings as they allow for the sensor to be replaced in the event of a failure and they also provide a fluid tight seal. A custom mechanical fitting used to install thermocouples into the crank shaft caps of a similar engine by Nottingham University is shown in Figure 5.24. The fitting consists of a small section of hypodermic needle down the middle of a threaded insert similar to that used by Alcock et.al for their traversing thermocouple [3]. Mechanical fittings are the preferred type of fixing, however, often due to space restraints it is required to use adhesives or puttys. For these reasons a mechanical method would be least desirable so an investigation into an appropriate adhesive was completed; which involved a market survey and evaluation process.

There were a variety of adhesives available, each designed for a specific task, dependent mainly on curing and operating conditions.

**Figure 5.24 – Thermocouple mechanical fitting used by Nottingham University**

In addition to fixing the multipoint sensors in place the adhesive was required to secure each of the five crank shaft caps with three thermocouples in the following locations:

A. Oil film temperature between the shell bearing and crank shaft
B. Inner Surface Metal temperature (1mm from Inner Surface)
C. Outer Surface Metal temperature (15mm from Inner Surface)

Thermocouple 'A' penetrated through the main cap and shell bearing into the oil film; therefore it was exposed to high pressures and temperatures. A location exposed to pressurised oil has the inherent risk of becoming dislodged which could result in engine failure due to producing an oil leakage path. Thermocouples 'B' and 'C' were not exposed to the increased pressure but were required to remain in position to measure accurate temperature values. It was important that the adhesive was tested to pressures which exceeded those that would be expected during running and to expose the adhesive to oil.

## Experimental approach and hydraulic test procedure

The chosen adhesive, Loctite™ 620 was designed specifically for the bonding of cylindrical fitting parts, where it was required for the product to cure in the absence of air and was capable of withstanding shock and vibration loading. The adhesive was hydraulically tested to best replicate conditions in the engine, which required the design and manufacture of a test piece. It was necessary for the test piece to be easily integrated into a pre-existing test circuit available at the University of Bath. Another prerequisite for testing was that if the adhesive were to fail, the test insert would be kept from entering the oil circuit and possibly

damaging components downstream. The adhesive contact area was designed to replicate that in the crank cap and is shown in Figure 5.25. The outlet was positioned close to the insert so that if a failure of the adhesive was to occur the insert would remain in the void of the test piece. From the manufacturer's technical data sheet a bond gap of 0.2mm diameter was used.

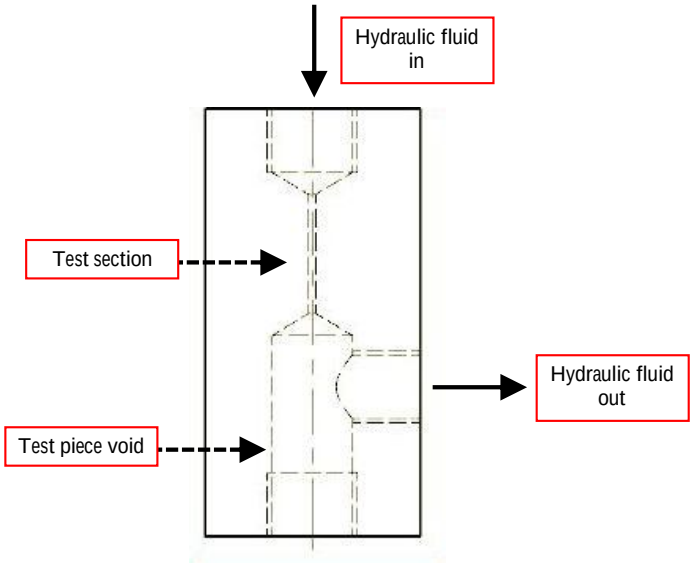


**Figure 5.25 – Adhesive test piece design**

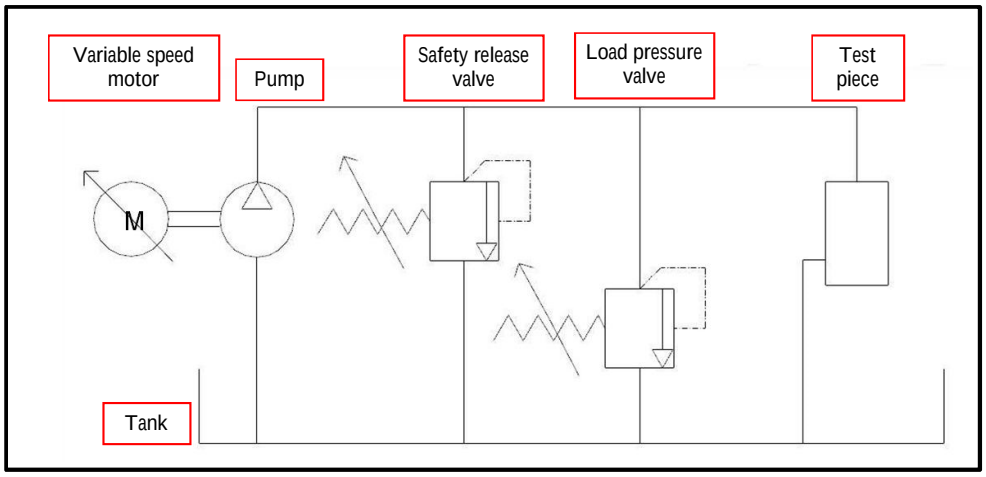


**Figure 5.26 – Hydraulic circuit for adhesive evaluation**

The hydraulic test circuit that was used is shown in Figure 5.26. Initially the load pressure valve and test piece were disconnected from the circuit allowing the safety relief valve cracking pressure to be set. As a load pressure of 50bar was required, the safety relief valve cracking pressure was set at 60bar. Once reconnected the load pressure valve was initially fully open allowing flow through the circuit. By restricting flow through the load pressure valve, pressure on the test piece was increased; if the adhesive were to fail a drop in pressure

would be experienced as oil was able to flow through the test piece. The pressure was maintained at 50bar for an extended period of time then cycled between 25bar and 50bar; the cyclic loading aimed to dislodge the test insert. If no failure was evident the load pressure would be further increased to 100bar.

**Figure 5.27 – Hydraulic test rig showing variable speed motor and pump**

## Discussion of results and conclusions

A flow rate of 4 l/min was established using the variable speed motor and pump and the pressure upstream of the load pressure valve was increased to 50bar. This pressure was maintained for 300 secs, and then cycled from 25 to 50bar for 15 repeats. During this time the oil flow rate increased by 0.21 l/min, this was due to the oil temperature rising by 5°C and the oil viscosity reducing. The safety relief valve cracking pressure was then set to 120bar to allow the load pressure to be increased. With increased pressure it was more efficient to increase the flow rate to 6 l/min. The load pressure was subsequently increased to 100bar and maintained for a further 300 secs. During the test there was no drop in load pressure; therefore the test insert was not dislodged. If failure had occurred a drop in load pressure would have been expected as the oil would have dislodged the test insert allowing flow through the test piece. Due to no flow through the test piece initially, it was expected that no oil would have been present on the outlet side of test piece. However on inspection the cavity on the outlet of the test piece contained oil. Further investigation into the physical connections used in the test circuit, shown in Figure 5.26, revealed that the oil in the outlet could have been due to backflow in the system from a 'Tee-Piece' in the return leg to tank. A further gravity leakage test was performed to prove that the adhesive had sealed around the insert. The test piece was cleaned thoroughly and oil was left in the inlet section of the

test piece. If the test section was sealed there would be no change in the oil level in the inlet and no evidence of oil would be found in the outlet side. It was found that the adhesive had formed a complete seal. This test also proved that oil in the test piece was due to backflow.

The adhesive, Loctite™ 620 performed as expected. It was capable of withstanding pressures far greater than expected in the running engine and produced a complete seal around the insert. If similar testing was required in the future, a check valve would be placed in the outlet side of the test piece which would prevent the back flow of oil into the test piece cavity.

## *5.5 Multipoint and thermocouple positioning*

This section will describe the position of the additional instrumentation installed on the engine for the purpose of the thermal investigation. A typical engine installation consists of a large number of sensors used to monitor the engine operating conditions during an experimental programme. Variables which are typically monitored include inlet and exhaust gas temperatures and pressures, engine temperature, oil temperature, intake air mass flow rate, fuel mass flow rate, coolant temperature, coolant flow rate at various points around the circuit and test cell ambient temperature. This instrumentation is designed to monitor the health of the engine during the experimental programme. In addition to this instrumentation, the multipoint sensors and a large number of thermocouples were installed. With such a large number of sensors a lot of care and precision was taken in routing the cables around the engine in order to improve the life expectancy of each of the sensors. The cables required heat shielding from any components where temperatures would exceed 125°C. The individual position of the sensors was designed to offer a strong understanding of the spatial temperature variation and to allow heat flux to be calculated over a wide range of operating conditions.

### Engine block

The engine block instrumentation consisted of 12 multipoint sensors and 19 single-point thermocouples. The multipoint sensors were installed in the combustion chamber walls whilst the thermocouple positions were designed to measure metal, oil and coolant temperatures. When designing the position of the sensors, it was essential to have no

sensors penetrating through the oil circuit, except where oil was the measurement medium, therefore eliminating the risk of cross contamination of coolant and oil, in addition to reducing the risk of an oil leak which could lead to a catastrophic failure of the engine.

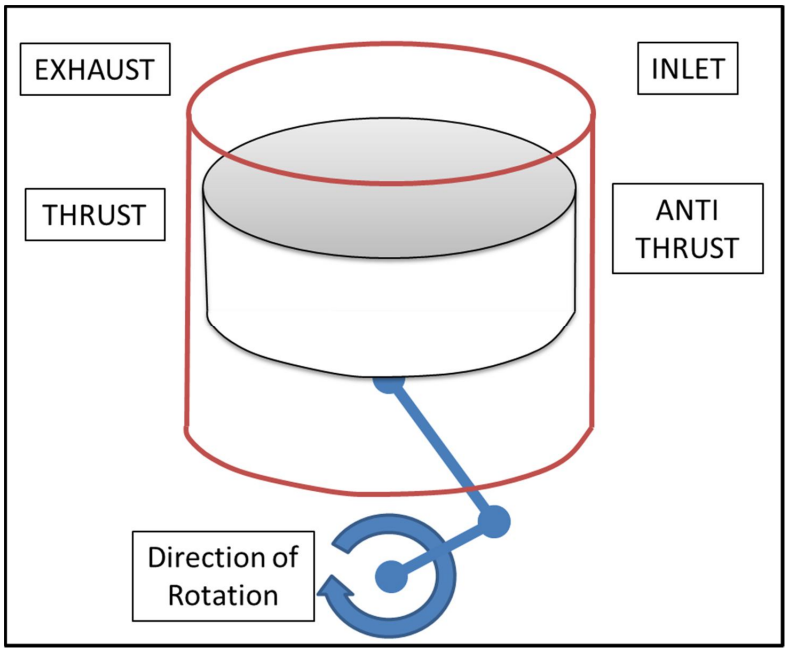


**Figure 5.28 – Diagram illustrating thrust and anti-thrust sides of cylinder bore**

Multipoint sensors were installed on both the exhaust and inlet sides of the engine. The reason behind this was to understand the difference, if any, of each side of the piston. The nature of the piston movement with relation to the crankshaft means that during each stroke there is a horizontal component to the force on the cylinder wall, this is commonly known as the thrust and anti-thrust sides. During compression the pressure within the cylinder will be opposing the piston motion, in Figure 5.28 this will cause the piston to be pushed against the right hand side of the bore (inlet side). In the power stroke the combustion process would be forcing the piston down, with the con-rod opposing this motion. In this situation if the motion was stopped mid-stroke the piston would be being pushed towards the left hand side of the cylinder (exhaust side). As the greater pressure is exerted during the power stroke, the exhaust side of the test engine is regarded as the thrust side.

The position of ancillary components and the shape of the engine block dictated that the instrumentation would be focused on cylinder 2 with further sensors located on cylinder 3 for comparison. The sensors were designed to provide a one-dimensional temperature gradient so therefore it was important that they were installed perpendicular to the combustion chamber. The internal structure of the engine block also influenced the

installation location of each of the sensors; therefore a second block was sliced into a number of sections to understand the cast structure. The block was sectioned vertically between each of the cylinders and at the midpoint of each of the cylinders, resulting in six sections. From this an understanding of the shape of the coolant jacket and the associated metal thicknesses was achieved. It was found that the cylinder had on average a 7mm wall thickness; however in some regions it reduced to 5.8mm which was taken into account in the sensor design. Figure 5.29 shows the position of the piston at both top dead centre (TDC) and bottom dead centre (BDC); this influenced the vertical position of the sensors. It was decided that four sensors would give adequate resolution down the length of the cylinder with three sensors covering the combustion chamber portion of the cylinder and an additional sensor below the top of the piston when at BDC. The coolant jacket was also found not to be equal on each side of the cylinder due to the coolant passageways to the cylinder head shown in Figure 5.29. Therefore at these locations the coolant flow pattern would be different due to the geometry.

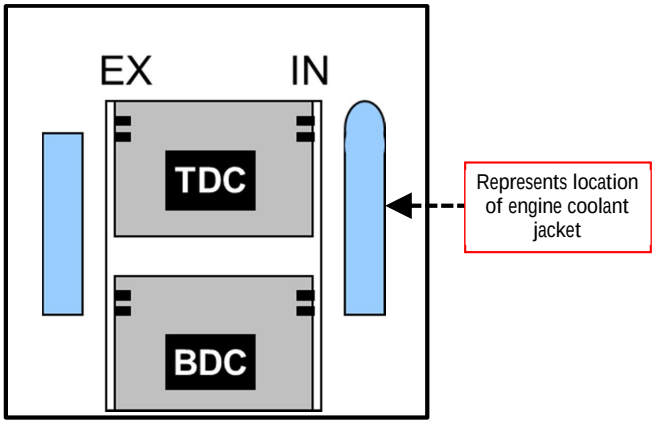


**Figure 5.29 – Representation of piston position within the cylinder**

Figure 5.30 shows a schematic of the sensor positions. The engine block was divided into four layers, 8mm, 60mm, 97.2mm and 160mm from the head gasket or top deck. The red markers indicate the multipoint sensors. The multipoint sensors which penetrated the coolant jacket each had an associated local coolant temperature thermocouple. The reason for the local coolant thermocouple was highlighted during a preliminary study, when calculating the coolant side convective heat transfer coefficient, it was found that using the average of the engine inlet and outlet coolant temperatures introduced a potential for error due to a very small difference between the wall temperature and the coolant temperature [123]. The green markers indicate the position of the inter-bore single-point thermocouples. It was not possible to install multipoint sensors in these areas as the heat transfer would not

be uniform in a single direction, but it was important to measure the temperature in these regions as there was restricted coolant flow due to the shape of the coolant jacket.

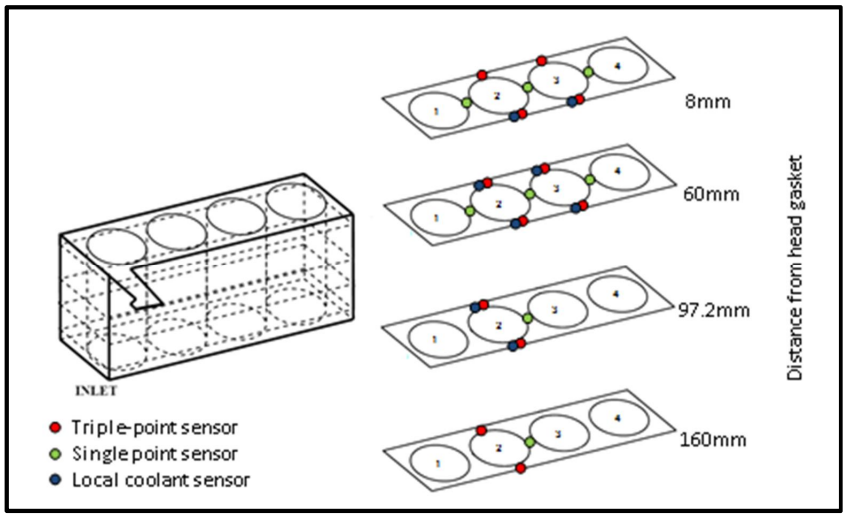


**Figure 5.30 – Cylinder block multipoint and inter-bore thermocouple positions**

Figure 5.31 shows the multipoint sensor positioning relative to the coolant jacket down cylinders 2 and 3. It shows the sensor positions down the length of the bore and illustrates their position with respect to the piston at both extents of its stroke. The sensors penetrated to a depth of 2mm from the combustion chamber inner surface and the holes were drilled with a flat bottom drill in order for the sensor to achieve the best contact with the metal surface.

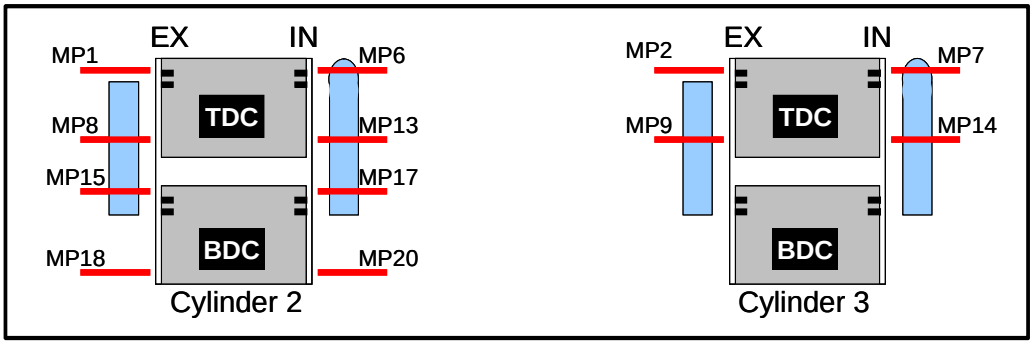


**Figure 5.31 – Multipoint sensor positions in cylinders 2 and 3**

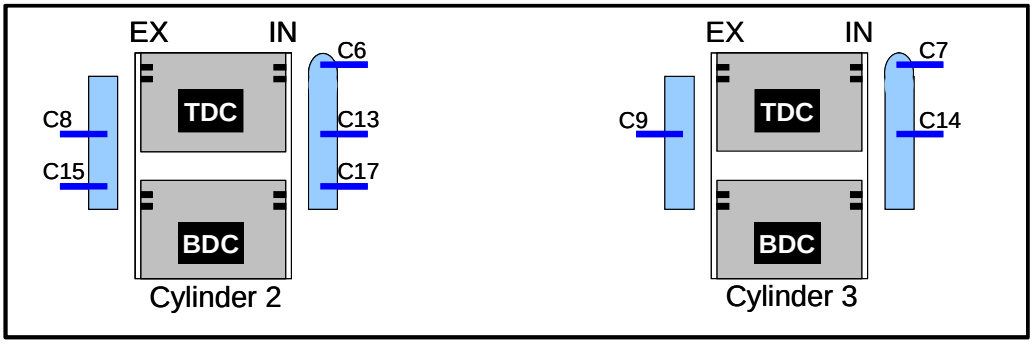


**Figure 5.32 – Local coolant thermocouple positions in cylinders 2 and 3**

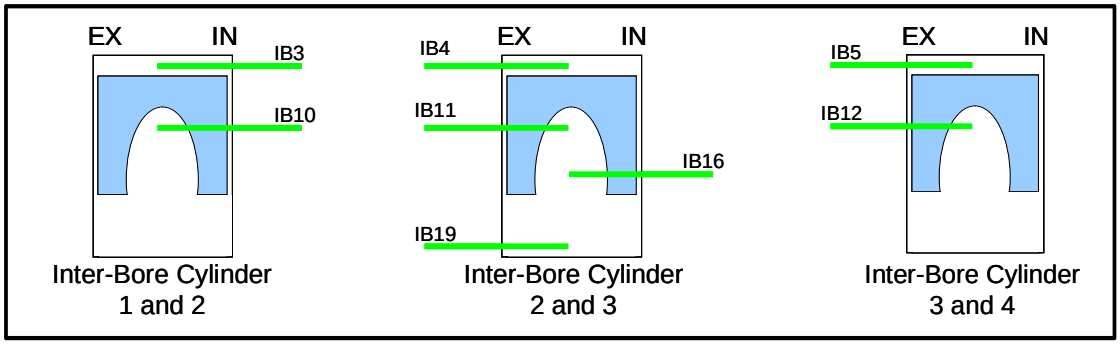


**Figure 5.33 – Inter-bore thermocouple positions**

Figure 5.34 shows an engine slice with a typical multipoint sensor install, this is only representative of the experimental install rather than an exact replica.

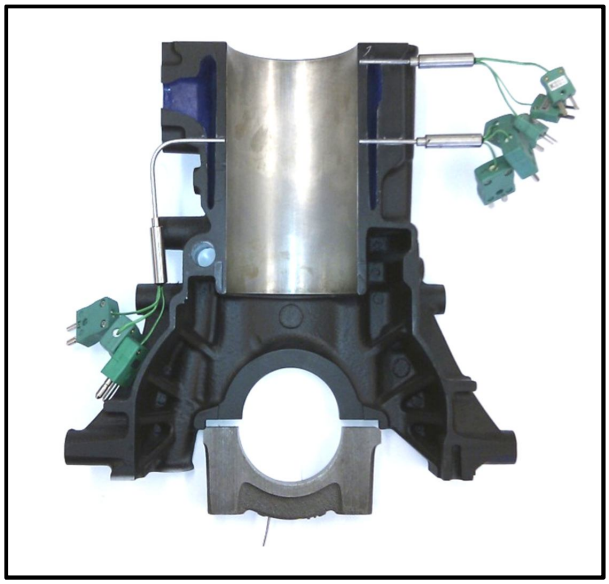

**Figure 5.34 – Example of instrumentation installed into a cutaway engine section**

All the engine instrumentation was subject to a large amount of vibration during the experimental programme, in addition to a number of engine build modifications which included component changes and coolant configurations; these had the possibility of causing damage to the instrumentation. Therefore it was important that the instrumentation was

sufficiently supported and the cables were routed in a manner so that the risk of damage was reduced, an example of this is shown in Figure 5.35.

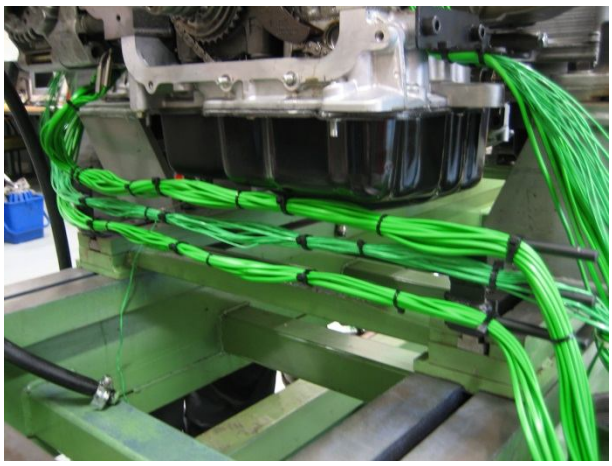

**Figure 5.35 – Thermocouple cable routing from multipoint sensors and crank cap instrumentation**

Once the sensors had been installed in the engine and the adhesive had been allowed to set, the engine was pressure tested to ensure that there were no leaks before the engine was rebuilt. A flat metal plate was bolted to the top deck of the block and a water feed was connected to the coolant inlet manifold. A system pressure of 4bar was reached and held whilst each of the sensor penetrations was observed.

## Main journal bearings and crank caps

Single point thermocouples were installed in each of the five crank caps. The aim of each of these thermocouples was to measure:

- Oil film temperature between the shell bearing and crank shaft
- Inner Surface Metal temperature (1mm from Inner Surface)
- Outer Surface Metal temperature (15mm from Inner Surface)

Figure 5.36 and Figure 5.37 show the three thermocouples installed in the crank caps with the shell bearing in position and with the shell bearing removed respectively. The central thermocouple penetrated the cap and protrudes into a hole in the shell bearing; this thermocouple was designed to measure the temperature of a small amount of oil which would accumulate in the hole, to give a representative temperature of the oil being used to lubricate the journal bearing. Crankshaft journal bearings operate in the hydrodynamic regime where the eccentricity of the rotating shaft allows an oil film to form. To ensure the

depth of this thermocouple was equal for all crank caps and that it did not interfere with the crankshaft, a mock cap was used as a depth gauge when installing the thermocouple. The other two thermocouples were drilled to 1mm and 15mm from the inner surface in order to calculate a thermal gradient through the cap. The outer surface thermocouple was installed at an angle of 26° from vertical on the exhaust side of the engine, which would be on the opposing side to the higher forces put on the bearing during the power stroke. The loading on the shaft and bearings is a result of inertia forces of the moving piston and the gas load from the compression, combustion and pumping events. The journal bearings were manufactured from aluminium with a slight eccentricity to allow oil to penetrate under the crankshaft. The greater the eccentricity, the greater the crank cooling and longevity, however at low speeds this can cause a drop in bulk engine oil pressure. The oil pressure in the main bearing has been shown to rise during the compression/combustion cycles of the adjacent cylinders and was measured to be 160MPa on a 1.4litre diesel at 4500 rpm [129].

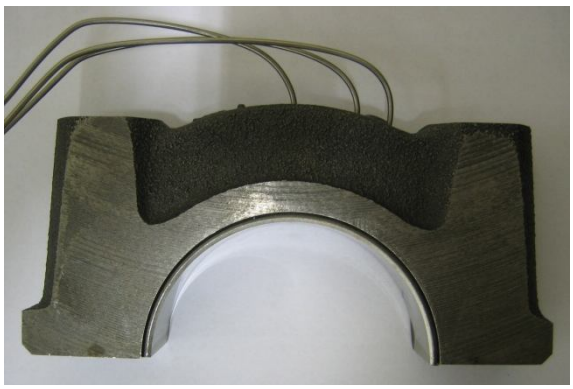

**Figure 5.36 – Crank cap instrumentation with shell bearing in position**

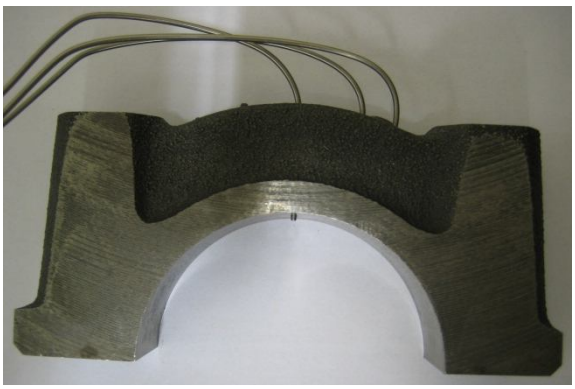

**Figure 5.37 – Crank cap instrumentation with shell bearing removed**

The thermocouple cables were routed out through the ladder frame and engine block interface as shown in Figure 5.38.

**Figure 5.38 – Crank cap thermocouple cables routing out through ladder frame and cylinder block interface**

## Cylinder head

Temperature sensors were also installed in the cylinder head to monitor oil and metal surface temperatures. Figure 5.39 shows a surface thermocouple installed in the cylinder head. It was positioned on the web between cylinder 2 and 3 and was designed to measure the metal surface temperature. The thermocouple consisted of a copper disc on which the hot junction was formed. Therefore the temperature reading is of the disc, rather than the cylinder head surface. This made the thermal contact between the disc and the surface crucial for accurate measurements. An equivalent sensor is also located on the exhaust side of the cylinder head. In addition to these sensors, thermocouples were positioned to monitor the oil temperature along its path through the cylinder head; these included the oil feed to the head and the oil groove temperature in the camshaft bearings on both the inlet and exhaust sides. The camshaft bearing measurement points were located in small pockets in the camshaft seats, shown in Figure 5.40. The groove is designed to feed oil around the plane bearing so will show a representative oil feed temperature to the bearing without interfering in the engine operation. These measurement points were located in camshaft bearings 1 and 5 on both the inlet and exhaust camshafts, thereby showing the oil temperature soon after delivery from the engine block and at the furthest point from the feed to the cylinder head.

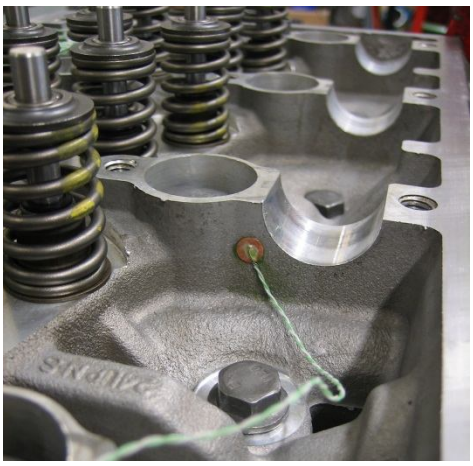

**Figure 5.39 – Surface thermocouples installed in the cylinder head**

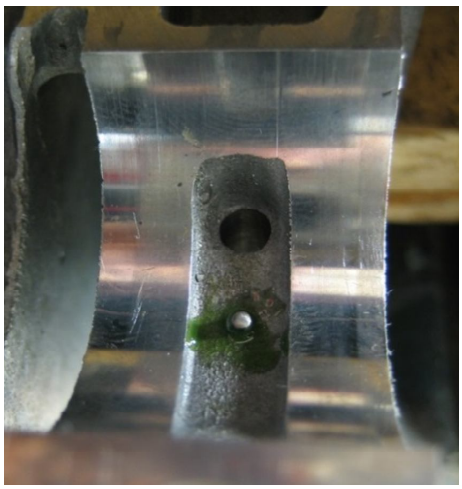

**Figure 5.40 – Thermocouple installed in oil feed groove to camshaft bearing**

## *5.6 Chapter summary and conclusions*

The method used to measure the heat transfer within the engine has been discussed in this chapter. The design and evaluation of a number of measurement devices was undertaken and the findings have been given, along with an analysis of the inherent uncertainties and the steps which have been taken to mitigate them. There were a number of key outcomes from this chapter which have been listed below:

- The assessment of the four multipoint temperature sensor designs led to one which was considered to be, experimentally robust, have an acceptable transient response of less than 3 seconds and capable of measuring a wide range of heat fluxes.

- The requirement for a calibration process was highlighted during the evaluation process and was implemented on all multipoint sensors prior to installation in the candidate engine, due to some inaccuracies in the location of the measurement point within the sensor body. The process aimed to reduce the systematic error in the thermal gradient measurement but uncertainty analysis of the sensor was still undertaken.

- The uncertainty in the temperature gradient was found to be dependent on the temperature difference across the sensor with a range of uncertainty from ±14% to

±28%, the majority of experimental work was performed in the region of ±14% error. Therefore at high engine powers the sensor accuracy was improved.

- A suitable installation method was researched and it was found that an adhesive allowed for the sensors to be secured in position whilst maintaining a liquid seal preventing any leakage of coolant. A Loctite™ 620 adhesive was successfully pressure tested prior to the installation in an engine.

- Twelve multipoint sensors and nineteen k-type thermocouples were installed in the engine block, with further thermocouples located in the crank caps and cylinder head. The location of all measurement points was devised to give an optimal understanding of the heat distribution throughout the engine without having to make any significant alterations to the engine architecture.

# Chapter 6. Experimental procedure and results

The aim of this chapter is to analyse and discuss the measured data from each experimental phase. The first experimental phase was the motored operation of the engine; this was completed to establish base levels of engine friction.

The second phase investigated the steady state operation of the engine at a number of operating conditions. The analysis aims to establish a detailed understanding of the effect of both engine speed and load on cylinder wall temperatures and rate of heat transfer. Also included in this section is the calculation of crank angle based heat transfer coefficients for evaluation and comparison with averaged heat transfer rates from measured data obtained from the multipoint sensors.

The third section aims to understand the effect of a number of adjustable actuators on the coolant and oil circuits on the wall temperatures and rate of heat transfer through the cylinder walls over transient drive cycle experiments.

## *6.1 Motored operation and friction measurement*

Motored tests were undertaken using the A.C. dynamometer at fixed speeds by cutting the fuel injection to the engine. The engine was initially fired until a thermal equilibrium was reached, however the lack of combustion during the measurement period will cause significantly lower in-cylinder temperatures which will impact the local lubricant viscosity. The lower in-cylinder pressures will also reduce the loading of the piston rings on the liner, and the loading of the crank shaft bearings and valve train. These inaccuracies have to be considered when evaluating the measured data. The motored tests were completed across the full engine speed range from 1000rpm to 4000rpm at intervals of 500rpm. At each engine speed condition 200 cycles of combustion data were recorded and the mean cycle calculated. There are a number of established correlations for predicting the total friction

mean effective pressure of an engine from the measured maximum cylinder pressure at each engine speed; the correlations were discussed in Chapter 3 Section 3.3. A comparison between the established correlations and the measured data is shown Figure 6.1.

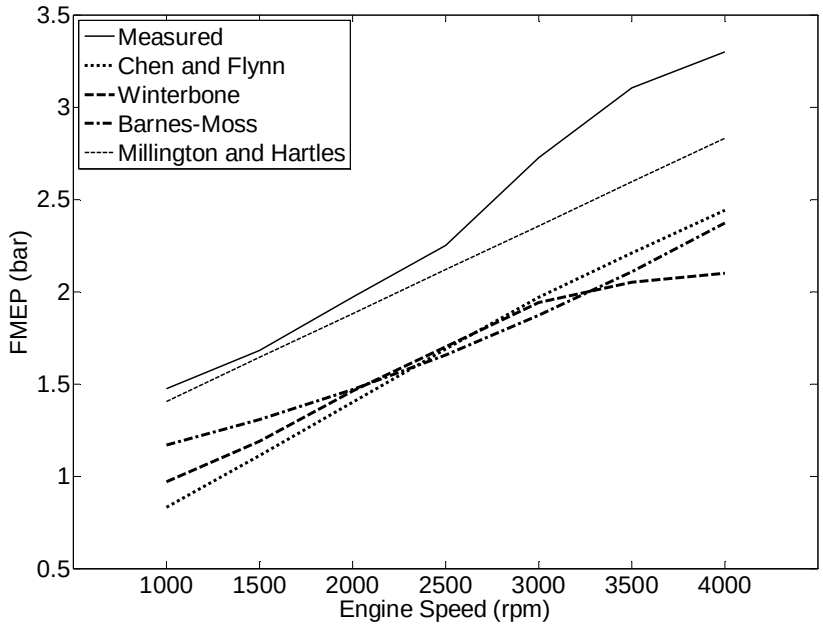


**Figure 6.1 – Friction mean effective pressure calculated using established correlations**

The correlations are shown to predict a lower $FMEP_{tf}$ compared to the measured numbers implying that the frictional losses of the experimental engine are greater than the engines used to develop the correlations. The correlations were all developed over twenty years ago with significant engine developments and additions being implemented since; this may have therefore increased the auxiliary loading. Auxiliary items on this engine include a variable flow oil pump, coolant pump and alternator. A method of isolating the effects of each component is to perform a friction teardown on the engine. This involves removing the loading from different components systematically whilst measuring the effect on the torque required to motor the engine across the speed range, thereby quantifying the load from each component. This process was not performed in this case due to time constraints, therefore only a measurement of the overall friction load is available. The closest correlation was found to be that by Millington and Hartles which was developed for diesel engines under motoring conditions ([130] via [2]). This shows strong agreement below 2500rpm, however the measured data shows a sharp increase in FMEP above this point, which is not reflected in any of the correlations. The Winterbone correlation shows the opposite effect above 3000rpm ([131] via [2]). The coefficient $C_1$ in the Heywood correlation can be determined

from experimental data and $c_m$ is the mean piston speed (m/s). Heywood found that mean piston speed gave better correlation than engine speed for the squared term [132]. A comparison of the motored data to the Heywood correlation is shown in Figure 6.2 where $C_1$ was equal to 89.

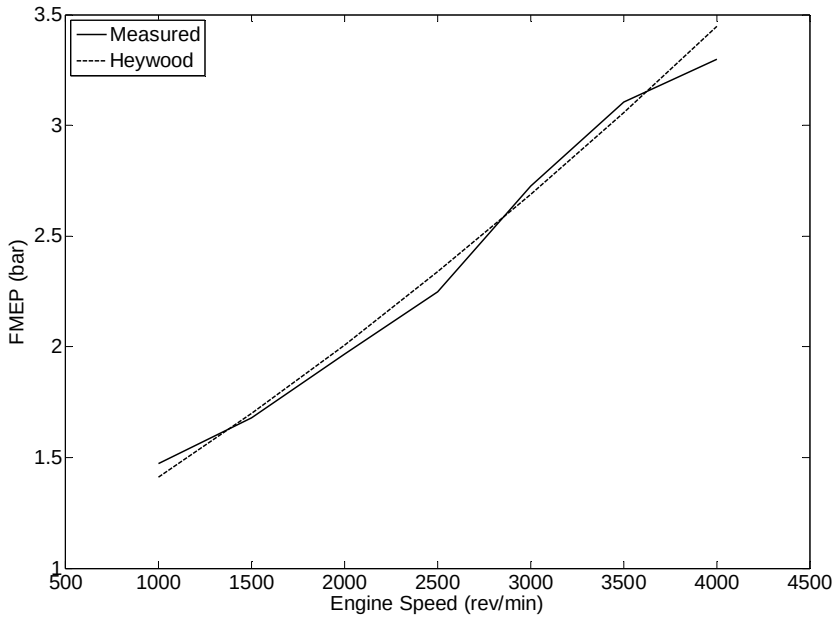


**Figure 6.2 – Heywood FMEP correlation**

The average motored cylinder pressure traces for each engine speed are shown in Figure 6.3. The highest maximum cylinder pressure was achieved at 3000rpm and was 59.5bar. The exhaust valve opening shows an increase in the in-cylinder pressure under some conditions due to the turbine obstruction in the exhaust system preventing the gas flow out of the cylinder as the exhaust stroke begins. There is an increase in the in-cylinder pressure during the valve overlap period as the piston is at TDC as the fresh charge begins flowing into the cylinder. The motored cylinder pressure data was used in the calculation of the gas side convective heat transfer coefficient when using the Woschni correlation.

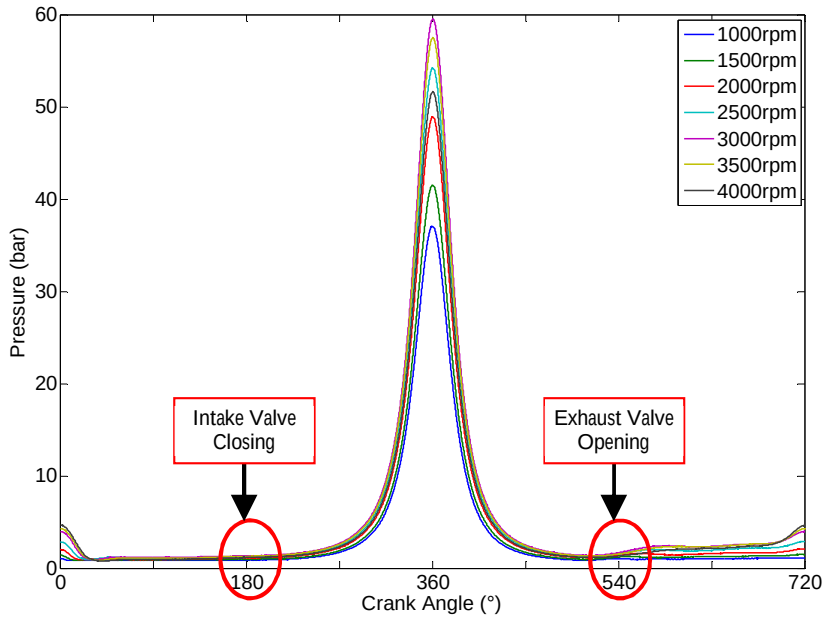


**Figure 6.3 – Average motored cylinder pressure for engine speed range**

## *6.2 Steady state thermal investigation and heat transfer coefficient evaluation*

The second series of tests were performed at steady state. The aim of the steady state test work was to understand the relationship between the temperatures down the cylinder and the rate of heat transfer to the operating condition of the engine, i.e. the engine torque and speed. The task of fully understanding this relationship across the complete torque and speed ranges of this engine would be very large, an area of greater interest was the New European Drive Cycle as this was the legislative cycle used to gauge the engine's performance and emissions levels for vehicle standards.

### The determination of the steady state operating conditions to evaluate the transient drive cycle

The New European Drive Cycle (NEDC) is shown in Figure 6.4, traces of vehicle speed, engine speed and engine torque are shown against time. The vehicle speed is the given criteria for the drive cycle and the speed and torque are determined by the vehicle inertia and gear ratios. The drive cycle is split into 2 phases, the 'Urban' phase and the 'Extra-Urban' phase, phase 1 and 2 respectively. Phase 1 is designed to represent inner city driving with a

number of accelerations, decelerations and steady state periods. Whereas phase 2 is designed to replicate a number of short higher speed cruises, such as dual-carriageway driving. Phase 1 can be further broken down into four repeats of the same conditions, also shown in Figure 6.4.

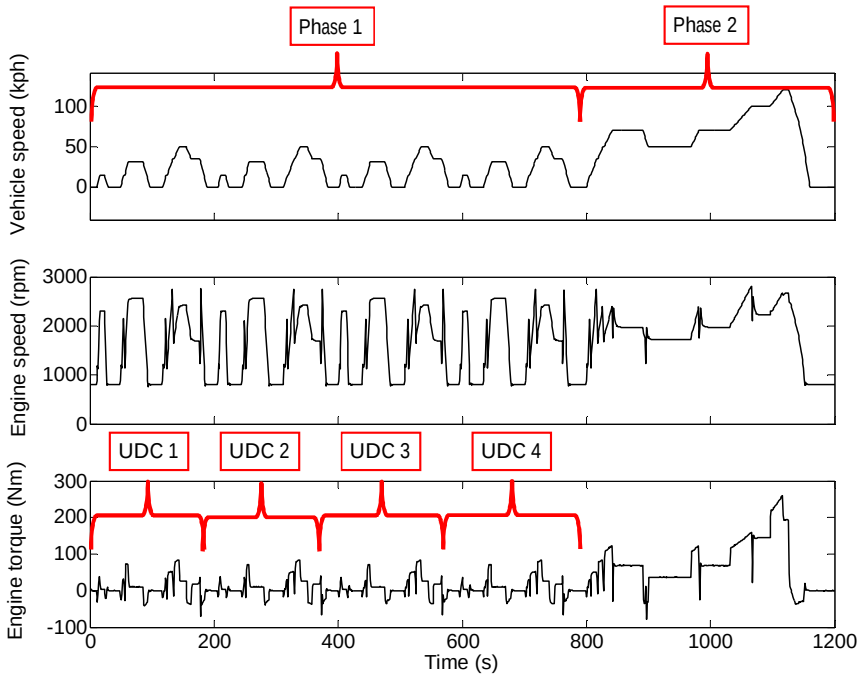


**Figure 6.4 – New European Drive Cycle specified vehicle speed and equivalent target engine speed and load for experimental engine in vehicle**

The drive cycle torque and speed is shown in relation to the limiting torque curve of this particular engine in Figure 6.5. The drive cycle does not exceed an engine speed of 3000rpm and has a peak torque of 259.1Nm, whereas the limiting torque curve peaks at 375Nm and the engine has a maximum speed of 4500rpm. This shows the limited engine performance used in the drive cycle and, from this it was decided that the steady state testing would be focused on the NEDC envelope in which the behaviour of the heat transfer was considered to be much more important for current engine designers, particularly with respect to fuel economy and $CO_2$ emissions improvement. However improvements at part load may be detrimental to full load cooling so therefore they cannot be regarded as mutually exclusive. An approach was developed to produce a number of steady state running conditions which would give an understanding of the heat transfer across the NEDC operating envelope.

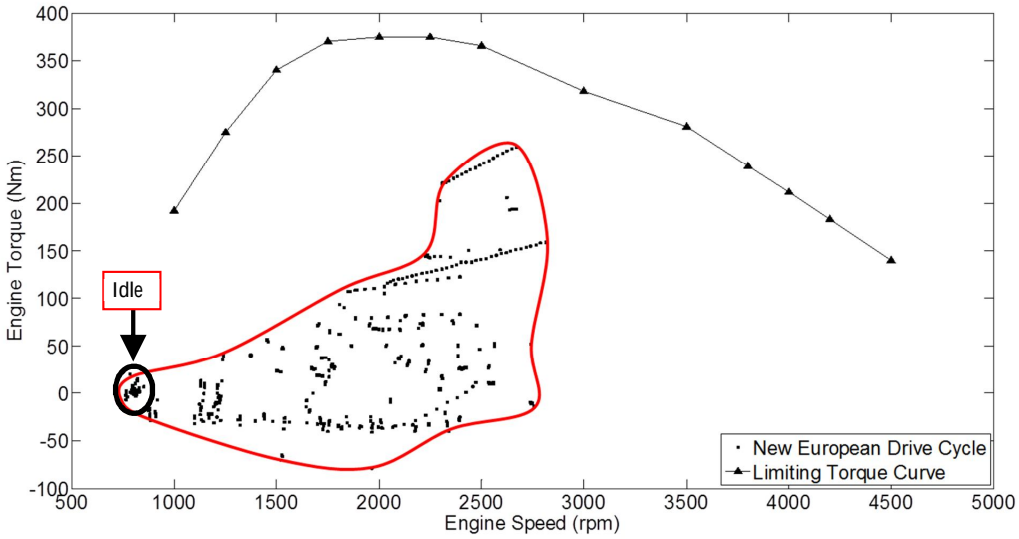


**Figure 6.5 – Limiting torque curve and NEDC operating envelope**

The data used in Figure 6.5 was measured at a frequency of 1Hz as used in the vehicle simulation for transient testing. The cycle includes a large number of periods where the engine speed is changing; for the purposes of the steady state evaluation all deceleration conditions, i.e. negative torque points were discarded as under these conditions the engine was not firing so would not be considered for this study, therefore would not be contributing to the heat generated and cannot be compared to steady state operation. The remaining operating points are shown in Figure 6.6.

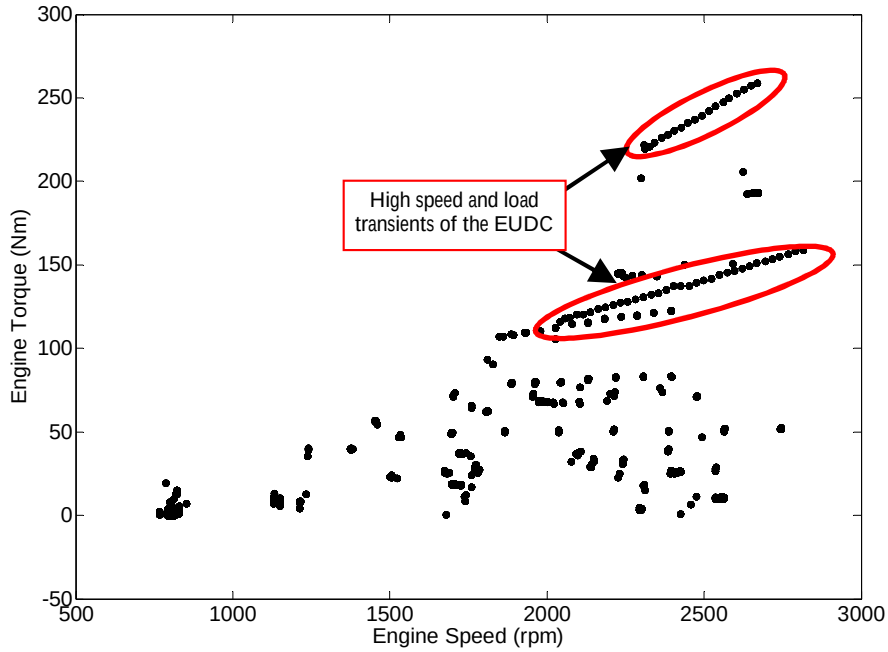


**Figure 6.6 – NEDC operating envelope without deceleration events**

Figure 6.6 consists of 879 operating conditions. The high speed and load transients during phase 2 of the drive cycle are clearly visible and have been highlighted. In addition the cycle contains a considerable number of idle periods resulting in a high number of conditions in the region of 800rpm and 0 to 25Nm. In order to reduce the number of conditions, the full operating envelope of the NEDC was divided into discreet speed and torque segments. These segments were equally spaced at 250rpm and 40Nm steps. A similar method has been applied in industry and can be described as a minimap test approach. The discretization resulted in 26 steady state conditions for this investigation. Each of these steady state conditions had a weighting factor which was dependent on the number of operating conditions within that particular segment. The sum of all weighting factors was equal to 1. The weighting factors were specific to this engine and vehicle combination but the same method could be employed for any powertrain or drive cycle. An approach of this nature allows for the number of steady state operating conditions to be dramatically reduced and hence reducing the overall test time.

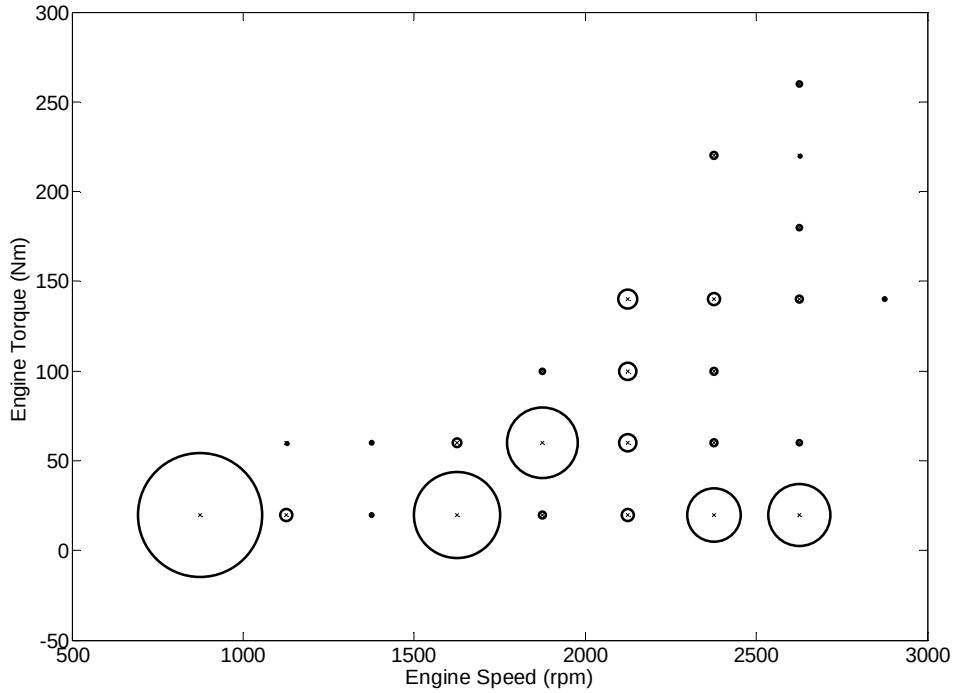


**Figure 6.7 – NEDC operating conditions with associated weighting factors shown**

Figure 6.7 shows the same operating envelope as Figure 6.6 but the number of data points has been reduced to the 26 operating conditions with the diameter of the circular marker dependent on the weighting factor and the centre point showing the operating condition for that test point. The test operating condition was located at the centre of the operating segment as this will provide the mean performance for that region of the operating map. In order to achieve the target engine operating conditions, the speed and torque set points were set by the dynamometer and controlled by the host system computer, whilst the ECU strategy managed the important parameters, such as fuelling and injection timing, to meet the particular demand. The additional hardware discussed in Chapter 4 Section 4.4 was installed on the engine during this phase of testing, however all items were set to their baseline conditions and did not affect the engine performance or heat transfer at a fully warm condition. In-cylinder pressure data was collected at each test point in addition to the temperature and flow data. The test operating conditions, weighting factors, engine power and brake mean effective pressure are given in Table 14 in the Appendix. Figure 6.7 shows that 21.7% of the NEDC takes place at a low speed and load operating point, in this case, equivalent to idle with ancillary loading, and a further 41.7% occurring at engine loads less than 40Nm. It is interesting to note that a total of 83.9% of the NEDC is achieved at engine loads less than 80Nm; therefore highlighting that a coolant system which has been designed

for peak torque and power conditions will be oversized for the drive cycle and require a large amount of energy to reach optimum operating temperature.

The experimental programme consisted of three repeats at each of the operating conditions in order to evaluate the test-to-test repeatability, and the engine thermal state was comparable to that of a fully warm drive cycle rather than a cold start cycle. At each condition three 30 second average data points and 500 cycles of in-cylinder pressure data for all four cylinders was recorded. Each variable was evaluated for a number of statistical metrics, such as standard deviation and coefficient of variation. The standard deviation was used to identify how much the measured values differ from the average value and the coefficient of variation is the standard deviation divided by the mean value. These statistical methods aimed to highlight any anomalous results which could be removed from the data set prior to analysis, such as thermocouple drift due to instrumentation degradation over the experimental programme. A constant air flow was passed over the engine with the ventilation inlet air temperature to the cell controlled to 15°C throughout the experimental period due to the long period of running at high load. The constant air flow meant that the engine was subject to a greater than necessary air flow during the low load conditions in order for there to be sufficient air flow at high speed and load. This decision was made in order to reduce the number of variables during the experimental programme. Steady state operation does not reflect real engine operating conditions as it is rare for an engine to maintain a single operating condition for an extended period of time; however it was essential that the engine was thermally stable to obtain suitable data for any future thermal modelling.

## Steady state results and discussion

This section aims to describe the data collected through the experimental programme and highlight the important findings. The data analysis can be broken down into different areas. Initially an investigation of the overall heat balance of the engine was undertaken, this led to the requirement of an understanding of the overall temperature distribution of different fluids and areas of the engine structure for each of the operating conditions. The third area of interest was the measured temperatures through the cylinder wall and how these were affected by the different engine speed and load conditions. Using the measured temperatures the rate of heat transfer from the combustion chamber could then be investigated. The final area of analysis was based on the cylinder pressure data captured at each of the operating points. This was to be used to calculate crank angle based convective heat transfer

coefficients which could be compared to those calculated from empirical correlations. In addition, by averaging the crank angle based data over time it can also be compared to the measured rates of heat transfer from the combustion chamber.

## Complete engine energy balance

Investigating the energy balance at the different engine speed and load conditions can be completed by implementing the overall first law energy balance with an imaginary control volume which surrounds the engine. The control volume is treated as an open system as there is a transfer of mass as well as heat and work across its boundaries. This method can only be applied to a steady state operating condition so is well suited to this application.

Figure 6.8 to Figure 6.11 present the results for the primary heat balance terms within the control volume versus engine speed and load. There were two inputs to the system, the fuel energy and the energy of the intake air charge. The fuel energy is shown in Figure 6.8, as the engine load was increased the mass of injected fuel also increased; therefore the fuel energy increased as this is based on the mass of fuel and its calorific value. Figure 6.9 to Figure 6.11 show the measureable outputs of the energy balance performed. The brake power shows energy output measured at the dynamometer. This again highlights that the operating conditions for this investigation did not achieve rated power of the engine. The rated power of the engine was 103kW at 3500 rev/min; the contour plot shows a gradual increase in this direction as it is a function of engine speed and torque. The second measurable output was the heat rejection to coolant; calculated using the engine coolant flow rate and temperature difference across the engine, this illustrates a similar shape to that of the brake power. At a constant percentage load, it was found that the heat rejection increased with engine speed, due to the coolant pump being driven by the front end pulley and, therefore being directly proportional to engine speed. An increase in the coolant mass flow resulted in an increase in the rate of heat transfer to coolant. The increase in engine speed also resulted in an increase in the exhaust enthalpy rejection, shown in Figure 6.11, as the exhaust enthalpy is a function of the exhaust mass flow and temperature. In addition the increase in load also resulted in an increase in the exhaust heat rejection, due to higher engine operating loads leading to higher in-cylinder pressures and temperatures, therefore higher exhaust gas temperatures. An additional output of the heat balance was the heat rejected to the atmosphere, in this experiment this was not measured, however it can be assumed to be the difference between the sum of the measured outputs and the sum of the inputs to the energy balance. The

external air flow over the engine was kept constant during these experiments, so any variation in heat rejection would be due to changes in component temperatures. Therefore it would be expected that the heat rejection would be similar in character to that of the exhaust gas enthalpy since this is the principle heat source.

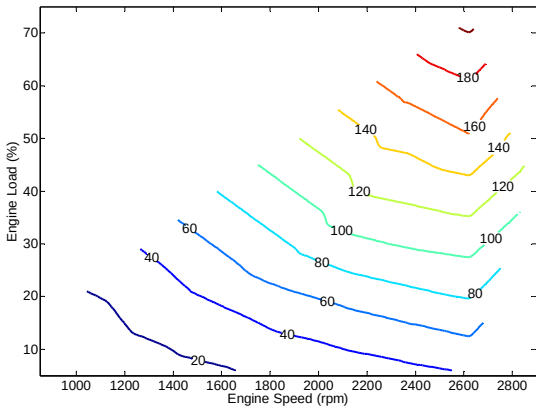


**Figure 6.8 – Fuel energy in kW**

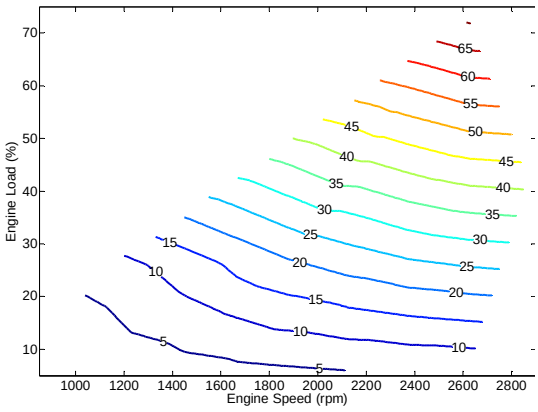


**Figure 6.9 – Useful brake power in kW**

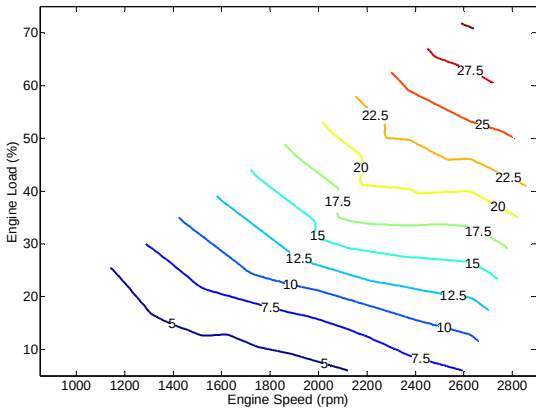


**Figure 6.10 – Heat rejection to coolant across engine structure in kW**

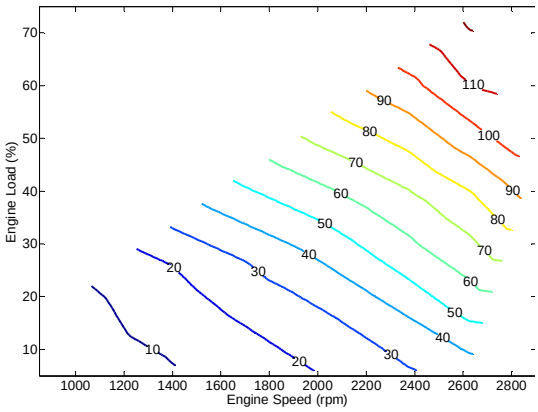


**Figure 6.11 – Exhaust enthalpy rejection in kW**

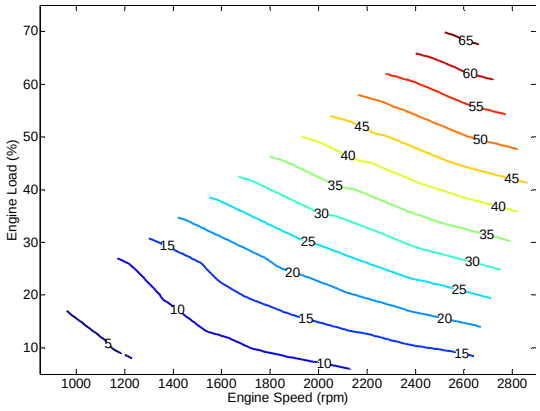


**Figure 6.12 – Indicated engine power in kW**

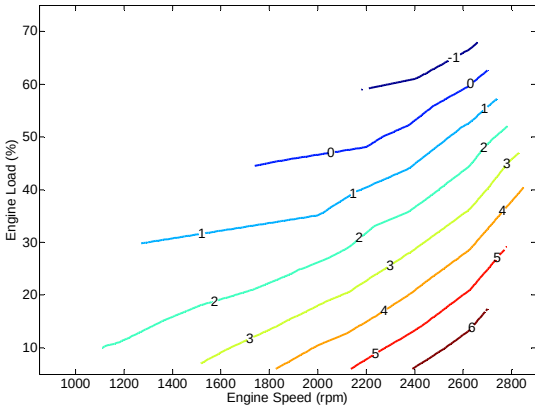


**Figure 6.13 – Friction Power in kW**

Figure 6.12 shows the indicated engine power calculated from the measured cylinder pressure data, therefore the difference between the calculated indicated power and the measured brake power is assumed to be the friction power, shown in Figure 6.13. The friction power is shown to be a function of both engine speed and load. The friction power increases with engine speed along a constant load line and reduces with an increase in engine load along a constant speed line. The indicated power was calculated across the whole cycle therefore includes the pumping, also regarded as $IMEP_n$. At high engine loads the turbocharger generates boost resulting in negative PMEP due to the increase in inlet manifold pressure and a positive pressure gradient across the engine. The PMEP for each of the operating conditions was calculated and found to not be the cause of the assumed error. As previously discussed, there are a number of factors which effect calculations based on cylinder pressure data, the most common being pressure phasing. An investigation into the TDC position of the motored pressure signals resulted in a possible TDC error of +0.3°CA. Figure 6.14 shows that the friction power reduces further at high load when calculated after the TDC offset has been applied to the cylinder pressure data prior to the calculation of $IMEP_n$. This is therefore not the cause of the negative friction at high load. Another possible cause is thermal shock of the pressure transducers. This will have very little impact on the calculation of gas side convective heat transfer coefficients as the in-cylinder pressure data is used primarily to obtain a crank angle based in-cylinder temperature and mass.

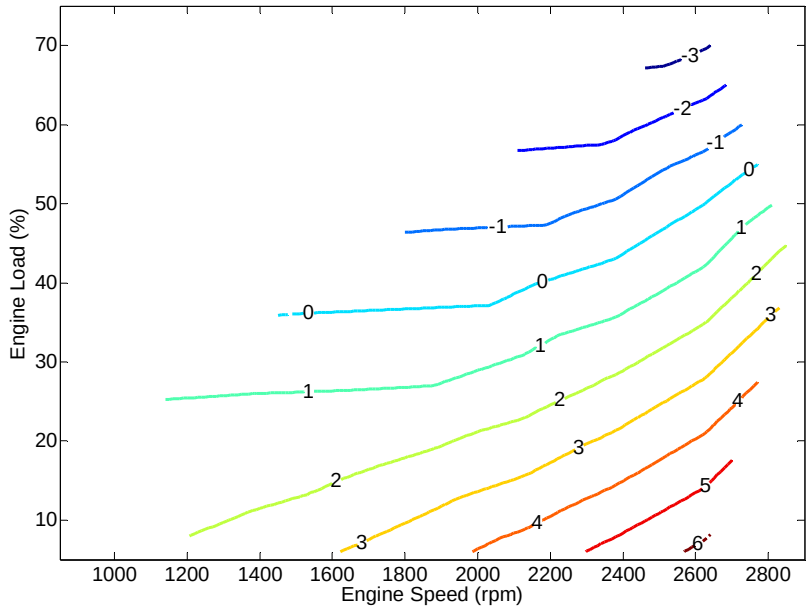


**Figure 6.14 - Friction power in kW with a TDC offset of -0.3°CA implemented**

The FMEP measurements obtained under motored conditions and the calculated friction under fired conditions (without TDC offset) are shown in Figure 6.15. The friction was calculated by different methods under motored and fired operation, therefore a direct comparison cannot be made. However, it is shown that the friction measured under fired condition also increases with engine speed; however the magnitudes were far less than that calculated under motored conditions. Ideally the fired operation derived friction would be larger as there would be additional components from bearing loads and increased gas pressures over the motored friction. There is also a reduction in the friction power when the engine torque is increased. The reduction in friction as torque is increased is contrary to the expected trend and indicates that within the calculation used to obtain the fired friction power, there was an increasing error with torque, as previously discussed.

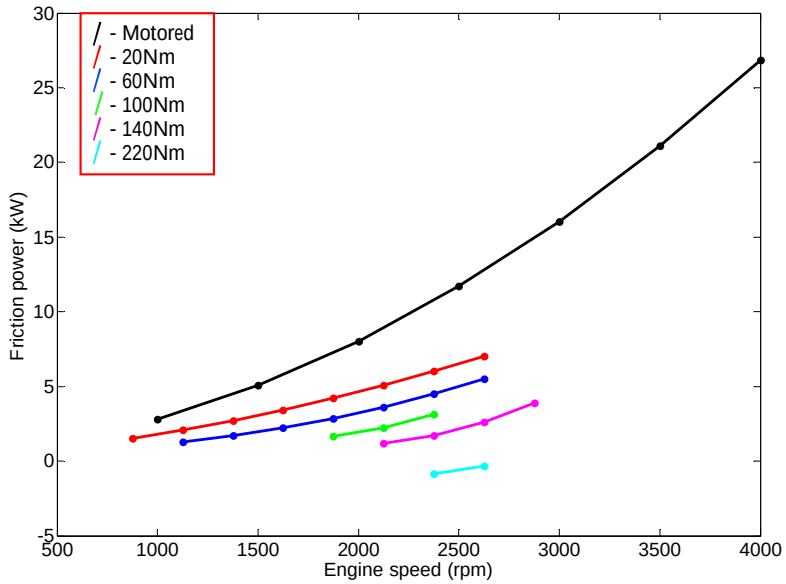


**Figure 6.15 – Motored friction power and friction power measured under fired conditions**

The contour maps provide a good overview to the engine's response to changes in speed and load; however it is not possible to compare the relative contributions at an operating condition. At a fixed engine speed the effects of changing loads on the coolant pump and oil pump are effectively removed as they are operating at a constant speed. Figure 6.16 shows the absolute magnitudes of the given contributions for 6 engine load points at 2625 rev/min. The data shows that the proportion to coolant has the smallest increase over the tested conditions and that most energy is lost to the exhaust with the proportion reducing as the engine load increases.

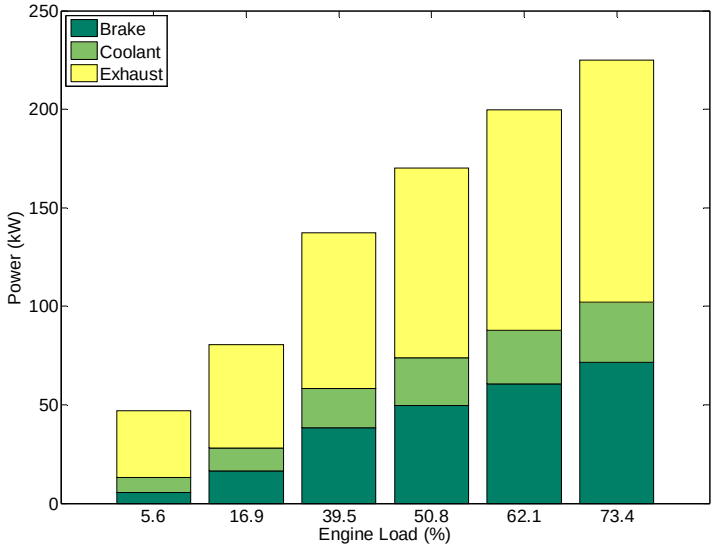


**Figure 6.16 – Heat balance at 2625rpm**

This data is better represented normalised to the sum of the input energy, shown in Figure 6.17. It is shown that as the operating load is increased, the proportion of useful energy obtained from the total input energy increases, with the most significant reduction shown from the miscellaneous losses. Across the engine load range the average energy lost to the coolant was found to be 12.2% (±0.6%), this does not fluctuate greatly due to the constant engine speed and therefore the constant coolant pump speed, with the small changes being attributed to the fluctuations in the thermostat control of the coolant flow.

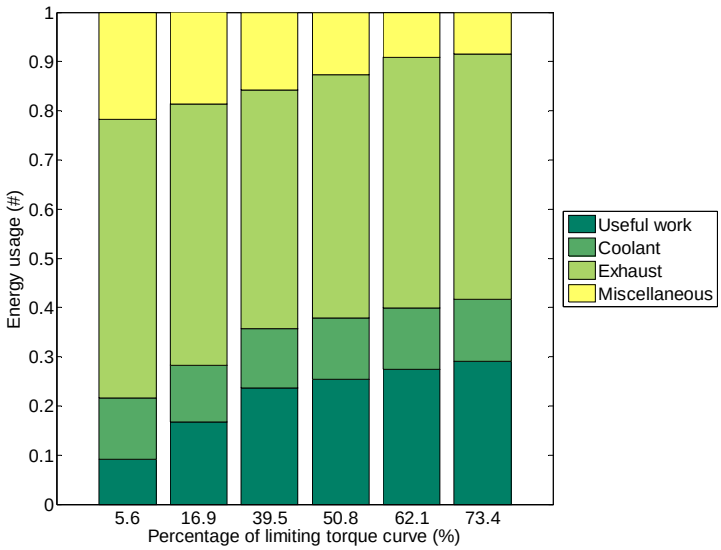


**Figure 6.17 – Energy usage data for each operating load at 2625rpm normalised to the total input energy**

The main finding from this investigation is that the proportion of input energy which is converted to useful work increases as the engine load is increased. The gains in efficiency reduce as the load increases.

## Oil and coolant temperature distribution

The aim of this section was to investigate the overall temperature distribution through the engine and how it was affected by the different operating conditions. An overview of the temperature distribution across the engine fluids is shown in Figure 6.18 and Figure 6.20 for the coolant and oil respectively, by way of a parallel coordinate plot. Each curve represents a minimap operating condition, with all repeat data included, and each x-coordinate is at a different location around the corresponding circuit. Figure 6.18 includes a number of temperatures within the engine cooling jacket, in addition to the coolant either side of the EGR cooler and oil cooler. Figure 6.20 shows the oil temperatures across the oil cooler, with the remaining locations being within the engine structure following the oil path through the engine, beginning at the oil sump, through the filter and continuing into the cylinder head. The temperatures used represent all areas of the engine to give a clear overview of the temperature distribution across the different fluids.

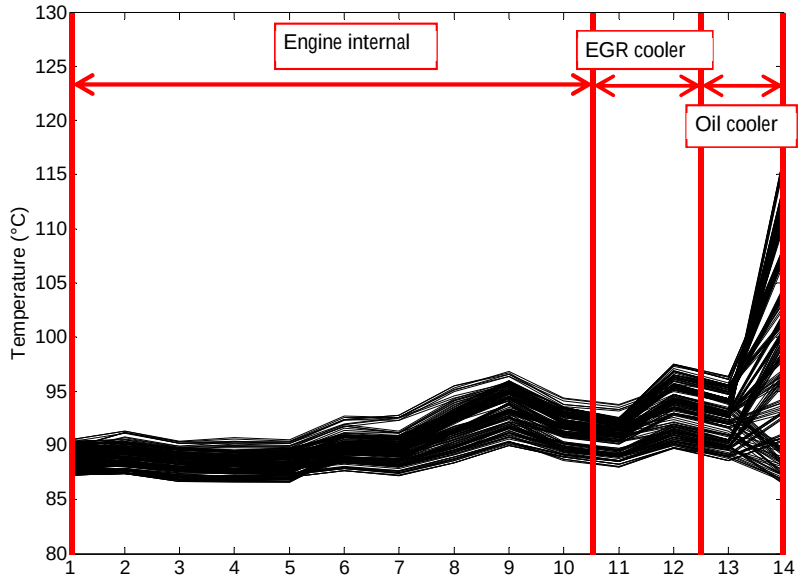


**Figure 6.18 – Coolant temperature distribution for all operating conditions**

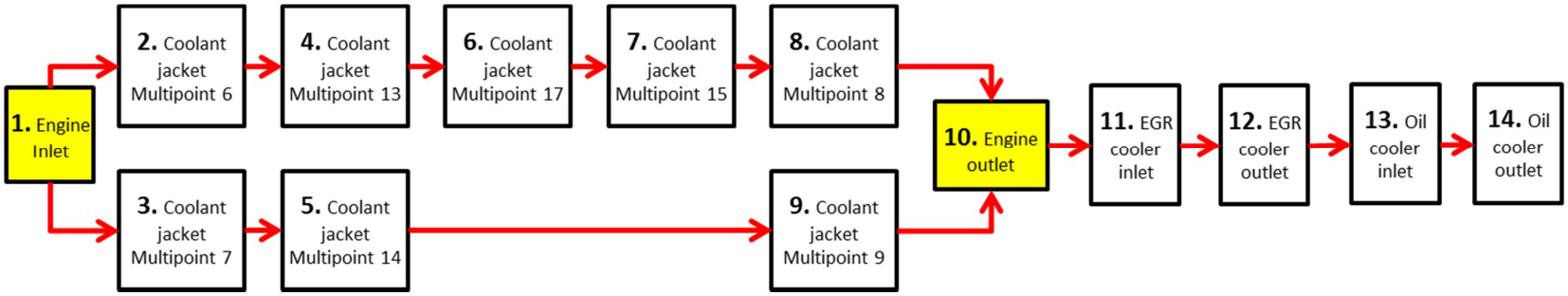


**Figure 6.19 – Flow diagram showing measurement locations used in coolant parallel coordinate plot**

Figure 6.18 shows very little temperature variation across all the operating conditions compared to the oil temperatures shown in Figure 6.20. The largest variation is in the coolant temperature out of the oil cooler, where at high load conditions the oil temperature was much higher, resulting in an increase in the coolant temperature. The small temperature difference across operating conditions shows that the thermostat is balancing the flow through the radiator and bypass routes to maintain a bulk coolant temperature around 90°C. The oil temperatures show a strong dependency on the operating condition, the high speed and load conditions were found to be 40°C hotter than the idle condition due to the higher oil pressure and combustion temperatures transferring energy to the oil. The impact of the stable coolant temperature through the oil cooler is also evident in Figure 6.20, oil temperatures below 90°C show a temperature rise across the oil cooler whereas above 90°C a temperature loss was measured. The oil shows a significant temperature reduction after the oil filter as it passes through the cylinder block to the main gallery and the feed to the cylinder head. The temperature rise was caused by the gradual reduction in pressure and temperature losses to the engine structure. A reduction in temperature on the inlet side, groove 1 (location 8) to groove 5 (location 9) is shown, whereas on the exhaust side a significant increase in these temperatures was shown from groove 1 (location 10) to groove 5 (location 11). The increase in temperature on the exhaust side was caused by the higher gas temperatures in the exhaust ports resulting in higher metal temperatures. The surface thermocouples mounted on the bridge containing the camshaft bearings support this finding, showing that on average the exhaust side was 7.2°C (peak of 20.3°C measured at high load) hotter than the inlet.

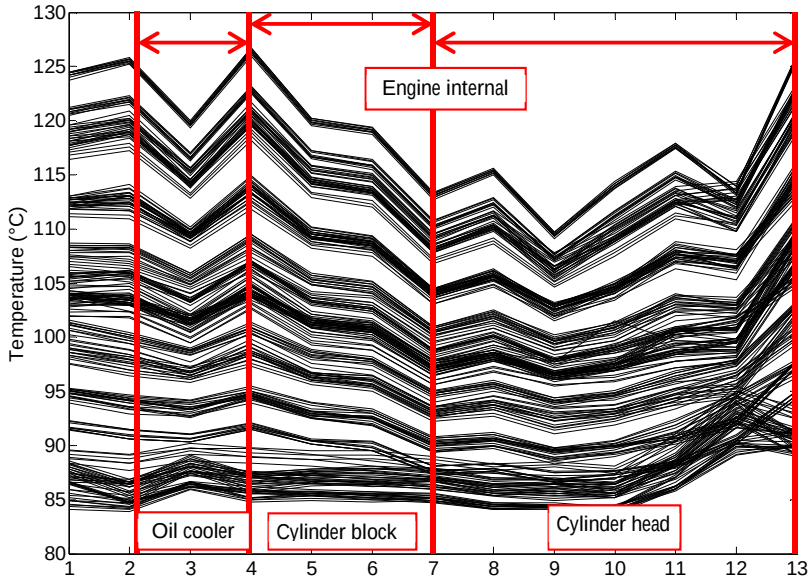


**Figure 6.20 – Oil temperature distribution for all operating conditions**

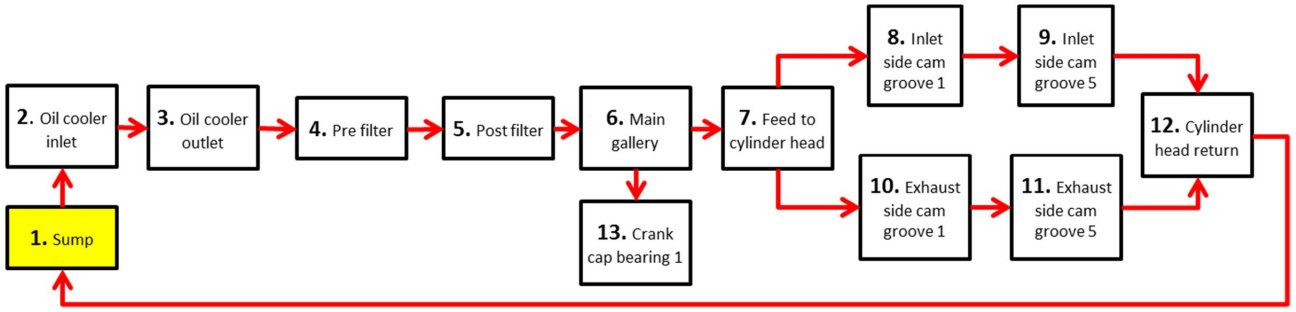


**Figure 6.21 – Flow diagram showing measurement locations used in oil parallel coordinate plot**

## The response of main journal bearing cap and cylinder head metal temperatures to changes in engine operating conditions

In addition to the instrumentation installed in the engine block, a series of thermocouples were installed in the cylinder head and crank caps to measure both oil temperatures and metal temperatures. This section aims to understand how the different steady state operating conditions affected the temperature distribution in these areas.

The oil used to lubricate the main journal shell bearings was fed through drillings to each bearing from the main oil gallery located on the intake side of the engine. This is shown in Figure 6.22, the upper bearing utilised a groove on the inner side to lubricate the bearing surface and to allow flow to the lower half of the bearing. The oil temperatures in the main gallery were found to fluctuate considerably with the different operating conditions, discussed earlier, and the variation was found to continue through into the bearing oil temperatures.

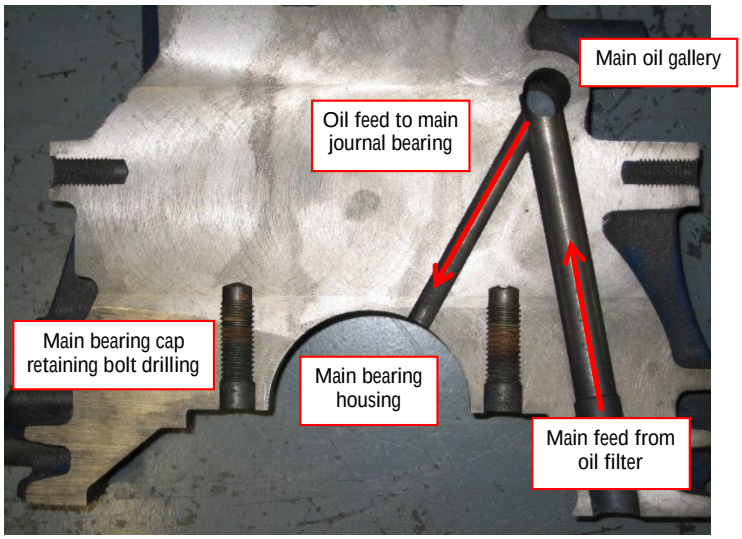


**Figure 6.22 – Photograph showing oil feed to main journal bearing**

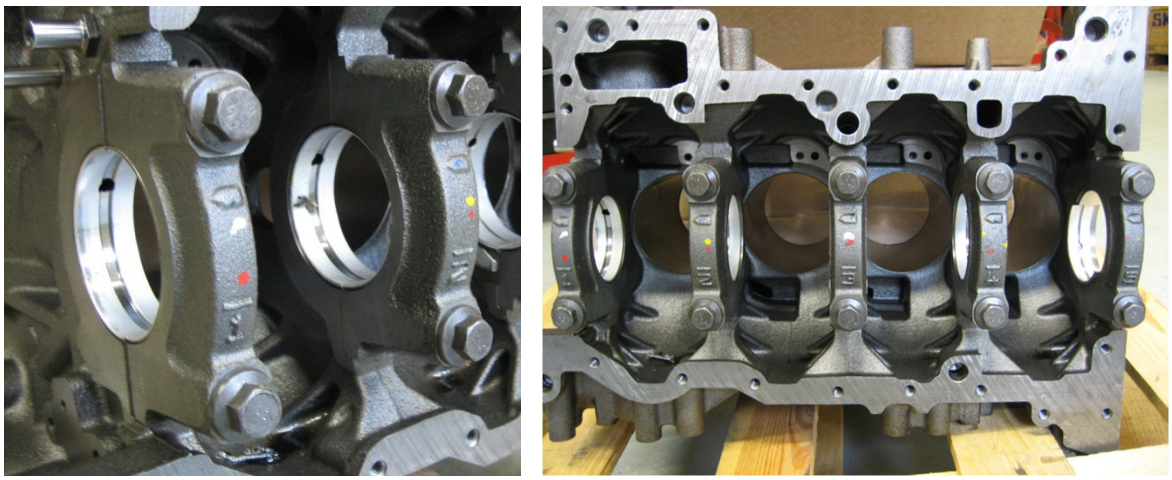

**Figure 6.23 – Main journal bearing detail showing a) oil delivery hole to lubricate shell bearing b) five main journal bearing caps**

The increase from the oil gallery temperature was found to be largest in bearings three and five, shown in Figure 6.24, Omar Mian et.al found that increasing the engine speed caused a rise in the oil temperature from the oil feed to the bearing of 10°C at 3000rpm up to 27°C at 6500rpm with a partial groove bearing [133]. Figure 6.24 was measured at 2625rpm and shows a temperature increase of 7°C (5.8%) between the feed temperature and bearing 1. It was found that across the five bearings and all operating conditions that bearing 3 was consistently hotter, ranging from 2 to 5°C (3.9%). The increased temperatures at bearing 3 are a result of the thrust bearing located at this position increasing the contact area to the rotating crankshaft, in addition to the consistently higher cylinder pressures measured on cylinder 3 in comparison to the other cylinders, it was found to be on average 3% higher during the high speed operating conditions. The higher temperatures at bearing 5 are caused primarily by the increased diameter of the bearing due to the friction power in a bearing being proportional to the cube of the bearing radius [134]. Bearing 5 was found to have the same surface area as the other bearings but an increased radius. In addition there would be increased load due to the flywheel and clutch assembly located at this end of the engine. The difference of this size could also be attributed to positional error of the thermocouple within the bearing. A contour plot showing the change in oil temperature in the recess in bearing 5 with operating condition is shown in Figure 6.25. The temperature was found to increase with both speed and load. This trend was consistent across the five bearings with a small change in magnitude.

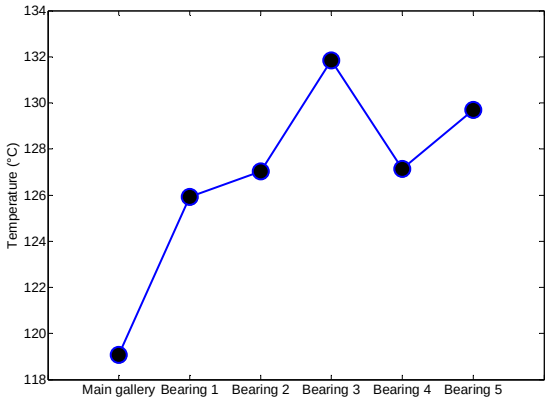


**Figure 6.24 – Comparison of oil temperatures across each bearing to the main oil gallery temperature at 2625rpm and 260Nm**

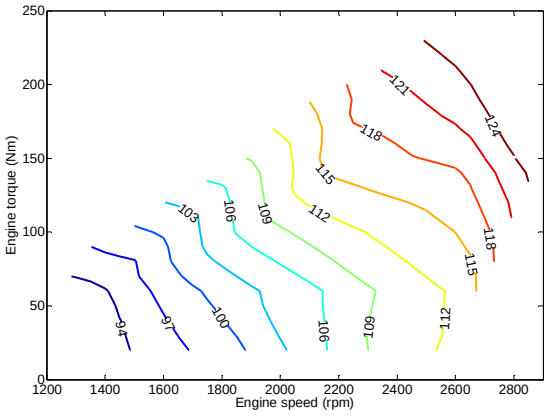


**Figure 6.25 – Main journal bearing number 5 oil temperatures for all operating conditions**

Figure 6.26 and Figure 6.27 show the metal surface temperatures in the cylinder head on the inlet and exhaust side respectively. The cylinder head was found to be consistently hotter on the exhaust side due to the heat transfer from the hot exhaust gases in the exhaust ports to the metal surface. The inlet side shows an island of increased temperature at higher operating conditions, whereas the response on the exhaust side is consistent with changing engine speed and load. At the low speed and load operating conditions, the temperatures were found to be comparable on both the inlet and exhaust sides, as the coolant temperature was dominant on maintaining a controlled temperature; at higher operating conditions it is unable to transfer the heat away from the metal at a sufficient speed to maintain a balanced temperature across the cylinder head.

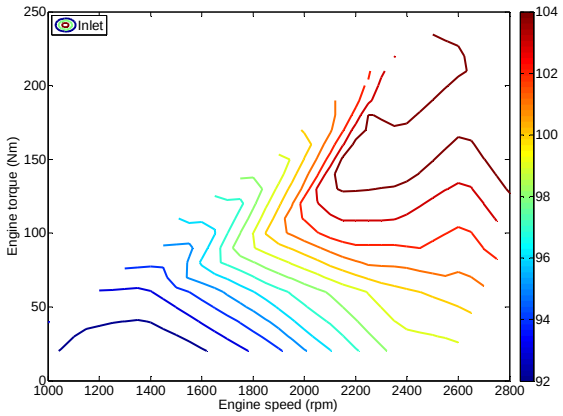


**Figure 6.26 – Metal surface temperature located**

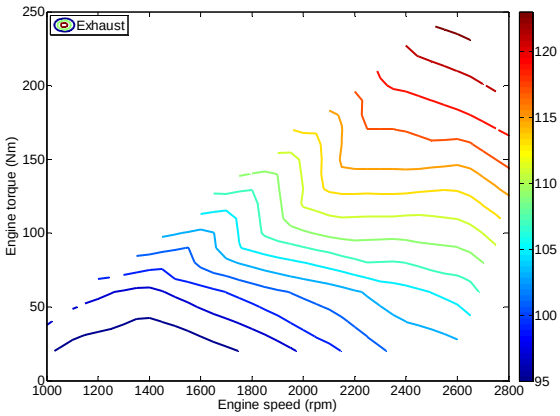


**Figure 6.27 – Metal surface temperature located on webbing on the exhaust side of the cylinder**

## Measured cylinder liner temperatures and heat transfer

An investigation into the cylinder wall temperatures was undertaken in order to understand the fundamental response to the changes in engine speed and load. The cylinder wall temperature data was initially broken down into BMEP groupings, an example is shown in Figure 6.28, which includes the extrapolated boundary temperatures. At each load condition it would be expected that as the engine speed increases, the cylinder wall temperature also increases, however below 1625 rpm this is not the case. In Figure 6.28 the marker size represents the engine speed and the low engine speed conditions are highlighted, the tip temperature measured 118.2 and 117.2°C at 1125 and 1375rpm respectively, which is 6°C greater than the high speed condition. The outer measured temperature reflects the temperature increase whereas at higher engine speeds the outer temperature remains constant, indicating a significant rise in the bulk metal operating temperature.

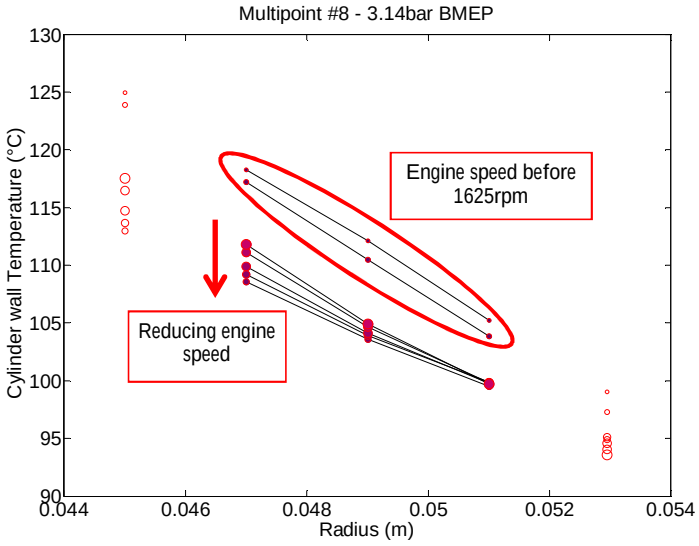


**Figure 6.28 – Cylinder wall temperatures measured by Multipoint sensor 8 at 3.14 bar BMEP, marker size indicates engine speed**

The increased temperatures at low speeds are reflected across all multipoint sensors. Further investigation found that:

- Low BMEP and low speed[5] = increasing engine speed caused a reduction in wall temperature
- Low BMEP and high speed = increasing engine speed caused an increase in temperature
- Mid BMEP and high speed = increasing engine speed caused a minimal increase in temperature
- High BMEP and high speed = increasing engine speed caused a minimal effect on temperature, i.e. ±0.5°C (some regions increasing and some decreasing)

These trends have been represented as areas on a brake mean effective pressure and engine speed map in Figure 6.29. The arrows indicate an increase in engine speed which results in the corresponding effect on cylinder wall temperature.

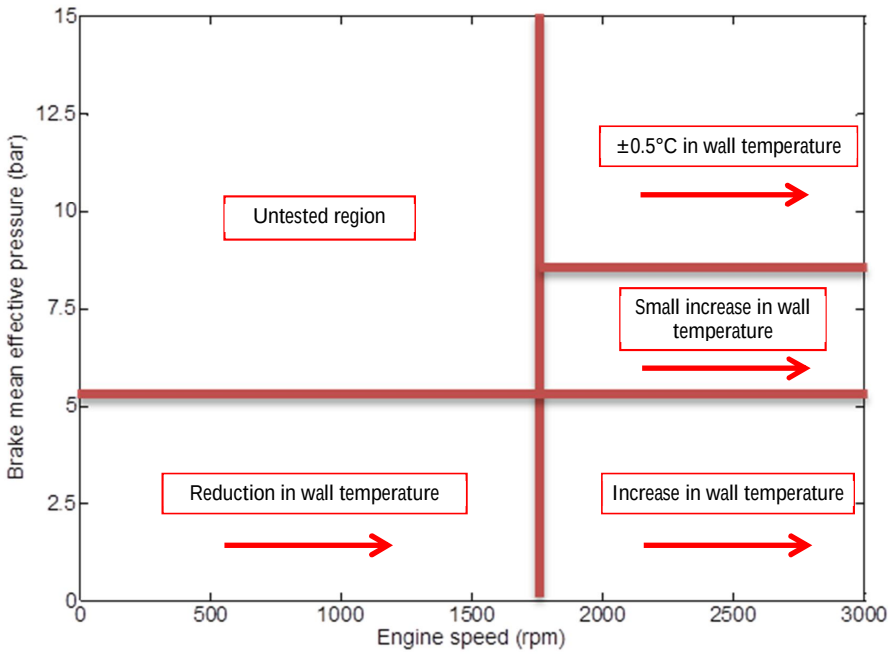


**Figure 6.29 - Wall temperature trend overview**

The coolant pump speed was directly proportional to the engine speed as the pump was driven by the front end ancillary drive belt. The relationship between engine coolant flow rate and engine speed is shown in Figure 6.30, above 1125rpm there is a clear linear relationship. Figure 6.30 also shows that load does not affect the coolant flow rate. A

[5] Low speed indicates engine speeds below 1625 rpm.

reduced coolant flow rate would be expected to cause a shallower temperature gradient through the cylinder wall rather than increasing the absolute temperature at the three locations through the wall. In addition the temperature rise was not reflected in the local coolant measurements. Therefore, this suggests that an additional variable caused the increased wall temperature.

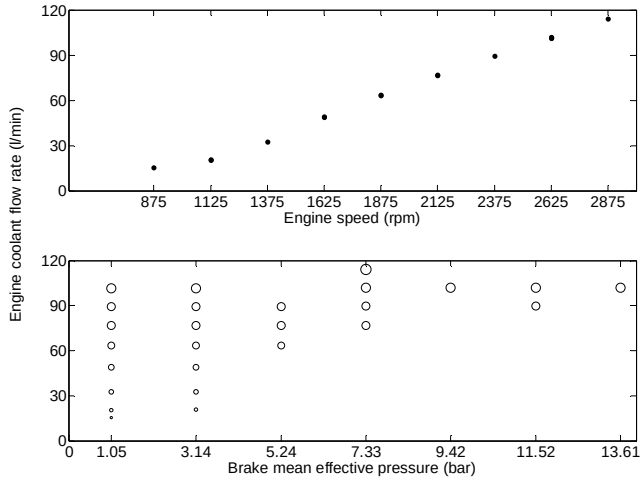


**Figure 6.30 – Engine out coolant flow rate against BMEP and engine speed**

The sources of additional heat within the combustion chamber are limited to higher combustion gas temperature, increased friction or reduced cooling of the piston. As this is a low speed and load condition, the combustion gas temperature would be reduced, increased friction would be caused by changes in the oil temperature and/or supply, and increased piston temperature would also be caused by a change in the oil feed to the piston cooling gallery. The test engine was fitted with standard piston cooling jets (PCJ) which were located in each of the cylinders and direct oil to the internal oil gallery on the underside of each of the pistons. Oil is fed from the main gallery to rigidly mounted nozzles on the crankcase at the bottom of each liner. As the piston approaches bottom dead centre the nozzle mates with a drilling in the piston skirt and a fresh charge of cooler oil is fed in. A drilling on the opposing side of the skirt allows oil to drain out and back to the sump. This technology helps to improve emissions and aids the engine in achieving higher peak powers. It is important that these function correctly to maintain the piston temperatures within the material operating range to prevent piston warping; also if the piston temperature was allowed to exceed the boiling point of the oil, then this can result in oil mist generation which can add to the unburnt hydrocarbon tail pipe emissions. Investigations into the effect

of piston cooling jets on piston temperatures, emissions and fuel consumption have been performed, which showed that with the jets switched off the piston temperatures could be between 20 and 88°C higher, resulting in an increase in NOx emissions by 3% and a reduction in CO of between 5 and 10% [135]. The PCJs used on this engine consist of a simple ball valve designed to open at a set pressure; they were tested prior to their installation and they were found to have a nominal opening pressure (NOP) of 150kPa (±4kPa). The post filter oil pressure for each of the operating conditions is shown in Figure 6.31[6]; the PCJ opening pressure is also indicated. The five test points below the NOP correspond to an engine speed below 1625rpm. It is important to note that the effect of the PCJ would not be noticeable during a transient cycle due to the steady state periods in the cycle being shorter in duration than the decay time of the oil pressure within the main gallery.

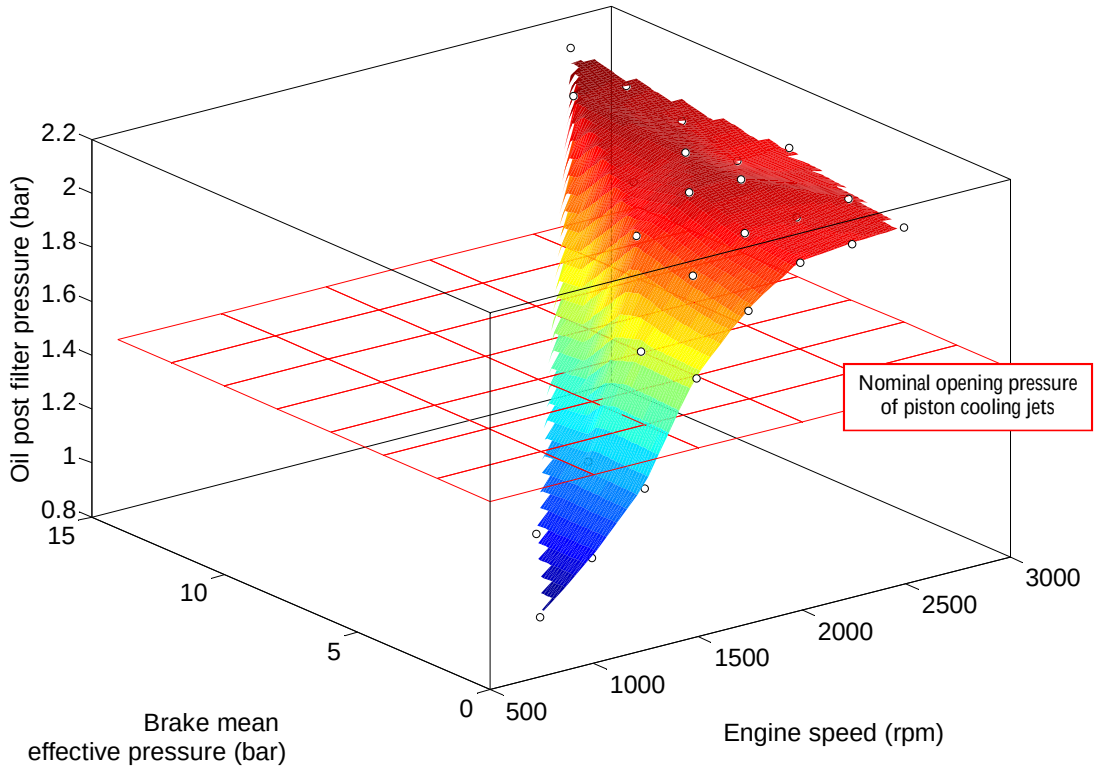


**Figure 6.31 – Post filter oil pressure response to changing engine load and speed, showing nominal opening pressure of the piston cooling jets**

[6] Plot shows steady state investigation operating region, no data was available for the low speed and high BMEP cases. A similar trend would be expected across the load range with high load and low speed region also showing the decay in oil post filter pressure.

In order to quantify the influence of PCJ's on the cylinder wall temperature, a relationship between the wall temperature and engine speed was established at each condition, as the engine speed had a direct impact on the oil pressure. A linear relationship was proposed for the wall temperature at each multipoint location. A prediction of the wall temperatures at lower speeds was extrapolated, which was then applied to each of the three thermocouples within the multipoint. Figure 6.32 shows both the measured and the adjusted inner wall temperatures against engine speed, and Figure 6.33 shows the adjusted temperature profile through the cylinder wall for all engine speeds at 3.14bar BMEP load condition, which can be compared with Figure 6.28. The adjustment has been made to allow for the steady state operating conditions to be directly compared to the transient data.

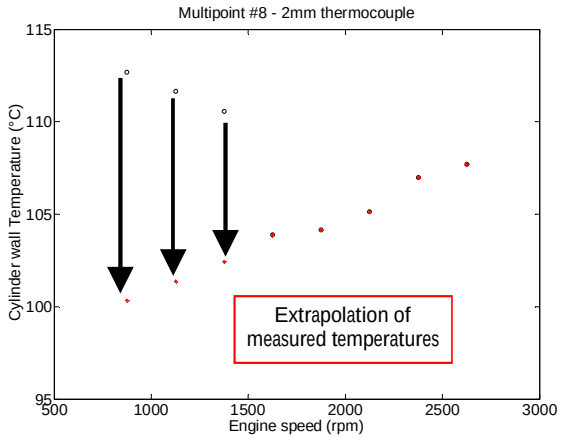


**Figure 6.32 – Comparison of PCJ adjustment for Multipoint 8 inner thermocouple against engine speed**

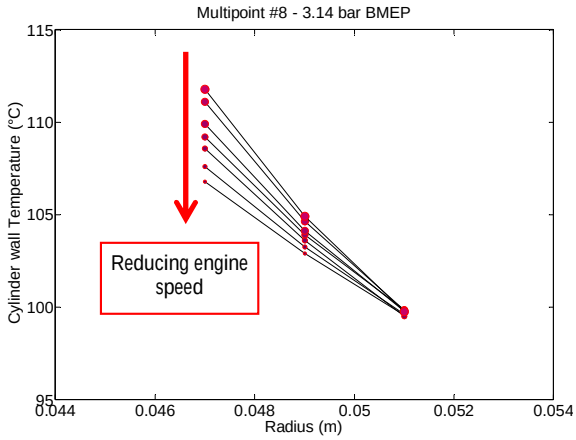


**Figure 6.33 – Resultant temperature profiles for Multipoint 8 at 3.14 bar BMEP and different engine speeds**

Figure 6.34 shows all temperature measurements taken around cylinder 2. The combustion chamber is positioned in the centre of the figure with the cylinder bore radius shown on the x-axis and the four plots on either side indicate the position down the length of the cylinder bore (8, 60, 97 and 160mm respectively). On each plot the marker size represents the BMEP of the operating condition and the blue areas indicate the location of the coolant jacket. This figure starts to explain the effect of the engine operating condition on the temperature profile through the cylinder wall. The three measurement locations show a linear temperature gradient through the cylinder wall across all operating conditions. However the profile through the wall is extremely different depending on the location relative to the coolant jacket. A positive temperature gradient is visible in all plots where the wall is exposed to combustion gases, i.e. down to 97mm from the top deck, whereas at the bottom

of the bore the gradient was found to be relatively shallow and negative in some cases. Figure 6.34*a*, *g* and *h* show an increase in the temperature across the width of the cylinder wall when the BMEP is increased but the locations penetrating the coolant jacket only show a similar temperature increase at the inner wall location, and a negligible increase in the outer wall temperature. This is most noticeable 60mm from the top deck where the coolant jacket width and flow rate are the greatest. The wall temperatures nearest the combustion chamber in this region are 14°C higher on the exhaust side than the inlet side during the high BMEP conditions, which can be attributed to an increase in the heat generated by friction due to the piston thrust exerted on the cylinder wall. The temperature difference was found to be only 1°C at low BMEP conditions reinforcing this conclusion. Cylinder wall areas below 60mm show an average temperature increase compared to higher up the wall by at least 10°C on both sides at higher loads, this is an interesting phenomenon and has been measured in previous studies [83, 102, 104]. Even though it has been measured in other engines the exact reason for the increase in temperature towards the bottom end of the engine block is unknown; however some possible causes may be that the coolant flow is greater higher up the coolant jacket, heat transfer to the cylinder head creates a heat transfer path in the cylinder block, or the large volume of metal around the bottom end and the reduced presence of coolant retains more heat elevating the overall temperature.

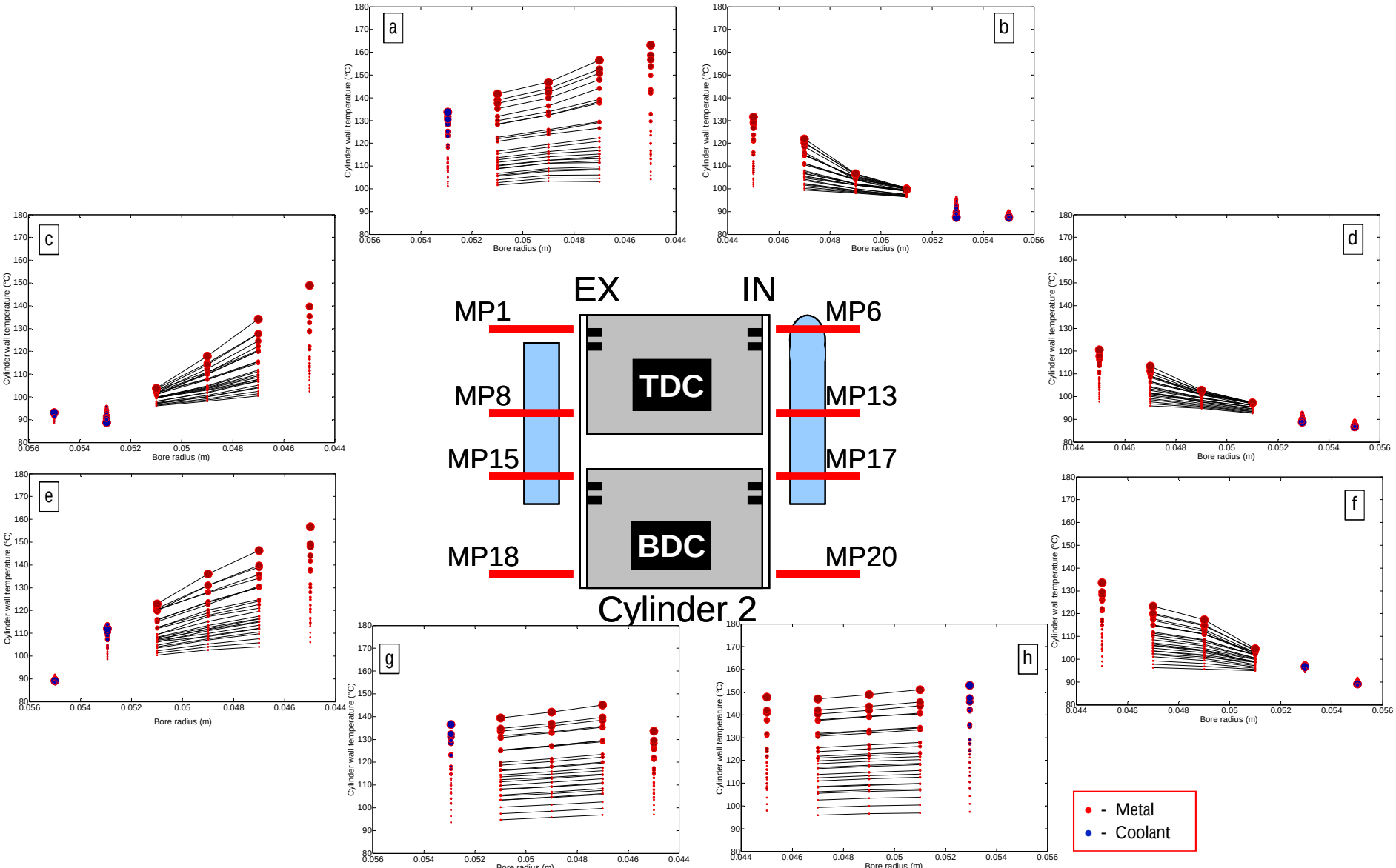


**Figure 6.34 – Cylinder 2 measured and extrapolated temperatures for all operating conditions (Marker size represents BMEP of operating condition)**

Further down the bore it would be expected that the reduced combustion temperatures and exposure time to the combustion gas would result in a reduction in temperature; however it is shown that the wall temperature is equal or greater than that that further up the cylinder bore where there is coolant present. Also shown are the extrapolated gas side and coolant side cylinder wall temperatures and the local coolant temperatures where available. The coolant temperatures were found to be in the region of 2°C less on the inlet side than the exhaust side, having some influence on the rate of heat transfer. Figure 6.35 shows the relationship down the length of the cylinder for each thermocouple within the multipoint sensors. A linear interpolation between the measurement locations has been assumed, without an increase in the number of measurement locations this is assumed to be the temperature profile, however some care must be taken when analysing the profile down the length of the bore. The measurement heights have been indicated on all figures in which a linear interpolation has been performed. The temperature profile on each side is quite different; the exhaust side shows much greater temperature variation due to the changing operating condition at all locations (except outer TC at 60mm) whereas on the inlet side, the temperatures in the region of the coolant jacket are much less affected by the operating condition but show a significant rise towards the bottom. It must be noted that the recorded temperatures at the bottom on both sides are comparable. At the bottom of the cylinder there is very limited cooling available, performed solely by oil splash, therefore explaining the higher temperatures and flatter temperature gradients. The consistently lower temperatures higher up the cylinder on the inlet side indicate that it is much more efficiently cooled and therefore able to maintain a much more stable temperature across the operating conditions. The coolant feed to the cylinder block was located on the inlet side and the coolant at 60mm was found to be in the range of 2°C to 4°C cooler compared to the exhaust side depending on the operating condition. At 97mm this range reduced to 1°C to 2°C, illustrating some of the impact of the coolant jacket shape resulting in flow rate variations. Similar trends were found on cylinder 3, where the impact of the coolant jacket position was very apparent with very little temperature spread on the outer thermocouple within the multipoint.

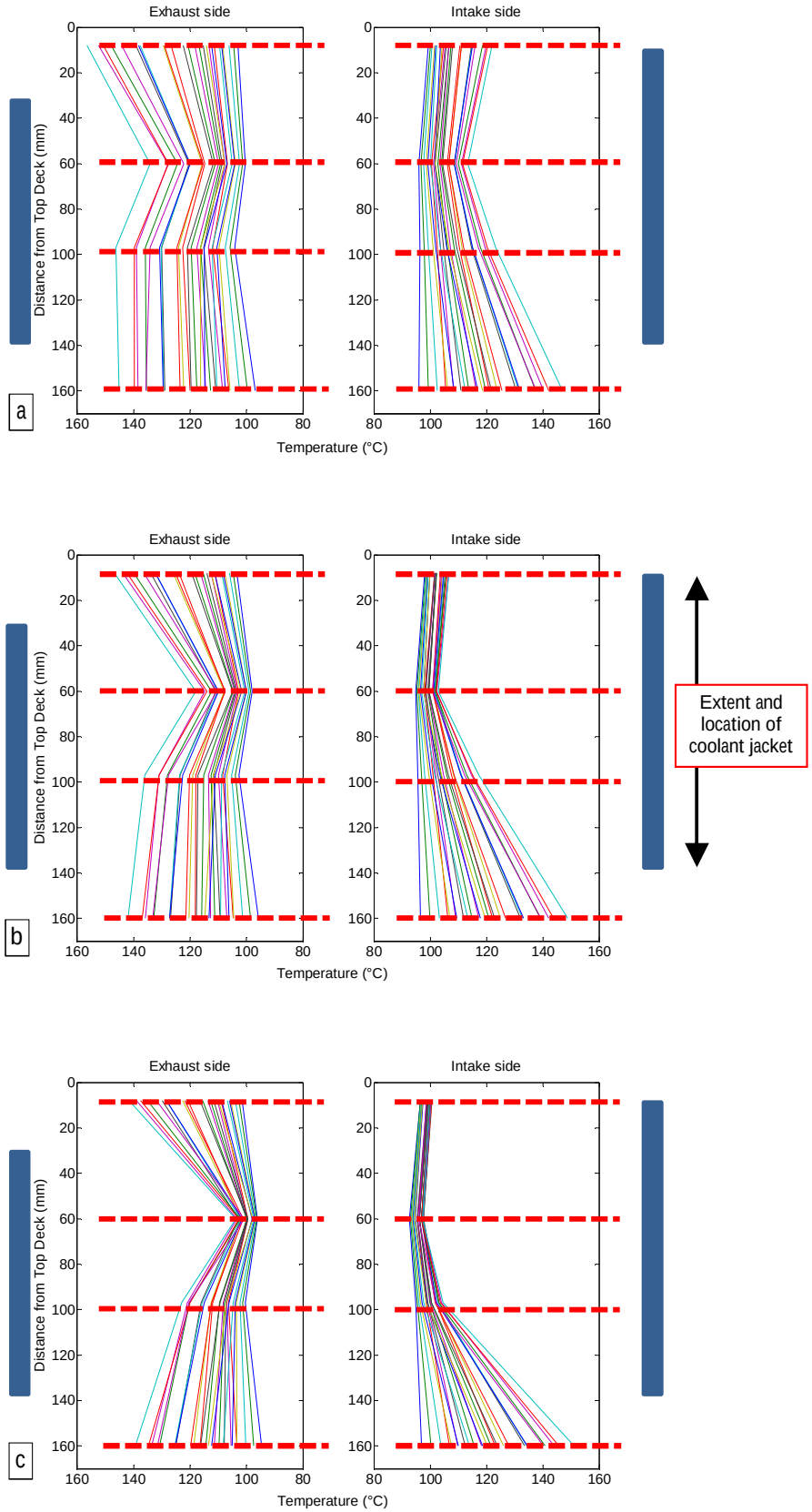


**Figure 6.35 – Temperatures down cylinder 2 for a) inner b) middle c) outer multipoint thermocouple for each operating condition – coolant jacket location and measurement point shown for both sides of the**

**cylinder**

To better visualise the response of cylinder wall temperature with changing engine speed and load, a contour plot for Multipoint 1 is shown in Figure 6.36. The figure shows that there is an increase in temperature with both speed and load with some bias towards load. This method can be applied to all temperatures providing a thorough understanding of the temperature response around the combustion chamber to changing engine speed and load.

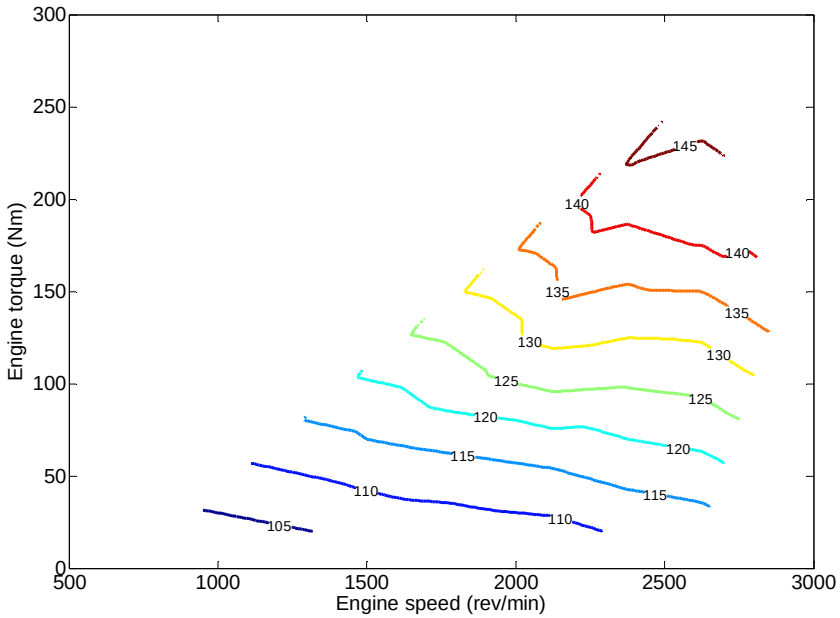


**Figure 6.36 – Multipoint 1 temperature response to changing engine speed and load in °C**

The temperatures shown in the above figures are measured along a single axis through the cylinder wall to provide a temperature gradient to calculate a rate of heat transfer. At all locations the conduction through the cylinder wall will have a longitudinal component, conduction in areas which are not subject to direct cooling will be more greatly affected by this three dimensional conduction as there will be no direct heat path along the axis of the sensor. The extent of the longitudinal conduction requires investigating as it could have significant influence on the calculated heat transfer rates as well as being a fundamental assumption in the calculation of the rate of heat transfer using Fourier's law. The temperature gradient was subsequently calculated both radially (i.e. through the sensor), and longitudinally down the length of the cylinder, using the average of the radial temperatures within the multipoint sensor. A positive gradient indicates a temperature reduction radially outwards from the combustion chamber and a reduction in the temperature down the cylinder. The longitudinal temperature gradient was found to be in the region of an order of

magnitude less than that measured radially due to the close proximity of the coolant in the radial direction. Figure 6.37 shows the longitudinal temperature gradient plotted against the radial temperature gradient between the 8 and 60mm, the 60 and 97mm, and the 97 and 160mm locations down the bore for all operating conditions. The colours indicate target engine torque, which shows that there is a linear increase in the radial temperature gradient as the engine speed increases for a fixed torque. The longitudinal temperature gradient was found to become more positive at the top of the exhaust side, indicating a larger heat transfer rate down the cylinder as the speed and/or torque increased, whereas at all other locations an increase in speed and/or torque resulted in a negative impact of the calculated temperature gradient, indicating an increase in the heat transfer towards the cylinder head. The bottom region of the exhaust side shows that at operating conditions above 1875rpm and/or above 60Nm the heat flow direction changed from down the cylinder to up the cylinder. In general the heat flow direction was found to show a convergence towards the middle of the cylinder indicating a strong relationship with the location of the highest flow within the coolant jacket and away from regions where there was no active cooling.

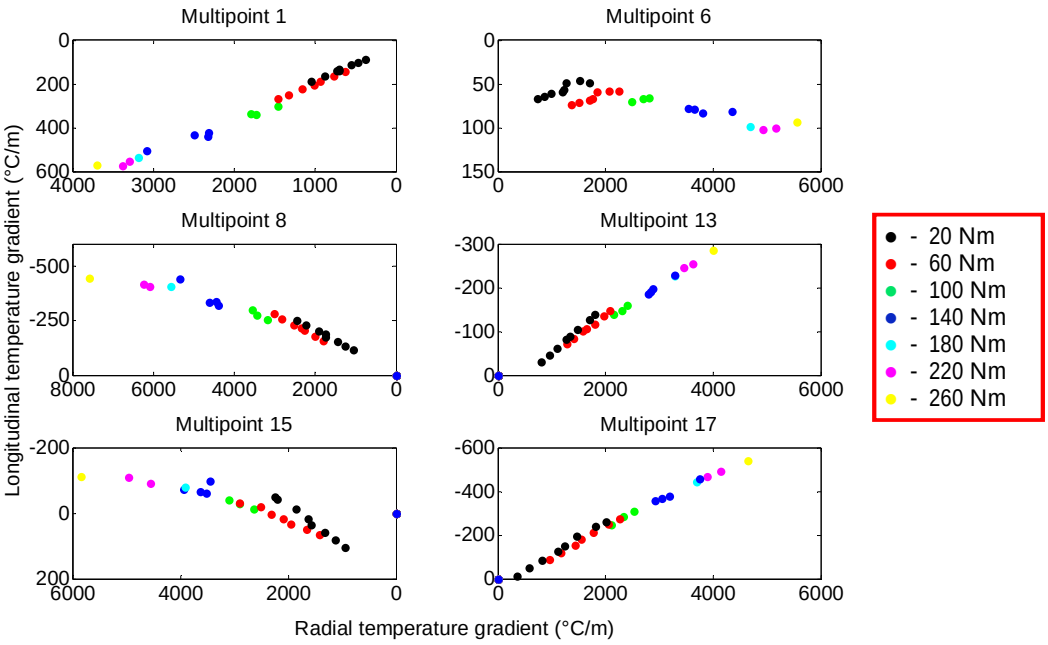


**Figure 6.37 – Temperature gradient longitudinally versus the radial temperature gradient for all operating conditions, colours indicate equivalent engine torque conditions**

The absolute magnitude of the longitudinal conduction as a percentage of the radial was found to vary significantly from a maximum of 23.0% at the top of the cylinder on the exhaust side at idle to 0% at the base of the exhaust side. This finding highlights that the

assumption of a completely 1-D conduction model radially from the combustion chamber is incorrect and is dependent on the operating condition and location down the cylinder; however the impact on the radial heat transfer may be negligible. Figure 6.38 illustrates the longitudinal temperature gradient towards the middle region of the coolant jacket and the radial temperature gradient along the length of the cylinder towards the coolant jacket. The primary heat transfer direction will always be towards the cooler regions, in this case the coolant jacket with the longitudinal heat transfer contributing to the energy transfer.

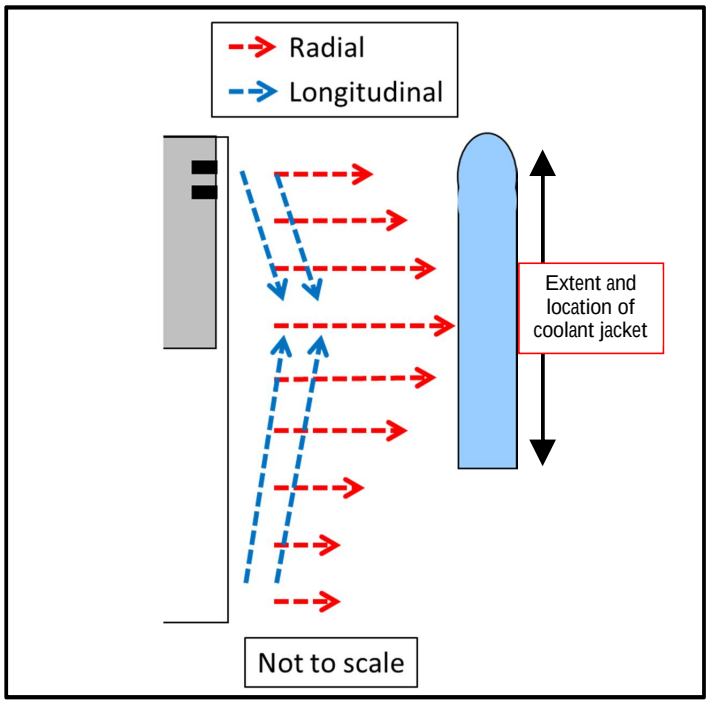


**Figure 6.38 – Illustration of longitudinal and radial temperature gradients**

The radial temperature gradient data can be used to calculate the heat flux through the cylinder wall from the combustion chamber, shown in Figure 6.39 for both sides of cylinder 2 and 3 at each BMEP operating condition. Different engine speeds at a fixed BMEP have resulted in a number of test points at each BMEP. All locations show that as the BMEP increases the rate of heat transfer through the cylinder wall increases. Figure 6.39a shows the highest heat flux at 60mm from the top deck, peak values of 340.9 and 311.5kW/m$^2$ were achieved at 13.6bar BMEP for cylinder 2 and 3 respectively, illustrating that there is some difference from cylinder to cylinder. The temperature data showed much higher inner cylinder wall temperatures but very similar outer cylinder wall and coolant temperatures leading to the larger rate of heat transfer on the exhaust side. The cylinder to cylinder variation is a result of the coolant temperature, flow velocity and the installation position of the sensor i.e. differences in the cylinder wall thickness and auxiliary obstructions on the

outside of the engine block result in small variations in sensor location. The inlet side, shown in Figure 6.39b, shows that the highest heat flux was measured at the top of the cylinder highlighting the effect of the sensor position relative to the coolant jacket.

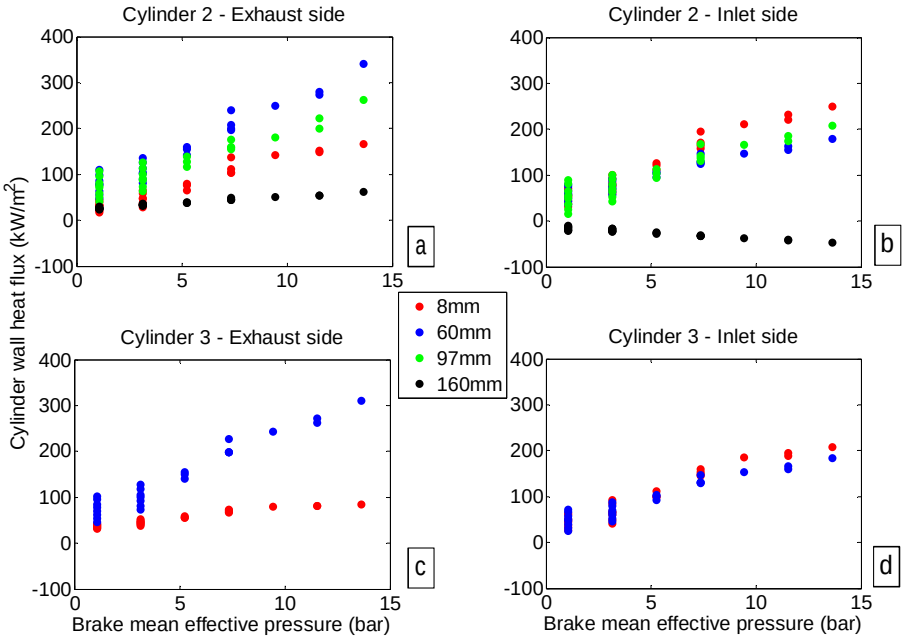


**Figure 6.39 – Calculated heat flux versus measured engine BMEP for both cylinder 2 and 3, colours indicate measurement height down the cylinder bore**

Figure 6.39b also shows the negative heat flux calculated at 160mm from the top deck. The impact of increasing the BMEP on the rate of heat transfer was found to be dependent on the location down the cylinder; a BMEP increase has the greatest effect mid-stroke. The cause of this is the increased combustion temperatures whilst the coolant jacket was maintained at a consistent temperature. Friction would have been a contributing factor to the increase in the cylinder wall temperature, higher cylinder pressure at high BMEP conditions would increase the piston forces on the cylinder wall, especially on the thrust side of the engine. The exhaust side of the engine illustrates a much larger variation in heat flux than the inlet, which is a consequence of the inner wall temperature variation.

Figure 6.40 conveys the heat flux data for both the intake and exhaust sides of cylinder 2, with each line representing an operating condition; the line was obtained from a linear interpolation between each of the measurement locations. This figure further highlights the different trends exhibited on the intake and exhaust sides of the cylinder block shown above. The low levels of heat flux at the top of the exhaust side are due to the elevated temperatures

across the length of the sensor as a result of no coolant jacket. A comparison with Figure 6.35 shows that a low temperature region does not result in a high heat transfer region or vice versa, as heat flux is a function of the temperature difference rather than the absolute temperature at any individual location. Therefore the efficiency of the cooling system on the outer side of the wall and the exposure to combustion gases and hot components on the inner side cause the differences in heat flux shown. The findings shown here contradict that of Alcock et.al who found that the heat flux changed very little with distance down the bore when the engine used aluminium pistons. The reason given was that the improved conductivity of the pistons when made from aluminium distributed the heat along the length of the bore more evenly [3, 136]. The conductivity of the pistons would be expected to have little impact on the heat flux through the combustion chamber wall as the heat transfer path from the combustion gas via the piston would be insignificant in comparison to that directly from the combustion gas to the wall. More important would be the operating temperature of the piston which is affected by the piston cooling jet effectiveness and has been shown to have a large effect on the combustion chamber wall temperature.

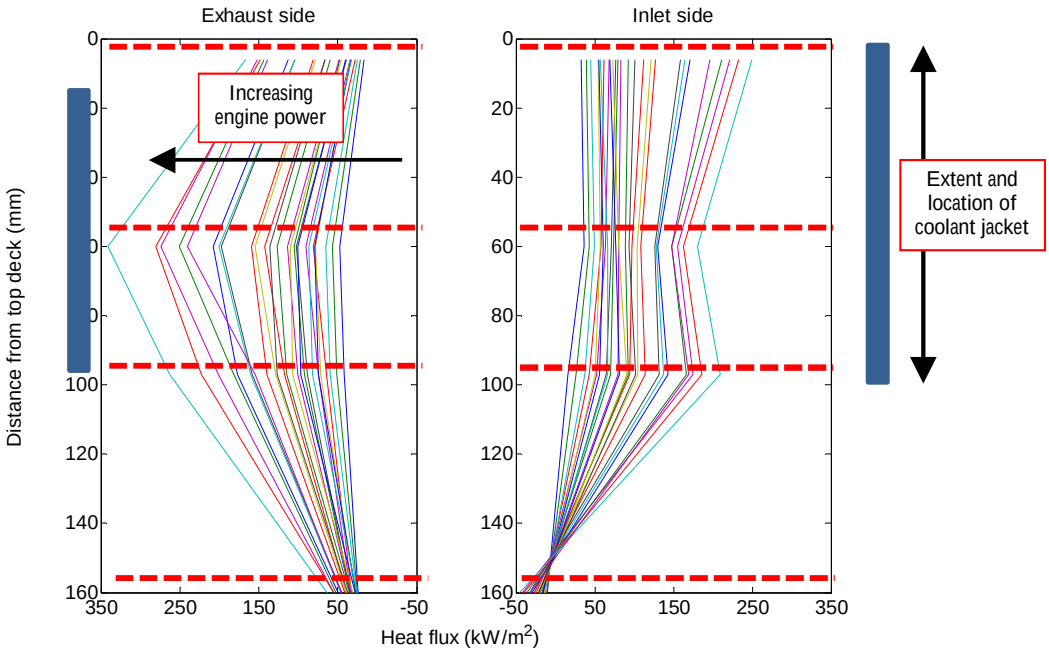


**Figure 6.40 – Calculated heat flux through the wall of cylinder 2 for all operating conditions, coolant jacket position shown**

As engine power is a function of engine speed and load, Figure 6.41 shows a surface plot of heat flux against distance down the bore and engine power for both the exhaust and inlet sides of cylinder 2. An interpolation has been performed between the engine power

operating conditions. The exhaust side shows that increasing engine power causes a steady increase in the rate of heat flux through the wall over the full length of the cylinder. The heat flux has a linear relationship with engine power at each distance from the top deck. The rate of heat transfer is much greater, 60mm from the top deck with a much smaller increase shown at the top and bottom of the cylinder as the engine power increases. This reflects the trend shown in Figure 6.40. The increase in engine power has caused a larger increase in the inner wall temperature, whilst the increase in engine speed and subsequent coolant flow velocity has maintained a more stable outer temperature resulting in a larger heat flux. The inlet side shows the same linear trend with engine power at each distance from the top deck, however there are 2 distinct peaks in the trend down the length of the cylinder where the heat flux is greatest. The reduction in heat flux at the 60mm location indicates either a reduction in the inner temperature or an increase in the outer temperature to reduce the thermal gradient. Figure 6.35 shows that at this location down the bore the overall temperature was less than at the neighbouring locations implying that the cooling in this region was more efficient at reducing the metal temperature. This is much more visible at high engine power conditions. At the bottom of the cylinder the heat flux shows a negative trend with engine power.

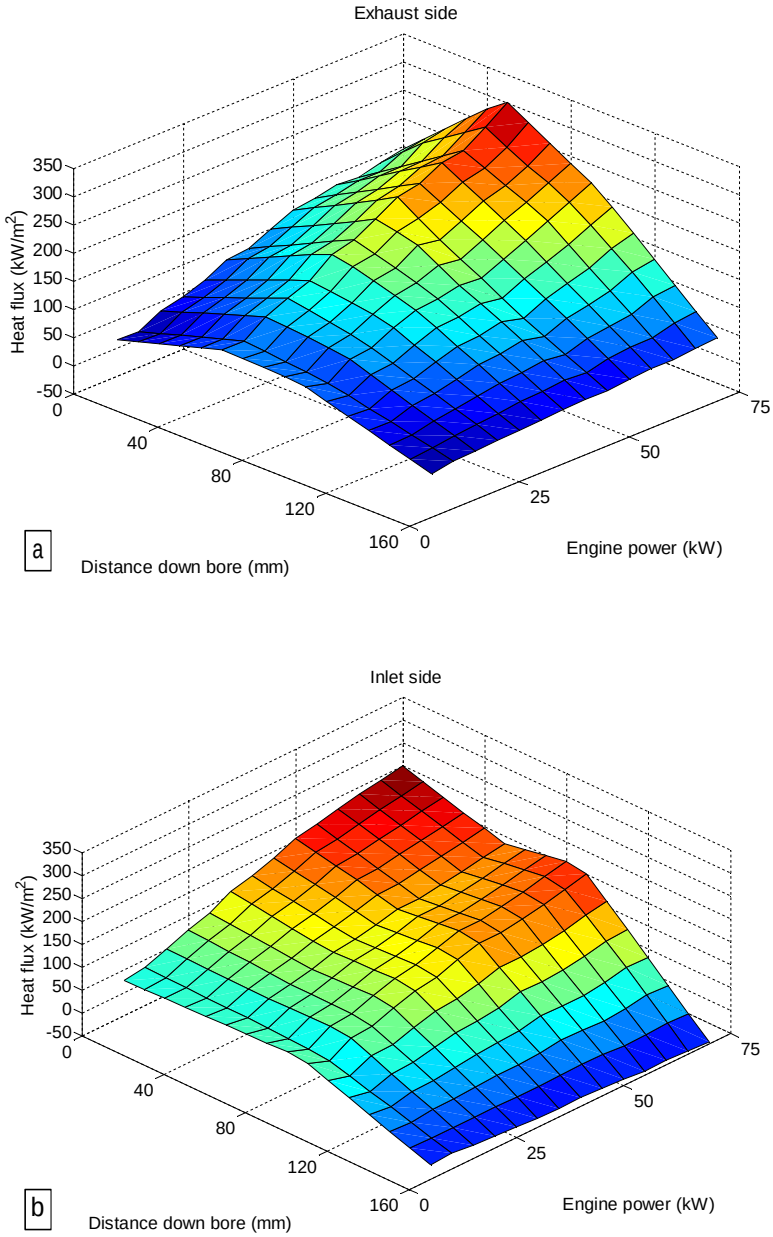


**Figure 6.41 – Effect of engine power on radial heat flux for a) exhaust side of cylinder and b) inlet side of cylinder**

A possible outcome of this investigation is to establish a correlation that can predict the heat flux for each cylinder given a number of inputs. In order to do this, it is important to incorporate all the parameters which affect the magnitude of heat flux. From a substantial literature review into correlations which have been developed to estimate the gas side heat transfer coefficient, the input factors typically used are a:

- Speed dependency (e.g. Engine speed, mean piston speed)

- Load dependency (e.g. Torque, BMEP)
- Engine characteristic length (e.g. Engine bore)

As the data collected was from a single test engine, it is not possible to establish a relationship for engines of different displacement; further testing would be required.

To evaluate each cylinder as a single unit, it is possible to calculate an average heat flux for the cylinder. In order to do this, the estimated heat flux from each of sensors was linearly interpolated around the circumference of the bore and vertically down the length of the cylinder. Interactions between engine speed and engine load on the estimated average heat flux through the cylinder wall can be visualised if the heat flux data is plotted against the operating condition number. Shown in Figure 6.42 is the average heat flux through the wall of cylinder 2 for each of the operating conditions plotted against the engine torque and grouped by engine speed for each of the operating conditions. A small increase in heat flux can be attributed to the increase in engine speed; however the increase in engine load has a much stronger influence on the rate of heat transfer.

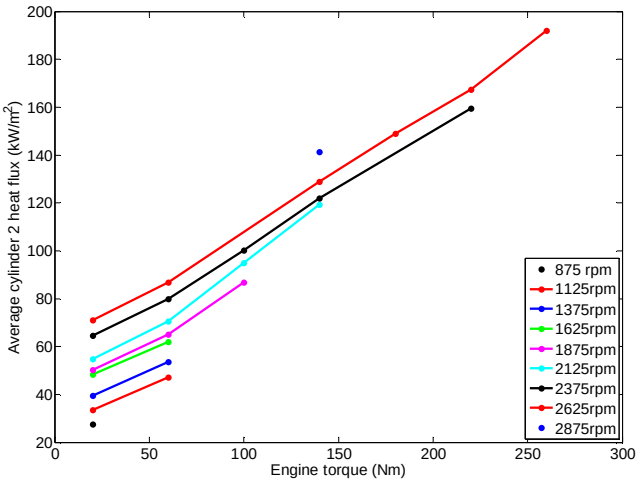


**Figure 6.42 – Calculated average heat flux for cylinder 2**

The average heat flux data, engine speed and BMEP data was subsequently imported into Matlab's Model Based Calibration (MBC) toolbox in order to create a heat flux model. A single stage modelling approach was chosen due to the simple dataset. The inputs to the model were as above and it was found that a linear model provided the best fit based on a

number of statistical metrics such as $R^2$, RMSE and PRESS equivalents[7]. PRESS $R^2$ and PRESS RMSE differ from their original forms in that they are the average values of the original statistic derived when one data point is omitted from the calculation. They provide a good indication of the predictive quality of the model and if they are significantly different to their original forms this implies a model over fitting. The equation given for the response model shown in Figure 6.43 is given in Equation (59). This relationship is only applicable to this engine.

$$Q\ (\frac{kW}{m^2}) = (59.7BMEP) + (25.8n) + 109.4 \quad (59)$$

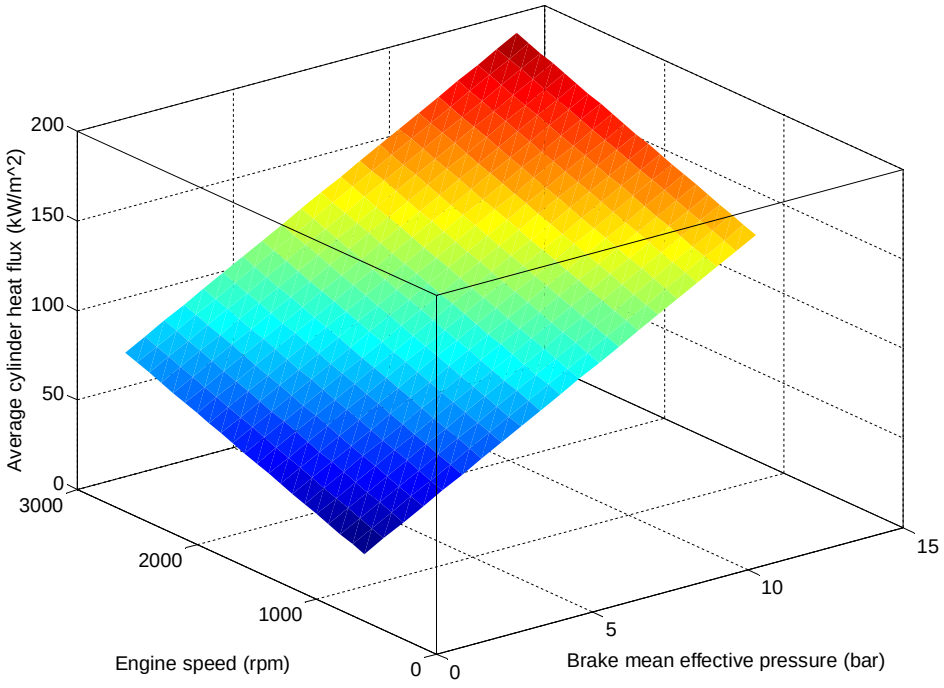


**Figure 6.43 – Linear response model for average cylinder heat flux as a function of engine speed and BMEP**

A similar model was created for the average cylinder wall temperature as a function of engine speed and BMEP, the equation is given in Equation (60) and the response surface is shown in Figure 6.44.

$$T_W\ (°C) = (15.4BMEP) + (7.17n) + 123.6 \quad (60)$$

[7] $R^2$ is a statistical measure of how close the data are to the fitted regression line, RMSE is the root-mean-square error and is a measure of the differences between values predicted by a model and the values actually observed and PRESS is the predicted error sum of squares.

The increase in average cylinder wall temperature was found to be linear with both engine speed and BMEP. The response with BMEP was much steeper due to the increase in in-cylinder pressure and temperature as a result of the higher fuel injection quantities and inlet air charge pressure. Equation (61) is only valid for this engine when fully warm; further investigation could expand this model based on a global engine temperature such as the cylinder head temperature which is used as an input to the ECU.

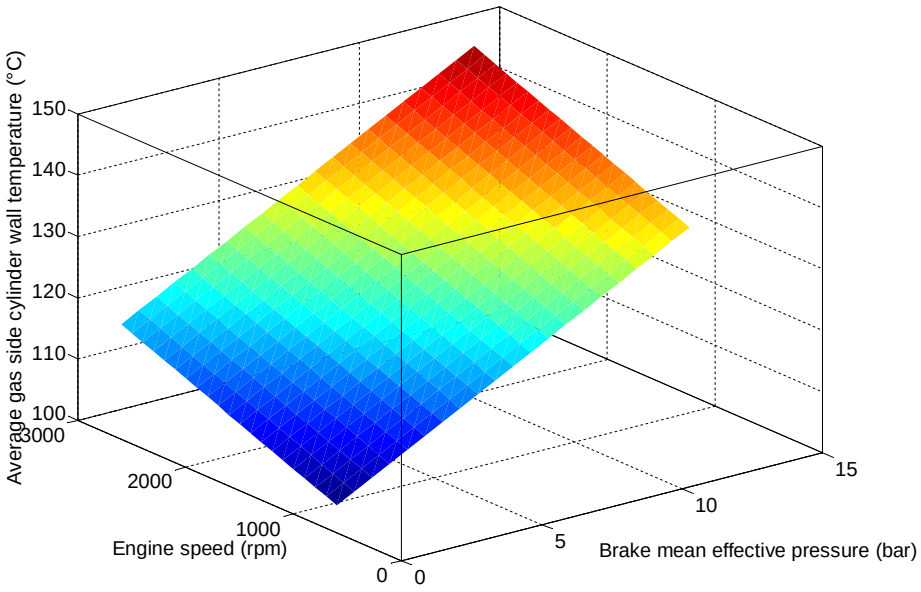


**Figure 6.44 – Linear response model for average gas side cylinder wall temperature as a function of engine speed and BMEP**

This section has enabled the following conclusions to be reached:

- An oil pressure of less than 1.5bar, found to be the piston cooling jet cracking pressure, results in a large increase in the bulk cylinder wall temperature during low speed steady state operation. Therefore, the increase in wall temperature was a result of an elevated piston temperature caused by reduced cooling. A variable flow oil pump has been shown to reduce parasitic losses and have significant benefits on fuel consumption at part load, compared to a fixed displacement pump in other studies, the impact of the reduced oil pressure on component temperatures must be accounted for when calibrating the operating oil pressure. In addition, this data showed that as well as reducing the parasitic losses the VFOP could potentially aid the engine warm-up by increasing the heat flow through the walls to the coolant, this

may be a contributing factor to the benefits measured in fuel consumption. The effect of the PCJs was accounted for in subsequent analysis.

- The temperature profile down the length of the cylinder was found to be different down each side of the cylinder reflecting changing in measurement location, cylinder wall thickness and coolant jacket dimensions. Temperatures were found to be 14°C higher on the exhaust side near the combustion chamber at 60mm from the top deck during high BMEP conditions. The temperature variation from side to side was also attributed to increased friction due to the thrust force generated by the piston motion.

- Local coolant temperature was also found to vary from the inlet side to the exhaust side of the engine by between 2°C and 4°C depending on the operating condition.

- The higher inner wall temperatures but consistent coolant temperatures led to the highest rate of heat flux occurring at the mid location down the coolant jacket.

- Longitudinal conduction was found to be significant with convergence towards the middle of the cylinder where the coolant flow rate was highest. In some cases the longitudinal temperature gradient was 20% of the radial however this was considered to have a negligible impact on the estimated radial conduction through a cylinder wall used in thermal modelling.

- The heat flux was found to have a linear relationship with engine power.

## The application of convective heat transfer correlations using measured in-cylinder pressure data

At each steady state operating condition 500 cycles of in-cylinder pressure data were captured. This data was then used to calculate a number of engine performance parameters. Prior to analysis the in-cylinder pressure signals were averaged and filtered using a low pass

Butterworth filter[8], followed by a thermodynamic pressure referencing process with the measured cylinder pressure being pegged to match the inlet manifold pressure at BDC. The filtered and corrected pressure data was used to calculate the net heat release as discussed earlier. To calculate the gross heat release, an estimate of the heat transfer from the combustion gases to the cylinder wall is required. Established correlations, such as Eichelberg, Annand, Woschni, Finol, Sitkei and Ramanaiah, and Hohenberg can be implemented to estimate this. A number of parameters are necessary in order to implement the different correlations, these include in-cylinder pressure data (both fired and motored), mean piston speed, instantaneous values of cylinder volume, cylinder surface area, in-cylinder mass, mean cylinder wall temperature, and a number of gas properties including viscosity, density, thermal conductivity and the ratio of specific heats. To simplify the analysis the in-cylinder temperature and mass were obtained through 1D modelling performed in Ricardo WAVE. A simplified four-cylinder engine model was created based on the known geometry for the experimental engine. The model used a number of boundary conditions such as the engine speed, measured inlet manifold temperature and pressure, exhaust manifold pressure, SOI, EGR rate and fuel injection rate, to estimate the total mass air flow and brake torque. Model iterations were performed until the calculated mass air flow and brake torque were within ±2% of the measured values. Outputs from the model included the in-cylinder temperature and mass throughout a single four stroke cycle. The in-cylinder mass was calculated based on the mass flow through the valves and was subsequently used, along with the in-cylinder pressure, to calculate the in-cylinder gas temperature. The experimental engine had four valves per cylinder and the inlet valves were larger in diameter to allow for higher maximum air flows for a given cylinder displacement. The valves were poppet type and the instantaneous flow area was dependent on the valve lift and the valve geometry. The flow area was calculated by breaking the valve lift into three stages. The first two stages, i.e. the minimum flow area for low and medium valve lift, can be calculated based on a frustum of a right circular cone and the high lift stage is simply the port flow area minus the sectional

[8] The filter was applied using the FiltFilt function from the Mathwork's Matlab Digital Filter library. This is a zero-phase filter as it is applied in both the forward and reverse directions. This ensures there is zero phase lag which is very important as the pressure signal must remain aligned with the crank angle position.

area of the valve stem. Further detail can be found in Heywood [132]. A diagram of a valve is shown in Figure 6.45 and the valve dimensions are given in Table 7.

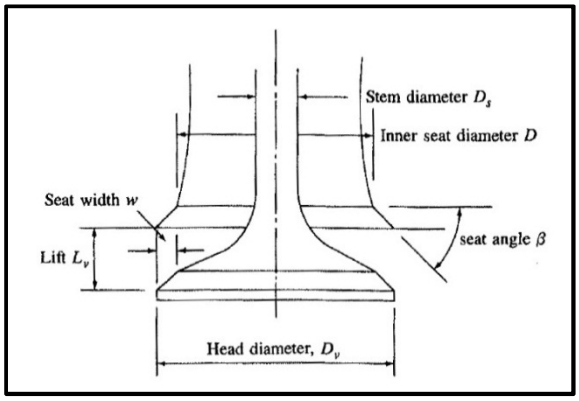


**Figure 6.45 – Common valve dimension diagram [132]**

**Table 7 – Valve dimensions**

| | Head diameter (mm) | Stem diameter (mm) | Port diameter (mm) | Seat width (mm) | β (°) |
|---|---|---|---|---|---|
| Inlet | 29.8 | 7.8 | 26.3 | 1.7 | 30 |
| Exhaust | 25.8 | 7.6 | 21.6 | 2.1 | 45 |

The mass flow rate through the calculated valve area can subsequently be described on a crank angle basis by the equation for compressible flow through a flow restriction. This equation was derived from one-dimensional isentropic flow analysis:

$$\dot{m} = \frac{C_D A_R p_0}{(RT_0)^{1/2}} \left(\frac{p_T}{p_0}\right)^{1/\gamma} \left\{ \frac{2\gamma}{\gamma - 1} \left[ 1 - \left(\frac{P_T}{P_0}\right)^{(\gamma-1)/\gamma} \right] \right\}^{1/2} \tag{61}$$

$\dot{m} = \frac{C_D A_R p_0}{(RT_0)^{1/2}} \gamma^{1/2} \left(\frac{2}{\gamma+1}\right)^{(\gamma+1)/2(\gamma-1)}$ when the flow is choked, i.e. $\frac{p_T}{p_0} \leq \left[\frac{2}{\gamma+1}\right]^{\gamma/(\gamma-1)}$

Equation (61) includes an experimentally determined discharge coefficient, $C_D$ to include the real gas flow effects, the stagnation conditions upstream of the flow restriction and the static pressure immediately after the restriction. The previously discussed valve flow area is used as the area of reference for the flow. The discharge coefficients and valve lift profiles for the experimental engine were supplied by Ford. The valve lift profile for the inlet and exhaust valves is shown in Figure 6.46 and the calculated flow area is shown in Figure 6.47. In all

figures combustion occurs around top dead centre (TDC) shown at a crank angle of 360°. The engine has fixed valve timing with a small amount of valve overlap shown in Figure 6.46 around TDC gas exchange.

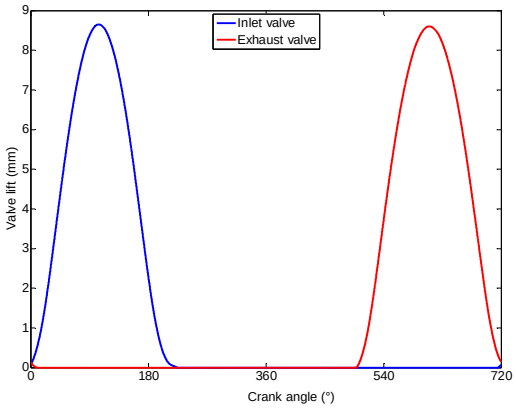


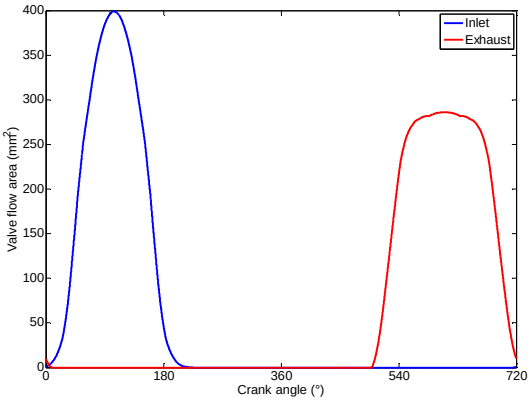


**Figure 6.46 – Inlet and exhaust valve lift profiles**

**Figure 6.47 – Inlet and exhaust valve flow areas**

An example of the in-cylinder temperature and mass is shown in Figure 6.48. The compression stroke causes a rise in the in-cylinder temperature but the start of combustion shows a significant increase in the temperature within the cylinder. A peak in-cylinder temperature of 1870K is seen during the cycle, and the average cycle temperature was found to be 805.8K. The temperature remains high during the exhaust stroke; however a significant drop in temperature is shown with the introduction of the fresh charge. The low EGR rate at this particular condition and efficient intercooler means that the inlet manifold temperature was 334K, resulting in the significant drop in in-cylinder temperature. The in-cylinder mass is shown to not reach zero, due to the mass contained in the clearance volume at TDC. The fuel injection is shown as a rise during the valve closed period between 200° and 500° crank angle, simple models show this as a step increase in in-cylinder mass, however WAVE utilises the fuel injector specification and rail pressure to determine the flow rate and subsequent rise in mass.

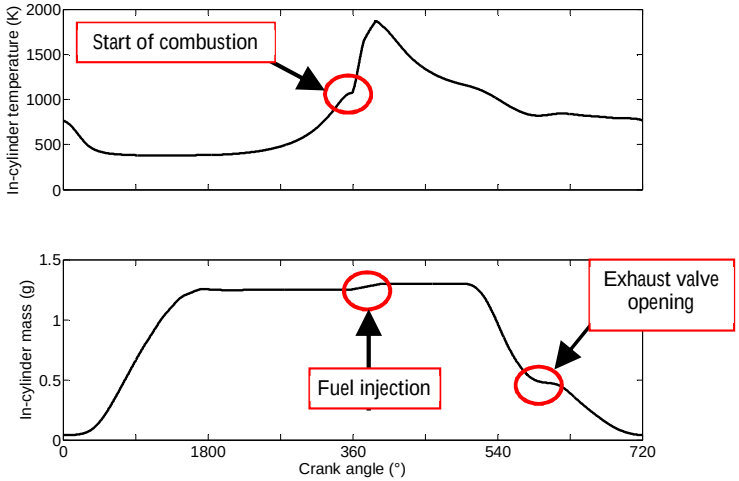


**Figure 6.48 – Example of in-cylinder temperature and mass profiles for high power operating condition**

The WAVE in-cylinder temperature and mass data for each operating condition was input into Matlab for calculation of heat release and for evaluation of the empirical heat transfer correlations against the calculated heat transfer coefficients from measured data. The heat flux data from the multipoint sensors has been averaged around the cylinder to result in a single average heat transfer rate for the cylinder. This was done by interpolating the measured heat flux around the circumference of the cylinder and linearly down the bore. A flow diagram showing how the measured data was combined with the WAVE data to give the gas side convective heat transfer coefficients (CHTCs) is given in Figure 6.49.

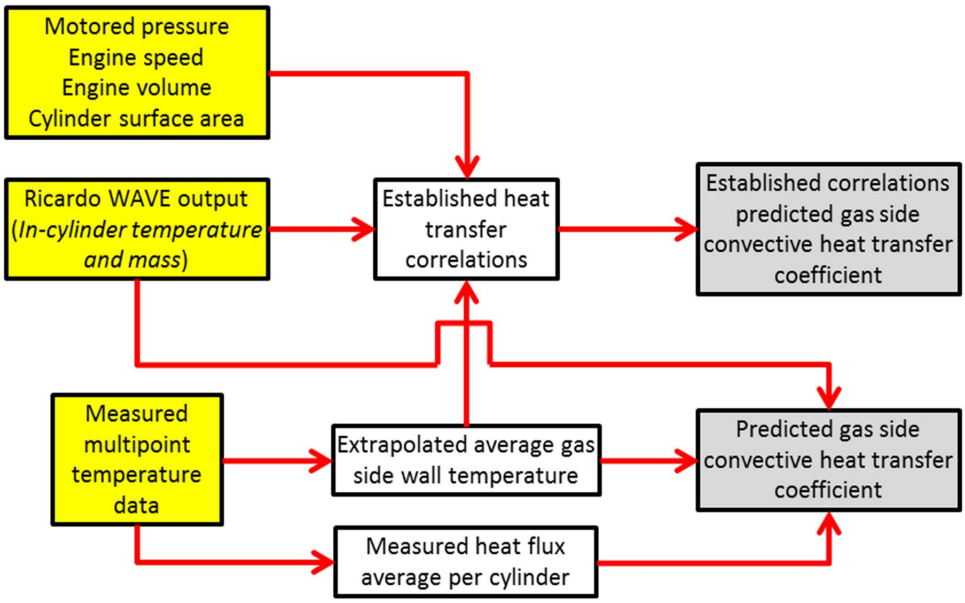


**Figure 6.49 – Flow diagram of data used for evaluation of established heat transfer correlations**

The yellow boxes indicate the input of measured and WAVE data and the grey boxes show the analysis outputs, in this case these are the gas side convective heat transfer coefficients. The thermal gradient calculated from the multipoint temperature data was used to extrapolate an average gas side wall temperature which was used in both the established heat transfer correlations and the measured heat flux method for calculating the gas side CHTCs. This analysis assumes a uniform heat transfer coefficient from the combustion gases to the cylinder liner. The measured data only takes into account the heat transfer from the combustion gases to the cylinder liner and not to the piston crown or the cylinder head which have been found to be significant in previous studies, this was taken into account in the analysis [48]. The analysis described above allowed for the outputs from the empirical correlations to be evaluated against measured engine data across a range of operating conditions.

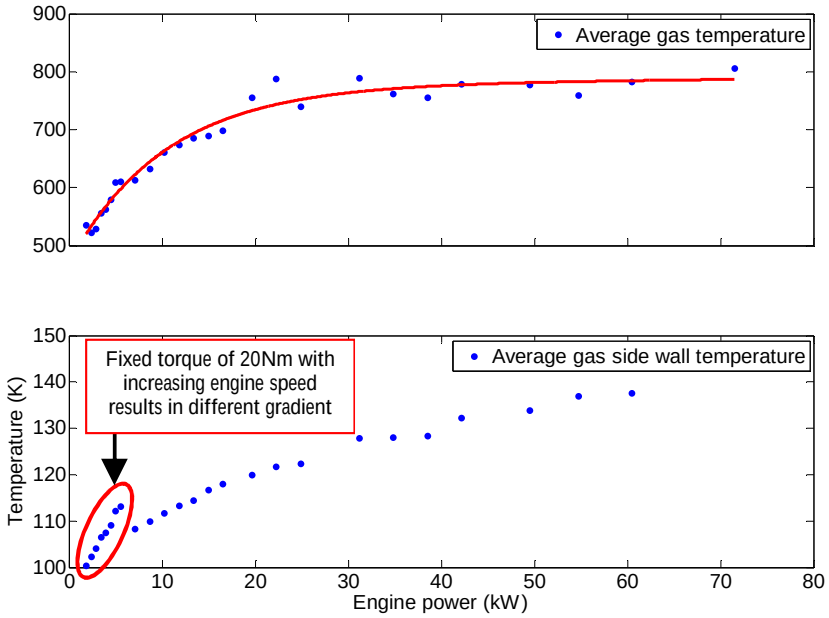


**Figure 6.50 – a) Average in-cylinder gas temperature from Ricardo WAVE and b) Average extrapolated gas side cylinder wall temperature for all operating conditions**

Shown in Figure 6.50 are the gas side cylinder wall temperatures and in-cylinder gas temperatures plotted against the engine power for all operating conditions. The in-cylinder gas temperature profile has been fitted with an exponential curve due to the steep increase between 2kW and 20kW, the gas temperature was found to plateau above 30 kW around 780K. The cylinder wall temperature shows two distinct trends. Below 7 kW there is a steep gradient, indicating a strong change in temperature with an increase in engine power, these

points were found to be at 20Nm and the increase in wall temperature was due to an increase in engine speed. Above 7 kW an increase in engine power results in an increase in temperature with less noticeable effects of engine torque and/or speed.

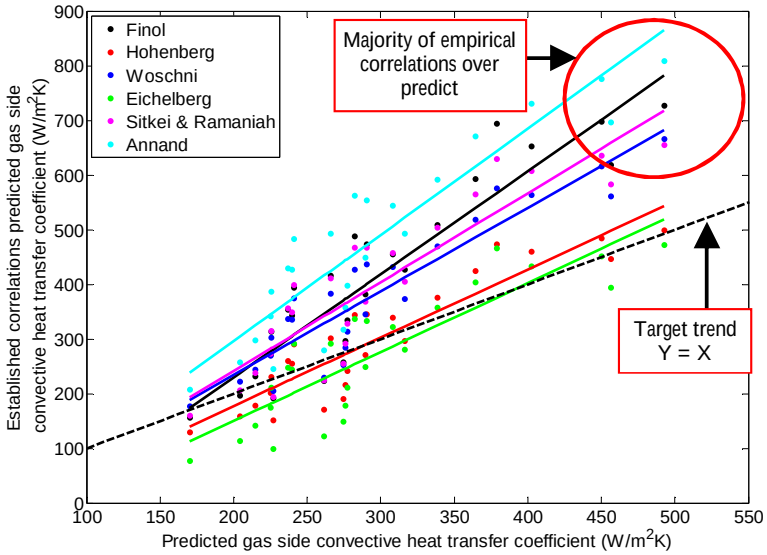


**Figure 6.51 – Comparison of gas side convective heat transfer coefficients calculated from empirical correlations to those estimated using measured multipoint temperature data and in-cylinder gas temperatures obtained from Ricardo WAVE**

The correlation derived CHTCs are shown plotted against the CHTCs derived from measured data. The dashed line shows the ideal relationship where the measured CHTC is equal to the predicted. For each set of CHTC, a linear regression curve fitting was performed and the data shows a linear correlation between the two calculation methods, with R-squared values ranging from 0.75 to 0.86. The lowest value of R-squared was obtained from the Eichelberg correlation; therefore this has the weakest relationship with the measured data, indicating that variations in the heat transfer performance are not taken into account in the estimation process. This correlation was derived in 1939 based on a slow acting two-stroke engine which is significantly different to the experimental engine used in this study. The strongest linear correlation was found from the Woschni correlation. The Finol correlation also showed a strong linear correlation to the measured data, this would have been expected as it was derived from a modern 2.0 litre diesel engine from the same engine family as the experimental engine. The correlations were found to significantly over-predict the CHTCs at the higher power operating conditions, with some under-prediction at the low power conditions, especially using the Eichelberg and Hohenberg correlations. Figure 6.52 shows the calculated percentage error at each operating condition for the

Hohenberg correlation, which shows significant error at the low engine power conditions. The largest error was found from the Annand correlation. The Finol correlation error is shown in Figure 6.53 as it is the most recent and relevant correlation to the experimental engine, however it was found to over-predict by up to 80% at higher engine powers. It is interesting to note the error trends at different engine loads, 20Nm and 60Nm are highlighted in red and blue respectively. A similar trend was found for the other correlations investigated. The constants employed in the Finol correlation were established from cycle averaged data obtained at 4000rpm and 100% of the limiting torque curve but were found to under-predict the CHTC at 70% and 40% of the limiting torque curve by 10%. Experimental data shows that in this case it was found to over-predict by at least 54%. Improvements to the prediction of the CHTCs are required to better predict the transfer of heat to the cylinder wall and through it. From these findings it was decided to take the Hohenberg correlation forward to improve its correlation with the measured data. The Hohenberg correlation illustrated the least error at higher engine power conditions.

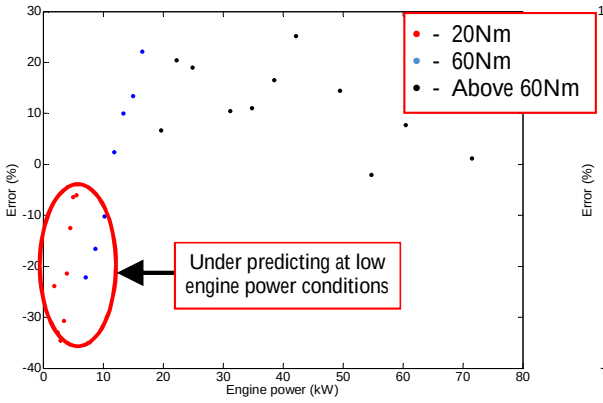


**Figure 6.52 – Hohenberg correlation CHTC error**

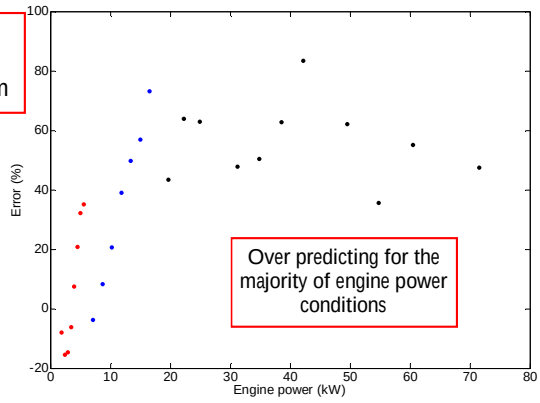


**Figure 6.53 – Finol correlation CHTC error**

In order to solve the Hohenberg equation globally for the operating conditions tested, a non-linear least-squares approach was undertaken. This was performed in Matlab using the optimisation toolbox. The 'lsqnonlin' function solves non-linear least-squares problems by computing a vector-valued function. The function is passed a start point and finds a minimum of the sum of squares of the desired function. Each of the coefficients can be constrained with an upper and lower limit or be allowed to search unconstrained. In this application no bounds were set. The solver works on the basis of a gradient error decent, therefore changes are applied to each of the coefficients and the sum of squares is compared to the previous iteration until the difference is below a given threshold.

As with most nonlinear function solvers, it is difficult to determine whether an obtained solution is a global solution or a local solution, which means that a local minimum has been found. This highlights that the choice of starting point is often critical to finding the right solution. A possible answer to this problem is to complete the optimisation from a number of starting points, commonly referred to as a multi-start optimisation. A variety of methods for selecting the starting points are available, including design of experiments, space filling designs or grid patterns. For this optimisation a range was given to each coefficient based on the established coefficients given in the Hohenberg correlation, shown in Table 8, based on Equation (62). In turn each coefficient was perturbed across the range whilst keeping the other coefficients constant, resulting in 1260 starting conditions.

$$h = C_1 \cdot V_S^a \cdot p^b \cdot T^c \cdot (c_m + C_2)^d \tag{62}$$

**Table 8 – Ranges used in nonlinear optimisation**

| Coefficient | Hohenberg | Lower limit | Upper limit | Step |
|---|---|---|---|---|
| $C_1$ | 130 | 122.5 | 137.5 | 2.5 |
| $C_2$ | 1.4 | 1.1 | 1.7 | 0.1 |
| a | -0.06 | -0.09 | -0.03 | 0.01 |
| b | 0.8 | 0.5 | 1.1 | 0.1 |
| c | -0.4 | -0.7 | -0.1 | 0.1 |
| d | 0.8 | 0.5 | 1.1 | 0.1 |

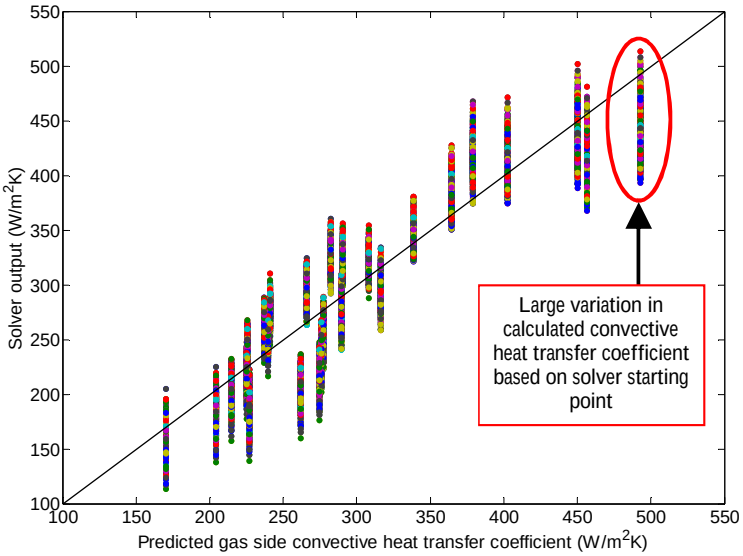


**Figure 6.54 – Convective heat transfer coefficients calculated using the solutions obtained from the non-linear optimisation from all starting points plotted against the predicted values from the measured data**

Figure 6.54 shows all the Hohenberg correlation outputs when employing the coefficients found using each of the starting points in the optimisation. The different starting points result in a large variation in the calculated convective heat transfer coefficients at each engine operating condition. This further highlights the non-linearity of gas side convective heat transfer within the cylinder, in addition to the large number of local minima which exist in the design space. To improve this error an iterative process was subsequently employed, where the solution to one optimisation was fed in as the starting point to the next optimisation, thus employing a gradient decent method. The results of which are shown in Figure 6.55. Also shown in this figure are the heat transfer coefficients obtained using the best solution from the single optimisation, and heat transfer coefficients using the original coefficients employed by Hohenberg. It shows that the optimisation has greatly improved the accuracy across the operating conditions, with particular improvement at low values of CHTC. The single run optimisation reduced the sum of the errors by 48.6%. The iterative process has shown further benefits over the multi-start optimisation further reducing the sum of the errors by 29% (77.6% improvement over the original Hohenberg coefficients). The optimised correlation coefficients are given in Table 9.

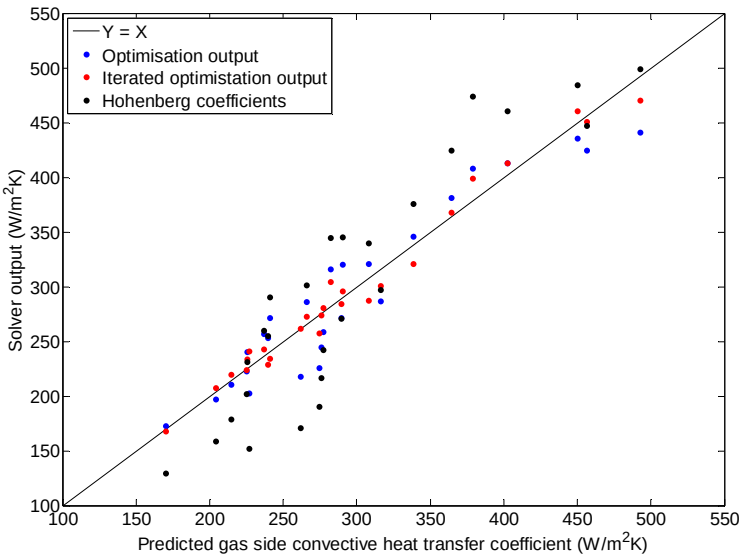


**Figure 6.55 – Comparison of single optimisation solution with iterated solution and Hohenberg original coefficients**

**Table 9 – Optimised Hohenberg correlation coefficients**

| Coefficient | Hohenberg | Single run | Iterative run |
|---|---|---|---|
| $C_1$ | 130 | $3.14x10^4$ | $1.074x10^{11}$ |
| $C_2$ | 1.4 | -1.76 | -2.61 |
| a | -0.06 | -0.04 | 0.76 |
| b | 0.8 | 0.85 | 1.02 |
| c | -0.4 | -1.01 | -2.33 |
| d | 0.8 | 0.22 | 0.17 |

It was decided to introduce a cylinder wall temperature component into the Hohenberg correlation to improve the curve fit. Equation (63) shows the function for the optimisation. A similar process to above was employed with an initial single optimisation performed with the same 1260 starting points, followed by an iterative process undertaken on the best result.

$$h = C_1 \cdot V_S^a \cdot p^b \cdot T^c \cdot (c_m + C_2)^d \cdot T_w^e \tag{63}$$

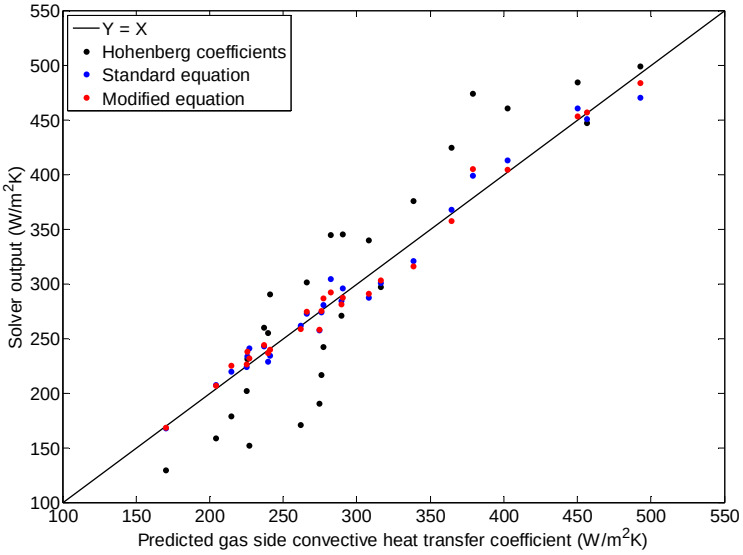


**Figure 6.56 – Comparison of modified Hohenberg equation to original**

Figure 6.56 illustrates the small improvement obtained by including cylinder wall temperature as a variable in the convective heat transfer function, especially at the higher heat transfer coefficients. The inclusion of cylinder wall temperature adds another degree of freedom and reduces the sum of the errors further over the original equation. Compared to the original Hohenberg coefficients the single run reduced the sum of the errors by 76.9%, whereas the iterative run reduced the errors by 81.5%. This is a 17.4% improvement compared to the

correlation without the inclusion of the cylinder wall temperature component. The final equation is shown below.

$$h = 1.18 \times 10^{-12} \cdot V_S^{-0.96} \cdot p^{0.48} \cdot T^{-2.33} \cdot (c_m - 2.54)^{0.17} \cdot T_w^{6.54} \quad (64)$$

Figure 6.57 shows the modified correlation in comparison with the established ones for the highest power condition that was tested. The modified correlation shows some clear differences during the gas exchange and expansion periods. The optimisation was performed with no constraints placed on the equation coefficients with the correlation to the cycle average being the primary objective; this has led to coefficients which are significantly different to the original equation. As a result the effect of changing cylinder volume, especially during gas exchange has a much greater impact on the calculated convective heat transfer coefficients resulting in much larger values than the other correlations, clearly seen during the gas exchange period. Therefore to achieve the cycle average the coefficient of the average in-cylinder temperature term has decreased, leading to the sudden reduction in convective heat transfer coefficient at the start of injection. The aim of the optimisation was to improve the accuracy of the cycle average heat transfer coefficient, which was successful. In order to apply this correlation on a crank angle base a repeat optimisation procedure would be required, where the equation coefficients are constrained and the focus of the optimisation was the combustion period, i.e. intake valve closing to exhaust valve opening.

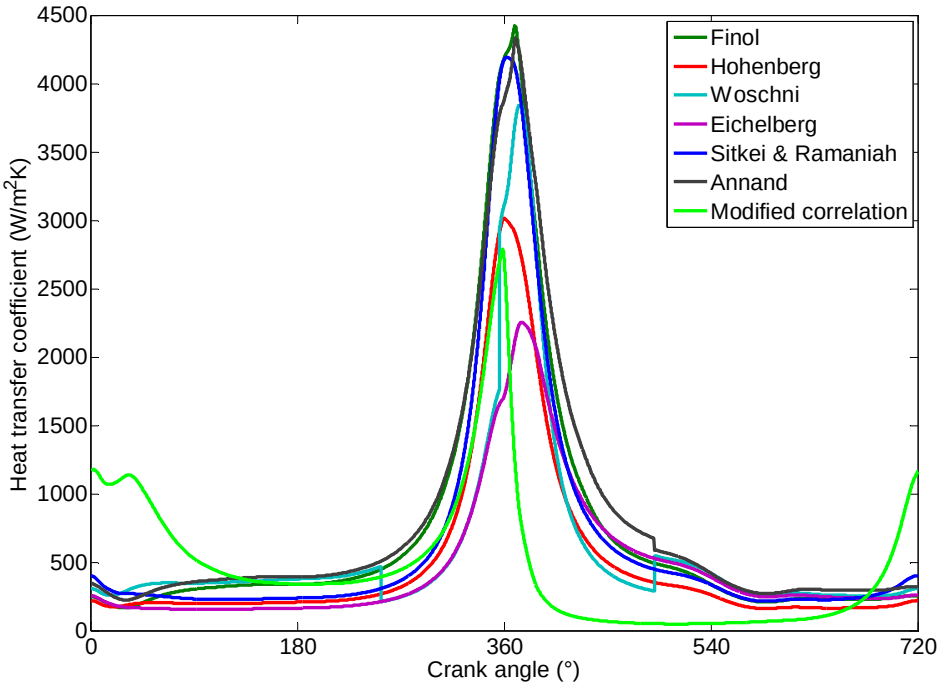


**Figure 6.57 – Predicted heat transfer coefficient including modified correlation**

A similar investigation was performed to derive an average heat flux through the cylinder walls based on the extrapolated gas side wall temperature using the CHTCs from the correlations explored above. A flow diagram on the analysis procedure is shown in Figure 6.58. The calculated heat flux was then compared against that measured by the multipoint sensors.

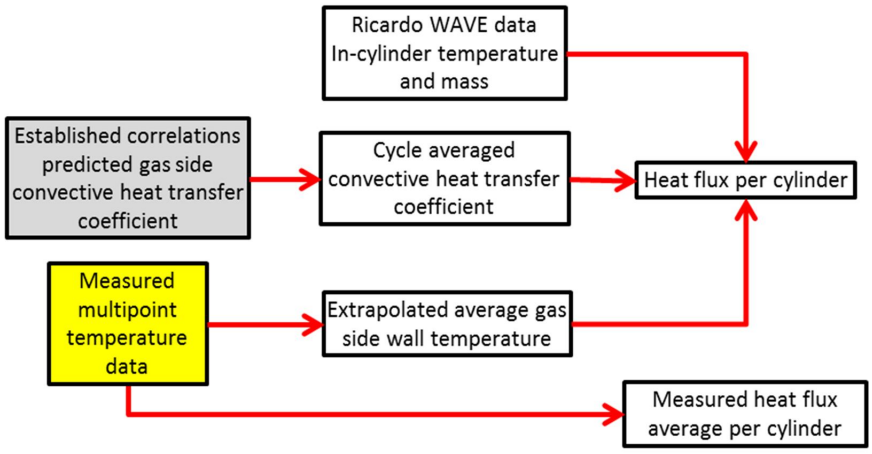


**Figure 6.58 – Flow diagram of heat flux calculation from heat transfer correlations and measured data**

The comparison of the cylinder-averaged measured heat flux to the predicted heat flux is shown in Figure 6.59. To calculate the heat flux, the CHTC was multiplied by the difference

in the in-cylinder gas and the wall temperature, therefore this is constant at each operating condition for all correlations and for the measured data. Due to this calculation method the error from the CHTC calculation is directly transferred to the calculation of heat flux, therefore the best correlation was found with the modified Hohenberg equation.

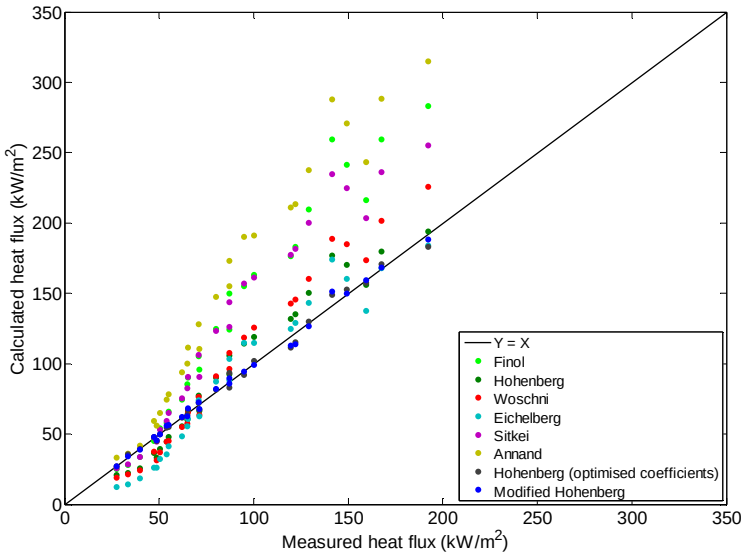


**Figure 6.59 – Comparison of measured average heat flux through the cylinder wall to those calculated from predicted convective heat transfer coefficients**

The following conclusions can be made from the findings in this sub-section:

- The average in-cylinder gas temperature over a complete engine cycle was found to plateau above an engine power of 30kW at around 780K. This is due to a combination of the concentration of EGR and the residency time of the gas within the cylinder controlling the temperature. Temperatures greater than this would result in component fatigue and therefore the use of more exotic materials for piston crown and inlet and exhaust valves.

- The average cylinder wall temperature across an engine cycle was found to have two distinct trends depending on the engine power. At low engine powers, i.e. below 7kW there was a large increase in temperature due to a small increase in engine power resulting in a steep gradient. The increase in engine power was a result in increasing engine speed at a fixed low load, implying that the injected fuel contributes significantly to the temperature control in the cylinder.

- An evaluation of established correlations found that the majority over-predicted the convective heat transfer coefficients, especially at higher power conditions. The advances in material properties used in engine block manufacture may be the cause of the reduction in heat transfer from the combustion charge to the cylinder wall. The largest error was given by the Annand equation.

- The Hohenberg equation coefficients were optimised using a non-linear least-squares regression employing a gradient decent approach. This resulted in a 77.6% improvement in the correlation between the calculated CHTC's and those measured at each operating condition.

- An average cylinder wall temperature component was added to the Hohenberg equation, which further improved the correlation. It was found that the inclusion of the average cylinder wall temperature reduced the sum of the errors by 17.4%, highlighting the influence of cylinder wall temperature on the convective heat transfer coefficient between the combustion charge and the cylinder wall.

- The modified equation was found to accurately predict the cycle average heat transfer coefficient but could not be currently used to estimate the CHTC's on a crank angle base without a repeat optimisation with the equation coefficients being constrained in order to prevent an over prediction during the gas exchange period.

## Section summary and conclusions

This section aimed to provide a description of how the engine operating conditions affected the cylinder wall temperature and the rate of heat transfer through the cylinder liner. In addition some understanding of the temperature distribution and energy balance at each operating conditions was targeted. Finally an investigation into the accuracy of established convective heat transfer correlations was undertaken. Some of the key findings of this section are outlined below:

- Ideally a larger proportion of the engine operating map would have been explored to fully understand the interactions of the engine speed and load on the thermal

distribution through the engine. An additional idle condition would have also been included in the steady state operating points as the low load condition which was included in the experimental program was at an elevated speed and torque due to the applied method.

- It was found that using the midpoint of the operating section did not provide an accurate approximation to the average outputs from that area. In hindsight the distribution of drive cycle operating points within the discretized area should have been taken into account and the tested operating condition should have been located to best replicate the spatial variation within the area, rather than choosing the arbitrary midpoint.

- It was found that in the region of 12% of the total input energy to the engine is lost to the coolant across the load range at 2625rpm. It was found that by reducing the engine speed and increasing the engine torque, a small proportion of the input energy was used to overcome friction. The experimental engine behaved as expected with less than 30% of the total input energy being converted to useful work.

- The coolant temperature distribution across the operating conditions was found not to vary significantly through the engine structure, with the largest increase shown across the oil cooler where a significant amount of heat was absorbed from the oil. The oil temperatures were found to change considerably with the operating condition, with the higher speed and load conditions showing oil temperatures 40°C higher than at idle. Interestingly the oil temperature was also found to reduce along its path through the engine structure and into the cylinder head. The oil in the camshaft bearings was also found to be on average 7.2°C hotter on the exhaust cam than the inlet cam due to presence of the hot exhaust gas in the ports resulting in higher cylinder head operating temperatures on the exhaust side.

- The piston cooling jets were found to impact the cylinder wall temperatures significantly at low speed. When operating at low speed, oil pressure remained below the nominal operating pressure of the jet and the cylinder wall was found to be significantly hotter. It was concluded that this phenomena only occurred during

steady state operating; when the oil gallery pressure was allowed to decay to below 1.5bar, therefore it was required to remove this contributing factor from the analysis.

- The temperature profile down the cylinder wall was found to vary significantly from exhaust side to inlet side, with the location of the coolant jacket also impacting on the temperature variation with operating condition.

- The cylinder liner heat transfer was found to be significantly different from the inlet to exhaust sides of the engine. The exhaust side of the engine recorded higher peak rates of heat transfer assumed to be caused by the higher levels of friction due to the thrust surface of the piston under the power stroke. The magnitude of heat flux was found to have a linear relationship to engine power at each position down the bore length on both sides of the cylinder.

- The crank caps were found to have a similar response to increasing to engine speed and torque as the other areas of the engine, illustrating a 7°C rise in oil temperature between the main gallery and bearing 1. Higher temperatures were measured at bearing 3 and 5.

- The cylinder head surface temperature located on the web between the cylinder 2 valves and the external structure was found to be on average 7.2°C hotter on the exhaust side than the inlet side due to the hot gases passing through the exhaust ports.

- Established correlations were found to over-predict the cycle average convective heat transfer coefficients, especially at higher operating conditions. Optimisation of the Hohenberg equation coefficients led to a 77.6% reduction in the sum of errors compared to the existing correlation. Further improvements to the correlation were achieved by introducing an average cylinder wall temperature component to the Hohenberg equation. This reduced the sum of the errors by a further 17.4%.

## 6.3 Transient investigation – Experimental Design of Experiments

The aim of this section is to assess the thermal effects of additional hardware during cold-start transient testing on the cylinder wall temperatures and the rate of heat transfer through them. It would be expected that the coolant flow rate through the engine and the temperature of the coolant into the engine would have the principle effect on the heat transfer through the cylinder liner. One hypothesis would be that a reduction in the coolant inlet temperature would promote a steep temperature gradient through the cylinder wall promoting heat transfer from the cylinder to the coolant. Whilst a reduced coolant flow rate would contain the heat from combustion within the engine minimising the heat transfer to components external of the main engine.

### A summary of the Design of Experiments operating condition determination process

The engine was fitted with a number of different hardware devices which had been integrated into the production configuration. The effect of these devices on the thermal conditions within the engine is very important if they are to be considered for production. The final series of experiments was designed to obtain a complete understanding of the interaction of each of these devices to the overall system. The control variables for this work are shown in Table 10. The selection process and reasoning behind these input variables are discussed in detail by Burke [137]. The DoE approach was designed to explore the responses of a number of individual parameters and their interactions with each other with an optimised amount of experimentation.

**Table 10 – Input variables for design of experiments**

| DoE Inputs | Setting 1 | Setting 2 | Setting 3 |
|---|---|---|---|
| Post engine throttle | Mapped | Mapped with minimum limit | Open |
| Oil cooler | On | N/A[9] | Bypassed |
| EGR coolant throttle | Low Flow: 20% | Mid Flow: 28%[10] | High Flow: 100% |
| EGR cooler type | Coolant | N/A | Oil |
| SOI | Standard | +1.5° | +3° |

The design of experiments, D-optimal test design approach produced a test matrix made up of 17 different conditions, shown in Table 11. An additional baseline test condition was added to the design and repeated a number of times through the test programme in order to monitor the stability of the engine within the experimental programme. As the effect on warm-up was the prime objective for the experiments, each test point represented a cold start NEDC and the calibration run order was randomised. Further details and reasoning behind the experimental programme are discussed by Burke [137]. The forced cool down procedure discussed in Chapter 4 Section 4.6 was implemented after each test point which allowed 2 tests to be performed each day. Investigation into the control and repeatability of each of the input parameters was illustrated by Burke and was found to be good [137]. This investigation also highlighted the scatter due to interaction between the different parameters. It was concluded that by throttling the coolant flow from the engine, the engine warm-up was improved by effectively isolating a proportion of the thermal mass and reducing the thermal inertia. Burke investigated the complete system response, the aim of this section is to delve deeper into the mechanism within the cylinder which caused the reduced warm-up time [138-140].

[9] Implies a two level system

[10] Percentage of throttle opening on outlet of coolant from EGR cooler

**Table 11 – 17 point D-Optimal design of experiments**

| DoE number | 1 – Post engine throttle | 2 – Oil cooler | 3 – EGR coolant throttle | 4 – EGR cooler type | 5 – SOI |
|---|---|---|---|---|---|
| Baseline | Open | On | High | Coolant | 0 |
| 1 | Mapped | Bypass | Low | Oil | 0 |
| 2 | Open | Bypass | Low | Oil | 1.5 |
| 3 | Mapped | Bypass | Low | Coolant | 0 |
| 4 | Open | Bypass | Low | Coolant | 3 |
| 5 | Open | On | Low | Oil | 0 |
| 6 | Open | Bypass | High | Oil | 1.5 |
| 7 | Mapped | Bypass | High | Coolant | 1.5 |
| 8 | Open | On | High | Coolant | 0 |
| 9 | Open | Bypass | Low | Coolant | 1.5 |
| 10 | Mapped | On | Low | Coolant | 1.5 |
| 11 | Mapped | Bypass | High | Oil | 3 |
| 12 | Mapped | On | Low | Oil | 3 |
| 13 | Mapped | On | High | Oil | 1.5 |
| 14 | Open | Bypass | High | Oil | 0 |
| 15 | Open | On | High | Coolant | 3 |
| 16 | Mapped | Bypass | High | Coolant | 0 |
| 17 | Mapped[11] | On | Mid | Coolant | 0 |

# Transient results and discussion

This section aims to describe the data collected through the experimental programme and highlight the important findings from the series of transient drive cycle experiments performed utilising the active thermal management system described above. The data analysis can be broken down into two areas. Initially a brief investigation into the overall system response will be given. This has been looked at in more detail by Burke, however some details are required to understand the subsequent investigation [137]. The main discussion within this section is the effect of the system responses on the heat transfer through the cylinder liner and how the external coolant and oil system changes have impacted the distribution of heat and fundamentally affected the rate of warm-up through the drive cycle.

[11] This test employed a reduced lower threshold which enforced a minimum throttle opening and hence a minimum engine out coolant flow. This produced a mid-flow setting throughout the test.

## System responses to changes in active thermal management actuators

A traditional DoE analysis method has not been utilised in this thesis as the overall system response and subsequent modelling of the system was undertaken by Burke. However, the effects of the input parameters on the overall system need to be understood before the effects on the cylinder wall temperatures and the heat transfer through the cylinder liner can be explained. The engine coolant flow is shown in Figure 6.60 and was found to produce 4 distinct groups. The post engine coolant throttle (IP1) has two modes, 'Open' or 'Mapped', the blue traces in Figure 6.60 indicate the 'Mapped' or low flow condition and the other 3 groupings are 'Open'. The mapped control of the engine out throttle shows minimal flow through the ECE sections of the drive cycle, the closed throttle forces all coolant flowing through the engine during this period around the EGR circuit; it is not until the EUDC section, when the cylinder head temperature has reached 85°C, that significant flow is measured. The large oscillations in the measured flow through the engine during the EUDC are caused by there being no hysteresis set on the coolant throttle so it is therefore responding to the cooling effects of the engine coolant on the cylinder head temperature. The mid flow conditions include four post engine coolant throttle mapped conditions where the EGR flow was high, resulting in an increased engine coolant flow. The maximum flow rate when IP1 is open interacts with the EGR coolant throttle; a high flow rate through the EGR cooler results in an increase in the coolant flow through the engine, therefore a low EGR flow reduced the peak flow rate through the engine, shown by the green lines. Figure 6.60b shows the cumulative engine coolant flow over the drive cycle; this shows the trends more clearly as it hides the effect of the changing engine speed on the coolant flow rate.

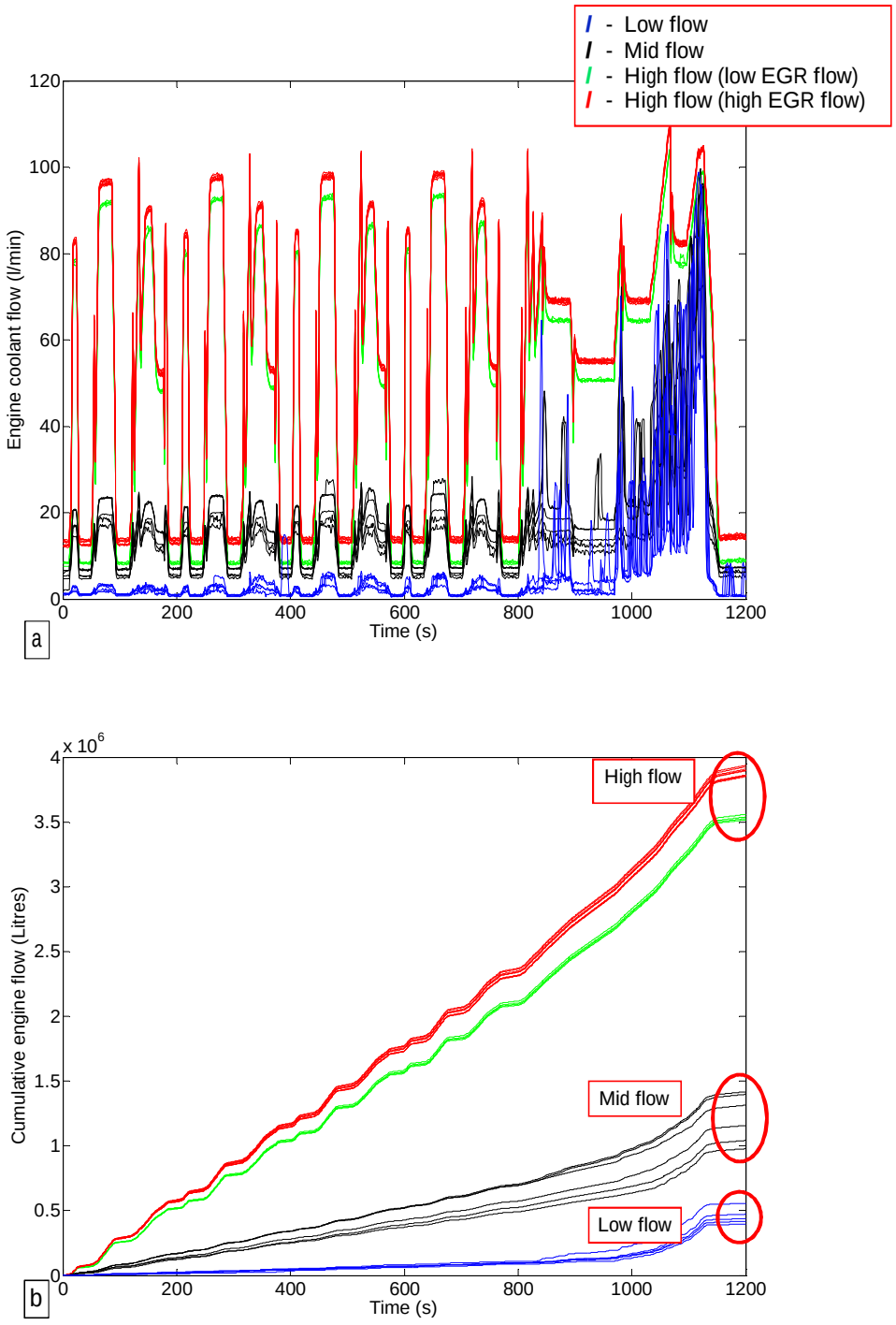


**Figure 6.60 – a) Coolant flow rate through the engine and cylinder head for all configurations, grouped together by the coolant flow rate condition. b) Cumulative coolant flow rate through the engine**

Figure 6.61, below, shows the cumulative EGR cooler coolant flow with three groups highlighted. Low flow through the EGR cooler throttle is clearly shown by the blue lines; the black lines indicate the mid-point position and the red lines indicate the high flow condition. The maximum flow variation is due to the interaction with both the engine out throttle (IP1) and the oil cooler (IP2) mode. The highest flow rate is produced when IP1 is

low and IP2 is in bypass. The flow rate subsequently reduces as IP2 is 'On' and then IP1 is 'Open', the baseline condition is in this grouping.

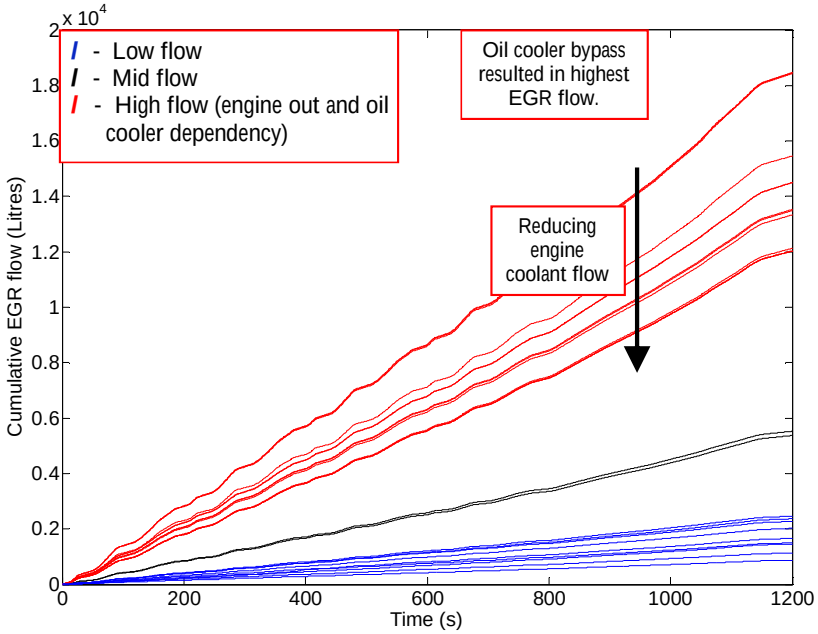


**Figure 6.61 – Cumulative coolant flow through the EGR Cooler for all configurations, grouped together by the EGR flow condition**

The impact of the EGR cooler type on the gas temperatures is shown in Figure 6.62, the oil cooled experiments are shown in red and the coolant cooled experiments in blue. Higher EGR gas outlet temperatures were measured when coolant was used, indicating that oil provides more cooling to the EGR gas than the coolant. Variation in the peak temperatures are more noticeable when employing coolant cooled EGR, indicating that the other input parameters have an influence on the post EGR temperature. The SOI was found to have 3 distinct groups with some variation due to the engine warm-up rates affecting the operating position on the temperature dependent ECU calibration maps. The SOI was found to have significant impact on the fuel consumption, offering up to a 20g (5.5%) benefit over the drive cycle, however this was found to be a secondary effect due to the changes in temperature in the combustion chamber affecting the ignition delay and subsequent premix combustion [137].

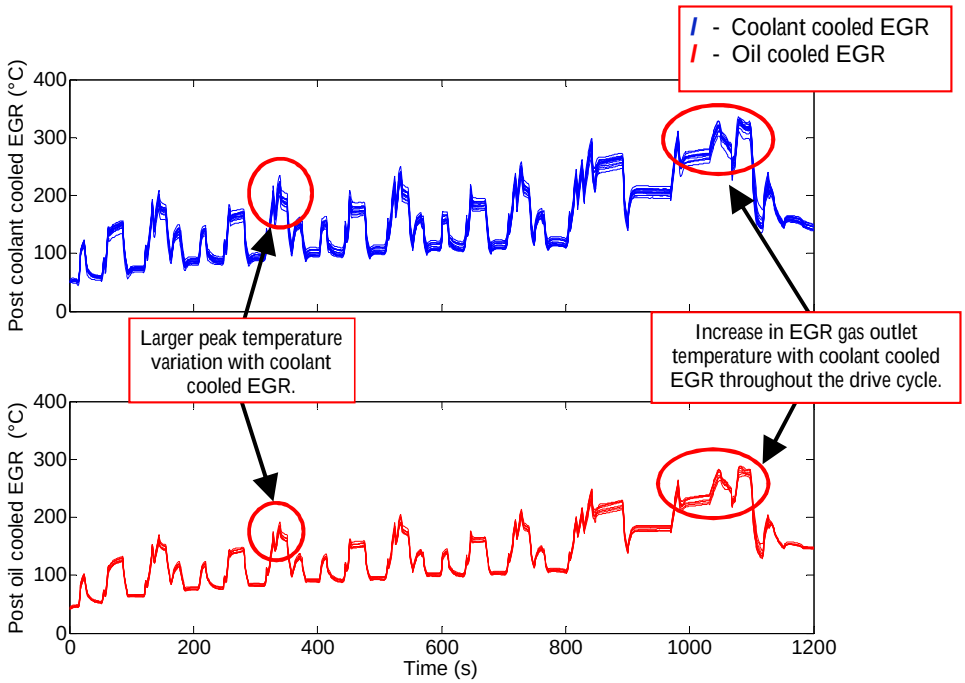


**Figure 6.62 – Post EGR cooler gas temperatures for Oil cooled and Coolant cooled EGR gas configurations**

## Response of cylinder wall temperatures and rates of heat transfer to changes in the active thermal management system

It was then possible to use these established groups to show the impact of the DoE parameters on the cylinder wall temperatures. An example of the instantaneous multipoint temperature is shown in Figure 6.63 for three repeats of the baseline experimental condition. In this figure the coloured groupings indicate the thermocouple position within the multipoint sensor. During the early stages of the drive cycle there is a 3°C variation in the recorded temperatures, the cause was found to be a 2°C difference in the overnight cell ambient condition and therefore the engine temperature. The effect of the ambient temperature variation is shown to reduce as the drive cycle progresses. The response time of the thermocouples within the sensor to a change in temperature can also be seen after each deceleration event as the difference between the tip and middle thermocouple becomes much smaller than that of the middle and outer. In order to simplify the temperature analysis, only the inner thermocouple within the sensor has been shown in the following figures, unless otherwise specified.

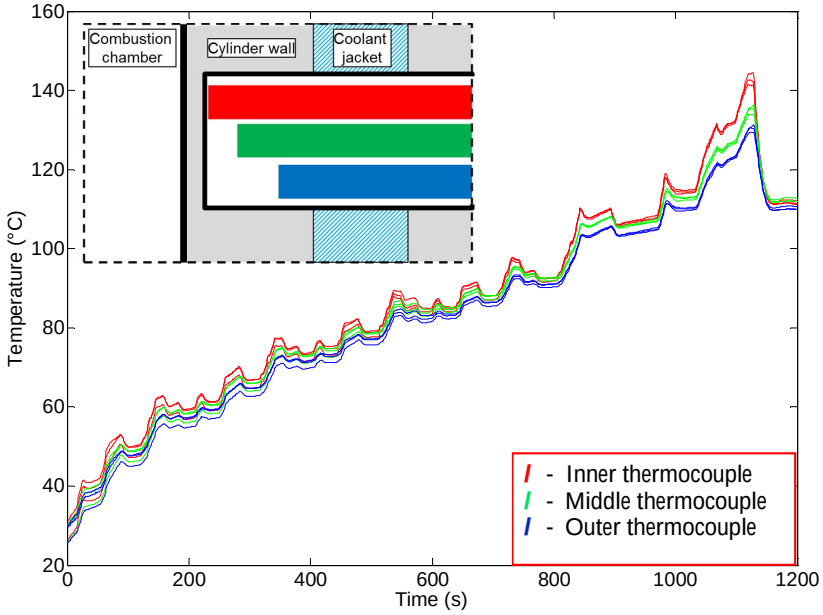


**Figure 6.63 – Multipoint temperature data over multiple baseline NEDC repeats (Coloured groups indicate thermocouple position within the sensor)**

Figure 6.64 shows the cumulative inner temperatures located around cylinder 2 grouped by the engine coolant flow rate as in Figure 6.60. Cumulative temperature is used as a device to visualise the temperature data disguising the interaction with engine speed and load through the drive cycle. The inlaid plot shows the final 100 seconds for Multipoint 6 located on the inlet side 8mm from the top deck. The low engine flow experiments clearly show higher cylinder wall temperatures, as well as the high EGR mid flow experiments. The high engine coolant flow experiments show a 12% reduction in the cumulative temperature over the drive cycle. A low EGR flow rate was found to reduce the total engine flow rate (Figure 6.60) during high engine speed conditions; this is shown to cause an increase in the cumulative inner wall temperature compared to high EGR flow conditions. This increase in wall temperature can be further compounded when the EGR gas is coolant cooled. A similar response was found for cylinder 3. Two mid flow conditions were found with cumulative inner wall temperatures similar to that of the low engine flow conditions, this was found to be as a result of the oil cooled EGR, as less heat was transferred to the coolant from the EGR gas.

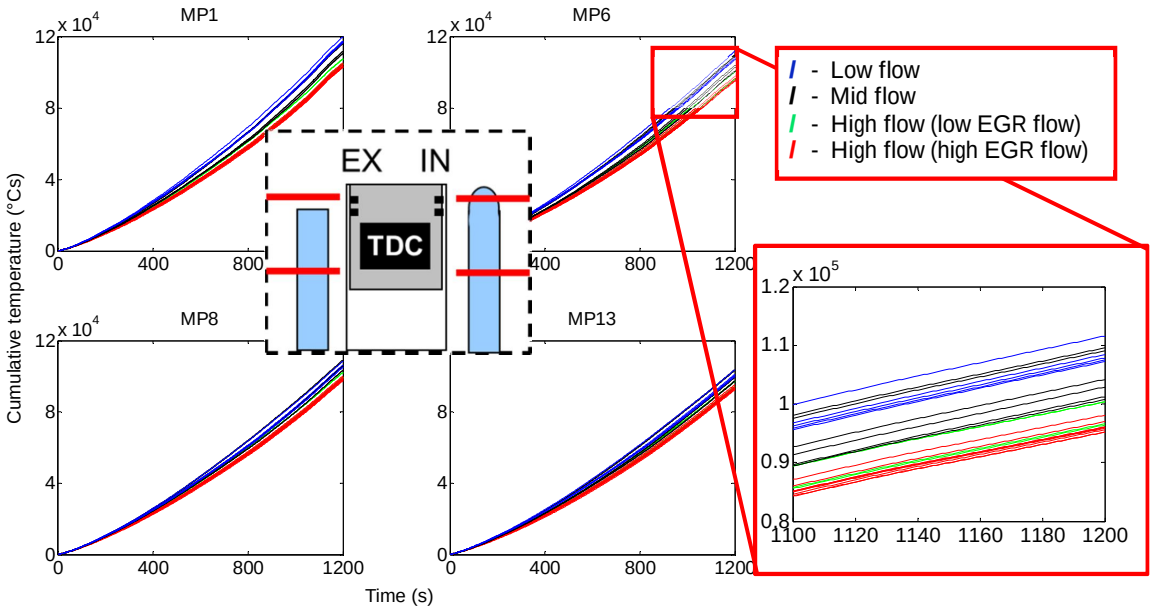


**Figure 6.64 – Cumulative inner thermocouple temperature for cylinder 2 at 8mm and 60mm from the top deck, colour groupings indicate engine out coolant flow rate condition**

To explain the higher cylinder wall temperatures during the low flow condition the cumulative energy transfer to coolant and the cumulative temperature difference across the engine are shown in Figure 6.65 and Figure 6.66 respectively. The closed post engine coolant throttle causes the energy transfer across the engine to be much smaller than the high flow experiments due to the low coolant mass flow. The low mass flow rate means that the heat energy generated in-cylinder, which is the same for all experiments, that is conducted through the cylinder liners is maintained within the engine structure. The highest rate of energy transfer to the coolant across the engine was found to be for two of the mid flow experiments. It was found that the mid flow experiments could be broken down into two further groups; one group where all flow through the engine subsequently passed through the EGR cooler or the second group in which the post engine coolant throttle was partly open and a proportion of the total engine flow passed through the radiator bypass circuit and the remainder flowed through the EGR circuit. The higher rate of energy transfer was found to be the part open post engine coolant throttle experiments. Therefore a large proportion of the engine coolant flow was directed around the radiator bypass circuit, resulting in a lower engine in coolant temperature than the other mid flow experiments. This combination of increased coolant flow rate compared with the closed post engine throttle experiments and the low engine in coolant temperature compared with the high flow experiments resulted in the high energy transfer across the engine. To further understand the interaction between

the coolant mass flow rate through the engine and the effect of the temperature difference across the engine, the cumulative temperature difference across the engine can be used.

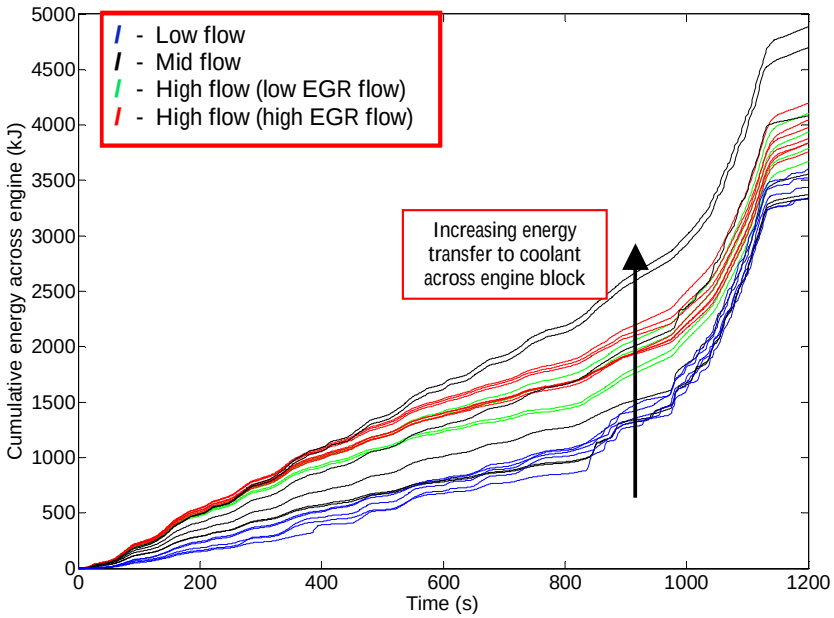


**Figure 6.65 – Cumulative energy transfer across the engine (Engine outlet - Engine inlet), coloured groups indicate engine coolant flow rate**

Figure 6.66 employs a cumulative temperature method to aid the visualisation of the impact of the coolant flow through the engine. It shows that the low engine coolant flow experiments have the largest temperature difference across the engine. This is a result of the low engine inlet temperature caused by the low engine flow rate maintaining a lower coolant temperature external to the engine. Whereas the high engine coolant and high EGR flow experiments show a much smaller temperature difference across the engine due to additional heat from the EGR gas and significant mixing of the coolant external to the engine structure elevating the engine inlet temperature. The mid flow experiments show the greatest variation in the measured temperature difference across the engine. This is a result of the high flow through the EGR cooler increasing the engine coolant inlet temperature; the mid flow experiments which have a large flow through the radiator bypass show the greatest temperature difference of the mid flow experiments. The variation within the remaining mid flow experiments was found to be caused by the EGR gas cooling medium; oil cooled EGR resulted in a larger temperature difference as the EGR gas heat transfer was not contributing to the engine in coolant temperature.

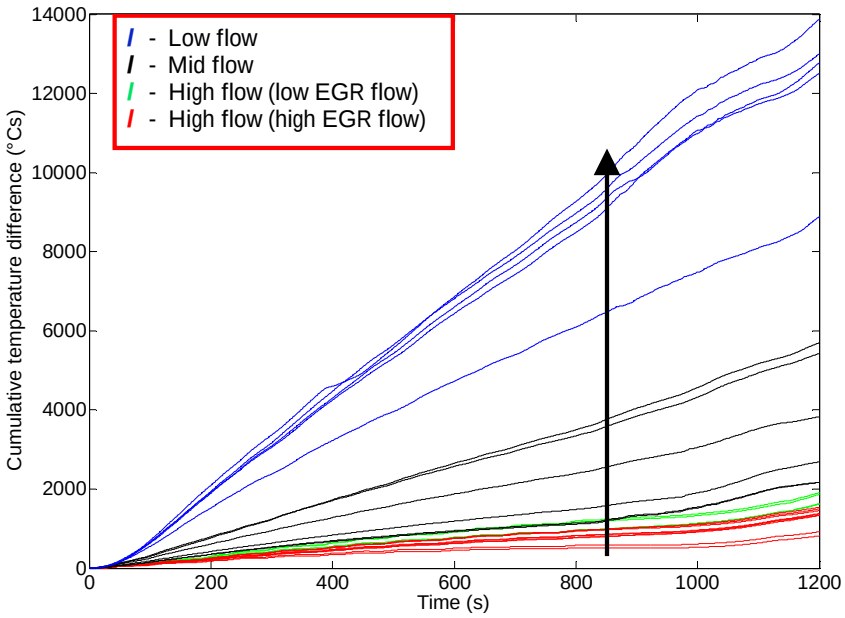


**Figure 6.66 – Cumulative temperature difference across the engine, grouped together by engine coolant flow**

As discussed in Chapter 6 Section 6.2, the drive cycle can be subdivided into a number of urban drive cycle repeats and an extra urban phase. For this discussion the key phase of the drive cycle is the first urban drive cycle as this has the greatest potential benefit for fuel savings from engine warm-up strategies and improved heat transfer understanding. Analysis of the complete drive cycle was performed alongside this investigation but is not reported here [141]. Figure 6.67 shows the mean heat flux over the first UDC repeat for each of the 17 experiments against the average engine coolant flow rate for each of the sensors around cylinder 2. The overall trend shows that as the average coolant flow rate increases the mean rate of heat transfer reduces, which contradicts the findings from the steady state investigation. These showed that an increase in the coolant flow rate through the engine resulted in an increase in the rate of heat transfer through the cylinder. The multipoint sensors at 60mm on the inlet side show the highest rate of heat transfer, supporting the findings in the steady state experiments. It was found that at a depth of 60mm the heat transfer was greater on cylinder 3 for both multipoint sensors, whereas at 8mm it was cylinder 2 which measured the larger rate of heat transfer. Multipoint 1 would not be exposed to this coolant controlled heat transfer phenomena. The small gradient is due to conductive heat transfer to neighbouring metal that is exposed to the coolant, inducing some heat transfer.

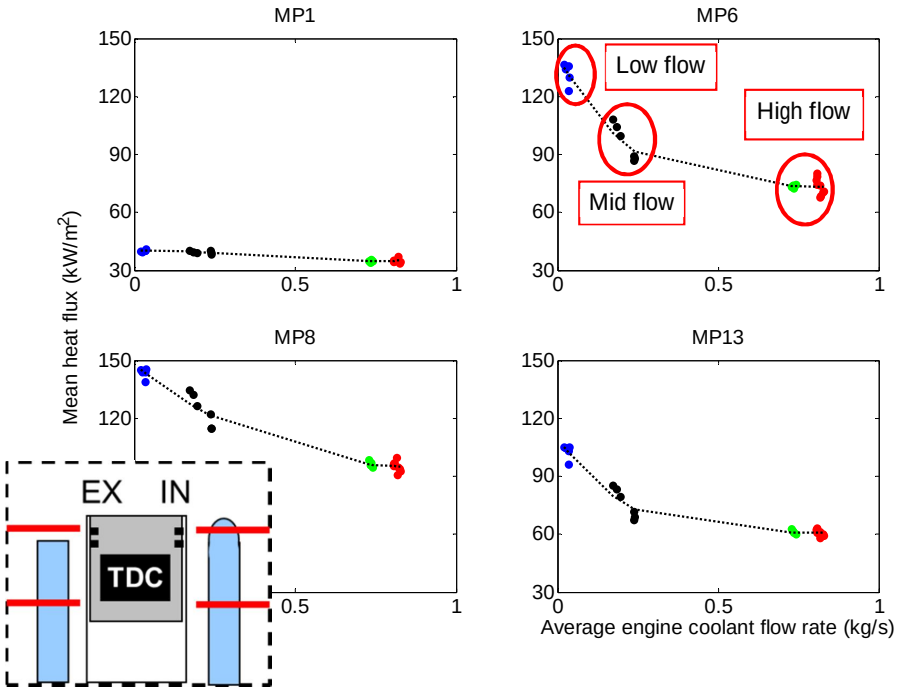


**Figure 6.67 – Mean heat flux on exhaust and inlet side of Cylinder 2 versus the average engine coolant flow rate – MP1 measurement location is not through the coolant jacket**

The position around the cylinder was found to influence the magnitude of the heat transfer with a reduction in the heat flux on the inlet side at MP13 compared to MP8, supporting the steady state experimental findings. The effect of coolant flow rate is shown to be much greater between the low and mid flow conditions on the inlet side compared to MP8. The energy transfer response to changing engine coolant flow rate and engine inlet coolant temperature is shown in Figure 6.68. The data for all experimental configurations over the first urban drive cycle repeat are included and it shows that an increase in the engine coolant flow rate results in an increase in the energy transfer to the coolant across the engine structure. The reduced energy transfer to the coolant is the fundamental reason why the engine was found to warm-up faster when the post engine throttle was closed. A reduction in the coolant temperature into the engine was found to further increase the energy transfer to coolant.

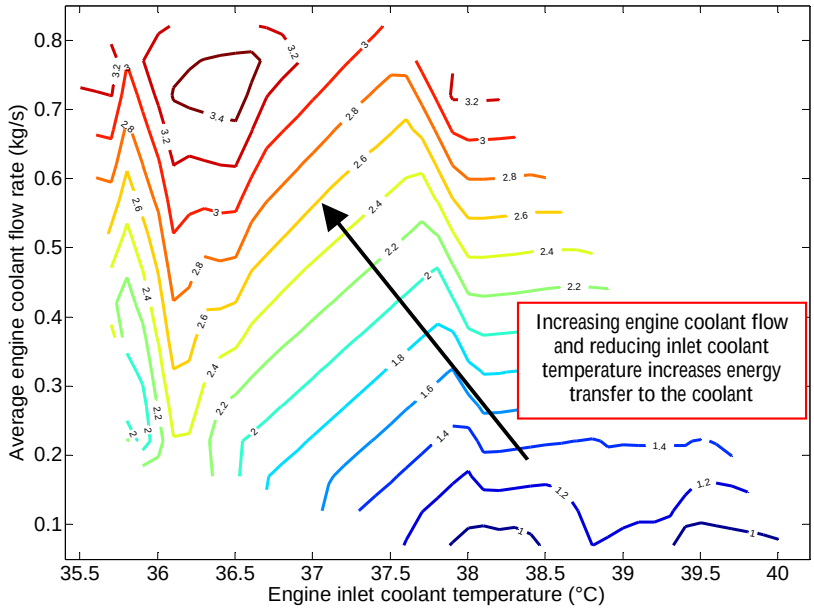


**Figure 6.68 – Energy transfer across the engine (kW) against the average engine coolant flow rate and engine coolant inlet temperature for all experimental configurations over UDC1**

To understand the effects of the DoE configurations on the cylinder wall temperatures Figure 6.69 shows the liner temperatures for Multipoint 8 for the low, mid and high engine coolant flow rate conditions for each configuration. In addition to the three metal temperatures the extrapolated gas and coolant side wall temperatures, local coolant temperature (shown at 0.055m) and engine coolant inlet temperature (shown at 0.06m) have been plotted. The local coolant measurement location is comparable to the position shown in the figures; however the engine coolant inlet temperature is shown for reference only. It is shown that the measured temperatures near the combustion chamber reduce as the coolant flow rate increases, whereas the outer metal temperatures were found to be comparable across all flow conditions. The reduction in the temperatures measured nearest the combustion chamber as the flow rate through the engine increases, could be attributed to the heat transfer in the cylinder head. During low engine coolant flow conditions the flow through the cylinder head is also reduced, therefore it will operate at a higher temperature which would have a knock-on effect on the combustion gases and the overall combustion chamber temperature. The different configurations were found to have very little impact on the measured temperatures in the high flow condition comparable to the 2-3°C temperature variation observed under mid and low coolant flow. This could be attributed to the variation in the local coolant temperature observed. Therefore there are two factors which have

impacted the temperature gradient through the wall. In the high flow regime the local coolant temperature was found to be higher and the measured temperature near the combustion chamber was lower resulting in a shallower gradient, i.e. lower heat transfer. An identical effect was found on the inlet side of the engine, however measured temperatures were found to be lower (2°C) and coolant temperatures comparable, leading to shallower temperature gradients across the flow regimes. In the steady state experiments the greater temperatures on the exhaust side were attributed to the influence of the hotter exhaust gases and increased heat from friction. There is also an observed rise in the engine inlet temperatures; with some cases showing a reduction between the engine inlet and the local measurement point. This reduction could be caused by the heat transfer from the warm coolant to the cold engine block during the early stages of the drive cycle especially during the low flow conditions.

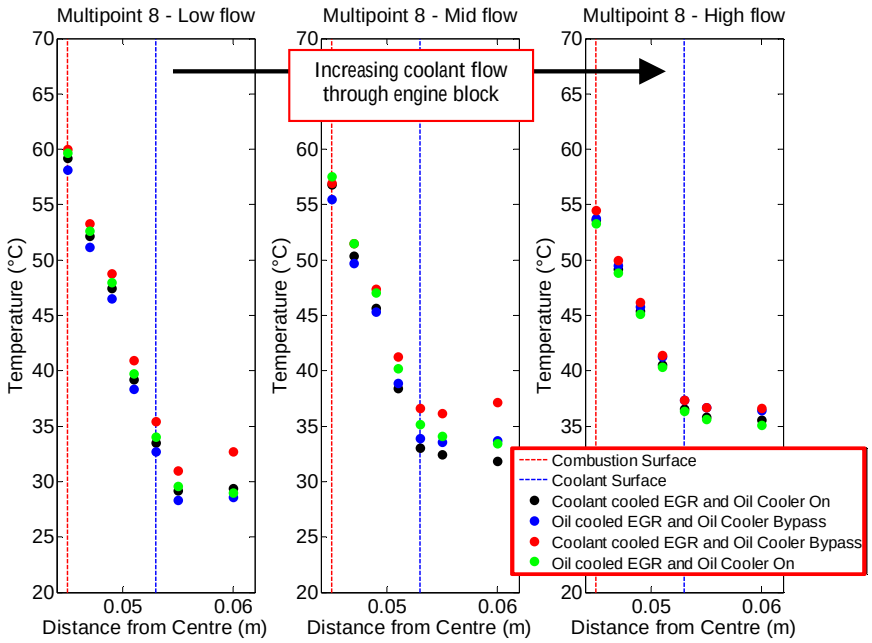


**Figure 6.69 – The effect of low, mid and high engine coolant flow rate and the DoE configuration on the cylinder liner and coolant temperatures for multipoint 8, located on the exhaust side at 60mm from the top deck**

The increase in engine inlet temperature was mainly caused by the increased engine coolant flow raising the temperature of the coolant external to the engine, in addition to a number of interactions between the build configurations. The coolant temperatures around the system were found to be highest during the coolant cooled EGR and oil cooler bypass configuration, attributed to additional heat energy transfer to the coolant via the EGR cooler

and heat energy not being transferred to the oil within the oil cooler. The other configurations show very little engine inlet temperature variation due to the energy transfer interactions within the EGR cooler and the oil cooler. The change in coolant temperature between the mid and high flow conditions for the coolant cooled EGR and oil cooler bypass configuration was very small due to the high coolant temperature out of the EGR cooler, whereas the other configurations show a stronger dependence on the engine coolant flow rate to increase the temperature of the coolant external to the engine.

The effect of the engine coolant flow rate on the liner and coolant temperatures for multipoint 8 for the coolant cooled EGR and oil cooler bypass configuration are shown in Figure 6.70 for each repeat of the urban drive cycle. The liner temperatures are shown to rise through the drive cycle as the engine warms up to its operating temperature which is not achieved until the early stages of the EUDC [137]. The low flow condition is shown to have the lowest coolant temperatures across the first 2 repeats with the mid flow condition showing the highest temperatures throughout. The low flow condition has the highest inner liner temperatures and the lowest outer temperature initially, therefore having the highest rate of heat transfer, which is maintained throughout the repeats. The mid flow condition was found to have the highest coolant temperatures as all the coolant which flowed through the engine was subsequently used to cool the EGR gas. The wall temperatures would eventually reach equilibrium during the EUDC phase when the engine is fully warm.

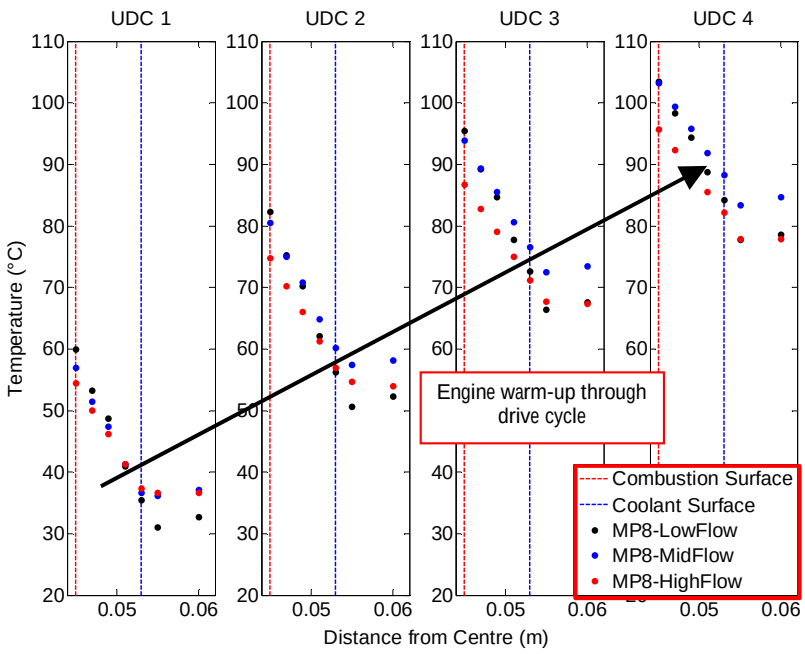


**Figure 6.70 – The effect of engine coolant flow rate on wall and coolant temperatures for multipoint 8 through each of urban drive cycle phases for coolant cooled EGR and oil cooler bypass.**

The boundary layer temperature gradient from the wall surface to the local coolant temperature for the low and high flow conditions for multipoint 8 over UDC1 is visualised in Figure 6.71. The equation for the convective heat transfer coefficient from the wall to the fluid is given in Equation (52). This states that if the heat transfer through the wall was constant, an increase in the temperature difference between the wall and coolant would result in a reduction in the convective heat transfer rate between the wall and the coolant, implying that there would be less energy transfer per unit area and temperature to the fluid. It is shown that the low flow condition, which was found to have the highest rate of heat transfer through the wall, also has the largest temperature difference between the extrapolated wall temperature and the local coolant temperature. Therefore the convective heat transfer coefficient, in this case is dependent on the relative increase of the rate of heat transfer to the increase in the temperature difference.

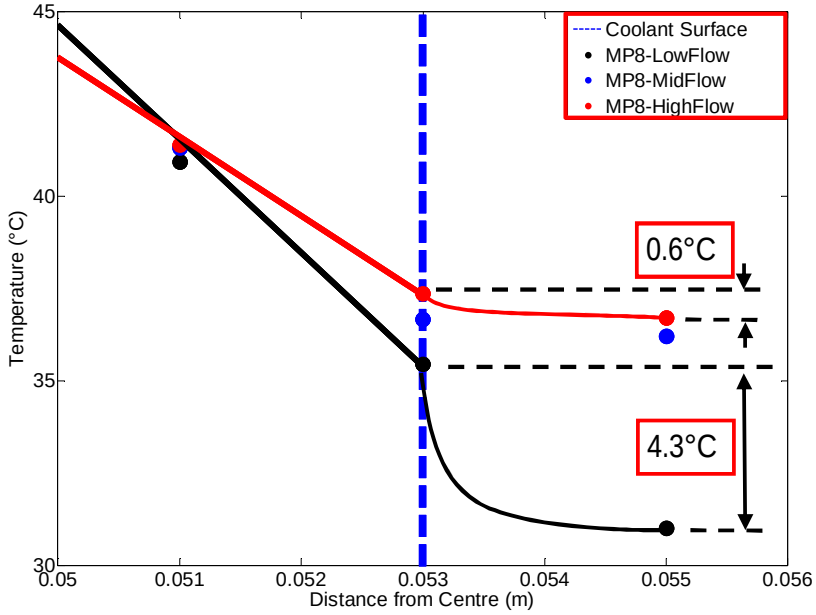


**Figure 6.71 – Visualisation of convective heat transfer profile for Multipoint 8 from the extrapolated cylinder wall temperature to measured local coolant temperature for mapped and high flow conditions**

Figure 6.72 helps to further understand the relationship between the convective heat transfer and the temperature difference between the extrapolated wall temperature and coolant temperature. The figure includes the data for all experimental configurations and all multipoint sensors which were exposed to coolant for both cylinders 2 and 3. It clearly shows a linear trend when plotted on a log scale. By plotting on a logarithmic scale the data is better represented and more visible due to the exponential nature of the coolant side convective heat transfer with the reduction in the temperature difference between the cylinder wall and the coolant temperature. The data presented here was found to be consistent with other studies.

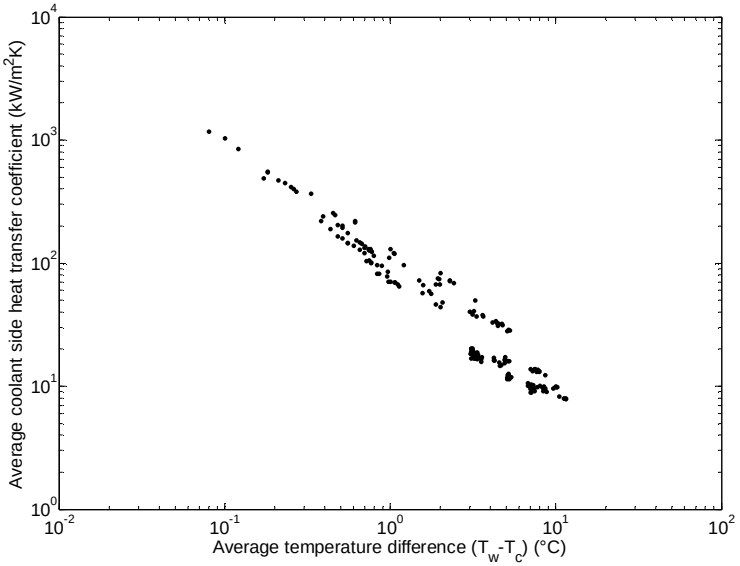


**Figure 6.72 – Convective heat transfer coefficient against average temperature difference between local coolant and cylinder wall for all Multipoints over UDC1**

# Section summary and conclusions

This section aimed to provide an understanding of how changes to the external oil and coolant circuits in the active thermal management system impacted the cylinder wall temperatures and rates of heat transfer through the cylinder liner. The external circuit changes were found to affect the rate of warm-up of the engine through the drive cycle and this section aimed to provide the fundamental reasons why. Some of the key findings of this section are outlined below:

- The low engine coolant flow was found to have the largest rate of heat transfer through the cylinder wall due to higher inner wall temperatures and much lower coolant temperatures. It had the largest temperature difference between the wall surface and the coolant indicating high convective heat transfer. The low engine inlet temperature was caused by the reduced mixing of the coolant external to the engine. Through the UDC repeats, the low engine flow condition maintained the highest inner wall temperature and the lowest coolant temperature, therefore the highest rate of heat transfer through the cylinder wall. This contradicts the findings of Chang et.al showing that the coolant temperature and the coolant flow rate have a significant impact on the heat flux, reinforcing the suggestion that it is only in HCCI

engines that the main driving force behind the heat transfer is the phasing of the combustion process [57].

- The low coolant flow rate resulted in much lower energy transfer to coolant across the engine and therefore a much faster warm-up as the heat energy remained within the engine structure. This finding may also highlight the importance of heat transfer from the cylinder head as well as from the combustion chamber during warm-up as it resulted in an increase in the wall operating temperature during the early stages of the drive cycle.

- The coolant cooled EGR and oil cooler bypass configuration was found to have the highest engine coolant temperatures due to the heat added to the coolant via the EGR gas and no heat being transferred to the oil within the oil cooler.

- The combination of low engine coolant flow and the coolant cooled EGR and oil cooler bypass configuration resulted in the fastest engine warm-up as the higher coolant inlet temperatures elevate the overall engine temperature but the low engine flow retains the heat in the engine structure. This finding suggests that the coolant system would benefit from additional controls which maximise flow through the EGR cooler to recuperate heat from the exhaust in order to elevate the bulk coolant temperature; an additional exhaust heat exchanger could also be incorporated. A secondary low flow circuit through the engine would then retain heat energy within the structure until warm-up has been achieved and the circuits could be combined.

## *6.4 The application of Steady State convective heat transfer findings on NEDC data*

The aim of this chapter is to combine the findings from the two experimental phases of this thesis, i.e. the steady state investigation and the transient analysis, to see if any benefits in the prediction of the gas side convective heat transfer for future modelling can be obtained.

To achieve the aim of this section each of the cruise conditions from the NEDC were investigated separately and compared to steady state operating conditions of similar torque and speed. The four vehicle cruise speeds are shown in Figure 6.73 alongside the engine speed and engine torque for each of these conditions. The NEDC cruise operating conditions have been summarised in Table 12, also shown in Table 12 is the steady state operating conditions used for comparison. The equivalent steady state condition for the 32kph has a much higher operating torque and this must be taken into account during the analysis.

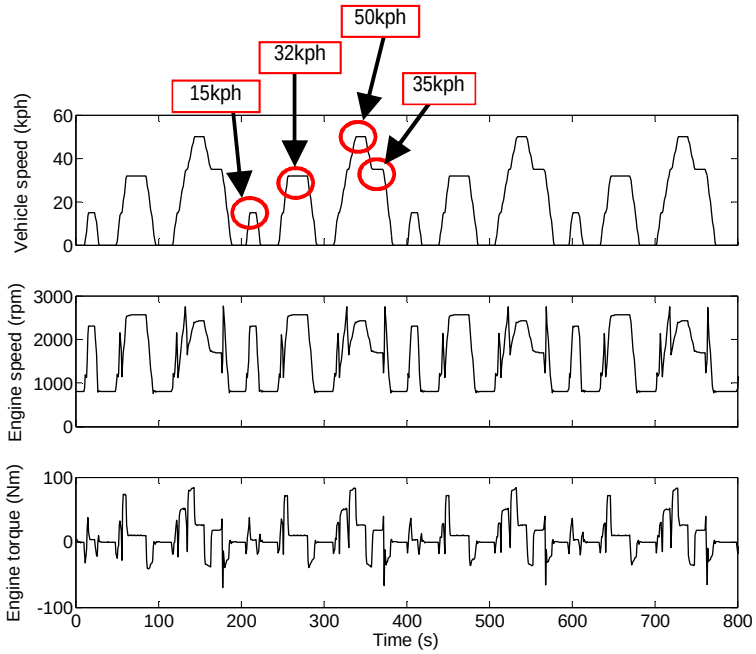


**Figure 6.73 – UDC phases of NEDC, highlighting the 4 cruise speeds**

**Table 12 – Summary of NEDC cruise conditions for target vehicle and steady state operating conditions used for comparison**

| | NEDC operating conditions | | Steady state operating conditions | |
|---|---|---|---|---|
| Cruise (kph) | Average engine speed (rpm) | Average engine torque (Nm) | Engine speed (rpm) | Engine Torque (Nm) |
| 15[12] | 2300 | 5.5 | - | - |
| 32 | 2560 | 11.3 | 2625 | 20 |
| 50 | 2415 | 27.3 | 2375 | 20 |
| 35 | 1705 | 18.1 | 1625 | 20 |

[12] 15kph cruise condition was not further investigated as it was concluded that there was no comparable steady state operating condition with the closest condition being 2375rpm and 20Nm.

For each UDC repeat an average gas side cylinder wall temperature was obtained from the drive cycle and averaged over the cruise period using the extrapolated data from the multipoint sensors located down the bore of cylinder 2. Then using the modified Hohenberg equation (Equation (64)), the in-cylinder pressure and temperature data from the corresponding steady state condition, an average gas side convective heat transfer coefficient was calculated for each of the Design of Experiment transient experiments and for each of the UDC repeats within those drive cycles. It must be noted that without the introduction of the cylinder wall temperature into the Hohenberg equation, it would be assumed that the convective heat transfer coefficient (CHTC) would be equal across all DoE conditions and across the drive cycle. The gas side CHTC was found to increase through the UDC phases for each of the DoE test conditions. The cooling regime resulted in the average cylinder wall temperature increasing at varying rates which directly impacts the CHTC calculation as all the other variables remain constant. The average cylinder wall temperature for the 32kph cruise of each UDC repeat is shown in Figure 6.74. The temperatures have been plotted against the DoE test ranked by the average cylinder wall temperature in UDC1 to illustrate the small temperature variation under the different cooling regimes which increase during the drive cycle. A number of temperature spikes are visible in UDC2 to 4, where the thermal regime has impacted the average cylinder wall temperature. The spikes located at points 13, 16, 19 and 22 correspond to conditions where the post engine coolant throttle was mapped and the oil cooler was bypassed. The oil cooler being bypassed would have resulted in higher oil temperatures and subsequently higher piston temperatures due to the reduced effectiveness of the piston cooling jets with elevated oil temperatures. Higher piston temperatures would have a knock-on effect onto the cylinder wall. Regimes which mapped the post engine coolant throttle resulted in a generally higher cylinder wall temperature early on in the drive cycle, however once the ECU temperature reached the desired value this affect would have diminished.

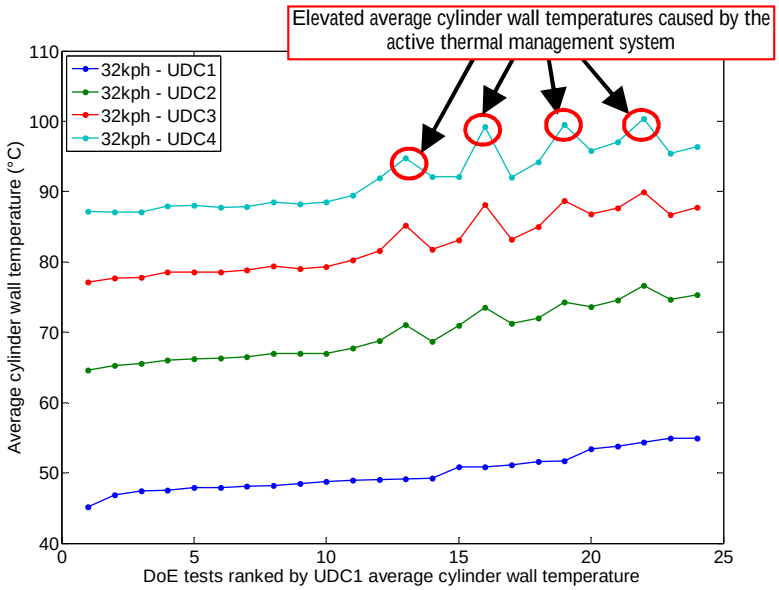


**Figure 6.74 – Average cylinder gas side wall temperature for the 32kph cruise of each UDC repeat plotted against the DoE test ranked by the average cylinder wall temperature in UDC1**

Figure 6.75 shows each of the average gas side convective heat transfer for each of the DoE test conditions plotted against the rate of energy transfer to coolant across the engine block for each of the cruises of UDC 1. It shows that as the rate of energy transfer reduces the gas side convective heat transfer coefficient was found to increase for each of the cruise speeds. The average cylinder wall temperature used in the modified Hohenberg equation was calculated using the time averaged extrapolated gas side wall temperature from each multipoint sensor linearly interpolated down the cylinder bore. During the early stages of the NEDC the wall temperature shows a temperature increase with time due to the structure warming up (a variation of 1.9°C to 8.8°C depending on the location down the bore and the cooling regime employed). In the later UDC phases the temperature variation over the cruise reduces and in some cases is negative due to the low torque requirement during the cruise. This results in the correlation between rate of energy transfer and the CHTC reducing through the UDC phases. Two anomalous baseline repeats were removed from the figures due to the calculation of very low rates of energy transfer compared with the other baseline tests. The low rates of energy transfer were found to be caused by a 3°C difference in the coolant starting temperature, reducing the temperature delta across the engine and introducing an error.

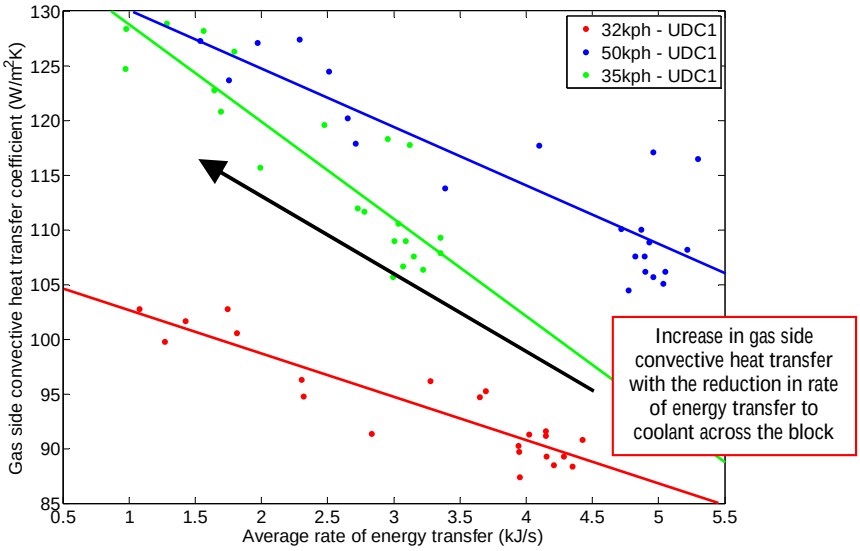


**Figure 6.75 – Energy transferred to coolant across engine block plotted against the calculated gas side convective heat transfer coefficient for each of the cruises of UDC 1 for each of the DoE points**

The data in Figure 6.75 was found to have an R-squared value of 0.77, 0.80 and 0.83 for 50kph, 35kph and 32kph respectively, showing a strong correlation. Figure 6.76 shows a very similar trend for UDC 2 however the R-squared values have reduced to 0.40 to 0.65.

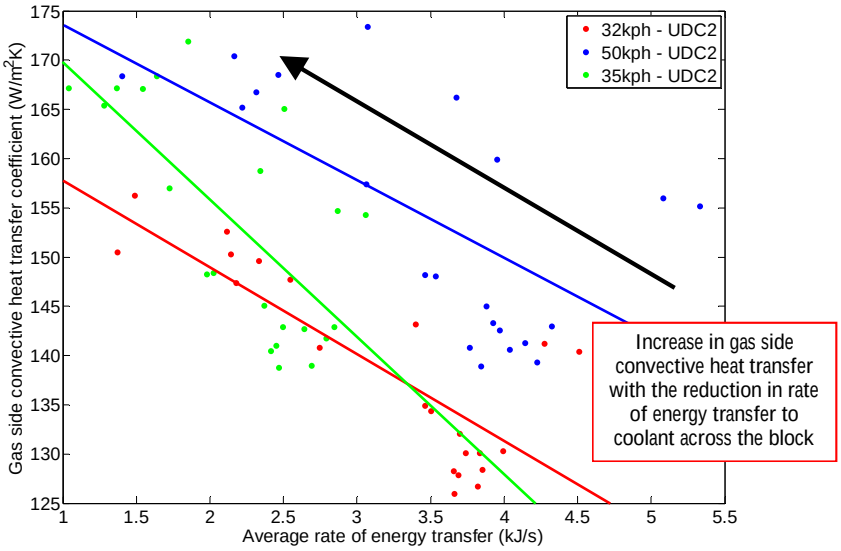


**Figure 6.76 – Energy transferred to coolant across engine block plotted against the calculated gas side convective heat transfer coefficient for each of the cruises of UDC 2 for each of the DoE points**

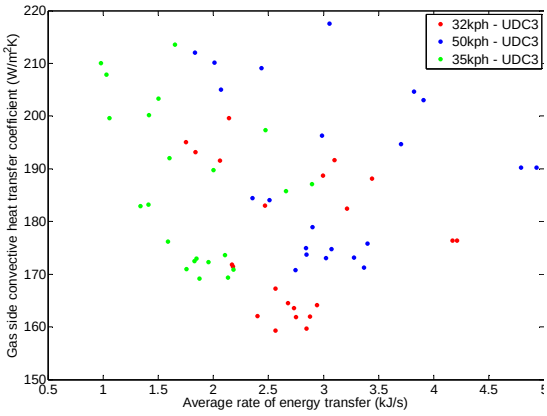


**Figure 6.77 – Gas side CHTC against rate of energy transfer to coolant across the engine for UDC 3**

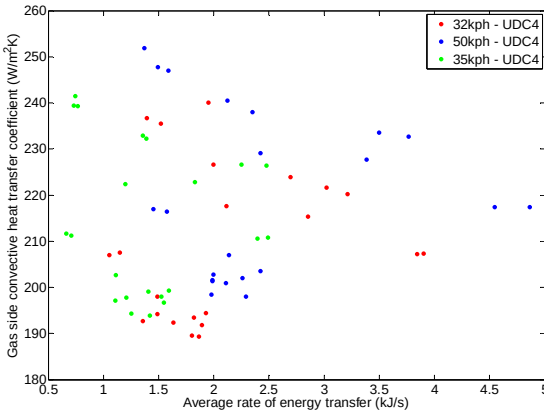


**Figure 6.78 – Gas side CHTC against rate of energy transfer to coolant across the engine for UDC 4**

The correlation between the energy transfer rate and the convective heat transfer coefficient further reduced as the NEDC progressed, this was attributed to the error introduced in the energy calculation when the difference in coolant temperature across the engine was reduced. Figure 6.77 and Figure 6.78 show the relationship between the gas side CHTC and rate of energy transfer to coolant across the engine for UDC 3 and 4 respectively. The model is clearly less useful when the engine is fully warmed but it has been shown that during warm-up the inclusion of the wall temperature in the model of convective heat transfer coefficient is required. This is typically where conventional models poorly predict heat transfer coefficients. The interactions taking place within the DoE variables such as the EGR cooler type, flow rate and oil cooler position would have influenced the results shown here. However in order to isolate these effects a more detailed study would have to be undertaken.

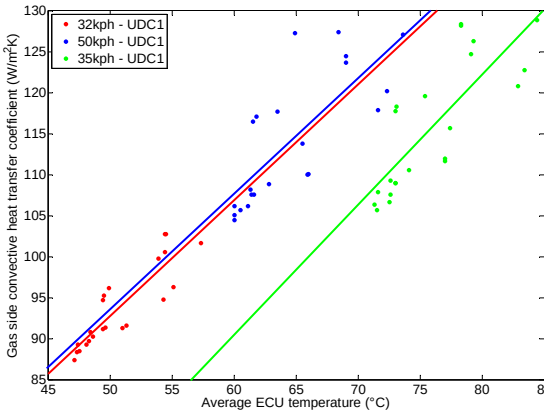


**Figure 6.79 – Gas side CHTC against average engine temperature as measured by the ECU for UDC 1**

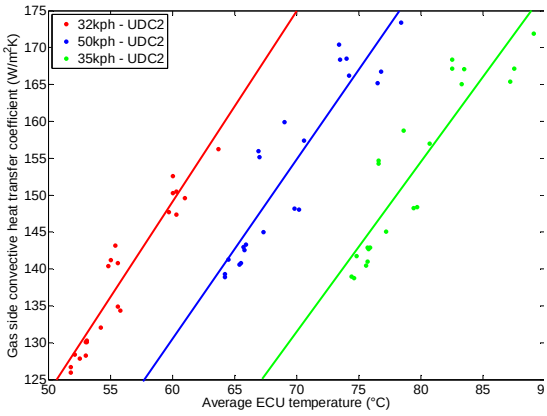


**Figure 6.80 – Gas side CHTC against average engine temperature as measured by the ECU for UDC 2**

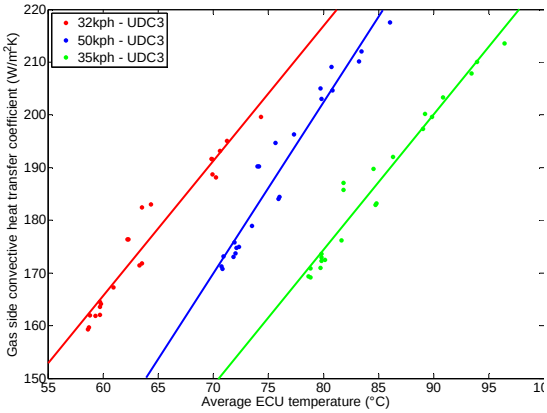


**Figure 6.81 – Gas side CHTC against average engine temperature as measured by the ECU for UDC 3**

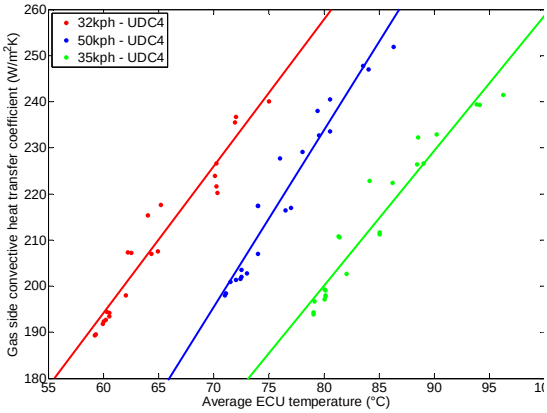


**Figure 6.82 – Gas side CHTC against average engine temperature as measured by the ECU for UDC 4**

The gas side CHTC for all DoE test conditions are also shown in Figure 6.79 to Figure 6.82 plotted against the average engine temperature as measured by the ECU for UDC1 to UDC 4 respectively. The R-squared values range from 0.6 to 0.95. The correlation is weaker during the UDC1 phase particularly during the 50kph cruise. The correlation of the engine temperature to the average cylinder wall temperature becomes stronger as the warm-up progresses. It was concluded that this was due to the transfer of heat within the engine structure and how it differs with the different active cooling strategies. For example, the low engine coolant flow strategy resulted in the cylinder wall temperature increasing at a faster rate than the bulk engine temperature, however with the high engine coolant flow strategies the cylinder wall temperature and the bulk engine temperature increased at a very similar rate. This difference reduced as the complete system reached warmer temperatures. In addition

the correlation would also be weakest at the low engine operating temperatures because the modified Hohenberg model used to calculate CHTCs was optimised at fully warm conditions.

As previously noted the standard Hohenberg equation predicted a single gas side convective heat transfer coefficient for each of the cruise conditions, not accounting for any differences in cylinder wall temperature or bulk engine temperature. Table 13 gives the gas side CHTCs for the standard Hohenberg model and compares it to the minimum, maximum and average calculated using the modified equation.

**Table 13 – Comparison of gas side convective heat transfer coefficients**

| | | Gas side convective heat transfer coefficient ($W/m^2K$) | | |
|---|---|---|---|---|
| | | 32 kph | 50 kph | 32 kph |
| Standard Hohenberg formula[13] | | 283.9 | 268.4 | 243.1 |
| Modified Hohenberg formula | Minimum | 84.4 | 102.5 | 103.3 |
| | Average | 153.4 | 168.0 | 166.1 |
| | Maximum | 240.1 | 251.9 | 241.5 |

The gas side CHTC was found to be much higher when calculated using the standard Hohenberg model. Table 13 shows the range obtained when calculated using the different cylinder wall temperatures and the modified equation. The elevated CHTCs from the standard equation are a result of the coefficients being based on cylinder wall heat flux of a fully warm engine, whereas the higher cylinder wall temperatures result in a smaller temperature difference between the combustion gases and the liner temperature, thus highlighting that the standard equation is only valid for a fully warm engine. However by introducing a cylinder wall component it is possible to estimate the gas side CHTCs for an engine at different stages through the warm-up process. This methodology could be applied to more complex cooling systems where there is split cooling between the cylinder head and block for example.

## Section summary and conclusions

This section aimed to combine the findings of the steady state investigation with those of the NEDC data to evaluate whether there are any benefits in incorporating a cylinder wall

[13] Estimation of gas side convective heat transfer coefficient performed using the iterated optimisation coefficients.

parameter into the equation used to predict gas side convective heat transfer coefficients. Some of the key findings of this section are outlined below:

- Each of the NEDC cruise conditions were approximated to a steady state operating condition for evaluation. The 15kph cruise operated at torque outside the steady state operating window so was not included in this study.

- The average cylinder wall temperature was calculated by averaging the extrapolated gas side wall temperature over the cruise period and linearly interpolated down both sides of the cylinder. The resultant average wall temperature was found to increase through the drive cycle. However during some cruise conditions a reduction in the wall temperature was noted.

- The DoE conditions resulted in a wide range of cylinder wall temperatures and it was found that as the CHTC increased, the average rate of heat transfer to the coolant across the engine reduced.

- The standard Hohenberg equation resulted in a single CHTC for each cruise condition which was much higher than those calculated using the modified equation.

- The correlation between the CHTC and the rate of energy transfer reduced as the engine warmed up partly due to the difference in coolant temperature across the engine reducing and influencing the energy calculation, in addition to the reduction in a direct heat transfer path from the combustion chamber to the coolant. A strong correlation was also found between the average engine temperature as measured by the ECU and the gas side CHTC. It was concluded that this correlation was due to the cylinder wall temperature reflecting the temperature used by the ECU as an overall engine temperature for the engine control strategy. However due to the cooling regimes implemented, the correlation was weaker during the early stages of the drive cycle when differences in the rate of change of the cylinder wall and bulk engine temperature relative to each other would have been largest.

## 6.5 Chapter summary and conclusions

The experimental procedure and results for the three experimental phases have been discussed in this chapter. The three phases undertaken were the motored operation and friction measurement, steady state operation and the application of convective heat transfer correlations at these operating conditions, and transient operation Design of Experiments. There were a number of key outcomes from this chapter which have been listed below:

- The motored friction was found to be much larger than that predicted from established models, such as Chen and Flynn, and Winterbone. The cause of this was attributed to the increased auxiliary load on the engine.

- The engine was found to convert less than 30% of the total input energy into useful work, which is typical of a modern diesel engine.

- Coolant temperatures around the engine were found not to vary significantly with operating condition due to the high flow rate and thermostat control. However the oil temperature was found to change considerably with a 40°C range between the high speed and load condition compared to the idle equivalent condition. The oil in the camshaft bearings was found to be over 7°C hotter on the exhaust side than the inlet as a result of the hot exhaust gases in the ports.

- The deactivation of the piston cooling jets at low speed was found to substantially increase the cylinder wall temperature. This is of limited concern as it would not impact the temperature during real world operation as the oil pressure would rarely drop below the nominal opening pressure of the jet. However steps had to be taken to remove this variable from the analysis.

- It was found that the assumption of 1-D conduction through the cylinder wall would not lead to an error in the estimation of heat transfer even though the longitudinal component was found to be up to 23% of the radial conduction under some operating conditions.

- The temperature and subsequently the heat transfer were found to differ from the inlet to the exhaust side of the cylinder, with a sizeable influence from the position of the coolant jacket relative to the measurement location.

- The overall heat flux from the cylinder was found to have a linear relationship with engine power.

- Established convective heat transfer models were found to over-predict the cycle average convective heat transfer coefficients, especially at higher operating conditions. Optimisation of the coefficients of the Hohenberg equation led to a reduction in the sum of the errors by 77.6% when compared with the measured data. However this was improved by a further 17.4% by incorporating a cylinder wall temperature component.

- A Design of Experiments was performed centred around the NEDC and a number of actuators to affect the transfer of energy to the coolant and oil during the engine warm-up. The overall system response has been reported by Burke so the focus of this study was to understand the impact of the system changes on the cylinder wall temperature [137]. The low engine coolant flow conditions were found to have the largest rate of heat transfer through the cylinder wall due to higher wall temperatures near the combustion chamber and much lower coolant temperatures.

- The lower engine inlet coolant temperatures were found to be a result of isolating the coolant from mixing with the coolant external to the engine. This approach led to the highest heat transfer rate through the cylinder wall due to the low coolant temperatures and the highest inner wall temperatures. The high inner wall temperatures were attributed to the reduced heat transfer to the cylinder head and therefore higher combustion gas temperatures. As a result of the low coolant flow rate through the engine the energy transfer to the coolant across the engine is very small retaining the heat within the engine structure and resulting in the reduced warm-up period.

- The fastest warm-up was found to be coolant cooled EGR, oil cooler bypassed and low engine coolant flow due to the higher coolant taking temperature from the EGR but the heat being generated in the engine being held within the structure by the low overall coolant flow rate.

- The findings from the optimisation of the convective heat transfer models was applied to the cruise conditions in the transient drive cycles for each of the DoE conditions. The average cylinder wall temperature was calculated based on the extrapolated liner temperature, averaged over the cruise and linearly interpolated down the cylinder bore. The CHTCs were found to increase as the average rate of energy transfer to the coolant across the engine reduced.

- The correlation between the CHTC and the energy transfer rate was found to reduce as the engine warmed up. The standard Hohenberg equation was found to estimate the CHTC to be much higher than calculated using the modified model. This was attributed to the coefficients of the standard equation being optimised on a fully warm engine.

- The introduction of the cylinder wall component allows for the CHTC to be estimated when the engine is not fully warm, and therefore allowing more complex cooling systems to be evaluated within modelling.

# Chapter 7. Conclusions and outlook

## 7.1 Summary

The work in this thesis has focused on the development of a robust method of measuring the cylinder wall temperature and rate of heat transfer within a modern production diesel engine without impacting the performance, the location of the auxiliary systems and the integrity of the engine. In Chapter 2 a review of relevant engine technologies and the trends within the thermal management system was given. Chapter 3 described the methods used in other studies to measure the combustion chamber wall temperature and summarised the outcome of these investigations, including the understanding of convective heat transfer correlation models based on in-cylinder conditions. Chapter 4 and Chapter 5 described the experimental facilities and the heat transfer measurement method. The detailed design of the measurement device was also detailed here, including the calibration procedure. Chapter 6 detailed the three main phases of experimental work undertaken and discusses the outcomes of each phase.

## 7.2 Conclusions

The conclusions from this work will be presented against the objectives laid out in Chapter 1. Each of these objectives is reminded below with the respective concluding remarks.

1) *Review literature relating to engine performance technologies, current trends in thermal management systems and their subsequent impact on the heat generation in modern diesel engines.*

The literature review was presented in Chapter 2. Key technologies have enabled a step increase in the peak performance of I.C. engines which leads to much higher cylinder pressures and subsequently higher temperatures. The rate of heat transfer from the combustion chamber was found to impact not only on the cooling system but also on the overall engine performance. Complex strategies and technologies have been proposed to combat the increase in heat generation without compromising the requirement for improved fuel economy, such as decoupling the coolant flow from the engine operating condition and

directing the waste heat to areas where it can be used in a productive way. It is these changes which have led to established methods of predicting heat transfer rates to become outdated.

2) *Review combustion chamber wall measurement techniques and the empirical convective heat transfer correlations which have been established.*

A wide variety of methods have been employed to measure the temperatures within the combustion chamber wall of reciprocating engines, however it was found that the primary consideration in all cases was the accuracy of measuring the 'true' temperature. The most common method for calculating heat transfer was the differential method applying Fourier's one dimensional law of conduction. There are a significant number of factors which influence the flow of heat from the combustion chamber and the prediction methods derived since 1939 vary in complexity and accuracy. No single empirical model has been concluded to be the most accurate when taking into account different engine sizes and operating conditions.

3) *Apply this knowledge in the design of a temperature sensor to be installed in the combustion chamber wall of a production engine at a number of different locations.*

A number of probes were designed and evaluated which utilised the differential temperature method to measure the heat flux through the cylinder wall. A calibration process was implemented to improve the measurement accuracy and to account for the systematic error of using dissimilar materials in the sensor construction. The sensor was designed to be robust and the installation method was evaluated prior to installation in the engine. The sensor was installed in twelve locations, with the majority located around a single cylinder; the additional sensors were used for cylinder to cylinder comparison.

4) *Develop and implement an experimental programme to evaluate the rate of heat transfer through the combustion chamber wall across a targeted operating envelope. Analyse the resulting data and use to evaluate established convective heat transfer models used in 1-D engine simulations.*

A series of steady state operating conditions were determined to evaluate the heat transfer over a New European Drive Cycle operating envelope. A number of assumptions were made to allow the use of the limited operating conditions to approximate to the NEDC heat transfer. The piston cooling jets were found to have a significant impact on the cylinder wall

temperature at low power operating conditions, increasing the wall temperature by up to 12°C when deactivated. The temperature profile and heat flux were found to be considerably different on the intake and exhaust sides of the engine due to the impact of the coolant feed position and the additional friction caused by the thrust force of the piston. Longitudinal conduction was found to be significant, in some cases the longitudinal temperature gradient was up to 20% of the radial; however this was considered to have a negligible impact on the estimated conduction through the cylinder wall. Linear response models were created for the average heat flux and gas side cylinder wall temperature for the range of engine speeds and BMEPs tested. The measured heat flux data was subsequently used to evaluate the convective heat transfer models and it was found that they over-predicted across the range of engine power conditions tested.

5) *Improve the accuracy and/or highlight fundamental deficiencies in the application of empirical convective heat transfer correlations in their current forms in 1-D simulation codes due to the inclusion of modern technologies in engine systems.*

An optimisation of the Hohenberg model was performed which showed a 77.6% reduction in the sum of the errors when comparing the existing correlation to the measured data. An average cylinder wall temperature component was subsequently introduced which further improved the correlation with the measured data, reducing the error by an addition 17.4%. A combination of the cylinder wall response model and the modified Hohenberg model could be implemented to predict the cycle average gas side convective heat coefficients for a range of engine operating conditions and at different points during the engine warm-up.

6) *Design and manufacture a number of mechanical components to allow for a series of thermal management system build changes to be performed.*

A Design of Experiments based test programme was undertaken to evaluate the effect of a number of key actuators within the thermal management system on the engine warm-up over a New European Drive Cycle. The additional hardware and instrumentation was developed and implemented in conjunction with Burke and was found to function correctly with little impact on the fluid volumes and structure compared to the installation used in the steady state investigation.

7) *Develop an understanding of how different active thermal management systems impact the rate of heat transfer from the combustion chamber through the cylinder wall.*

It was found that the fastest warm-up was a result of the low engine coolant flow rate, combined with the use of coolant-cooled EGR and bypassing the Oil Cooler. The low engine coolant flow maintained a low coolant inlet temperature to the engine, whilst allowing the cylinder wall temperature to rise. The low coolant flow rate then kept the heat within the engine rather than it mixing with the coolant external to the engine. The coolant-cooled EGR allowed for some waste heat to be recovered aiding the warm-up process.

8) *Combine findings from both the steady state experiments and the transient experiments to improve the understanding of heat transfer within a modern diesel engine.*

The cruise conditions in the UDC phase of the NEDC were approximated to steady state operating conditions and the in-cylinder data from the steady state operation was used to calculate the convective heat transfer based on the modified Hohenberg equation and measured cylinder wall temperature from each of the transient experiments. It was found that during the early UDC phases, the gas side convective heat transfer correlated to the rate of energy transfer to the coolant across the engine structure. The correlation reduced as the engine warmed up, which was attributed to the reduction in the change in the cylinder wall temperature. The findings showed that by introducing the cylinder wall component to the Hohenberg model, some prediction of the convective heat transfer coefficients at part warm conditions could be made.

The aim of this project was to achieve an improved understanding of the heat transfer in modern diesel engines through the measurement of combustion chamber wall temperatures under both steady state and transient operation. Measurement methods have been employed on a wide variety of single cylinder engines with different levels of complexity in previous studies. In this work, sensors were integrated into a production engine to give a more representative understanding of the heat transfer within an engine currently in production, incorporating a large number of new technologies which aim to improve the fuel consumption, especially during cold start operation. Through this work, the inaccuracy of established models has been highlighted and the effect of engine operating condition on both the rate of heat transfer and cylinder wall temperature explained. In addition the impact of a

number of devices integrated into the production engine cooling circuit has been described and how the candidate hardware fundamentally affected the heat transfer through the combustion chamber wall.

Additionally from the obtained understanding, a change to an established model has been proposed in order to improve the accuracy and allow it to be applied to an engine at different stages of warm-up. These findings can be applied to 1-D simulation codes and are beneficial both within the University and in other experimental facilities.

## 7.3 Outlook and further work

The work conducted for the purpose of this thesis has impacted on a number of projects since its completion in 2009. The TSB project was not continued but the improved understanding of the fundamentals of heat transfer has provided significant insight and some direction in current projects. The future of I.C. engine development, especially within gasoline is towards lower displacement and much higher peak power. Engine downsizing requires the use of air charge systems to maintain the performance of larger displacement engines and by doing so increases the in-cylinder temperatures and pressures. The increased temperatures within the cylinder and the increasing complexity of active engine cooling regimes to improve cold start fuel consumption require the ability to predict the effect on the engine structure.

The conclusions made in this thesis are based on strong experimental data and add to the knowledge that was reviewed. The findings can be used to predict convective heat transfer coefficients during warm-up conditions for this particular engine. In addition the mechanisms within the engine structure which result in a faster warm-up have been explored. This gives a clear indication that expansion of work of this nature would prove useful in the development of modelling and simulation of engines in the future. The findings are useful as a starting point but are very limited due to only one engine configuration being tested; however there is still a large amount of information and understanding which can be extracted from the current data. Possible continuations and expansions of this work would involve increasing the number of sensors installed in the engine to reduce the level of interpolation required. This would include temperature measurement in the cylinder head and piston; however increased instrumentation would result in an engine which does not resemble a production unit, therefore a compromise would have to be made. It would also

be beneficial to employ a similar measurement technique on different types of engine in order to widen the application of the proposed improvements to the convective heat transfer model and the cylinder wall temperature prediction. This would also allow for some model validation to be employed.

The outcomes of this work are useful to engine designers, combustion simulation engineers and thermal management teams who are continuously looking for ways to improve the predictability of their systems.

# References


1. Khemani, H. **Thermodynamic Diesel Cycle: Air Standard Cycle: Part – 3**. [Website] 8/9/2008 [cited 2103 12th December].
2. Stone, R., **Introduction to Internal Combustion Engines**. Third Edition ed. 1999: MacMillan Press Ltd.
3. Alcock, J. F., Robson, J. V. B. and Mash, C., **Distribution of Heat Flow in High-Duty Internal-Combustion Engines**. 1957.
4. Taylor, C. F., **The internal combustion engine in theory and practice**. Vol. 1. 1985a, Cambridge, Massachusetts: MIT Press.
5. Smith, L. A., Preston, W. H., Dowd, G., Taylor, O. and Wilkinson, K. M., **Application of a First Law Heat Balance Method to a Turbocharged Automotive Diesel Engine**. 2009, SAE International.
6. Donn, C., Zulehner, W., Ghebru, D., Spicher, U. and Honzen, M., **Experimental Heat Flux Analysis of an Automotive Diesel Engine in Steady-State Operation and During Warm-Up**. 2011, SAE International.
7. Brace, C. J. and Burke, R. D, **Increasing accuracy and repeatability of fuel consumption measurement in chassis dynamometer testing**. Proceedings of the Institution of Mechanical Engineers, Part D: Journal of Automobile Engineering, 2009. 223(9): p. 1163-1177.
8. British Standard Institution, **Reciprocating internal combustion engines. Exhaust emission measurement. Test-bed measurement of gaseous and particulate exhaust emissions**. 2009
9. Hawley, J. G., Bannister, C. D., Brace, C. J., Cox, A., Ketcher, D. and Stark, R., **Vehicle modal emissions measurement techniques and issues**, in Proceedings of the Institution of Mechanical Engineers -- Part D -- Journal of Automobile Engineering. 2004, Professional Engineering Publishing. p. 859-873.
10. Benz, Daimler, in Aachen Colloquium. 2011.
11. Sanli, A., Ozsezen, A. N., Kilicaslan, I. and Canakci, M., **The influence of engine speed and load on the heat transfer between gases and in-cylinder walls at fired and motored conditions of an IDI diesel engine**. Applied Thermal Engineering, 2008. 28(11-12): p. 1395-1404.
12. Lakshminarayanan, P. A. and Dani, A. D., **Heat transfer from a diesel engine and estimation of lubricating oil temperature**. ARCHIVE: Proceedings of the Institution of Mechanical Engineers, Part C: Journal of Mechanical Engineering Science 1989-1996 (vols 203-210), 1994. 208(33): p. 199-205.
13. Smith, L. W. L., Angus, H. T. and Lamb, A. D., **Cracking in cast iron diesel engine cylinder heads**. Proceedings of the Institution of Mechanical Engineers, 1970. v185 1970-71: p. 16.
14. Cheung, C. S., Leung, C. W. and Leung, T. P., **Modelling spatial radiative heat flux distribution in a direct injection diesel engine**. Proceedings of the Institution of Mechanical Engineers, Part A: Journal of Power and Energy, 1994. 208(Compendex): p. 275-283.
15. Woschni, G. **Universally applicable equation for instantaneous heat transfer coefficient in internal combustion engine**. in *SAE Meeting, Oct 30-Nov 3 1967*. 1967. New York, NY, United States: Society of Automotive Engineers (SAE).

16. Eichlseder, W., Marzy, R., Hager, J. and Haidinger, M., **Optimization of heat management of vehicles using simulation tools**, in Vehicle thermal management systems 4. 1999, Professional Engineering Publishing Limited.
17. Campbell, N. A. F., Tilley, D. G., MacGregor, S. A. and Wong, L., **Incorporating Nucleate Boiling in a Precision Cooling Strategy for Combustion Engines**. 1997.
18. Kubozuka, T., Ogawa, N., Hirano, Y. and Hayashi, Y., **An application study of evaporative cooling to heavy duty diesel engines**, S. International, Editor. 1987.
19. Watanabe, Y., Ishikawa, H. and Miyahara, M., **An application study of evaporative cooling to heavy duty diesel engines**, S. International, Editor. 1987.
20. Pretscher, M. and Ap, N. S., **Nucleate boiling engine cooling system - vehicle study**, S. International, Editor. 1993.
21. Chen, J. C., **Correlation for boiling heat transfer to saturated fluids in convective flow**. Industrial and Engineering Chemistry -- Process Design and Development, 1966. 5(3): p. 322-329.
22. Robinson, K., Hawley, J. G., Hammond, G. and Owen, N., **Convective coolant heat transfer in internal combustion engines**. Proceedings of the Institution of Mechanical Engineers, Part D: Journal of Automobile Engineering, 2003. 217(2): p. 133-146.
23. Robinson, K., Wilson, M., Leathard, M. J. and Hawley, J. G., **Computational modelling of convective heat transfer in a simulated engine cooling gallery**. Proceedings of the Institution of Mechanical Engineers, Part D: Journal of Automobile Engineering, 2007. 221(Compendex): p. 1147-1157.
24. Robinson, K., Hawley, J. G. and Campbell, N. A. F., **Experimental and modelling aspects of flow boiling heat transfer for application to internal combustion engines**. Proceedings of the Institution of Mechanical Engineers, Part D: Journal of Automobile Engineering, 2003. 217(10): p. 877-889.
25. Warrier, G. R. and Dhir, V. K., **Heat Transfer and Wall Heat Flux Partitioning During Subcooled Flow Nucleate Boiling---A Review**. Journal of Heat Transfer, 2006. 128(12): p. 1243-1256.
26. Boyle, R. J., Finlay, I. C., Biddulph, T. and Marshall, R. A., **Heat transfer to non-aqueous engine coolants**. SAE (Society of Automotive Engineers) Transactions, 1991. 100(Compendex): p. 377-386.
27. Cozzone, G. E., **Effect of coolant type on engine operating temperatures**, in SAE International Congress and Exposition. 1999, SAE International: Detroit, Michigan, USA.
28. National Engineering Laboratory, **The influence of wall material on heat transfer to engine coolants under conditions of nucleate boiling**. 1986.
29. Alexander, M. V., **A modern approach to evaluation of ethylene glycol based coolants**. 1988, SAE.
30. Pang, H. H. and Brace, C. J., **Review of engine cooling technologies for modern engines**. Proceedings of the Institution of Mechanical Engineers, Part D: Journal of Automobile Engineering, 2004. 218: p. 7.
31. Janowski, P., Shayler, P. J., Robinson, S. and Goodman, M., **The effectiveness of heating parts of the powertrain to improve vehicle fuel economy during warm-up**, in VTMS 10. 2011: Gaydon.
32. Couetouse, H. and Gentile, D. **Cooling system control in automotive engines**. in *International Congress and Exposition, Febrary 24, 1992 - Febrary 28, 1992*. 1992. Detroit, MI, USA: Publ by SAE.
33. Brace, C. J., Burnham-Slipper, H., Wijetunge, R. S., Vaughan, N. D., Wright, K. and Blight, D., **Integrated cooling systems for passenger vehicles**, in SAE. 2001.

34. Wagner, J. R., Ghone, M. C., Dawson, W. and Marotta, E. E., **Coolant flow control strategies for automotive thermal management systems**, in SAE. 2002.
35. Chalgren, R. D. J., **Thermal confort and engine warm-up optimization of a low-flow advanced thermal management system**, in SAE. 2004.
36. Allen, D. J. and Lasecki, M. P., **Thermal management evolution and controlled coolant flow**, in Vehicle Thermal Management Systems Conference and Exhibition. 2001, SAE International: Nashville, TN, USA.
37. Brace, C. J., Hawley, J. G., Akehurst, S., Piddock, M. and Pegg, I. **Cooling system improvements - assessing the effects on emissions and fuel economy**. in *8th Vehicle Thermal Management Systems Conference*. 2007. Nottingham, ENGLAND: Professional Engineering Publishing Ltd.
38. Choukroun, A. and Chanfreau, M., **Automatice control of electronic actuators for an optimized engine cooling thermal management**, in SAE. 2001.
39. Andrews, G. E., Ounzain, A. M. and Li, H., **The Use of a Water/Lube Oil Heat Exchanger and Enhanced Cooling Water Heating to Increase Water and Lube Oil Heating Rates in Passenger Cars for Reduced Fuel Consumption and CO2 Emissions During Cold Start**, in 2007 JSAE/SAE International Fuels and Lubricants Meeting. 2007, SAE International: Kyoto, Japan. p. 14.
40. Varghese, M. B., Goyal, S. K. and Agarwal, A. K., **Numerical and Experimental Investigation of Oil Jet Cooled Piston**. 2005.
41. Campbell, N. A. F., Charlton, S. J. and Wong, L, **Designing towards Nucleate Boiling in Combustion Engines**. Proceedings of the Institution of Mechanical Engineers, Part D: Journal of Automobile Engineering, 1995.
42. Robinson, K., Campbell, N. A. F., Hawley, J. G. and Tilley, D. G., **A Review of precision engine cooling**. 1999, SAE International.
43. Clough, M. J., **Precision cooling of a four valve per cylinder engine.** 1993, SAE
44. Osman, A., Sabrudin, A., Hussin, M. and Bakri, Z. A., **Design and Simulations of an Enhanced and Cost Effective Engine Split Cooling Concept**. 2013, SAE International.
45. Brace, C. J., Hawley, J. G., Cox, A., Pegg, I. and Stark, R., **The Effect of Variable Flow Oil Pumps on Vehicle Fuel Economy**. University of Bath.
46. Baek, D. K. and Khonsari, M. M., **Temperature analysis of a gasket for an internal combustion engine**. Proceedings of the Institution of Mechanical Engineers, Part D: Journal of Automobile Engineering, 2006. 220: p. 11.
47. Suzuki, Y., Shimano, K., Enomoto, Y., Emi, M. and Yamada, Y., **Direct Heat Loss to Combustion Chamber Walls in a Direct-injection Diesel Engine: Evaluation of Direct Heat Loss to Piston and Cylinder Head**. International Journal of Engine Research, 2005. 6(2): p. 119-135.
48. Yoshida, M., Harigaya, Y. and Sato, K., **Variation of Heat Flux through a Combustion Chamber wall of Pre-Chamber type diesel engine - Heat Flux through piston crown, cylinder head, suction vale, exhaust valve, pre-combustion chamber and exhaust port wall**. Bulletin of the JSME, 1982. 25(201): p. 426-437.
49. Jafari, A. and Hannani, S. K., **Effect of fuel and engine operational characteristics on the heat loss from combustion chamber surfaces of SI engines**. International Communications in Heat and Mass Transfer, 2006. 33(1): p. 122-134.
50. Genix, M., Vairac, P. and Cretin, B., **Local temperature surface measurement with intrinsic thermocouple**. International Journal of Thermal Sciences, 2009. 48(9): p. 1679-1682.

51. Sapozhnikov, S. Z., Mitiakov, V. Y. and Mitiakov, A. V. **Heat flux sensor for heat transfer investigation**. in *11th International Heat Transfer Conference*. 1998. Kyongju, South Korea: Taylor & Francis Ltd.
52. Eichelberg, G., **Some new investigations on old combustion engine problems - Part 1**. Engineering, 1939. 148: p. 463 - 466.
53. Eichelberg, G., **Some new investigations on old combustion engine problems - Part 2**. Engineering, 1939. 148: p. 547-550.
54. Eichelberg, G., **Some new investigations on old combustion engine problems - Part 3**. Engineering, 1939. 148: p. 603-606.
55. Eichelberg, G., **Some new investigations on old combustion engine problems - Part 4**. Engineering, 1939. 148: p. 682-686.
56. Eichelberg, G., **Some new investigations on old combustion engine problems - Part 5**. Engineering, 1940. 149: p. 297-299.
57. Chang, J., Filipi, Z., Assanis, D., Kuo, T. W., Najt, P. and Rask, R., **Characterizing the thermal sensitivity of a gasoline homogeneous charge compression ignition engine with measurements of instantaneous wall temperature and heat flux**. International Journal of Engine Research, 2005. 6(4): p. 289-310.
58. Chang, J., Guralp, O., Filipi, Z., Assanis, D., Kuo, T. W., Najt, P. and Rask, R., **New Heat Transfer Correlation for an HCCI Engine Derived from Measurments of Instantaneous Surface Heat Flux**, in SAE International. 2004, SAE International: Tampa, Florida. p. 18.
59. Chang, J., Filipi, Z., Kuo, T. W., Assanis, D., Najt, P. and Rask, R., **Investigation of Mixture Preparation Effects on Gasoline HCCI Combustion Aided by Measurements of Wall Heat Flux**. Journal of Engineering for Gas Turbines and Power, 2008. 130(6): p. 062806.
60. Cho, K-W., Assanis, D., Filipi, Z., Szekely, G., Najt, P. and Rask, R., **Experimental investigation of combustion and heat transfer in a direct-injection spark ignition engine via instantaneous combustion chamber surface temperature measurements**. Proceedings of the Institution of Mechanical Engineers, Part D: Journal of Automobile Engineering, 2008. 222: p. 15.
61. Enomoto, Y. and Furuhama, S., **Heat transfer to wall of ceramic combustion chamber of internal combustion engine**. Nippon Kikai Gakkai Ronbunshu, B Hen/Transactions of the Japan Society of Mechanical Engineers, Part B, 1985. 51(Compendex): p. 2781-2786.
62. Mohammed, H., Salleh, H. and Yusoff, M. Z., **Design and fabrication of coaxial surface junction thermocouples for transient heat transfer measurements**. International Communications in Heat and Mass Transfer, 2008. 35(7): p. 853-859.
63. Assanis, D. N. and Friedmann, F. A., **A Thin-Film Thermocouple for transient heat-transfer measurements in Ceramic-Coated Combustion-Chambers**. International Communications in Heat and Mass Transfer, 1993. 20(4): p. 459-468.
64. Hoag, K. L. **Measurement and analysis of the effect of wall temperature on instantaneous heat flux**. in *Adiabatic Engine: Global Developments.* 1986. Detroit, MI, Engl: SAE.
65. Bendersky, D., **A special thermocouple for measuring transient temperatures**. Mechanical Engineering, 1953. 75.
66. Heichal, Y., Chandra, S. and Bordatchev, E., **A fast-response thin film thermocouple to measure rapid surface temperature changes**. Experimental Thermal and Fluid Science, 2005. 30(2): p. 153-159.
67. Burgess Jr, D., Yust, M. and Kreider, K. G. **Thin film thermocouples for measurement of wall temperatures in internal combustion engines**. in *Parallel and Vector Computation in Heat Transfer - Presented at AIAA/ASME Thermophysics and*

*Heat Transfer Conference, June 18, 1990 - June 20, 1990*. 1990. Seattle, WA, USA: Publ by ASME.
68. Meingast, U., Reichelt, L. and Renz, U., **Measuring transient wall heat flux under diesel engine conditions**. International Journal of Energy Research, 2004. 5(5): p. 10.
69. Marr, M. A., Wallace, J. S., Chandra, S., Pershin, L. and Mostaghimi, J., **A fast response thermocouple for internal combustion engine surface temperature measurements**. Experimental Thermal and Fluid Science, 2010. 34(2): p. 183-189.
70. Overbye, V. D., Bennethum, J. E., Uyehara, O. A. and Myers, P. S. **Unsteady heat transfer in engines**. in *SAE Meeting, Jun 5-10 1960*. 1960. New York, NY, United States: Society of Automotive Engineers (SAE).
71. Yamada, Y., Emi, M., Ishii, H., Suzuki, Y., Kimura, S. and Enomoto, Y., **Heat loss to the combustion chamber wall with deposit in D.I. diesel engine: variation of instantaneous heat flux on piston surface with deposit**. JSAE Review, 2002. 23(4): p. 415-421.
72. Childs, P. R. N., Greenwood, J. R. and Long, C. A., **Heat flux measurement techniques**. Proceedings of the Institution of Mechanical Engineers, Part C: Journal of Mechanical Engineering Science, 1999. 213(7): p. 22.
73. Buttsworth, D. R., **Transient response of an erodable heat flux gauge using finite element analysis**. Proceedings of the Institution of Mechanical Engineers, Part D: Journal of Automobile Engineering, 2002. 216: p. 6.
74. Rakopoulos, C. D. and Mavropoulos, G. C., **Experimental evaluation of local instantaneous heat transfer characteristics in the combustion chamber of air-cooled direct injection diesel engine**. Energy, 2008. 33(7): p. 1084-1099.
75. Rakopoulos, C. D., Mavropoulos, G. C. and Hountalas, D. T., **Measurements and analysis of load and speed effects on the instantaneous wall heat fluxes in a direct injection air-cooled diesel engine**. International Journal of Energy Research, 2000. 24(7): p. 587-604.
76. Rakopoulos, C. D., Rakopoulos, D. C., Mavropoulos, G. C. and Giakoumis, E. G., **Experimental and theoretical study of the short term response temperature transients in the cylinder walls of a diesel engine at various operating conditions**. Applied Thermal Engineering, 2004. 24(5-6): p. 679-702.
77. Mavropoulos, G. C., Rakopoulos, C. D. and Hountalas, D. T., **Experimental Assessment of Instantaneous Heat Transfer in the Combustion Chamber and Exhaust Manifold Walls of Air-Cooled Direct Injection Diesel Engine**, in SAE 2008 World Congress. 2008, SAE International, Warrendale, Pennsylvania, USA: Detroit, Michigan, USA. p. 25.
78. Desantes, J. M., Torregrosa, A. J., Broatch, A. and Olmeda, P., **Experiments on the influence of intake conditions on local instantaneous heat flux in reciprocating internal combustion engines**. Energy, 2011. 36(Compendex): p. 60-69.
79. Rakopoulos, C. D. and Mavropoulos, G. C., **Effects of transient diesel engine operation on its cyclic heat transfer: an experimental assessment**. Proceedings of the Institution of Mechanical Engineers, Part D: Journal of Automobile Engineering, 2009. 223: p. 22.
80. Rakopoulos, C. D. and Mavropoulos, G. C., **Experimental instantaneous heat fluxes in the cylinder head and exhaust manifold of an air-cooled diesel engine**. Energy Conversion and Management, 2000. 41(12): p. 1265-1281.
81. Demuynck, J., Raes, N., Zuliani, M., De Paepe, M., Sierens, R. and Verhelst, S., **Local heat flux measurements in a hydrogen and methane spark ignition**

**engine with a thermopile sensor**. International Journal of Hydrogen Energy, 2009. 34(24): p. 9857-9868.
82. Hart, J. S., Stryker, P. C. and Ciaravino, J., **Multi-point temperature probe for measuring combustion chamber heat fluxes and surface temperatures**. IMechE, 1999: p. 10.
83. Finol, C. A. and Robinson, K., **Thermal Profile of a Modern Passenger Car Diesel Engine**, in Powertrain & Fluid Systems Conference & Exhibition. 2006, SAE International: Toronto, Canada. p. 10.
84. Emi, M., Suzuki, Y., Yamada, Y., Ishii, H., Kimura, S., Ogawa, H. and Enomoto, Y., **Development of thin film thermocouple for measurement of instantaneous heat flux flowing into the cast iron combustion chamber wall**. JSAE Review, 2002. 23(3): p. 379-382.
85. Torregrosa, A., Olmeda, P., Degraeuwe, B. and Reyes, M., **A concise wall temperature model for DI Diesel engines**. Applied Thermal Engineering, 2006. 26(11-12): p. 1320-1327.
86. Sharief, A., Chandrashekar, T. K., Antony, A. J. and Samaga, B. S., **Study on Heat Transfer Correlation in IC Engines**. 2008.
87. Wu, Y., Chen, B., Hsieh, F. and Ke, C., **Heat transfer model for small-scale spark-ignition engines**. International Journal of Heat and Mass Transfer, 2009. 52(7-8): p. 1875-1886.
88. Taylor, C. F. and Toong, T. Y., **Heat transfer in internal-combustion engines**. 1957, ASME.
89. Annand, W. J. D., **Heat Transfer in the cylinders of reciprocating internal combustion engines**. Proceedings of the Institution of Mechanical Engineers, 1963. 177: p. 24.
90. Sitkei, G. and Ramanaiah, G. V., **Rational approach for calculation of heat transfer in diesel engines**. 1972(Compendex).
91. Annand, W. J. D. and Ma, T. H., **Instantaneous heat transfer rates to the cylinder head surface of a small compression-ignition engine**. Proceedings of the Institution of Mechanical Engineers, 1970. 185.
92. Schmidt, E., **Z. VDI 81**. 1937(1041).
93. Stone, C. R., Lim, E. P., Ewart, P., Lloyd, G. and Williams, R. B., **Temperature and heatflux measurements in a spark-ignition engine**, in SAE 2000 World Congress. 2000, SAE International: Detroit, Michigan, USA. p. 11.
94. Sihling, K. and Woschni, G., **Experimental investigation of the instantaneous heat transfer in the cylinder of a high speed diesel engine**. SAE Special Publications, 1979(Compendex): p. 95-103.
95. Lawton, B., **Effect of compression and expansion on instantaneous heat transfer in reciprocating internal combustion engines**. Proceedings of the Institution of Mechanical Engineers. Part A. Power and process engineering, 1987. 20 I(Compendex): p. I75-186.
96. Watson, N. and Janota, M. S., **Turbocharging - The Internal Combustion Engine**. 1982, Southampton: MacMillan Publishers Ltd.
97. Wang, X., Price, P., Stone, C. R. and Richardson, D., **Heat release and heat flux in a spray-guided direct-injection gasoline engine**. Proceedings of the Institution of Mechanical Engineers, Part D: Journal of Automobile Engineering, 2007. 221: p. 12.
98. Heinle, M., Bargende, M. and Berner, H., **Some Useful Additions to Calculate the Wall Heat Losses in Real Cycle Simulations**. SAE Int. J. Engines, 2012. 5(2): p. 469-482.

99. Hohenberg, G. F., **Advanced Approaches for Heat Transfer Calculations**, in SAE Spec Publ SP-449, Diesel Engine Therm Loading. 1979, SAE: Milwaukee, WI, USA. p. 61-79.
100. Woschni, G. and Huber, K., **The influence of soot deposits on combustion chamber walls on heat losses in diesel engines**, in International Congress and Exposition. 1991, SAE International.
101. Soyhan, H. S., Yasar, H., Walmsley, H., Head, B., Kalghatgi, G. T. and Sorusbay, C., **Evaluation of Heat Transfer Correlations for HCCI Engine Modeling**. Applied Thermal Engineering, 2009. 29(2-3): p. 541-549.
102. Finol, C. A. and Robinson, K., **Thermal modelling of modern diesel engines: proposal of a new heat transfer coefficient correlation**. Proceedings of the Institution of Mechanical Engineers, Part D: Journal of Automobile Engineering, 2011. 225(11): p. 1544-1560.
103. Finol, C. A., **Heat Transfer Investigations in a Modern Diesel Engine**, in Mechanical Engineering. 2008, University of Bath: University of Bath. p. 245.
104. Finol, C. A. and Robinson, K., **Thermal modelling of modern engines: a review of empirical correlations to estimate the in-cylinder heat transfer coefficient**. Proceedings of the Institution of Mechanical Engineers, Part D: Journal of Automobile Engineering, 2006. 220: p. 17.
105. LeFeuvre, T., Myers, P. S. and Uyehara, O. A., **Experimental Heat Fluxes in a Diesel Engine and Their Correlation**, in Mid-Year Meeting. 1969, Society of Automotive Engineers: Chicago, Illinois. p. 22.
106. Oude Nijeweme, D. J., Kok, J. B. W, Stone, C. R. and Wyszynski, L, **Unsteady in-cylinder heat transfer in a spark ignition engine: experiments and modelling**. Proceedings of the Institution of Mechanical Engineers, Part D: Journal of Automobile Engineering, 2001. 215: p. 13.
107. Davis, R. S. and Patterson, G. J., **Cylinder Pressure Data Quality Checks and Procedures to Maximise Data Accuracy**, in SAE World Congress 2006. 2006, SAE International: Detroit, Michigan.
108. Brunt, M. F. J. and Platts, K. C., **Calculation of heat release in direct injection diesel engines**, in International Congress and Exhibition. 1999, SAE International: Detroit, Michigan.
109. Lapuerta, M., Armas, O. and Hernández, J. J., **Diagnosis of DI Diesel combustion from in-cylinder pressure signal by estimation of mean thermodynamic properties of the gas**. Applied Thermal Engineering, 1999. 19(5): p. 513-529.
110. Lapuerta, M., Armas, O. and Bermúdez, V., **Sensitivity of diesel engine thermodynamic cycle calculation to measurement errors and estimated parameters**. Applied Thermal Engineering, 2000. 20(9): p. 843-861.
111. Shayler, P. J., Baylis, W. S. and Murphy, M., **Main Bearing Friction and Thermal Interaction during the Early Seconds of Cold Engine Operation**. ASME, 2002. 39: p. 15.
112. Zammit, J. P., Shayler, P. J., Gardiner, R. and Pegg, I., **Investigating the Potential to Reduce Crankshaft Main Bearing Friction During Engine Warm-up by Raising Oil Feed Temperature**. SAE Int. J. Engines, 2012. 5(3): p. 1312-1319.
113. Zweiri, Y. H., Whidborne, J. F. and Seneviratne, L. D., **Instantaneous friction components model for transient engine operation**. Proceedings of the Institution of Mechanical Engineers, Part D: Journal of Automobile Engineering, 2000. 214: p. 15.
114. Abu-Nada, E., Al-Hinti, I., Al-Sarkhi, A. and Akash, B., **Effect of piston friction on the performance of SI engine: A thermodynamic approach**. Journal of Engineering for Gas Turbines and Power, 2008. 130.

115. Livanos, G. and Kyrtatos, N. P., **A model of friction losses in Diesel Engines**. 2006.
116. Patton, K. J. and Nitschke, R. G., **Development and Evaluation of a Friction Model for Spark-Ignition Engines**. 1989.
117. Wakuri, Y., Soejima, M., Ejima, Y., Hamatake, T. and Kitahara, T., **Studies on Friction Characteristics of reciprocating Engines**. 1995.
118. Bannister, C. D., Hawley, J. G., Brace, C. J., Cox, A., Ketcher, D. and Stark, R., **Further Investigations on Time-Alignment**. SAE Technical Paper Series, 2004: p. 15.
119. Lewis, A. G. J., Brace, C. J. and Cox, A., **The Effect of Forced cool down on Cold Start Test Repeatability**, in Powertrains, Fuels and Lubricants. 2009, SAE: Florence, Italy. p. 6.
120. Kunze, K., Lade, I. and Wolff, S., **A Systematic Analysis of C02-reduction by an Optimized Heat Supply during Vehicle Warm-up**, in 2006 SAE World Congress. 2006, SAE International: Detroit, Michigan. p. 401-410.
121. Brace, C. J. and Hawley, J. G., **Fuel Consumption Measurement - Techniques and Issues** in UnICEG. 2006.
122. Bannister, C. D., Hawley, J. G., Brace, C. J., Pegg, I., Dumenil, J.C. and Brown, A., **Determining the effect of lubricating oil properties on the diesel engine fuel economy**, in Internal Combustion Engines: Performance, Fuel economy and Emissions. 2007.
123. Lewis, A. G. J., Akehurst, S., Brace, C. J., Finol, C. A. and Robinson, K., **Dynamic Measurement of Heat Flux through the Cylinder Wall of a Modern HSDI Engine over a New European Drive Cycle**, in SAE 2010 World Congress. 2010, SAE International, Warrendale, Pennsylvania, USA: Detroit, Michigan, USA. p. 11.
124. Slifka, A. J., Filla, B. J. and Phelps, J. M., **Thermal Conductivity of Magnesium Oxide from Absolute, Steady-State Measurements**. Journal of Research of the National Institute of Standards and Technology, 1998. 103(4): p. 357-363.
125. Bevington, R. P., **Data Reduction and Error analysis for the Physical Sciences**. 1969, New York: McGraw-Hill.
126. Kline, S. J. and McClintock, F. A., **Describing uncertainties in single-sample experiments**. Mechanical Engineering, 1953. 75: p. 3-8.
127. Ltd., TC, **Guide to Thermocouple and Resistance Thermometry**. 2001.
128. Assanis, D. N. and Badillo, E., **On Heat Transfer Measurements in Diesel Engines Using Fast-Response Coaxial Thermocouples**. Journal of Engineering for Gas Turbines and Power, 1989. 111(3): p. 458-465.
129. Kataoka, T., Suzuki, Y., Kato, N., Kikuchi, T. and Mihara, Y., **Measurement of Oil Film Pressure in the Main Bearings of an Operating Engine Using Thin-Film Sensors**, in SAE 2008 World Congress. 2008, SAE International. p. 7.
130. Millington, B. W. and Hartles, E. R., **Frictional Losses in Diesel Engines**. 1968, SAE International.
131. Winterbone, D. E., **The Thermodynamics and Gas Dynamics of Internal Combustion Engines**. Vol. 2. 1986: Oxford University Press.
132. Heywood, J. B., **Internal Combustion Engine Fundamentals**. 1988: McGraw-Hill.
133. Omar Mian, A., Parker, D. and Williams, B., **Measured crankshaft bearing oil flow and temperatures with a full and partial groove mainbearing**, in SAE 2000 World Congress. 2000, SAE International: Detroit, Michigan, USA. p. 7.
134. Martin, F. A., **Developments in engine bearing design**. Tribology International, 1983. 16(3): p. 147-164.

135. Luff, D. C., Law, T., Shayler, P. J. and Pegg, I., **The Effect of Piston Cooling Jets on Diesel Engine Piston Temperatures, Emissions and Fuel Consumption**. SAE Int. J. Engines, 2012. 5(3): p. 1300-1311.
136. Laboratory, National Physical, **Thermal Conductivity of an Aluminium Alloy**. 2000.
137. Burke, R. D., **Investigation into the Interactions between Thermal Management, Lubrication and Control Systems of a Diesel engine**, in Mechanical Engineering. 2012, University of Bath. p. 251.
138. Burke, R. D., Brace, C. J., Cox, A., Lewis, A. G. J., Hawley, J. G., Pegg, I. and Stark, R., **Systems approach to the improvement of engine warm-up behaviour**. Proceedings of the Institution of Mechanical Engineers, Part D: Journal of Automobile Engineering, 2010. 224: p. 16.
139. Burke, R. D, Brace, C. J., Hawley, J. G. and Pegg, I., **Review of the systems analysis of interactions between the thermal, lubricant and combustion process of diesel engines**. Proceedings of the Institution of Mechanical Engineers, Part D: Journal of Automobile Engineering, 2009. 224: p. 24.
140. Burke, R. D, Brace, C. J., Lewis, A. G. J., Cox, A. and Pegg, I., **Analysis of energy flows in engine coolant, structure and lubricant during warm-up**, in VTMS10. 2010: Gaydon.
141. Lewis, A. G. J., Brace, C. J., Akehurst, S., Robinson, K. and Pegg, I., **Spatially resolved heat flux measurements from a HSDI engine over NEDC**, in VTMS 10. 2011, IMechE: Gaydon.

# Appendix

**Table 14 – All minimap operating conditions**

| Minimap number | Engine speed (rpm) | Engine torque (Nm) | Engine power (kW) | Brake mean effective pressure (bar) | Weighting factor |
|---|---|---|---|---|---|
| 1 | 875 | 20 | 1.8 | 1.0 | 0.217 |
| 2 | 1125 | 20 | 2.4 | 1.0 | 0.023 |
| 3 | 1125 | 60 | 7.1 | 3.1 | 0.001 |
| 4 | 1375 | 20 | 2.9 | 1.0 | 0.005 |
| 5 | 1375 | 60 | 8.6 | 3.1 | 0.007 |
| 6 | 1625 | 20 | 3.4 | 1.0 | 0.150 |
| 7 | 1625 | 60 | 10.2 | 3.1 | 0.016 |
| 8 | 1875 | 20 | 3.9 | 1.0 | 0.013 |
| 9 | 1875 | 60 | 11.8 | 3.1 | 0.125 |
| 10 | 1875 | 100 | 19.6 | 5.2 | 0.011 |
| 11 | 2125 | 20 | 4.5 | 1.0 | 0.023 |
| 12 | 2125 | 60 | 13.4 | 3.1 | 0.031 |
| 13 | 2125 | 100 | 22.3 | 5.2 | 0.031 |
| 14 | 2125 | 140 | 31.2 | 7.3 | 0.034 |
| 15 | 2375 | 20 | 5.0 | 1.0 | 0.094 |
| 16 | 2375 | 60 | 14.9 | 3.1 | 0.014 |
| 17 | 2375 | 100 | 24.9 | 5.2 | 0.014 |
| 18 | 2375 | 140 | 34.8 | 7.3 | 0.022 |
| 19 | 2375 | 220 | 54.7 | 11.5 | 0.014 |
| 20 | 2625 | 20 | 5.5 | 1.0 | 0.109 |
| 21 | 2625 | 60 | 16.5 | 3.1 | 0.011 |
| 22 | 2625 | 140 | 38.5 | 7.3 | 0.013 |
| 23 | 2625 | 180 | 49.5 | 9.4 | 0.010 |
| 24 | 2625 | 220 | 60.5 | 11.5 | 0.001 |
| 25 | 2625 | 260 | 71.5 | 13.6 | 0.009 |
| 26 | 2875 | 140 | 42.2 | 7.3 | 0.003 |